Biomaterials-Tissue Interaction of an Injectable Collagen-Genipin Gel in a Rodent Hemi-Resection Model of Spinal Cord Injury

By

Daniel J. Macaya

B.S. Materials Science & Engineering

Cornell University, 2008

SUBMITTED TO THE HARVARD-MIT PROGRAM IN HEALTH SCIENCES AND TECHNOLOGY IN PARTIAL FULFILLMENT OF THE REQUIREMENTS FOR THE DEGREE OF

DOCTOR OF PHILOSOPHY IN MEDICAL ENGINEERING AND MEDICAL PHYSICS
AT THE
MASSACHUSETTS INSTITUTE OF TECHNOLOGY

SEPTEMBER 2013

Signature of Author:_____
Harvard MIT Program in Health Sciences & Technology
June 28, 2013

Certified by:_____
Myron Spector, Ph.D.
Professor of Orthopedic Surgery (Biomaterials), Harvard Medical School
Senior Lecturer, Department of Mechanical Engineering, MIT
Thesis Supervisor

Accepted by:_____
Emery Brown, MD, Ph.D.
Director, Harvard-MIT Program in Health Sciences and Technology
Professor of Computational Neuroscience and Health Sciences and Technology

Biomaterials-Tissue Interaction of an Injectable Collagen-Genipin Gel in a Rodent Hemi-Resection Model of Spinal Cord Injury

By

Daniel J. Macaya

Submitted to the Harvard-MIT program in Health Sciences and Technology on June 28th, 2013 in Partial Fulfillment of the Requirements for the Degree of Doctor of Philosophy in Medical Engineering and Medical Physics

ABSTRACT

Spinal cord injury (SCI) is a significant health issue resulting in life-long disability and associated secondary complications, affecting approximately 300,000 individuals in the United States. Primary barriers to functional recovery after SCI include the formation of a growth inhibitory astrocyte scar at the lesion border and a lack of a supportive stroma within the defect allowing for axon regeneration. Interestingly, in animals capable of spinal cord regeneration, astrocytes create a tissue bridge across the injury site to facilitate the regeneration of axons through the defect and thus enable functional recovery.

The **overall goal** of this thesis was to develop an injectable collagen-genipin (Col-Gen) hydrogel to facilitate the intrinsic regenerative response after SCI by promoting the population of the defect with astrocytes through a provisional scaffold permissive of astrocyte migration. The **specific aims** of the thesis involved: **1)** development and materials characterization of an injectable collagen hydrogel for neural tissue regeneration, capable of undergoing covalent crosslinking *in vivo;* **2)** evaluation of the permissiveness of Col-Gen gels with and without Fibroblast growth factor-2 (FGF-2), a known astrocyte chemoattractant, incorporated within lipid microtubules (LMTs) to infiltration by primary astrocytes using an *in vitro* cellular outgrowth assay; **3)** evaluation of select formulations of the gel, based on the *in vitro* findings, in a standardized hemi-resection defect in the rat spinal cord. Functional, locomotor, and histopathological outcome measures, recorded up to 4 weeks post-SCI were correlated with each other and with micro MRI studies.

In vivo, the implantation of Col-Gen gels containing FGF-2 LMTs resulted in the enhancement of astrocyte, blood vessel, and laminin infiltration of the defect; increased the amount of spinal cord tissue spared from secondary degeneration; and increased functional recovery, at four weeks post injury as compared to control or Col-Gen treatment groups. Micro MRI was found to be a suitable modality to non-destructively observe the features of the injury *in situ*. This work commends an injectable, covalently cross-linkable formulation of collagen gel incorporating FGF-2-releasing LMTs for further investigation for the treatment of SCI.

Thesis Supervisor: Myron Spector

Title: Professor of Orthopedic Surgery (Biomaterials), Harvard Medical School. Senior Lecturer, Department of Mechanical Engineering, MIT

Acknowledgements:

This work is dedicated to Randy Duchesneau. Randy, your perseverance to lead a successful and fun-filled life despite your injury has been an inspiration for me throughout my PhD. I hope we are now one step closer to a brighter future.

I am immensely grateful to my advisor Dr. Myron Spector. Dr. Spector is my role model for what a great mentor and teacher should be. In addition to guiding my project, he has preened me as a scientist, and fully supported my personal and professional development in any way he could. He always made time for me when I needed it and helped me run workshops aimed at supporting graduate students throughout MIT. I could not have asked for a more dedicated and supportive advisor.

I would like to thank my fellow lab members who I came to know over the years at the VA for their help and support of my work: Karen Ng, Alix Weaver, Paul Elias, Cathal Kearney, Rahmat Cholas, Lily Jeng, Teck Chuan Lim, Toh Wei Seong, Thomas Cheriyan, Wanting Niu. Ravikumar Rajappa, Swetha Rokkappanavar, and Casper Foldager. I am especially grateful to Dr. Hu-Ping Hsu for his exceptionally skillful hands in performing the animal surgeries and Ravi for his invaluable assistance with animal care. I would also like to thank my thesis committee Dr. Michael Cima, Dr. Zhigang He, and Dr. Ken Arai for their guidance through the process of forming my work, as well as my collaborators who made many aspects of this work possible. Specifically, Dr. Gareth McKinley for use of his rheometer, Michelle Farley and Dave Bennet for their technical expertise with MRI, and Dr. Kazuhide Hayakawa for isolation of the primary astrocytes.

A special thank you to my parents Iris and Joseph Macaya for inspiring the scientist inside of me for as long as I can remember. You fed my thirst for knowledge with books, plastic reptiles/dinosaurs, and countless trips to the zoo, aquarium, and museum of natural history. You always encouraged me to shoot for the stars and pursue my dreams. To my grandma Pauline Freundlich, thank you for helping to raise me and bring me to where I am today. I know you are proudly looking down at me from above.

To Christine Hsieh: My love, we have seen each other grow and develop as people and as scientists since I first entered graduate school. We talked deeply and intimately about life and we were there for each other through all the highs and lows. You looked out for me as I looked out for you, and you carried me through my toughest moments in grad school. Our adventures, whether they be urban festivals, suburban getaways, or epic hikes have been a cornerstone of my happiness these past few years.

To Ryan Cooper: You have been my best friend since we both embarked on this journey to get our PhDs many years ago. You opened my eyes to the outdoors and have changed my life ever since. I will always remember those first few years when almost every weekend was another adventure. I can trust you with everything and anything.

To the rest of my friends (my buddies from Sidney-Pacific, HST, MIT, and back home in NYC) and family who have helped me along this journey of the PhD, I sincerely appreciate all of your love and support.

The funding for this work was provided by: The National Science Foundation Graduate Research Fellowship Program; The GEM consortium; the Harvard-MIT division of Health Sciences & Technology; U.S. Department of Veterans Affairs, Veterans Health Administration, Rehabilitation Research and Development Service; and the Department of Defense.

Table of Contents

Chapter 1:
Introduction

Spinal cord injury (SCI) is an extremely debilitating condition often resulting in complete or partial paralysis. In the United States there are approximately 12,000 new cases per year with an additional 232,000-316,000 people currently living with SCI [1]. Since most SCI patients are young, with an average age at injury of 40.7 years, the lifetime cost to care for these individuals is high, ranging from $300,000 for incomplete motor function at any level to over $4,000,000 for high tetraplegia [1]. Currently, there are no clinically available treatments to restore significant function after injury.

SCI presents a complex regenerative problem due to the multiple facets of growth inhibition that occur following trauma to the cord parenchyma and stroma. Clinically, SCI is further complicated by the heterogeneity in the size, shape, and extent of human injuries. Many of these injuries do not breach the dura mater and have continuous viable axons through the injury site that can later lead to some degree of functional recovery. In these cases, surgical manipulation of the spinal cord by implanting a preformed scaffold or drug delivery device may lead to further damage. Given these circumstances, utilizing in situ-forming scaffolds are an attractive approach for SCI regeneration. These synthetic or natural polymers undergo a rapid transformation from liquid to gel upon injection into the cord tissue, conforming to the individual lesion site and directly integrating with the host tissue. Injectable materials can be formulated to have mechanical properties that closely match the native spinal cord extracellular matrix, and this may enhance axonal ingrowth. Such materials can also be loaded with cellular and molecular therapeutics to modulate the wound environment and enhance regeneration.

Overall **goal** of this thesis is to develop an injectable gel capable of undergoing covalent cross-linking *in vivo*, which can modulate the native tissue response to spinal cord injury, allowing for the formation of a regenerative template of astrocytes and blood vessels within the defect formed after spinal cord injury.

In order to enhance the infiltration of the gel-filled defect with astrocytes, a known chemoattractant for these cells, fibroblast growth factor (FGF)-2, was incorporated into the collagen solution prior to its injection. In addition to acting as a chemoattractant for astrocytes, FGF-2 is commended for use in this study for its ability to: promote revascularization of the injury site and act as a neuroprotective factor for the spared tissue. The gel formulations were evaluated in a hemi-resection defect model in the rat spinal cord.

The **specific aims** of the thesis involve: **1.)** Development of an injectable collagen hydrogel for neural tissue regeneration, capable of undergoing covalent crosslinking *in vivo*. . **2.)** Enhancement of astrocyte infiltration into Col-Gen gels through the sustained delivery of fibroblast growth factor 2 (FGF-2) encapsulated within lipid microtubules (LMTs). **3.)** *In vivo* histological and behavioral study of the

acute- early chronic tissue response to injection of Col-Gen gels in a standardized hemi-resection defect in the rat spinal cord.

The overall **hypothesis** is that by designing a provisional matrix with the proper attractive cues for axon supportive cellular ingrowth (i. e. astrocytes and endothelial cells), a regenerative template will be formed within the spinal cord defect, allowing for the ingrowth of axons.

This thesis consists of several chapters, summarized below, which provide a detailed background, methods, results, and discussion of the present study:

Chapter 2 details the background and motivation underlying the work performed in this thesis. It includes a through literature review of the pathophysiology of SCI, current treatments, the role of injectable therapies in SCI, the design parameters and classes of materials appropriate for use as injectable gels for SCI, and finally an overview of the prior *in vivo* studies using injectable collagen gels for the treatment of SCI. A majority of the content in this chapter has been published in Biomedical Materials [2].

Chapter 3 characterizes the injectable collagen-genipin gel in terms of its mechanical behavior, cross-linking kinetics (via absorbance and fluorescence measurements), resistance to enzymatic degradation, and cell viability when incorporated into these gels. A majority of the content in this chapter has been published in Advanced Functional Materials [3].

Chapter 4 describes the cellular outgrowth assay used to assess the permissiveness of select collagen-genipin gel formulations containing FGF-2 to astrocyte infiltration. This chapter also provides insight in to the phenotype of the astrocytes in response to FGF-2, the benefits of sustained release of FGF-2 via lipid microtubules (LMTs), the effects of genipin on astrocytes, and the role of proliferation and viability in the observed response. A majority of the content in this chapter has been published in Biomaterials [4].

Chapter 5 describes a pilot *in vivo* biocompatibility study in a standardized rodent hemi-resection model of SCI using collagen-genipin gels with and one without FGF-2 LMTs. The formulations used in this study were guided by the experiments in chapters 3 and 4. The animals were assessed at one and four weeks post injury and evaluated histologically and behaviorally.

Chapter 6 describes a full *in vivo* study of the biomaterials-tissue interaction of collagen-genipin gels in a standardized rodent hemi-resection model of SCI. Histologic and behavioral analysis was performed on three groups: control, collagen-genipin gel, and collagen-genipin gel with FGF-2 LMTs, at four weeks post injury. The formulations of the collagen-genipin gels were determined based on the pilot study in chapter 5.

Chapter 7 details a pilot *ex vivo* magnetic resonance imaging study of the hemi-resection defect with and without implanted gel at 1 day, 1 week, and 4 weeks post injury. The results correlate features of the injury, gel localization, and tissue remodeling with histology on the same samples.

Chapter 8 lists the conclusions that are supported by the work presented in this thesis.

Chapter 9 discusses the limitations of the worked performed and identifies areas for future investigation.

Following the main chapters of the thesis is an appendix with detailed protocols for the fabrication and assays performed in the thesis.

References:

[1] Center NSCIS. Spinal cord injury facts and figures at a glance. Birmingham Alabama: University of Alabama at Birmingham; February 2012.
[2] Macaya D, Spector M. Injectable hydrogel materials for spinal cord regeneration: a review. Biomed Mater. 2012;7:012001.
[3] Macaya D, Ng KK, Spector M. Injectable Collagen-Genipin Gel for the Treatment of Spinal Cord Injury: In Vitro Studies. Adv Funct Mater. 2011;21:4788-97.
[4] Macaya DJ, Hayakawa K, Arai K, Spector M. Astrocyte infiltration into injectable collagen-based hydrogels containing FGF-2 to treat spinal cord injury. Biomaterials. 2013;34:3591-602.

Chapter 2:
Background and Motivation

2.1. Introduction to SCI

2.1.1. Pathology and current treatment

An understanding of the pathophysiology of SCI is essential for the rational development of therapeutic strategies. We now have available a wide array of agents which can be employed as treatments for SCI individually or in combination: biomaterials; exogenous cells of various types; protein regulators of cell function (*e.g.*, growth factors and chemoattractants), and their genes; antagonists of inflammation and nerve growth inhibitors; and enzymes for extracellular matrix (ECM) molecules which interfere with the regenerative process. The informed selection of specific agents and the timing of their administration require an understanding of the intrinsic components of the response to SCI that prevent or interfere with a regenerative response.

The mechanism of SCI is usually a mechanical insult to the spinal cord parenchyma following a fractured vertebra or disk intruding into the spinal canal [1]. This results in various degrees of contusion, laceration, and in very rare cases a complete transection of the spinal cord tissue [1-3]. Human cases of SCI vary widely with respect to the site and degree of tissue destruction, and may involve multiple lesions with sizes smaller than a single vertebral segment [3] SCI rarely results in a complete disruption of tissue through the lesion site [1]. Approximately 61% of SCIs are classified as incomplete, meaning that there is still a degree of function in segments of the spinal cord innervated below the injury [4]. Complete injuries may also have continuous parenchyma through the lesion, although there is no function in distal segments [1, 3, 5]. Taken together, these studies show that after injury, the protective dural covering of the spinal cord may be intact and there is almost always some amount of viable tissue traversing the site of the lesion. Given these observations, minimally invasive therapies are an attractive treatment option for SCI.

Although our knowledge of the pathology of human SCI is limited, it is believed that most injuries are caused by cord contusion. In one classification system, a contusion/compression type SCI presents with extensive damage and cyst formation in the cord parenchyma with no breach or disruption in the surface anatomy or adhesions to the dura [2]. Another class of SCI, solid cord injury, appears normal grossly but displays tissue that is clearly damaged histologically [2].

One of the challenges in the treatment of SCI is that such injuries may not show gross morphological changes until hours post injury, but eventually encompass 1-2 vertebral segments proximal and distal to the lesion site [6]. The major clinical manifestations of the injury result from damage and subsequent degeneration of the ascending and descending white matter tracks (axons) [1]. In the case of a contusion injury, viable and intact axons are still present at the injury site but are rendered virtually useless from demyelination due to oligodendrocyte loss, which greatly reduces their conduction velocity

[7]. While some plasticity may be observed, the function of areas innervated by segments below the injury is lost.

Current treatment for SCI addresses 2 features of the injury: the persistent mechanical compression of the cord and the acute inflammatory response. Surgical decompression of the injured segments is immediately followed by the administration of steroids to neutralize acute inflammation and decrease swelling to further reduce compression on any remaining neurons [8, 9].

2.1.2. Chronology of pathophysiological changes

SCI pathology can be divided into immediate, acute (*0-7 days)*, sub-acute (*7-14 days)*, and chronic (*months/years*) stages [9]. The microenvironment of the injured spinal cord presents many significant obstacles to regeneration at these various stages (**Table 2-1**). The initial injury causes necrotic cell death due to direct mechanical trauma and ischemia from vascular disruption and hemorrhage. During the acute phase, a cascade of secondary injury processes occurs that leads to further cell death, scarring, and loss of function. Continued vascular injury, ischemia, inflammation, free-radical production, and the massive release of excitatory neurotransmitters by the injured cells cause secondary necrosis, apoptosis, and swelling 1-2 segments above and below the original lesion site. Supportive glial astrocytes at the lesion periphery begin to hypertrophy and proliferate into a "reactive" phenotype that contains the injury [10]. The most widely used indicator of the reactive astrocytic response to injury is cellular hypertrophy and the enhanced expression the intermediate filament, glial fibrillary acidic protein (GFAP) [11]. The cytoskeletal intermediate filaments, vimentin and nestin, which are typically found in immature astrocytes, and the following non-cytoskeletal proteins are also expressed in reactive astrocytes: class II histocompatibility antigens, glutamine synthetase, and glutamine transporters [11, 12].

Table 2-1: Key cellular and molecular events after SCI

Event Type	Timeframe	Underlying Pathological Mechanism
Necrosis	min-hours	Oxidative stress, edema, hemorrhage and disruption of BBB, ischemia, physical trauma, excitatory neurotransmitters, infiltration of acute inflammatory cells.
Apoptosis	days/week	Oxidative stress, limited ability to replace damaged glia & neurons via endogenous progenitors. Activation of apoptotic pathways.
Demyelination	days-months	Oligodendrocyte loss
Glial scar formation	days-weeks	Reactive astrocytes, ECM remodeling
Axon degeneration	days-months	Loss/block of function (signaling) Inhibitory/repulsive environment blocks regrowth (Nogo, OMG, MAG, CSPG)

In the sub-acute phase, microglia begin to clear the injured area of debris leaving behind a cystic cavity, which is subsequently surrounded by a glial scar consisting of reactive astrocytes. The glial scar is composed of long astrocytic processes that interweave to form a dense mesh and ECM material including chondroitin sulfate proteoglycans (CSPGs) [13, 14]. Macrophages, fibroblasts, and Schwann cells are also known to infiltrate the wound from outside of the CNS, usually from the spinal nerve roots, especially in the case of laceration injuries where the dura is disrupted [3, 15].

Finally, in the chronic phase, the astrocytic scar stabilizes around cysts/syrinxes and extends down the path of degenerated axons [16]. Depending on the extent of fibroblast infiltration, there may also be a dense collagenous scar within the injury site. The fibrous scar formed after SCI can present a greater barrier to regeneration than glial scarring due to its dense framework and ability to bind growth inhibitory molecules [17]. Over the course of the next few months, oligodendrocyte populations continue to undergo apoptosis, which leads to progressive demyelination of axons. Wallerian degeneration, the destruction of the distal end of severed axons, also occurs over the next few months-years leaving behind a trail of myelin debris that further inhibits axon growth [16, 18]. Additionally, Schwannosis, the infiltration of Schwann cells and their associated axons from the peripheral nervous system (PNS), is prevalent in human SCI after approximately four months and is attributed to the loss of astroglial framework at the injury site[3]. This ingrowth by elements of the PNS potentially serves as an impediment to neurite outgrowth and may cause pain, spasticity, and other abnormal physical responses.

Unlike experimental models of SCI, human injuries are highly heterogeneous and the exact pathology and time course of events will vary depending on the type of injury [1, 2]. It is worth noting that the time course of human SCI is typically extended with respect to rodents [19]. In humans, the loss of myelin in degenerating axon tracts takes approximately 2-3 years, as opposed to months in rodents [18]. Schwann cell invasion of the lesion is seen as early as 1 week in rodents but is not noted in humans until 3 weeks [15]. Interestingly, human SCI exhibits less glial scarring and CSPGs are mainly localized to the lesion site. There is also a lower incidence of chronic demyelination in humans when compared to rodents [15, 19]. Such variation in pathology between human and animal models should be considered when designing and testing potential therapies for SCI (**Table 2-2**) [19].

Table 2-2: Differences in pathophysiology between rodent models and clinical human spinal cord injury. From Hagg et al.

	Rodent	*Human*
Degenerative processes		
Vascular response	Hemorrhage, angiogenesis	Hemorrhage, angiogenesis
Inflammation	Extensive	Much less pronounced, despite similar cytokine expression
Demyelination	Yes	Yes, but perhaps less pronounced
Axonal degeneration	Some die-back and Wallerian degeneration	Wallerian degeneration much more protracted
Glial scar	Extensive, with astroglial CSPG	Not extensive, CSPGs mostly in blood vessels
Cyst formation	Rat yes; mouse no	Yes
Schwann cell response	Some invasion	Extensive Schwannosis
Regenerative processes		
Sprouting	Yes	Yes
Remyelination	Yes	Yes
Plasticity of uninjured systems	Yes	Yes

CSPG, chondroitin sulphate proteoglycan.

2.1.3. Inflammatory and vascular events after SCI

The time course of inflammatory cell infiltration after injury is illustrated in **Figure 2-1** [20]. Further detail about the contributions of specific inflammatory cells to injury and tissue repair is summarized in **Table 2-3** [20].

One specific inflammatory cell type, the macrophage has been extensively studied due to its role as an important modulator of tissue injury and repair after SCI. Macrophages are recruited to the site of injury immediately after SCI, reach a peak density at 14 days post injury, and finally decrease to an elevated by stable value by 3-4 weeks post injury and remain around the injury site indefinitely [20-22]. Interestingly, chondroitin sulfate proteoglycans (CSPGs) most noted for their role in axon inhibition, actually have a pivotal role in spatially and temporally controlling the activity of infiltrating blood-borne monocytes and resident microglia during the acute phase after the injury. Rolls et al. demonstrated that immediate inhibition of CSPG production after SCI in mice caused a dramatic effect on the spatial organization of infiltrating macrophages and an alteration in their cytokine/growth factor release leading to enhanced tissue destruction and decreased functional recovery [23]. In contrast, allowing CSPG synthesis during the first 2 d post injury, followed by inhibition, improved recovery.

Two main phenotypes of macrophages, M1 and M2 can be seen after SCI. M1 macrophages (pro-inflammatory) clear tissue debris from the injury site and areas of Wallerian degeneration but may contribute to the axonal retraction and secondary tissue damage after SCI. M2 macrophages (anti-

inflammatory) secrete a variety of neurotropic factors may be responsible for neuroprotection, angiogenesis, and the promotion of axon growth however, an excessive or prolonged presence of M2 macrophages may result in fibrosis and scarring, which could hinder axon regeneration [21]. Therefore, an important balance must be struck between M1 and M2 macrophages to achieve the clearance of tissue debris, reduce secondary tissue damage, and promote repair.

Recent work by Kigerl et al. suggests that after injury to the cord there is a transient appearance

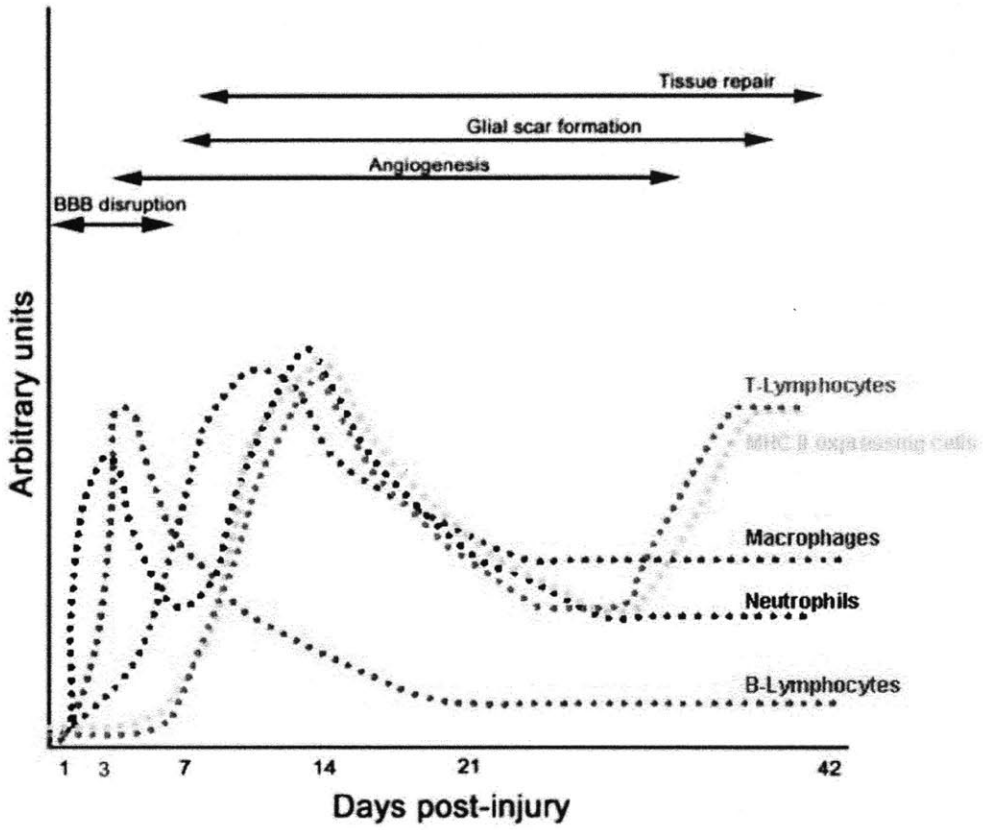

Figure 2-1: Time course of inflammatory cell infiltration of the defect site after rodent spinal cord injury with relation to major pathogenic and wound healing events. From Trivedi et al.

of M2 macrophages early (1-7 days) after injury with 40-50% of the macrophages adopting an M2 phenotype [21]. However, by 28 days post injury, fewer than 10% of the macrophages are M2. This work shows that the environment of SCI is conducive to M1 macrophage polarization despite the phagocytosis of red blood cells and cellular debris, which normally promote a M2 phenotype. Within the M2 phenotype there are three subtypes, which modulate different aspects of the inflammatory response, however these have been poorly characterized in the context of SCI.

The vascular events after spinal cord injury play a critical role in the degree of secondary damage, which occurs after the primary injury. Mechanical trauma to the spinal cord (contustion, compression, lasceration) causes vasospasm of superficial vessels and intraparenchymal hemorrhage particularly in the highly vascular central gray matter [24]. There is also a disruption of the blood-spinal cord barrier leading to edema, an alteration of tissue perfusion from the release of vasoactive molecules, and a loss of autoregulation (the ability to maintain blood flow despite differences in perfusion pressure). Additionally, there may be post-traumatic systemic events, which affect blood flow such as hypotension, bradycardia, and decreased cardiac output [24]. Together, these events lead to ischemia and necrosis within the spinal cord parenchyma. The resulting cell death further initiates a cascade of events such as the release of excitotoxicity neurotransmitters from dead/dying cells and the generation of free radicals from the reperfusion if ischemic tissue or degradation of hemoglobin, which results in additional (secondary) damage to previously viable spinal cord tissue.

Cell Type	Type of Immunity	Pro-inflammatory molecules	Mediators of cell injury/ death	Pro-regeneration/ wound healing events
Neutrophils	Innate [41]	Express receptors for various chemokines and cytokines, MMP-9	Produce metalloproteinases , reactive oxygen and nitrosyl radicals neutrophil elastase	Phagocytosis
Dendritic cells	Innate and adaptive	Produce TNF-agr;, IL-1, IL-2, IL-6, IL-12, 1L-18, IFN-γ	Function as antigen presenting cells	Production of neurotrophin-3
Monocytes/ Macrophages	Innate	Produce TNF-agr;, IL-1. IL-2, IL-6, IL-12, 1L-18	Produce reactive oxygen species and nitrosyl radicals	Phagocytosis, production of trophic factors. IL-10, TGF-β
Microglia/ Macrophages	Innate and adaptive	Produce TNF-agr;, IL-1. IL-2, IL-6, IL-12, 1L-18	Function as antigen presenting cells; produce reactive oxygen species and nitrosyl radicals	Phagocytosis, production of trophic factors. IL-10, TGF-β
B-Lymphocytes	Adaptive	Express receptors for various chemokines and cytokines	Produce antibodies	Unknown
T-Lymphocytes	Adaptive	Express receptors for various chemokines and cytokines, IFN-γ, TGF-β	Pro-inflammatory cytokines and chemokines	Production of trophic factors. IL-10. IL-4, IL-13

Abbreviations: matrix metalloproteinase-9 - MMP-9; tumor necrosis factor-alpha - TNF-agr;; interleukin - IL; interferon-gamma - IFN-γ; transforming growth factor-beta - TGF-β;

Table 2-3: Overview of inflammatory cells, their inflammatory mediators, and mechanism of tissue destruction or wound healing. From Trivedi et al.

The hemorrhage which occurs after vascular injury to the spinal cord is greatest at the injury epicenter and can be seen extending into the dorsal columns both rostral and caudal to the injury [24]. Zhang et al, studied the regenerative response within these dorsal column lesions and found they were extensively infiltrated by macrophages and the beginnings of blood vessel growth by 1 week [25]. By 2 weeks, there was a network of blood vessels and clusters of glial cells within the defect and regenerating nerve fibers could be seen at the interface of the lesion and adjacent normal tissue.

1.3. Considerations for regeneration

There are a number of intrinsic and extrinsic factors that lead to regenerative failure in the CNS. Therefore, one may consider multiple targets for intervention (**Figure 2-2**).

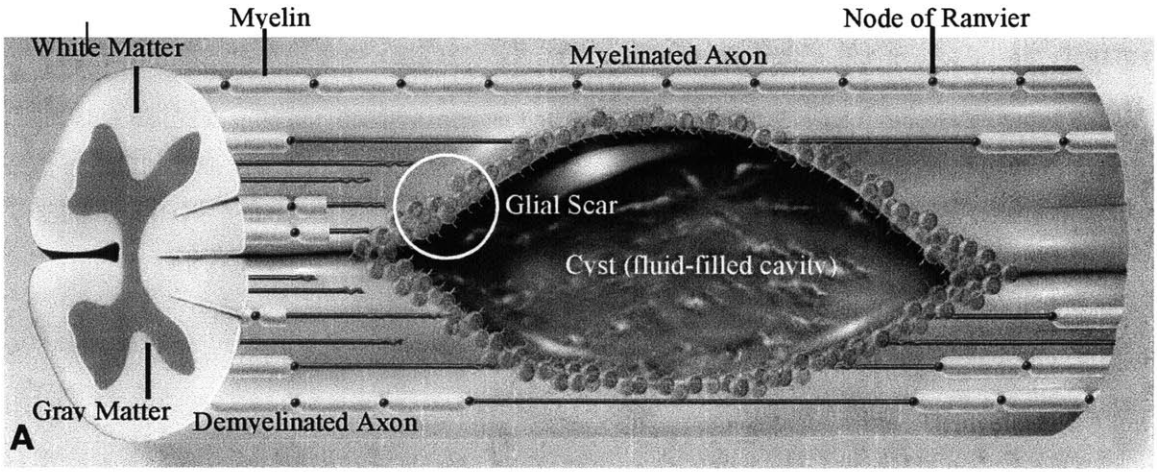

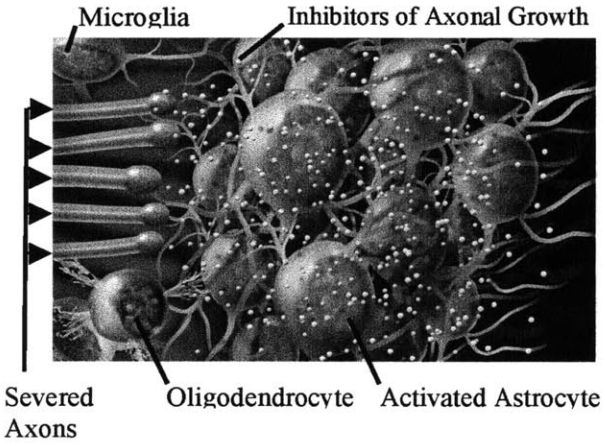

Figure. 2-2. A) A fluid-filled cystic cavity in a spinal cord resulting from injury, surrounded by a glial scar (white circle) shown in more detail in (B). The glial scar (B) is made up of activated astrocytes and contains inhibitors of axonal growth (depicted as yellow dots).

Unlike the CNS, the PNS is capable of spontaneous regeneration. Nerve grafts and guidance tubes have been shown to enable severed axons to grow through large gaps in the PNS and promote recovery [26, 27]. After a PNS injury, the axons at the distal end degenerate while those at the proximal end begin to sprout, elongate, develop growth cones, and eventually reform synapses to nerves/muscles. The major support and myelinating cell of the PNS (Schwann cell) assists the process by re-myelinating axons, secreting growth factors and synthesizing ECM (laminin, fibronectin), and guiding axon growth [28-30]. There is a 1:1 ratio of axons to Schwann cells in the PNS and after injury cells from the degenerated portions of axons assist in the regeneration process. In contrast in the CNS, oligodendrocytes myelinate between one and eighteen axons, making the loss of these cells detrimental to a larger

proportion of nerve fibers [31]. Perhaps the most interesting example of the difference between the regenerative potential of the CNS and PNS relates to the dorsal root ganglia (DRG). DRGs are areas beside the spinal cord where the bodies of sensory neurons are located. Although these neurons have axons within the spinal cord and the PNS, they can only regenerate their peripheral process [32]. In the case of complete SCI, Schwann cells infiltrate the spinal cord and associated PNS axons can be seen growing within the former spinal cord parenchyma [15].

As noted above, in the CNS, the major support and myelinating cell, the oligodendrocyte is associated with multiple neurons. Consequently, after injury, many of these cells die; demyelinating their associated neurons and greatly reducing the support for regenerating axons. Degraded myelin contains potent growth inhibitors such as Nogo-A, oligodendrocyte myelin glycoprotein (OMG), and myelin-assisted glycoprotein (MAG) [33-35]. In the PNS these products are cleared by macrophages and Schwann cells, but in the CNS, microglia cells are much slower in clearing this debris which may be present as long as 3 years post injury [18].

The cyst and glial scar formed after injury to the CNS also act as significant physical and chemical barriers to spontaneous regeneration. But the astrocytic response can be beneficial as well as detrimental to regeneration [10, 36]. At early times, it serves limit further damage by: reestablishing the blood brain barrier (BBB) and ionic homeostasis; limiting immune cell infiltration; and containing excitatory neurotransmitters. At later times, however, the dense scar and associated CSPGs are inhibitory towards regeneration. Reactive astrocytes secrete an ECM containing chondroitin sulfate proteoglycans (CSPGs), which have been implicated as a major growth inhibitory molecule for neurons [37-39]. In cases of SCI where there is disruption of the dura, there is also substantial fibrous infiltration of the spinal cord, which leads to an even greater physical and chemical barrier to axon regeneration.[17, 40]

Although there are many barriers to regeneration in the CNS, it has the potential for repair. CNS white matter can support axon regeneration in uninjured as well as degenerating white matter tracts in rodents [41, 42]. The inhibitory factors deposited at sites of chronic SCI do not form absolute boundaries. Early work by David, *et al.*, using a peripheral nerve graft, demonstrated it was possible to achieve significant axon elongation through a lesion site in the spinal cord by providing a permissive environment for growth similar to the PNS [43]. Axons can regenerate through scars into sites of chronic SCI using diffusible signals such as neurotrophin (NT)-3 from modified mesenchymal stem cells (MSCs) [44]. Numerous others have shown that neurotrophic factors, antibodies against myelin debris receptors, and CSPG degrading enzymes can promote regeneration and axonal sprouting after SCI [45].

The regeneration of a large number of tracts may not be necessary to promote substantial recovery after SCI. Signals can be re-routed to downstream targets over other pathways through neural

plasticity. Significant neurological function may be preserved with as few as 5-10% of the original number of axons present in the white matter [46]. Basso, *et al.*, showed that after a graded contusion by a weight drop, an increase in spared white matter from 5% to 10% allowed rats to go from not supporting their own weight to supporting their own weight and exhibiting consistent stepping [47]. This ability has also been noted in humans. Cordotomy procedures for the relief of pain following cancer showed that the anterior half of the thoracic cord could be cut without any disturbance to motility, and cutting one lateral corticospinal tract (CST) and 85-90% of the opposite tract and the reticulospinal fibers anterior to the tract caused total paralysis of the lower limbs which recovered over 2 months so that the patient eventually walked again [48].

In sum, the local environment after SCI plays a significant role in the regenerative response of neurons. If a minimally invasive therapy is utilized to spare viable axons, reduce the amount of secondary damage after the insult, and promote axon regeneration and collateral sprouting, a significant amount of functional recovery can potentially occur. By addressing the multiple facets of growth inhibition in SCI, it may be possible to restore a healing response similar to that of the PNS.

2.2. Injectable materials for SCI: Overview

Research into injectable biomaterials holds great promise in the fields of tissue engineering and regenerative medicine. A wide variety of injectable materials have been developed for various tissue specific applications such as bone, cartilage, intervertebral disk, brain, and spinal cord [49-51]. Each tissue poses its own unique set of properties and challenges that must be addressed by the scaffold material. In particular, the CNS presents a complex regenerative obstacle due to the multiple mechanisms of degeneration and growth inhibition that occur after injury. These obstacles require a combinational approach utilizing scaffolds, cellular, and molecular therapies tailored to the specific injury at hand.

2.2.1. Current status of injections into the spinal cord

The injection of substances directly into the spinal cord or surrounding tissue has been used clinically for a variety of scenarios. Intrathecal infusion of medication via catheters has been used for chronic/severe pain relief [52]. For drug delivery applications, mini-pumps and catheters are sub-optimal for sustained delivery as they are prone to blockage and subsequent infection [53]. Currently, there are a few clinical trials are underway for the injection of cells into the spinal cord including autologous macrophages, olfactory ensheathing cells, oligodendrocyte progenitor cells [7, 54, 55].

2.2.2. Advantages of injectable materials

Hydrogels are natural or synthetic hydrophilic polymers capable of binding large percentages (50-99.9% by wt.) of water. Hydrogels are viscoelastic materials resulting from the physical or chemical bonding of molecules in a liquid state: physical gels by van der Waals interactions and hydrogen bonding, and for the purpose of this review, ionic bonding; and chemical gels by covalent crosslinking. The conversion of the injected liquid into a physical or chemical gel *in vivo* enables the filling of small defects such as the cavities/cysts, which form after SCI or the space between transected parts of the spinal cord. The gel, serving as a scaffold, can eliminate void spaces and form a regenerative template to direct cellular infiltration and matrix deposition towards repair of the injured region.

Injectable materials that form scaffolds *in situ* can conform to the shape of the defect and create an integrative implant-tissue interface to restore the continuity of the tissue and reduce significant contraction/deformation of the scaffold [56]. This injectable gel property obviates the need to create preformed scaffolds for each individual patient and avoids excising viable tissue at the injury site to accommodate implantation of the preformed scaffold, which could cause further tissue damage and loss of functionality. Poor graft integration is often the cause of graft failure and pathological changes in the host spinal cord including extensive glial-connective scar and cyst formation [57]. For incomplete cases of SCI where the BBB has not been disrupted and the dura mater is intact, injectable therapies will be beneficial since they will not further disrupt the dura. Damage to this important structure has been implicated in scar formation, cellular invasion, and cystic cavity formation after SCI [40].

Injectable materials, in their liquid state, can be uniformly mixed with cells and other therapeutics prior to delivery within the spinal cord defect. Spatial and temporal control over the release of these agents can be tailored through multiple mechanisms including incorporation within secondary release vehicles such as micro- and nano-particles, liposomes, and microtubules [50, 58], covalent tethering to the gel with subsequent enzymatic release [59], or harnessing the ability of macromolecules such as heparin to bind growth factors such as NT-3 and platelet derived growth factor (PDGF) [60].

The mechanical properties of gel scaffolds can more closely match the properties of the native spinal cord tissue, compared to most preformed biomaterial matrices. The implications of this include providing a permissive substrate for neuronal growth and will be discussed in subsequent sections.

For patients, injectable therapies hold the promise of minimally invasive procedures. The prime and most clinically practical window for intervention may not be immediately after injury but delayed until the sub-acute stage (7-14 days post injury), when the initial inflammatory response has subsided [7, 61]. Having flexibility on the time course of administration could enhance the clinical outcome of

patients without risking further damage.

2.2.3. Requirements for injectable systems

2.2.3.1. Main functions

The development of injectable therapies for spinal cord regeneration may be designed with a focus on three broad functions.

1) Scaffolding for cellular infiltration and axonal ingrowth. The gel material itself will serve to bridge the lesion site. Scaffolding acts to reduce cyst formation, inflammation, and the associated secondary cell damage, while accommodating the infiltration of supportive cell populations and the growth of axons into the gel-filled lesion site [62]. The gelation kinetics, final gel microstructure, mechanical properties, degradation rate, and bioactive properties of the scaffold can be tuned to optimize its regenerative potential.

2) Encapsulation of drugs and maintenance of bioactivity throughout gelation and release. Therapeutics such as neurotrophic factors, antibodies against degrading myelin products, chondroitin sulfate-degrading enzymes, and others, can stimulate axonal regeneration through lesion and encourage neural plasticity [63]. Injectable systems can provide a sustained and tunable delivery of these agents locally to the lesion site. This is especially important for therapeutics such as NT-3, which has an *in vivo* half-life of only 30 minutes, but have a therapeutic effect when delivered over the course of days to weeks [64, 65].

3) Support of suspended cell populations prior to injection, throughout solidification process, and within in the lesion site. The incorporation of transplanted cell populations have been shown to enhance functional recovery after SCI in animal models by providing necessary trophic factors and extracellular cues for axon regeneration, myelination, and a source to restore lost cell populations [66, 67]. Cellular therapies are more effective when delivered and maintained locally in the injured area as opposed to delivered systemically.

2.2.3.2. Design parameters

It should be noted that in most polymer systems it is difficult to isolate crosslink and macromer concentration-dependent material properties such as mechanical stiffness, mesh or pore size, degradation rate, and bioactive ligand density. Therefore several group have created multi-component systems to study the effects of each variable on neuronal behavior [68-70].

Biocompatibility. The reactants and degradation products of the material must be non-toxic and non-immunogenic to reduce excessive inflammation at the injury site leading to additional cellular

damage. Materials obtained from natural sources should be carefully screened and treated to reduce the risk of disease transmission and immunological responses. Initiators, crosslinkers, or other additives required for scaffold formation should not adversely affect encapsulated cells or cross-react with therapeutics.

Solidification Solidification of the injectable material should occur under mild conditions to avoid additional tissue damage at the lesion site, adversely affecting encapsulated cell populations, or sensitive drug compounds. The speed of gelation must be rapid enough to contain the material within the injection site and maintain the localization of incorporated cells or therapeutic agents. Ideal solidification times are on the order of seconds to minutes depending on the initial viscosity of the injectable material. Factors affecting the gelation time include, temperature, crosslinker concentration, ionic strength, pH, light, surface area, among others [50].

Porosity/mesh size The overall mesh size of nanoporous fibrillar scaffolds, and the porosity, and pore diameter and interconnectivity of microporous scaffolds are crucial for tissue ingrowth, the removal of nutrients and waste, and the diffusion of therapeutic agents from the polymer matrix. A growth-permissive substrate for endogenous/exogenous cell populations may recapitulate the three-dimensional (3-D) organization of the native ECM. *In situ*-forming scaffolds typically have >99% water content and a typical mesh/pore size on the order of 0.1-10 μm. Neurons are 20-30 μm in length with approximately 1-μm diameter growth cones [71, 72]. The relative dimensions of the growth cones and mesh opening may hinder cell motility unles the material can be moved or degraded by the cells [68, 73]. For example, agarose gels with decreasing mesh size and increasing stiffness severely inhibited neurite outgrowth below a mesh opening of 150 nm [74]. Additionally, decreasing the mesh size of collagen gels from 7.2 μm at 0.4 mg/ml to 3.1 μm at 2.0 mg/ml impeded neurite extension of encapsulated DRG cells [73]. The polymer size and concentration of the monomer/polymer, as well as the initiator and crosslinker concentrations, can be used to control the mesh or pore size of injectable scaffolds.

Mechanical properties The mechanical properties of the gel should match the native tissue to withstand *in vivo* forces, maintain structural integrity, and transmit physiological forces until it can be replaced by native tissue. While the spinal cord itself is not a load-bearing structure, injected materials should not collapse under the weight of the surrounding tissue. Additionally, the mechanical properties of substrates have a profound effect on cell behavior especially in the CNS [70, 75, 76]. The soft and viscoelastic nature of native CNS tissue and hydrogels make rheology an ideal technique to study their mechanical properties. In this regard, the shear modulus is often reported as the measure of "stiffness."

Numerous model systems using several materials have been created to investigate the effects of substrate stiffness on neurite behavior. Flanagan, *et al.*, created a system to isolate the mechanical effects

on primary mouse spinal cord neurons using polyacrylamide gels coated with matrigel to provide a constant mesh size and number of adhesion ligands. Neurons exhibited a high branching density on substrates of 50Pa-350 Pa which is on the order of bovine (50 Pa) or human (200 Pa) spinal cord tissue [70]. In comparison, the branching frequency on 550 Pa gels was reduced, and was similar to glass. Similarly, Leach, *et al.*, used a 2-D polyacrylamide gel with a constant fibronectin density to explore neurite outgrowth and branching of PC12 cells induced to a neuronal phenotype [77]. Unlike Flanagan's experiment, the cells displayed a threshold response to substrate stiffness from a shear modulus of 100 – 10,000 Pa. In this stiffness range, a greater percentage of cells expressed neurites, which were also longer and more branched than the softer gels (<0.1 kPa).

Wilits, *et al.*, cultured DRG cells in 3-D collagen gels of varying protein content, ranging in shear modulus from 2.2-17 Pa and found that maximum lengths of neurites occurred in softer gels [73]. It should be noted that increasing the collagen concentration had multiple effects, which factored into the observed results including a decreased interfiber spacing, increased ligand density, and increased shear modulus. Using a 3-D agarose culture of DRG cells, Balgude, *et al.*, found the average rate of axon elongation was inversely correlated to the concentration of the agarose gel, which ranged in modulus from 5-130 Pa [71]. Banerjee, *et al.*, explored a greater range of gel stiffness ~180-20,000 Pa with alginate gels encapsulating neural stem cells (NSCs) and found that the softest gels, which were on the order of magnitude of the stiffness of brain tissue, resulted in significantly higher NSC proliferation and neuronal differentiation (B-tubulin III staining) than stiffer gels [78]. Seidlits, *et al.*, used acrylated high molecular weight hyaluronic acid (HA) gels to investigate ventral midbrain neural progenitor cell (NPC) differentiation and spinal astrocyte behavior in a 3-D culture environment with tunable mechanical properties [79]. By adjusting the degree of acrylate substitution, the compressive modulus could be modified between 3-10 kPa, which is similar to adult rat spinal cord (8.1 ± 1.1 kPa). After 3 weeks in culture, NPCs on the softest gels were furthest differentiated towards the neuronal phenotype and exhibited β-III tubulin-positive long branching processes while NPCs on the stiffest gels did not survive the full 3 weeks. On the other hand, spinal astrocytes survived the full 3 weeks in all gels and only showed evidence of migration on the stiffest gel.

Overall, the difference in the observed optimal stiffness for neurite branching among the different studies is due to specific factors, which have an effect on the response of cells to compliant substrates, such as: the cell type (*i.e.*, PC12, DRG, primary neurons); material type and adhesive ligand density; mesh/pore size; and range of modulus investigated. Interestingly, glia, which are implicated in scarring after SCI, had poor survival on soft substrates [70]. Other groups demonstrated that DRG neurons tend to elongate processes down gradients in stiffness and fibroblasts, implicated in mesenchymal scarring,

preferentially migrate back towards stiffer areas of patterned hydrogels [80-82].

Degradation rate The degradation rate of injectable scaffolds should proceed on the time scale of tissue formation so that axons are provided with a constant stable platform for growth. If the scaffold degrades prematurely, the injury site will also be subject to compressive stresses that would cause further inflammation and glial scaring [83], and there will be lack of sufficient stromal support for the ingrowth of axons. If the scaffolding degrades too slowly, it will impinge on new tissue formation and hinder axonal growth. Mahoney, *et al.*, investigated the process of extension of neural tissue into polyethylene glycol (PEG)-polylactic acid (PLA) gel matrices with controllable degradation rates. The group was able to control the time course of neurite extension from 1-3 weeks depending on the degradation rate of the polymer and concomitant change in the matrix mesh size [68]. Subsequent work by this group showed a relationship between the degradable macromer content of the PEG-PLA matrix and the cellular proliferation of neural cells cultured within the material after 7 days [84]. In rodents, degradation rates on the order of weeks to months would be appropriate. This timeframe corresponds to the rate of axon sprouting from the CST, which can be observed 3 weeks to 3 months after injury [85, 86].

Additionally, neuronal growth cones secrete serine proteases and calcium dependent matrix metalloproteinases that assist in matrix remodeling for axonal path finding during development and regeneration [87, 88]. Pittier, *et al.*, showed that inhibiting serine proteases greatly decreased neurite extension in fibrin matrices [89]. Therefore, synthetic material with bioactive sequences sensitive to these enzymes as well as natural materials such as collagen can be specifically remodeled by the regenerating axons. To this point, Straley, *et al.*, engineered protein polymers containing bioactive sequences for serine protease specific degradation (see section 3.3.3) [69]. By altering the bioactive sequence, scaffolds could be fabricated with a 200-fold difference in degradation half-lives. However, using PC12 cells, the difference in degradation rate of the scaffolds had no significant effect on cell morphology or neurite extension after 6 days of exposure to neuronal differentiation media.

The degradation mechanisms of biomaterials will influence their behavior *in vivo*. Since total body water is conserved, materials undergoing hydrolytic degradation have the advantage of having low animal-animal and location variability, however the degradation is non-specific. Enzymatic mechanisms can respond to local changes in cell behavior during the regenerative process but may suffer from high individual variability [69]. For drug delivery applications, the biodegradability also determines the release of incorporated drugs within the scaffold matrix.

Bioactivity Scaffolds should present specific soluble and insoluble cues to direct cell behavior, such as adhesion ligands present in the natural ECM. Injectable scaffolds have a high pore volume, interconnectivity, and a 3-D architecture, which allow for significant cell-surface interactions. For

scaffolding applications, cell adhesion is crucial as neurons are anchorage-dependent for their growth and survival and will undergo apoptosis when detached from the ECM [90]. Straley, *et al.*, found the density of the cell-adhesive RGD peptide present in the protein directly affected cell adhesion and neurite outgrowth of undifferentiated and differentiated PC12 cells [69]. However, the effect was still smaller than the control collagen gels suggesting that cues other than RGD motifs are important for controlling neuronal cell behavior.

Neurites are sensitive to environmental cues, which can both promote and inhibit their growth. To explore the interaction of neurites with bioactive cues, Kofron, *et al.*, cultured DRG explants at the interface between a 3-D collagen matrix and a glass coverslip coated with laminin or CSPGs, a promoter and inhibitor of neurite outgrowth, respectively [91]. The coating was arranged as either a uniform layer or patterned tracks. They found that most of the neurites extended away from the coverslip and into the collagen gel when CSPGs were present, while most of the neurites extended at the surface of the gel when laminin was present. There was also an alignment of the neurites to the tracks of laminin on patterned surfaces [91]. Extending this work to a 3-D system, Yu, *et al.*, used DRG cells cultured in layered agarose hydrogels to explore the chemical effects of neurite extension. They found that at the interface of unmodified agarose gels and agarose gels with covalently bound chondroitin sulfate B (CS-B), neurite extension was significantly inhibited as compared to homogeneous gels. The inhibition was significantly decreased by either degradation of CS-B with chondroitinase (Ch) ABC or addition of laminin-1 to the CS-B containing hydrogels [92].

Additionally, for drug delivery applications to the intrathecal space, materials with limited adhesion ligands should be used to avoid cellular infiltration. The material-drug interactions will play a role in their release kinetics depending on their relative size, charge, and hydrophobicity to one another. The material also needs to preserve the bioactivity of the encapsulated drug.

2.2.4. Considerations for administration in the context of SCI

Therapies for SCI must take into account the timeframe of intervention and the specific condition of the cord during administration. The injured spinal cord presents a dynamic environment that evolves through years after injury. The composition of the ECM, cytokines, excitatory neurotransmitters, inhibitory molecules, degree of necrosis, and cellular makeup change with time after injury. This will affect which therapeutic agents would be most beneficial to incorporate into the device. Additionally, the size and location of cysts within the lesion site may affect how an injectable therapy is administered. In the acute phase of SCI, fluid filled cysts will not be present in significant number while during the sub-acute phase, the necrotic cyst defects will present as cavities to fill with an injectable material. In later

stages of SCI, there may be extensive Schwannosis and connective tissue scarring will result in dense tissue difficult to inject into.

Once the material is injected, the final space-filling morphology of the implant may affect its behavior. The gel may completely fill a defect/cavity or intermix with the remaining parenchymal tissue. The material should be delivered so that it can set without extruding back out of the needle tract or collapsing under the weight of the surrounding tissue in the case of hemisection injury. To address this, groups have used multiple injections of material at different lesion depths and left the needle in place until gelation is complete [86, 93], or used artificial dura such as agarose or collagen sheets [86, 93, 94].

Finally, to extend the clinical usefulness and application of injectable scaffolds for SCI, it must be shown that these materials can be injected without adverse effects into intact CNS tissue. This is important, particularly for acute and chronic cases where the disruption of intact neural tissue in and around the lesion site may lead to further functional deficits.

2.3. Classes of injectable hydrogel materials for SCI

Injectable materials may be in the form of chemical or physical gels, which form through a variety of mechanisms.

2.3.1. Natural vs. synthetic materials

Natural polymers, *i.e.*, biopolymers, are advantageous as many contain intrinsic amino acid motifs for cell adhesion and are readily degraded by the body [58, 95]. Gels made from biopolymers closely simulate the morphology and mechanical properties of the native ECM and are conducive to neuronal and axonal growth. These materials are composed of proteins and/or polysaccharides and can be formed into 3-D nanofilament networks with high water content allowing for the migration of cells and diffusion of nutrients and waste through the material. They can be easily obtained and may be composed of materials naturally present in the ECM of the spinal cord such as HA [96]. Gels of natural materials have been used extensively to culture and study CNS cell behavior *in vitro* and *in vivo* [97, 98]. The disadvantages of natural materials include the risk of disease transmission and the ability to provoke an immune response if left untreated for pro-inflammatory antigens. The mechanical properties, adhesion sites, and degradation rate are difficult to decouple from one another. Additionally, the degradation rate of natural scaffolds can be difficult to control as enzyme levels vary among species, individuals, and injection location.

Synthetic materials can be custom made with specific bioactive sequences and degradation mechanisms. Synthetic materials do not suffer from batch-to-batch source variations and have more controllable final properties. Disadvantages of synthetic materials include the biocompatibility of the

material and degradation products, and the lack of adhesion sites for integrins. Synthetic materials are also currently unable to recapitulate the complexity of organization and bioactive motifs present in natural ECM materials.

2.3.2. In situ physical gels

Physical gels formed from synthetic or natural polymers can undergo a transition from liquid to a gel upon a change in environmental conditions such as temperature, ionic concentration, or pH, or other condition such as mixing two components. Physical gels are attractive for injectable materials because the gelation reaction is mild and occurs from an aqueous solution without the addition of crosslinking agents, which could lead to additional damage at the site of injection due to un-reacted monomers, initiators, or exothermic reactions [50]. The system is compatible with cells and sensitive therapeutic agents and the reaction rate can be tuned to occur rapidly upon injection into the body. Although initial reactions are able to confine the material to the injection site, full setting of the material may take up to an hour in some systems. Physical gels are typically weak with moduli on the order of tens to hundreds of Pascals, which is on par with the mechanical properties of the spinal cord and is best suited for promoting neuronal growth and deterring scar formation [99].

2.3.2.1. Thermogels

The most common form of physical gel utilized in SCI regenerative approaches are thermo-gelling polymers. Thermo-gelling systems are aqueous monomer/polymer solutions, which have the ability to form a gel upon temperature change [49]. These systems either undergo gelation/solidification as the temperature decreases or have an inverse gelling property characterized by a lower critical solution temperature (LCST) at which the material undergoes a sol-gel phase transition and forms a solid network. For biomedical applications, thermo-gelling injectable systems with an LCST around or below 37°C would be ideal, as they would transform from a solution to a gel upon injection into a body cavity.

Collagen Type I collagen is a major component of tissue ECM throughout the body and is used in a number of U.S. Food and Drug Administration - approved medical devices [100]. It has been widely shown to support the growth and differentiation of neurons *in vitro* and has been applied as a gel scaffold numerous times *in vivo* [72, 73, 101-103]. Collagen can also inhibit glial proliferation which may decrease glial scarring after SCI [104]. Collagen displays an inverse gelation reaction where soluble collagen triple helixes aggregate under physiologic conditions (pH and ionic strength) to form a fibrillar gel network. The reaction kinetics are temperature dependent and depending on the volume may take up to 30 minutes. Additionally, the telopeptide regions between triple helixes play an important role in crosslinking between molecules during gel formation. However, these telopeptides are also implicated in

antigenicity of collagen and are usually removed for medical grade materials resulting in slightly weaker gels [105]. Collagen is readily degraded by endogenous proteases secreted at the tips of neuronal growth cones [87].

Agarose Agarose is a polysaccharide derived from seaweed. It does not cause adverse reactions when implanted *in vivo* and can support neurite extension *in vitro*. Since the average mesh size decreases exponentially as the concentration of agarose increases, neurites cannot extend processes over a threshold of 1.25% [74]. Also the hydrophilic chains are poor substrates for cell attachment and will limit outgrowth and viability over time [72]. Agarose is thermally induced to form a gel through intermolecular hydrogen bonding interactions as it is cooled. Solidification upon cooling presents an obstacle for applications that require injection into the body. To overcome this, Jain, *et al.*, utilized a nitrogen cooling system to gel hydroethylanated agarose with a gelation temperature of 17°C within 30 seconds *in situ* [106]. It is also not broken down naturally by mammalian cells so it persists *in vivo* until the chains dissociate and are excreted. Its inability to degrade may hinder the migration of neurons through agarose gels.

Methyl cellulose (MC) MC is a natural polysaccharide from plant sources. It is non-cell adhesive and does not elicit an immune response. It displays an inverse gelling property above physiologic temperatures, which can take on the order of minutes or hours to complete. As the temperature increases, hydrogen bonds between the polymer and surrounding water break and hydrophobic junctions form to produce a gel. MC alone forms a weak gel in at 37°C in water and does not form quickly enough for drug or protein delivery applications. However, the gelation temperature decreases with increasing salt concentration due to a decrease in the solubility of MC molecules [107]. Through ionic and hydrogen bonding with other polymers such as HA and chitosan, methyl cellulose mixtures can gel at lower temperatures (even below room temperature) and behave more gel-like then the constituent components [108, 109]. Shearing the mixture (via injection) can break these hydrogen bonds resulting in a shear thinning property that facilitates injection even if the material is in gel form prior to delivery. MC disperses and is excreted fairly quickly under physiological conditions if it is not previously crosslinked [109].

Hyaluronic acid (HA) – HA is a non-immunogenic, biocompatible anionic glycosaminoglycan native to connective, epithelial, and neural tissue [110]. On its own, it is non-cell adhesive but may be used in conjunction with other natural polymers to create an ECM-like scaffold that supports neuronal cell populations [102]. The long chains form random coils and gel due to molecular entanglements. This imparts HA with a shear thinning property as under shear force, the molecules align with the direction of stress and flow. Typically HA alone is highly water-soluble and disperses when injected into an aqueous

environment therefore physical gels must be made by combining HA with other polymers such as MC before gelation [109, 111]. The molecular weight (MW) of HA is also believed to affect its biological activity with high MW HA resulting in reduced astrocyte proliferation and CSPG deposition after SCI [112].

Chitosan is a natural linear cationic polysaccharide derived from shellfish and insects [113]. Its mechanical properties can be tuned to match the native ECM. It offers limited support for neuronal cells in its natural form and must be coupled with another bioactive polymer or peptide.[113] The gelation of chitosan is typically pH dependent but a pH-neutral chitosan solution was developed by adding a glycerophosphate salt, which forms a gel scaffold in approximately 30 minutes when raised to 37°C [114]. Crompton, *et al.,* investigated the optimization of neuronal survival and outgrowth in injectable chitosan- glycerophosphate scaffolds copolymerized with poly-L-Lysine [113]. Functionalization with poly-L-Lysine did not significantly affect cell survival as compared to chitosan in 2-D culture and provided a slight benefit in 3-D culture.

Poly(N-isopropylacrylamide) (PNIPAAm)-PEG PNIPAAm-PEG is a synthetic inverse-gelling block copolymer with an LCST of 29-32°C due to hydrophobic interactions [115]. Gelation takes approximately an hour to complete. This polymer may have applications for drug delivery due to its unique structure and properties. Unlike most hydrogels, it did not have a large interconnected porous structure and its hydrophobic chains prevent water from rapidly diffusing through the scaffold, which inhibits the transport of hydrophilic drugs [115]. *In vitro* experiments showed a sustained released of bioactive NT-3 and brain-derived neurotrophic factor (BDNF) from the scaffold, which promoted chick embryo DRG process extension in an explant assay after 31 days of incubation in the scaffold. Since there are no intrinsic cell adhesion motifs, human MSCs seeded in the scaffold did not attach until 14 days but survived through 31 days [115].

Tetronic-oligolactide (TL) TL is a coplymer thermogel, which is liquid at room temperature but gels in seconds at temperatures close to 37°C. The main structure consists of a thermo-sensitive poly propylene oxide (PPO) and polyethylene oxide (PEO) block connected to a degradable lactide oligomer. Go, *et al.,* coupled heparin to TL to create a cell compatible scaffold capable of growth factor delivery [116]. Kang, *et al.,* explored a TL scaffold containing the anti-inflammatory agent minocycline in a hemisection model of SCI [117].

2.3.2.2 Ionic crosslinking

Alginate- is a naturally linear anionic polysaccharide derived from algae. An aqueous solution of alginate can undergo a gelation in the presence of divalent cations such as Ca^{2+} and Zn^{2+} by forming ionic

inter-chain bridges between guluronic acid blocks of adjacent alginate chains [118]. The reaction occurs in about 30 minutes. The resulting gel is biocompatible, ECM-like, and has tunable properties via regulation of the cation and alginate concentrations, and the molecular weight of alginate. While injectable alginates have not been directly used in *in vivo* studies of SCI, it is a candidate material for SCI regenerative approaches. Like other non-animal polysaccharides, alginate does not support robust neuronal survival and outgrowth [119]. Alginate hydrogel inhibited the metabolic activity of olfactory ensheathing cells (OECs), Schwann cells (SCs), and bone marrow-derived MSCs in culture as well as DRG neurite outgrowth. This was improved after enriching alginate with fibronectin or cell adhesive peptides [119, 120]. Alginate is also slow to dissolve and dissolution occurs by the diffusion of cations out of the polymer matrix.

2.3.2.3. Enzymatic

Fibrin is the main component of blood clots. It results from the rapid polymerization of soluble fibrinogen monomers by the activation of the proteolytic enzyme thrombin under physiological conditions. Endogenous plasmin enzymes subsequently degrade fibrin. The advantages of fibrin include the following: extremely elastic resisting a 5x deformation from its resting length without breaking; forms a soft scaffold; contains ligands for CNS cell integrins; and binds growth factors, fibronectin, and protease inhibitors [121]. The gelation rate and mechanical properties of fibrin can be tuned by adjusting the ratio of fibrinogen and thrombin in the injection mix. Fibrin glue has been used in *in vivo* applications as a preformed gel to stabilize intercostal nerve grafts and to deliver acidic FGF or NT-3 to a model of SCI [122-124]. In another study, dorsal root axons regenerated across the dorsal root-spinal cord interface of rats with fibrin glue containing NT-3, BDNF, or ciliary neurotrophic factor, and entered the spinal cord. However, only a few axons regenerated into the spinal cord of animals with fibrin glue implants that lacked neurotrophic factor, and their growth within the spinal cord was extremely limited [123]. In a series of studies, Johnson, *et al.*, evaluated fibrin scaffolds implanted two weeks after a dorsal hemisection model of SCI [60, 125-127]. The scaffolds were pre-polymerized into a sphere on the tip of a pipette before implantation and stabilized in place by a second injection of fibrin allowed to polymerize *in situ* on top of the sphere. This two-step procedure was performed because fully *in situ*-polymerized fibrin scaffolds were assumed to be completely degraded after one week and could not be visualized in the lesion [126]. Fibrin alone showed an increase in neural fiber staining at the lesion site at 2 and 4 weeks post treatment and delayed the accumulation of reactive astrocytes [126]. Neural fiber density within the lesion site was significantly increased by the controlled release of 500 ng/ml NT-3 via a heparin binding delivery system (HBDS) incorporated within the fibrin scaffolds [125]. Further work used the scaffolds to deliver embryonic stem cell-derived neural progenitor cells (ESNPCs) along with the

growth factors, NT-3 and PDGF-AA, which were added directly to the scaffold or entrapped within the HBDS [60]. The presence of the growth factors (with or without the delivery system) increased the number of implanted cells at 2 weeks and the presence of the delivery system resulted in more NeuN-positive neurons derived from the ESNPCs.

Fibrin has also been investigated as a fully injectable biomaterial scaffold and drug delivery system for SCI (see section 4). Briefly, King, *et al.*, examined fibrin and fibronectin based injectable scaffolds in a dorsal hemisection model of SCI, and Hyatt, *et al.*, explored highly concentrated fibrin gels as a delivery vehicle for ChABC [128, 129].

The disadvantages of fibrin use *in vivo* include the potential for an immune response and disease transmission. Fibrin also degrades very rapidly *in vivo*: ~25 % remained after a 9-day implantation period. The degradation rate of fibrin is subject to variations in plasmin concentrations [123]. Non-mammalian sources of fibrin, such as from salmon, are promising for their reduced antigenicity, lower clotting temperature and *in vitro* enhancement of neurite outgrowth in comparison to bovine or human fibrin [130].

2.3.2.4 Self-assembling peptide systems

Self-assembling peptides are synthetic amino acid based molecules that undergo a sol-gel transition within seconds when brought to neutral pH and ionic concentration. The resulting gel is a nanofibrous mesh similar in some respects to the native ECM [131]. Several types of self-assembling peptides have been found to be biocompatible and non-cytotoxic, and not to cause immunologic reactions like some natural materials. They are broken down into L-amino acids and excreted in urine within 3-4 weeks of implantation [86]. These systems do not use crosslinking agents so they can safely encapsulate cells and/or drugs without exposing them to toxic agents. The fiber density can be tuned by the initial concentration of peptide in solution. Drawbacks of these systems include: lack of adhesion sites for integrins; low mechanical strength; and non-tunable crosslinking density. Some peptide systems also exhibit a low initial pH that must be rapidly buffered to prevent cytotoxic conditions [132].

Self-assembled peptide-amphiphiles (PA) PAs have hydrophobic and hydrophilic domains, and upon injection into a neutral ionic aqueous environment can self assemble into a nanofiber gel composed of peptide nanofilaments. These molecules can be modified with bioactive peptides such as the neuronal integrin-binding motif IKVAV [133]. A 1 wt% PA solution mixed in a 1:1 ratio with a suspension of NPCs in media resulted in a transparent gel-like solid within seconds. The same occurs upon injection into a physiologic environment. Self-assembled PAs are capable of presenting a high density of IKVAV epitopes, 10^3 fold higher than native ECM molecules like laminin [133]. These

IKVAV-presenting PAs support neuronal cell growth and differentiation from progenitors towards neuronal cell types *in vitro* and have been used as a regenerative scaffold for SCI *in vivo* [86].

Self-assembling peptide nanofiber scaffolds (SAPNSs) SAPNSs are synthetic biomaterials formed of ionic self-complementary peptides (alternating positive and negative L-amino acids). One such SAPNS, RADA16-1, commercially available under the name PuraMatrix™ (3DM, Inc., Cambridge, MA, USA), is a 16-amino acid peptide which assembles into β-sheets with alternating charges [134]. The gelation process is charge dependent and these materials rapidly form nanofilamentous, highly-hydrated scaffolds in physiological ionic or pH conditions. RADA16-1 supports neuronal growth and development *in vitro* [135]. A main disadvantage of this material is its low pH, which must be buffered to avoid cell necrosis. While SAPNSs have been injected into the brain of guinea pigs *in vivo* with successful regenerative results, the low buffering ability of the spinal cord resulted in a severe inflammatory reaction when a SAPNS was used as an *in situ* scaffold in a model of SCI [132, 136]. This severe reaction was not, however, observed by Cigognini, *et al.*, when using a SAPNS modified with bone marrow homing protein (BMHP) [93].

Amphiphilic diblock copolypeptide hydrogels (DCHs) DCHs are synthetic polymers, composed of lysine, homoarginine, or glutamate combined with leucine, which physically associate in water into elastic gels with porous fibril-like nanostructures by hydrophobic association [137]. These gels have a shear thinning property, which allows them to be injected. The properties of the gel can be altered by the copolymer chain length or composition, and the amino acid side chains of DHCs allow for further functionalization with bioactive molecules. Injections of DCHs into the mouse forebrain showed no detectable toxicity or inflammatory response compared with injections of physiological saline, for up to 8 weeks. The gel exhibited good tissue integration, and a timedependent ingrowth of blood vessels, glia, and a limited ingrowth of nerve fibers .

Mixing induced two component protein gels (MITCHs) MITCHs are synthetic protein gels can be fabricated to undergo gelation in the absence of specific external environmental cues. Using protein-protein interactions between specific peptide domains, Foo, *et al.*, prepared a two-component protein gel containing multiple repeats of WW (tryptophan residues) and proline-rich peptide domains, which undergo a sol-gel phase transition in upon mixing [138]. The shear modulus of the gel could be varied from 9-50 Pa by the frequency of repeated association domains per chain and the association energy between the domains. The physical hydrogel which is formed is shear thinning and "self-healing," which allows it to be reformed after injection through a syringe. Functionalizing the backbone of the MITCH material with the cell adhesive sequence, RGDS, supported the 3-D culture and proliferation of PC-12 human umbilical vein endothelial cells, and murine adult neural stem cells. Neural stem cells

encapsulated in these gels were able to self-renew, differentiate, and sprout extended neurites.

2.3.3. In situ chemical gels

Chemical crosslinking imparts mechanical integrity and degradation resistance to otherwise weak materials. It can occur through a variety of mechanisms, but principally involves covalent bonding which utilizes a reactive moiety that can either be conjugated to the pre-polymers or added as a small molecule/enzyme to create the free radicals to form covalent bonds between adjacent polymer chains. Unlike preformed scaffolds, the crosslinking agent contained in the injectable gel cannot be washed away or quenched prior to implantation, so all reactants must be non-cytotoxic at the concentrations that they are employed.

2.3.3.1 Photoinitiated polymerization and crosslinking

Photo-initiated polymerization and crosslinking typically utilizes ultraviolet (UV) light and a photo-initiator molecule, which react to create free radicals and subsequent covalent bonding via reacting groups such as acrylates. The wavelength of light, concentration of photo-initiator, and monomer chemistry are used in order to achieve a rate-controlled procedure with control over the final gel morphology. The reaction can be completed with seconds or minutes. The main limitations of photo-crosslinking polymers are concerns for cell viability and the inability to use such systems in minimally accessible areas such as deep within tissue. Free radical-induced cell death by photo-initiators is dependent on concentration as well as the cell type; specifically, cells with higher proliferation rates are more sensitive to photo-initiator-induced cell death [139]. A cytocompatibility study of a common water soluble photo-initiator, I2959, with NPCs showed a significantly decreased cell survival at concentrations in culture above 2.5 mg/ml (0.25%) which would be required for rapid polymerization *in vivo* [140]. However, when the NPCs were encapsulated within a PEG-poly-L-lysine (PEG-PLL) gel polymerized with 5 mg/ml I2959, the cells showed minimal apoptosis following the photo-polymerization reaction, most likely due to the rapid polymerization of the macromers. Given these concerns, there exists a balance among properties such as solidification time and crosslink density and cytotoxicity.

Acrylated PLA-PEG-PLA **PLA-PEG-PLA** is a tri-block copolymer (ABA) containing degradable PLA and non-degradable PEG units. The macromers are then end-capped by methacrylated groups to allow for photo-polymerization. This material degrades by a hydrolytic mechanism and is less sensitive to the variation in enzymes at injection sites. For drug delivery applications, the crosslink density, number of degradable PLA units, and hydrophobicity of the encapsulated drug can tune the release rate of drugs. *In vivo* injection of this material containing NT-3 into rodent spinal cords showed sustained delivery of the neurotrophic factor for a period of two weeks [141]. This material is also

capable of encapsulating cells and has been used as a model system for studying the effects of select properties on neural cell types (see section 2.3.2). The degradation products of PLA-PEG-PLA may also have a therapeutic benefit themselves. Neural cell populations cultured in a copolymer mix of PEG and PLA-PEG-PLA hydrogels had higher metabolic activity and proliferation with increasing percentage of the degradable PLA-PEG-PLA component [84]. It was proposed that the lactic acid released upon degradation had a positive effect on encapsulated neural cell populations due to its radical-scavenging effects.

PEG-poly-L-lysine (PLL) PEG-PLL is a photo-polymerizable copolymer scaffold consisting of PEG and PLL. *In vitro* results show that these gels support NPC survival and differentiation due to the presence of PLL segments [140]. The gelation reaction occurred in 4-10 minutes and the mechanical properties of the gel could be tuned to match the native spinal cord ECM. The morphology (pore size) of the resulting scaffold was larger than ECM analogous scaffolds (20-200 μm) and degraded very slowly since PEG-PEG linkages are not enzymatically cleavable.

Acrylated hyaluronic acid (HA) High molecular weight HA gels were used to investigate ventral midbrain NPC differentiation and spinal astrocyte behavior in a 3-D culture environment with tunable mechanical properties (see section 2.3.2) [79]. In a subsequent experiment, pre-formed hydrogels with stiffness matching the native spinal cord were then implanted in a dorsal hemisection rat model of SCI [142]. In the acute setting, the hydrogel resulted in a decreased number of immune cells around the lesion site and lower CSPG expression. By 9 weeks post injury, the tissue adjacent to the implants exhibited a significantly decreased astrocytic response but no significant difference in CSPG deposition. Few cells were found to infiltrate the gels, most likely due to the non cell adhesive nature of HA and the very small amount of gel. No significant degradation of the gel occurred over the 9-week study. It should be noted that in these experiments, hydrogels were pre-formed and rinsed of excess photo-initiator before implantation or promptly after contact with cells. For cell encapsulation experiments, low UV irradiation times were used to preserve NPC viability.

PEGylated fibrinogen Covalently modifying fibrinogen with PEG macromolecules results in a biosynthetic hydrogel with separate control over mechanical properties via PEG and degradation rate and bioactivity via fibrinogen [143]. 3-D neurite outgrowth of DRG explants from the hydrogels could be controlled with relatively small changes in either fibrinogen concentration or PEG content. Cell outgrowth was increased with decreasing fibrinogen concentration or ratio of PEG to fibrinogen. It was proposed that the dominant mechanism controlling outgrowth was the physical obstruction of the polymer network (mesh size, stiffness, and proteolytic resistance of fibrinogen). Higher ratios of PEG reduced fibrinogen's susceptibility to degradation, and increased fibrinogen content increased the hydrogel

modulus and slowed the invasion of neurites and non-neuronal cells from the explant. Interestingly, at low PEG concentrations, the non-neuronal outgrowth from the DRGs lagged behind the neurite extensions implying that it may be possible to tune the movement of individual cell types within the material.

2.3.3.2 Molecular/chemical crosslinking

Chemical crosslinking results in the formation of covalent bonds of varying length among fibers of polymeric scaffolds depending on the length of the crosslinking molecule and its ability to oligomerize. A common method of crosslinking pre-formed scaffolds is though the addition of amine or carboxylic acid reactive small molecules such as aldehydes, diepoxy compounds, N-hydroxysulfosuccinimid (NHS), and 1-ethyl-3-(3-dimethylaminopropyl) carbodiimide (EDC). However these molecules are highly cytotoxic even at low concentrations, and are not feasible to use in an injectable scaffold [144, 145]. As an alternative, less toxic small molecules like the iridoid compound, genipin, and naturally occurring ECM crosslinking enzymes such as lysyl oxidase and transglutaminase have been investigated to crosslink biopolymers such as collagen and fibrin [129, 146-148]. Studies of genipin-crosslinked collagen gels showed good cytocompatability with mesencyhmal and neural stem cells even though free genipin was in direct contact with the cells throughout the gelation process [149]. Additionally, cross-linking of collagen with genipin induces colorimetric and flourometric changes within the gel, which can be correlated to crosslink-dependent properties such as shear modulus and degradation resistance [149, 150].

Elastin-like protein Elastin-lile protein can be used to prepare a highly tunable scaffold which can be designed to contain: bioactive sequences for serine protease specific degradation; RGD sequences for cell adhesion; and lysine residues incorporated in the elastin-like regions as sites for polymer crosslinking [69]. In this system, the degree of crosslinking could be modulated by the frequency and location of lysine residues and the ratio of lysine to NHS esters formed by reacting the polymer with bifunctional crosslinker disuccinimidyl suberate. This compartmentalizing of functionality allowed for independent tuning of initial elastic modulus, degradation rate, and cell adhesive ligand density. By altering the degradation-sensitive sequences, scaffolds could be fabricated with a 200-fold difference in degradation half-life. These gels could support the growth and differentiation of PC12 cells. However, the chemical crosslinking method is highly cytotoxic, and required a rinse step before the introduction of cells into the material, which is not feasible for an injectable material.

PEG-star heparin Star shaped PEG (star-PEG) and heparin can be crosslinked using EDC/NHS chemistry to create a hybrid material with independently tunable mechanical and bioactive properties [151]. The mesh size, swelling, and elastic modulus could be tuned by the degree of gel component

crosslinking while keeping the heparin content constant. Heparin was used to non-covalently bind fibroblast growth factor-2 (FGF-2), a modulator of neural stem cell and astrocyte response. Heparin was further covalently modified with RGD peptides to promote cell adhesion. The gel was assayed using primary nerve cells and neural stem cells. Injection of 2 μl of the gel into the striatum of rats caused a transient nonspecific reaction to the brain injury and no chronic inflammatory processes.

2.4. *In vivo* studies of injectable materials for SCI

In contrast to the many investigations of preformed scaffolds, relatively few studies have explored the use of injectable materials for SCI repair **(Table 2-4)**. The primary functions of the injectable materials can be divided into two categories: scaffolding for cellular in growth and drug delivery.

Table 2-4: *In vivo* studies of injectable materials in SCI

Material	Injury model(s)[a,b]	Vol. inj.	Formulation(s)	Degradation time	Ref.
Scaffolding					
Collagen	- T8-T10 Tx (1-1.5 mm) - T8-T10 Hx - T10 Tx (3 mm), 10 days after 200 g/cm Ct - T8-T10 Tx (3-4 mm)	5 μl	Collagen (2.4 mg/ml) +1mM glyoxal +.0144% condroitin-6-sulfate (C-6-S) +.024% carbodiimide (CD)	4 weeks 8 weeks (glyoxal) 6 months (C-6-S, CD)	[128, 152-156]
SAPNS (RADA-16) (RADA-16-I-4G-BMHP1)	Dorsal column C6-C7 Tx (1mm) T9 moderate Ct (10g rod/25 mm height)	5 μl 3μl	1% aqueous solution	3 weeks (solid) 8 weeks	[93, 132]
IKVAV-PA	T10 Ct (24 g modified aneurysm clip 1 minute-therapy applied 24 hours after injury)	2.5 μl	1% solution in isotonic glucose	3 weeks	[86]
Fibrin Fibrin & Fibronectin	T9 Dorsal hemisection 1.2 mm depth T7-T9 Dorsal hemisection (2x1x1 mm)	10 μl "filled lesion"	10 mg/ml fibrinogen, 12.5 U/ml thrombin 10 mg/ml fibrinogen, 2 mg/ml FN, 5.4 U/ml thrombin	< 7days 4 weeks	[126] [128]

Drug delivery					
Collagen	T2 Ct: (20g or 35 g modified aneurysm clip 1 minute Intrathecal injection of therapy at T2 level)	20 µl	Collagen (24-28 mg/ml) +22.7 µg/ml EGF & FGF-2	>8 weeks	[157]
hyaluronic acid-methylcellulose (HA-MC)	T2 Ct: (35 g modified aneurysm clip 1 minute Intrathecal injection of therapy at T2 level)	10 µl	2% HA:7% MC +100IU/µl EPO + PLGA nanoparticles	7 days	[109, 158]
Agarose	T8-T10 Dorsal Hx (2x2x1.5 mm)	5 µl	Agarose + BDNF, ChABC, NT-3 loaded microtubules	>6 weeks	[94, 106]
PLA-PEG-PLA	T8 hx (1.5 mm depth)	10 µl	10% pre-polymer +100 µg /ml NT-3	3 weeks (*in vitro*)	[141]
Fibrin	C4 scissor cut to 2 mm depth	8 µl	108 mg/ml fibrinogen + 0.29 IU thrombin + 2.5 µg genipin + 0.25 U ChABC	Not examined	[129]
Tetronic-oligolactide	T7-T8Dorsal Hx	20µl	35% TL + minocycline (0.5, 5 µM)	7 days	[117]

a. Tx= transection, Hx= hemisection, Ct= contusion.

b. Dimensions after injury model represent amount of tissue removed

2.4.1 *Major findings and correlations between in vivo studies*

2.4.1.1. Cellular interaction with injectable scaffolds is beneficial for decreasing the astrocytic response and scar formation, and for the promotion of axonal growth after SCI. *In situ*-forming scaffolds are capable of bonding directly to the host, thus restoring the continuity of the spinal cord and allowing for cellular infiltration. Scaffolds permissive to cellular migration do not exhibit a cap of GFAP+ astrocytes at the host-graft interface. Instead, astrocytic processes extend within the gel to form a framework that may be associated with ingrowing axons. The overall astrocyte reactivity and production of CSPGs is lower in permissive gels as when compared to controls or non-permissive substrates. The initial studies employed collagen in complete transection models with tissue resection that led to extensive invasion by fibroblasts. Despite the formation of mesenchymal ECM, collagen scaffolds redirected the tissue formation from a dense scar towards a loosely connected highly vascularized tissue that was conducive to axonal ingrowth [152]. IKVAV-PA had a decreased astroglial response, decreased apoptosis, and axonal growth long after it was degraded showing that modulating the glial response after SCI may drive the reparative process away from scarring and towards regeneration.

2.4.1.2. Cellular infiltration of scaffolds is dependent on scaffold microstructure, degradability, and the presence of soluble or insoluble cues for cell growth. Non-cell adhesive materials such as methylcellulose, tetronic-oligolactide or PLA-PEG-PLA, or non-permissive morphologies such as agarose and high concentration collagen showed no cellular ingrowth unless neurotrophic factors were present. For example, BDNF was able to promote astrocyte and axon growth within otherwise non-permissive agarose. However, the intensity of neurofilament staining in BDNF-loaded agarose scaffolds significantly dropped off by 500 μm into the scaffold, which is shorter than expected for optimal conditions after 6 weeks [106]. Poorly cell adhesive PLA-PEG-PLA scaffolds had no effect on the astrocytic response after SCI and little axon regrowth was seen in gels releasing phosphate buffered saline [141]. This was likely due to the lack of cell adhesion motifs or mesh sizes too small to allow for growth cone movement.

Under optimal conditions such as those existing during development, neurites can extend up to 1 mm a day [159]. That rate of axonal growth, however, was not achieved in these gel studies. There appeared to be a balance between the persistence of scaffolding material and the rate of axon elongation. Rapidly degrading scaffolds such as PAs showed good axon elongation; however, this occurred in a contusion model, which maintained a residual structure of the spinal cord and was not highly prone to infiltration from cells outside of the CNS (*viz.*, fibroblasts and Schwann cells). Collagen scaffolds with different degrees crosslinking demonstrated the importance of maintaining structural rigidity in hemisection and transection models of SCI to prevent the organization of newly formed ECM into scar-

like tissue. No scaffolds showed axon re-growth before 3 weeks and regenerating axons could be seen at high densities within several implants at 2-3 months, suggesting that the scaffold should continue to provide a provisional matrix through this period.

2.4.1.3. Placement of DDS determines release profile and localization of the therapeutics

Injectable DDSs provide advantages over bolus injection and implantable mini-pumps/catheters. Depending on the extent of injury, the blood flow in the spinal cord and intrathecal space may result in different release profiles. The local CSF and blood flow after injury is greatly decreased which leads to more localized delivery. Penetration of the therapeutic into the cord also depends on the actual drug and the interaction with the delivery system (ionic or hydrophobic interactions). Another consideration is the placement of the DDS. A non-scaffold DDS may impede on axon growth if injected into the lesion cavity while cell permissive scaffolds may cause cellular buildup in unwanted areas such as the intrathecal space. The therapeutic window will also determine what type of DDS would be most beneficial.

2.4.1.4. Combinational approaches will be required to achieve significant recovery after SCI

Neurotrophic, anti-inflammatory, CSPG degrading, and cellular therapies hold great promise to enhance recovery after SCI and should be used in conjunction with scaffolding to enhance spinal cord regeneration. It was noted in the scaffolding studies that a low proportion of any regenerating axons crossed through the lesion site into the distal cord suggesting that the growth inhibitory environment outside of the lesion site must be addressed to promote full regeneration. A multifaceted approach delivering therapeutics inside the graft as well as distal to the lesion may overcome this barrier.

While, the collagen and PA systems showed enhanced axonal ingrowth they are too porous to provide a sustained release of therapeutics to the injury site and could benefit from the addition of drug delivery systems such as microparticles or heparin binding. Conversely, the PLA based drug delivery system showed excellent release profiles with little axon growth through the graft and most recovery coming from collateral sprouting distal to the lesion site. The incorporation of synthetic or natural biopolymers with adhesive motifs (*e.g.*, fibronectin, collagen, or synthetic peptides with RGD or IKVAV sequences) would enhance cellular interaction with the material. In the reviewed literature, there are few examples of scaffolds incorporating a separate drug delivery device. The BDNF-loaded microtubules within the alginate gel provided a chemotactic gradient which caused the initially non-cell permissive agarose scaffold to become infiltrated by astrocytes and neurites [106]. Similarly, ChABC- and NT-3-loaded microtubules synergistically improved axonal growth by addressing two growth inhibitory barriers [94]. Additionally, PLGA nano/microparticles have been used to encapsulate a number of neurotrophic factors (GDNF, CTNF, BDNF, NT-3) and have been injected alone or within hydrogels [158, 160, 161].

Modular therapies with the individual components optimized towards the specific functions of scaffolding, drug delivery, and cell encapsulation/delivery will provide a substantial advantage for regenerative approaches.

2.4.2 Description of prior studies using collagen as a scaffold for SCI

There were significant commonalities among the six *in situ* gelling collagen studies reviewed in this chapter [128, 152-156]. All of the studies used a liquid collagen gel, which polymerized *in situ* to form a fibrillar scaffold. Additionally three studies further investigated alternative forms of collagen scaffolds for comparison with solubilized collagen implants. Marchand, *et al.*, examined three additives to enhance the stability of the collagen gels *in vivo*, including chondroitin-6-sulfate (C-6-S), and the crosslinking agents, glyoxal and carbodiimide (CD) [152, 156]. Joosten, *et al.*, compared the *in situ*-forming collagen scaffold to a preformed solid collagen scaffold of the same concentration [155].

Studies by Marchand and Joosten provide extensive histological descriptions of the graft-host environment throughout the acute to early chronic time course of SCI progression in rodents. Liquid collagen injected directly into the spinal cord was able to gel sufficiently fast to localize the material and form a continuous interface between the graft and host tissue in hemisection or transection lesions. It was important to have a "clean" lesion site with little hemorrhage or contusion so gelation was not impeded.

The laceration injury model resulted in significant mesenchymal cell infiltration from the pial surfaces. Control saline-injected rodents had cystic cavities at the edges of the defect and a proliferative scar of variable thickness and orientation consisting of astrocytes, fibroblasts, and microglia. Collagen gel-treated animals formed a loose highly vascularized connective tissue matrix that became populated by a heterogeneous group of cells including ingrowing axons.

During the acute phase (<8 days) the *in situ* collagen implants behaved similarly regardless of additives. Rapid angiogenesis occurred and the implants were invaded by a heterogeneous group of cells including fibroblasts and Schwann cells. In the collagen-treated groups, this did not lead to the creation of a dense scar or extensive Schwannosis. The astrocytic response was also modulated in collagen-treated groups. The overall reactivity and proliferative response of the astrocytes was decreased as compared to control injections. Instead of astrocytes forming a cap around the ends of transected axons, astrocytes migrated into the graft and were noted to extend long processes within the matrix. This was partially attributed to the presence of a permissive scaffold for cellular migration and may be related to the ability of type I collagen inhibits glial proliferation *in vitro* [162].

At four weeks, the grafts were heavily infiltrated by a heterogeneous group of cells including astrocytes, microglia, and fibroblasts [152]. Thick randomly oriented collagen bundles and astrocytic

processes bridged the inter-stump gap creating continuity between the ends of the host tissue. The structure of the newly synthesized collagenous ECM was studied using polarized light microscopy enhanced by sirius red staining [156]. At four weeks, collagen-only implants contained more numerous thick red birefringent type I collagen bundles. The CD- and C-6-S–collagen gels on the other hand showed disorganized thin green collagen fibers by polarized microscopy. Collagen fiber organization into thick yellow and red bundles could be seen starting at the surface of the lesion near the meninges and extended gradually towards the center of the lesion.

There was no ingrowth of labeled CST axons until approximately 4 weeks post injury when a cellular and ECM support structure was in place. Marchand noted that the ingrowth of axons tended to follow the collagen architecture and microcysts within the collagen matrix. A collagen and a carbohydrate rich fibrogranular material was deposited in and around the follicular shaped microcysts, and astrocytic processes bent around the walls of these cysts. At 4 weeks, several long axonal processes could be seen extending into the C-6-S-collagen implant. The histological results suggested that axon regeneration occurred only after a secondary carbohydrate-rich matrix containing glial cells and processes formed in place of the primary matrix. In area of the C-6-S-collagen matrix, several axons were reported to extend through the distal tissue-implant interface and re-enter the spinal cord [156].

From 4-8 weeks, there was an increase in the number of axons growing from the lesion ends into the matrix in longitudinal fascicles. Collagen crosslinked with the addition of 1mM glycoxl showed better stability than collagen alone during cellular infiltration phase, and the also displayed the establishment of a newly formed ECM. At 2 months, the implant site of the glycoxl-crosslinked collagen group exhibited a tissue-like framework spanning the defect, while the defect site of the non-crosslinked collagen group appeared highly disorganized. Beyond 2 months, the defect filled with crosslinked collagen was profusely invaded by regenerating nerve fibers originating from both grey and white matters.The maturation of the endogenously produced collagen extended into the whole lesion site and into the adjacent spinal tissue. The pattern of deposition and maturation of the endogenous collagen was similar in normal and glyoxal-treated collagen.

Marchand noted that at about 2-3 months, the collagen-only implants became highly disorganized and contained thick collagen aggregates, which was detrimental to axon regeneration. In comparison, at 3 months, axons could be seen in both C-6-S- and CD-collagen implants and by 6 months numerous axons had grown into the lesions in the C-6-S- and CD-collagen groups. There was a greater number of axons in the C-6-S-collagen gels and their path was more rectilinear. These hydrogels were also still visible at the lesion site. The C-6-S-collagen implant had a more open structure and showed less endogenous collagen deposition and aggregation than the CD-collagen scaffolds. This was because the C-6-S-collagen matrix

delayed the formation of thick collagen aggregates for a longer period than the CD–collagen samples. The extent of collagen aggregation in both samples was still lower than control or collagen only implants.

Except in the case of C-6-S-collagen implants, axons were not noted caudal to the lesion (~8 weeks) suggesting the persistence of an inhibitory environment outside of the graft. However, De La Torre, *et al.*, demonstrated that 90 days after a full transection and implantation of a similar collagen implant, sensory evoked potential showed early wave-forms suggesting some re-growth through the graft [153].

Overall, the presence of the collagen hydrogel attenuated scar formation following injury. The stability of the collagen gel was important for preventing contraction and maintaining a loose vascularized matrix within the lesion, which allowed for the ingrowth of glia and axons. These studies show that there may be a relationship between the mechanical properties of the primary matrix and the tendency for dense scar formation; increasing the mechanical stability of the collagen implant could prevent scar formation. To further this point, a study by King, *et al.*, examining injectable collagen scaffolds in a knife-cut model of SCI, showed that by 1 week, the material had dense inclusions, which inhibited axonal infiltration as well as various other cellular and non-cellular elements [128]. It was proposed the dense inclusions were due to uneven gelation of the material within the lesion or focal contraction by infiltrating cells.

2.5. Summary

In situ-gelling systems are promising therapeutic interventions after SCI. They are capable of filling the heterogeneous defects, which occur after human SCI and can modulate the wound environment to decrease scarring and encourage regeneration. A multitude of other cellular and molecular therapeutics can also be encapsulated and released by the gel to enhance regeneration, sprouting, and recovery of functional axon connections.

In vivo studies unveiled some of the obstacles for *in* situ gel therapies. It is important that the scaffold persists until a native ECM framework can be synthesized to support and guide cellular growth. Gels are intrinsically soft and weak structures, and while their relatively low moduli may be beneficial for axon ingrowth, their attendant degradation rate may be too rapid. Further work needs to be conducted to find non-toxic *in situ* covalent crosslinkers for materials such as collagen, HA, and self-assembled peptides. Other materials such as alginate, agarose, and chitosan, which have longer persistence but lack cell adhesiveness and supportive domains, can be copolymerized with other bioactive polymers or peptides. The pore size, stiffness, degradation rate, and bioactivity of all scaffold materials must be finely tuned to allow for cellular ingrowth of both supportive glia and axons throughout the course of regeneration through the lesion, which is on the order of several weeks.

Drug delivery systems should consider the site of application, target the therapeutic agents and release profile to maximize the regenerative potential of the therapy. Many of the studies revealed a distinct increase in axon regeneration when combining therapeutic agents with scaffolding materials. Further development of modular therapies (*i.e.*, drug delivery systems incorporated within a scaffold polymer) would allow for independent tuning of gelation kinetics, stiffness, degradation rate, and bioactivity of scaffolds as well as their drug release kinetics. In the reviewed literature, there was also virtually no mention of incorporating cells within the scaffolds.

The flexibility of using injectable systems would allow therapies to be administered during the most suitable time for regeneration. The sub-acute stage ,7-14 days post injury, may be a prime intervention time. As described earlier, this period is after the cascade of initial inflammation and at the point of a beneficial astrocyte response. The microenvironment would be less harsh for exogenous cells and for the damaged axons beginning to re-extend growth cones towards the lesion site after having initially retracted after the injury [159].

While animal models are essential for *in vivo* comparison of the behavior of candidate materials in standardized defects, there are understandably shortcomings to the models of SCI, as there are to animal models for all human diseases and traumatic conditions. While many animal species and injury

types have been explored, each have distinct differences in relation to the pathology of human SCI [163]. It is also difficult to compare studies with different injury models since transection and resection of tissue may hinder axon elongation through a scaffold and the mechanisms of sprouting and regeneration are different between transection and contusion type SCI [46, 159]. It is challenging in some studies to differentiate actual axon regeneration from sprouting (*e.g.*, based on time frame, labeling, or tortuosity), and there is question as to which is more beneficial for functional recovery. There is also currently no reliable *ex vivo* model to assay or screen for application-specific properties of injectable materials prior to *in vivo* studies.

Over the past 10 years there have been dramatic and encouraging results of *in vivo* investigations of biomaterials and therapeutic agents for the treatment of SCI. It seems clear that there will be a role for multifunctional injectable gels, serving as scaffolds for endogenous cell migration into the gel-filled lesion and as delivery vehicles for therapeutic agents. There is hope that these gels along with our deepening understanding of the pathophysiology of SCI will result in advances in the treatment of SCI in human subjects in the next 10 years.

2.6. References:

[1] Kakulas BA. A review of the neuropathology of human spinal cord injury with emphasis on special features. J Spinal Cord Med. 1999;22:119-24.
[2] Bunge R, Puckett W, Becerra J, Marcillo A, Quencer R. Observations on the pathology of human spinal cord injury: a review and classification of 22 new cases with details from a case of chronic cord compression with extensive focal demyelination. Advances in neurology. 1993;59:75-89.
[3] Norenberg M, Smith J, Marcillo A. The pathology of human spinal cord injury: defining the problems. Journal of neurotrauma. 2004;21:429-40.
[4] Center NSCIS. Spinal cord injury facts and figures at a glance. Birmingham Alabama: University of Alabama at Birmingham; February 2012.
[5] Bunge R, Puckett W, Hiester E. Observations on the pathology of several types of human spinal cord injury, with emphasis on the astrocyte response to penetrating injuries. Advances in neurology. 1997;72:305.
[6] Profyris C, Cheema S, Zang D, Azari M, Boyle K, Petratos S. Degenerative and regenerative mechanisms governing spinal cord injury. Neurobiology of disease. 2004;15:415-36.
[7] Keirstead HS, Nistor G, Bernal G, Totoiu M, Cloutier F, Sharp K, et al. Human embryonic stem cell-derived oligodendrocyte progenitor cell transplants remyelinate and restore locomotion after spinal cord injury. J Neurosci. 2005;25:4694-705.
[8] Baptiste DC, Fehlings MG. Update on the treatment of spinal cord injury. Prog Brain Res. 2007;161:217-33.
[9] Rowland JW, Hawryluk GW, Kwon B, Fehlings MG. Current status of acute spinal cord injury pathophysiology and emerging therapies: promise on the horizon. Neurosurg Focus. 2008;25:E2.
[10] Faulkner JR, Herrmann JE, Woo MJ, Tansey KE, Doan NB, Sofroniew MV. Reactive astrocytes protect tissue and preserve function after spinal cord injury. J Neurosci. 2004;24:2143-55.
[11] Norenberg MD. Astrocyte responses to CNS injury. J Neuropathol Exp Neurol. 1994;53:213-20.
[12] Kalman M. Glial reaction and reactive glia. In: Leif H, editor. Advances in Molecular and Cell Biology: Elsevier; 2003. p. 787-835.
[13] Puckett W, Hiester E, Norenberg M, Marcillo A, Bunge R. The astroglial response to Wallerian degeneration after spinal cord injury in humans. Experimental Neurology. 1997;148:424-32.
[14] Yiu G, He Z. Glial inhibition of CNS axon regeneration. Nature Reviews Neuroscience. 2006;7:617-27.
[15] Buss A, Pech K, Kakulas B, Martin D, Schoenen J. Growth-modulating molecules are associated with invading Schwann cells and not astrocytes in human traumatic spinal cord injury. Brain. 2007;130:940-53.
[16] Buss A, Pech K, Merkler D, Kakulas B, Martin D. Sequential loss of myelin proteins during Wallerian degeneration in the human spinal cord. Brain. 2005;128:356-64.
[17] Klapka N, Muller HW. Collagen matrix in spinal cord injury. J Neurotrauma. 2006;23:422-35.
[18] Buss A, Brook G, Kakulas B, Martin D, Franzen R. Gradual loss of myelin and formation of an astrocytic scar during Wallerian degeneration in the human spinal cord. Brain. 2004;127:34-44.
[19] Hagg T, Oudega M. Degenerative and spontaneous regenerative processes after spinal cord injury. J Neurotrauma. 2006;23:264-80.
[20] Trivedi A, Olivas AD, Noble-Haeusslein LJ. Inflammation and Spinal Cord Injury: Infiltrating Leukocytes as Determinants of Injury and Repair Processes. Clinical neuroscience research. 2006;6:283-92.
[21] Kigerl KA, Gensel JC, Ankeny DP, Alexander JK, Donnelly DJ, Popovich PG. Identification of two distinct macrophage subsets with divergent effects causing either neurotoxicity or regeneration in the injured mouse spinal cord. J Neurosci. 2009;29:13435-44.
[22] Beck KD, Nguyen HX, Galvan MD, Salazar DL, Woodruff TM, Anderson AJ. Quantitative analysis of cellular inflammation after traumatic spinal cord injury: evidence for a multiphasic inflammatory response in the acute to chronic environment. Brain. 2010;133:433-47.

[23] Rolls A, Shechter R, London A, Segev Y, Jacob-Hirsch J, Amariglio N, et al. Two faces of chondroitin sulfate proteoglycan in spinal cord repair: a role in microglia/macrophage activation. PLoS medicine. 2008;5:e171.
[24] Mautes AE, Weinzierl MR, Donovan F, Noble LJ. Vascular events after spinal cord injury: contribution to secondary pathogenesis. Physical therapy. 2000;80:673-87.
[25] Zhang Z, Guth L. Experimental spinal cord injury: Wallerian degeneration in the dorsal column is followed by revascularization, glial proliferation, and nerve regeneration. Exp Neurol. 1997;147:159-71.
[26] Fu SY, Gordon T. The cellular and molecular basis of peripheral nerve regeneration. Mol.Neurobiol. 1997;14:67-116.
[27] Huebner E, Strittmatter S. Axon Regeneration in the Peripheral and Central Nervous Systems

Cell Biology of the Axon. In: Koenig E, editor.: Springer Berlin / Heidelberg; 2009. p. 339-51.
[28] Sulaiman OAR, Gordon T. Effects of short- and long-term Schwann cell denervation on peripheral nerve regeneration, myelination, and size. Glia. 2000;32:234-46.
[29] Tucker BA, Mearow KM. Peripheral sensory axon growth: from receptor binding to cellular signaling. Can J Neurol Sci. 2008;35:551-66.
[30] Hilliard MA. Axonal degeneration and regeneration: a mechanistic tug-of-war. J Neurochem. 2009;108:23-32.
[31] Butt AM, Ibrahim M, Berry M. Axon-myelin sheath relations of oligodendrocyte unit phenotypes in the adult rat anterior medullary velum. Journal of Neurocytology. 1998;27:205-17.
[32] Grimpe B, Pressman Y, Bunge M, Silver J. The role of proteoglycans in Schwann cell/astrocyte interactions and in regeneration failure at PNS/CNS interfaces. Mol Cell Neurosci. 2005;28:18-29.
[33] Caroni P, Schwab ME. Antibody against Myelin-Associated Inhibitor of Neurite Growth Neutralizes Nonpermissive Substrate Properties of CNS White Matter. Neuron. 2008;60:404-5.
[34] Mckerracher L, David S, Jackson DL, Kottis V, Dunn RJ, Braun PE. Identification of Myelin-Associated Glycoprotein as a Major Myelin-Derived Inhibitor of Neurite Growth. Neuron. 1994;13:805-11.
[35] Mukhopadhyay G, Doherty P, Walsh FS, Crocker PR, Filbin MT. A Novel Role for Myelin-Associated Glycoprotein as an Inhibitor of Axonal Regeneration. Neuron. 1994;13:757-67.
[36] Rolls A, Shechter R, Schwartz M. The bright side of the glial scar in CNS repair. Nat Rev Neurosci. 2009;10:235-41.
[37] McKeon R, Schreiber R, Rudge J, Silver J. Reduction of neurite outgrowth in a model of glial scarring following CNS injury is correlated with the expression of inhibitory molecules on reactive astrocytes. J Neurosci. 1991;11:3398-411.
[38] Lemons ML, Howland DR, Anderson DK. Chondroitin sulfate proteoglycan immunoreactivity increases following spinal cord injury and transplantation. Exp Neurol. 1999;160:51-65.
[39] Barritt AW, Davies M, Marchand F, Hartley R, Grist J, Yip P, et al. Chondroitinase ABC promotes sprouting of intact and injured spinal systems after spinal cord injury. Journal of Neuroscience. 2006;26:10856-67.
[40] Iannotti C, Zhang Y, Shields L, Han Y, Burke ... D. Dural repair reduces connective tissue scar invasion and cystic cavity formation after acute spinal cord lasceration in adult rats. J Neurotrauma. 2006;23:853-65.
[41] Davies SJ, Goucher DR, Doller C, Silver J. Robust regeneration of adult sensory axons in degenerating white matter of the adult rat spinal cord. J Neurosci. 1999;19:5810-22.
[42] Davies SJ, Fitch MT, Memberg SP, Hall AK, Raisman G, Silver J. Regeneration of adult axons in white matter tracts of the central nervous system. Nature. 1997;390:680-3.
[43] David S, Aguayo A. Axonal elongation into peripheral nervous system" bridges" after central nervous system injury in adult rats. Science. 1981;214:931-3.
[44] Lu P, Jones L, Tuszynski M. Axon regeneration through scars and into sites of chronic spinal cord injury. Exp Neurol. 2007;203:8-21.

[45] Thuret S, Moon LD, Gage FH. Therapeutic interventions after spinal cord injury. Nat Rev Neurosci. 2006;7:628-43.
[46] Fehlings M, Tator C. The relationships among the severity of spinal cord injury, residual neurological function, axon counts, and counts of retrogradely labeled neurons after experimental spinal cord injury. Exp Neurol. 1995;132:220-8.
[47] Basso D, Beattie M, Bresnahan J. Graded histological and locomotor outcomes after spinal cord contusion using the NYU weight-drop device versus transection. Exp Neurol. 1996;139:244-56.
[48] Nathan P. Effects on movement of surgical incisions into the human spinal cord. Brain. 1994;117:337-46.
[49] Klouda L, Mikos A. Thermoresponsive hydrogels in biomedical applications. European Journal of Pharmaceutics and Biopharmaceutics. 2008;68:34-45.
[50] Kretlow J, Klouda L, Mikos A. Injectable matrices and scaffolds for drug delivery in tissue engineering. Advanced Drug Delivery Reviews. 2007;59:263-73.
[51] Hoare T, Kohane D. Hydrogels in drug delivery: Progress and challenges. Polymer. 2008;49:1993-2007.
[52] Tutak U, Doleys DM. Intrathecal infusion systems for treatment of chronic low back and leg pain of noncancer origin. South Med J. 1996;89:295-300.
[53] Amar AP, Larsen DW, Teitelbaum GP. Percutaneous spinal interventions. Neurosurg Clin N Am. 2005;16:561-8, vii.
[54] Knoller N, Auerbach G, Fulga V, Zelig G, Attias J, Bakimer R, et al. Clinical experience using incubated autologous macrophages as a treatment for complete spinal cord injury: Phase I study results. J Neurosurg-Spine. 2005;3:173-81.
[55] Feron F, Perry C, Cochrane J, Licina P, Nowitzke A, Urquhart S, et al. Autologous olfactory ensheathing cell transplantation in human spinal cord injury. Brain. 2005;128:2951-60.
[56] Gillette BM, Jensen JA, Tang B, Yang GJ, Bazargan-Lari A, Zhong M, et al. In situ collagen assembly for integrating microfabricated three-dimensional cell-seeded matrices. Nat Mater. 2008;7:636-40.
[57] Nomura H, Katayama Y, Shoichet MS, Tator CH. Complete spinal cord transection treated by implantation of a reinforced synthetic hydrogel channel results in syringomyelia and caudal migration of the rostral stump. Neurosurgery. 2006;59:183-92; discussion -92.
[58] Willerth S, Sakiyama-Elbert S. Approaches to neural tissue engineering using scaffolds for drug delivery. Advanced Drug Delivery Reviews. 2007;59:325-38.
[59] Straley KS, Heilshorn SC. Dynamic, 3D-Pattern Formation Within Enzyme-Responsive Hydrogels. Advanced Materials. 2009;21:4148-52.
[60] Johnson PJ, Tatara A, Shiu A, Sakiyama-Elbert SE. Controlled Release of Neurotrophin-3 and Platelet-Derived Growth Factor From Fibrin Scaffolds Containing Neural Progenitor Cells Enhances Survival and Differentiation Into Neurons in a Subacute Model of SCI. Cell Transplantation. 2010;19:89-101.
[61] Coumans J, Lin T, Dai H, MacArthur L, McAtee M, Nash C, et al. Axonal regeneration and functional recovery after complete spinal cord transection in rats by delayed treatment with transplants and neurotrophins. Journal of Neuroscience. 2001;21:9334-44.
[62] Zhong Y, Bellamkonda RV. Biomaterials for the central nervous system. J R Soc Interface. 2008;5:957-75.
[63] Bradbury E, McMahon S. Spinal cord repair strategies: why do they work? Nat Rev Neurosci. 2006;7:644-53.
[64] Krewson CE, Klarman ML, Saltzman WM. Distribution of nerve growth factor following direct delivery to brain interstitium. Brain Res. 1995;680:196-206.
[65] Sayer FT, Oudega M, Hagg T. Neurotrophins reduce degeneration of injured ascending sensory and corticospinal motor axons in adult rat spinal cord. Exp Neurol. 2002;175:282-96.
[66] Eftekharpour E, Karimi-Abdolrezaee S, Fehlings MG. Current status of experimental cell replacement approaches to spinal cord injury. Neurosurg Focus. 2008;24:E19.

[67] Willerth SM, Sakiyama-Elbert SE. Cell therapy for spinal cord regeneration. Adv Drug Deliv Rev. 2008;60:263-76.
[68] Mahoney M, Anseth K. Three-dimensional growth and function of neural tissue in degradable polyethylene glycol hydrogels. Biomaterials. 2006;27:2265-74.
[69] Straley KS, Heilshorn SC. Independent tuning of multiple biomaterial properties using protein engineering. Soft Matter. 2009;5:114-24.
[70] Flanagan LA, Ju YE, Marg B, Osterfield M, Janmey PA. Neurite branching on deformable substrates. Neuroreport. 2002;13:2411-5.
[71] Balgude AP, Yu X, Szymanski A, Bellamkonda RV. Agarose gel stiffness determines rate of DRG neurite extension in 3D cultures. Biomaterials. 2001;22:1077-84.
[72] O'Connor S, Stenger D, Shaffer K, Ma W. Survival and neurite outgrowth of rat cortical neurons in three-dimensional agarose and collagen gel matrices. Neuroscience Letters. 2001;304:189-93.
[73] Willits R, Skornia S. Effect of collagen gel stiffness on neurite extension. Journal of Biomaterials Science, Polymer Edition. 2004;15:1521-31.
[74] Bellamkonda R, Ranieri JP, Bouche N, Aebischer P. Hydrogel-based three-dimensional matrix for neural cells. J Biomed Mater Res. 1995;29:663-71.
[75] Georges P, Miller W, Meaney D, Sawyer E. Matrices with compliance comparable to that of brain tissue select neuronal over glial growth in mixed cortical cultures. Biophysical journal. 2006;90:3012-8.
[76] Discher D, Janmey P, Wang Y. Tissue cells feel and respond to the stiffness of their substrate. Science. 2005;310:1139-43.
[77] Leach JB, Brown XQ, Jacot JG, Dimilla PA, Wong JY. Neurite outgrowth and branching of PC12 cells on very soft substrates sharply decreases below a threshold of substrate rigidity. J Neural Eng. 2007;4:26-34.
[78] Banerjee A, Arha M, Choudhary S, Ashton RS, Bhatia SR, Schaffer DV, et al. The influence of hydrogel modulus on the proliferation and differentiation of encapsulated neural stem cells. Biomaterials. 2009;30:4695-9.
[79] Seidlits SK, Khaing ZZ, Petersen RR, Nickels JD, Vanscoy JE, Shear JB, et al. The effects of hyaluronic acid hydrogels with tunable mechanical properties on neural progenitor cell differentiation. Biomaterials. 2010;31:3930-40.
[80] Lo C, Wang H, Dembo M, Wang Y. Cell movement is guided by the rigidity of the substrate. Biophys J. 2000;79:144-52.
[81] Sundararaghavan HG, Monteiro GA, Firestein BL, Shreiber DI. Neurite Growth in 3D Collagen Gels With Gradients of Mechanical Properties. Biotechnol Bioeng. 2009;102:632-43.
[82] Norman LL, Stroka K, Aranda-Espinoza H. Guiding Axons in the Central Nervous System: A Tissue Engineering Approach. Tissue Eng Part B-Re. 2009;15:291-305.
[83] Sung HJ, Meredith C, Johnson C, Galis ZS. The effect of scaffold degradation rate on three-dimensional cell growth and angiogenesis. Biomaterials. 2004;25:5735-42.
[84] Lampe KJ, Bjugstad KB, Mahoney MJ. Impact of degradable macromer content in a poly(ethylene glycol) hydrogel on neural cell metabolic activity, redox state, proliferation, and differentiation. Tissue Eng Part A. 2010;16:1857-66.
[85] Hill CE, Beattie MS, Bresnahan JC. Degeneration and sprouting of identified descending supraspinal axons after contusive spinal cord injury in the rat. Exp Neurol. 2001;171:153-69.
[86] Tysseling-Mattiace VM, Sahni V, Niece KL, Birch D, Czeisler C, Fehlings MG, et al. Self-assembling nanofibers inhibit glial scar formation and promote axon elongation after spinal cord injury. Journal of Neuroscience. 2008;28:3814-23.
[87] Seeds N, Siconolfi L, Haffke S. Neuronal extracellular proteases facilitate cell migration, axonal growth, and pathfinding. Cell and Tissue Research. 1997;290:367-70.
[88] Pittman R, WILLIAMS A. Neurite penetration into collagen gels requires Ca2+-dependent metalloproteinase activity. Dev Neurosci-Basel. 1989;11:41-51.
[89] Pittier RG, Sauthier F, Hubbell JA, Hall H. Neurite extension andin vitro myelination within three-dimensional modified fibrin matrices. J Neurobiol. 2005;63:1-14.

[90] Steller H. Mechanisms and Genes of Cellular Suicide. Science. 1995;267:1445-9.
[91] Kofron C, Fong V, Hoffman-Kim D. Neurite outgrowth at the interface of 2D and 3D growth environments. J Neural Eng. 2009;6:016002.
[92] Yu X, Bellamkonda R. Dorsal root ganglia neurite extension is inhibited by mechanical and chondroitin sulfate-rich interfaces. J Neurosci Res. 2001;66:303-10.
[93] Cigognini D, Satta A, Colleoni B, Silva D, Donega M, Antonini S, et al. Evaluation of Early and Late Effects into the Acute Spinal Cord Injury of an Injectable Functionalized Self-Assembling Scaffold. PLoS One. 2011;6:e19782.
[94] Lee H, McKeon RJ, Bellamkonda RV. Sustained delivery of thermostabilized chABC enhances axonal sprouting and functional recovery after spinal cord injury. Proc Natl Acad Sci U S A. 2010;107:3340-5.
[95] Mano JF, Silva GA, Azevedo HS, Malafaya PB, Sousa RA, Silva SS, et al. Natural origin biodegradable systems in tissue engineering and regenerative medicine: present status and some moving trends. Journal of the Royal Society, Interface / the Royal Society. 2007;4:999-1030.
[96] Rauch U. Modeling an extracellular environment for axonal pathfinding and fasciculation in the central nervous system. Cell and Tissue Research. 1997;290:349-56.
[97] Samadikuchaksaraei A. An overview of tissue engineering approaches for management of spinal cord injuries. J Neuroeng Rehabil. 2007;4:15.
[98] Nomura H, Tator C, Shoichet M. Bioengineered strategies for spinal cord repair. Journal of Neurotrauma. 2006;23:496-507.
[99] Levental I, Georges P, Janmey P. Soft biological materials and their impact on cell function. Soft Matter. 2007;3:299-306.
[100] Chevallay B, Herbage D. Collagen-based biomaterials as 3D scaffold for cell cultures: applications for tissue engineering and gene therapy. Med Biol Eng Comput. 2000;38:211-8.
[101] Joosten E, Veldhuis W, Hamers F. Collagen containing neonatal astrocytes stimulates regrowth of injured fibers and promotes modest locomotor recovery after spinal cord injury. J Neurosci Res. 2004;77:127-42.
[102] Ma W, Chen S, Fitzgerald W, Maric D, Lin H, O'Shaughnessy T, et al. Three-dimensional collagen gel networks for neural stem cell-based neural tissue engineering. Macromol Symp. 2005;227:327-33.
[103] Ma W, Fitzgerald W, Liu Q-Y, O'Shaughnessy TJ, Maric D, Lin HJ, et al. CNS stem and progenitor cell differentiation into functional neuronal circuits in three-dimensional collagen gels. Experimental Neurology. 2004;190:276-88.
[104] Eccleston P, Mirsky R, Jessen K. Type I collagen preparations inhibit DNA synthesis in glial cells of the peripheral nervous system. Experimental Cell Research. 1989;182:173-85.
[105] Sato K. Possible Involvement of Aminotelopeptide in Self-assembly and Thermal Stability of Collagen I as Revealed by Its Removal with Proteases. Journal of Biological Chemistry. 2000;275:25870-5.
[106] Jain A, Kim Y, McKeon R, Bellamkonda R. In situ gelling hydrogels for conformal repair of spinal cord defects, and local delivery of BDNF after spinal cord injury. Biomaterials. 2006;27:497-504.
[107] Xu Y, Wang C, Tam KC, Li L. Salt-assisted and salt-suppressed sol-gel transitions of methylcellulose in water. Langmuir. 2004;20:646-52.
[108] Martin BC, Minner EJ, Wiseman SL, Klank RL, Gilbert RJ. Agarose and methylcellulose hydrogel blends for nerve regeneration applications. J Neural Eng. 2008;5:221-31.
[109] Gupta D, Tator CH, Shoichet MS. Fast-gelling injectable blend of hyaluronan and methylcellulose for intrathecal, localized delivery to the injured spinal cord. Biomaterials. 2006;27:2370-9.
[110] Tom VJ, Doller CM, Malouf AT, Silver J. Astrocyte-associated fibronectin is critical for axonal regeneration in adult white matter. J Neurosci. 2004;24:9282-90.
[111] Kurisawa M, Chung J, Yang Y, Gao S, Uyama H. Injectable biodegradable hydrogels composed of hyaluronic acid–tyramine conjugates for drug delivery and tissue engineering. Chemical Communications. 2005;2005:4312-4.

[112] White RE, Rao M, Gensel JC, McTigue DM, Kaspar BK, Jakeman LB. Transforming growth factor alpha transforms astrocytes to a growth-supportive phenotype after spinal cord injury. J Neurosci. 2011;31:15173-87.
[113] Crompton KE, Goud JD, Bellamkonda RV, Gengenbach TR, Finkelstein DI, Horne MK, et al. Polylysine-functionalised thermoresponsive chitosan hydrogel for neural tissue engineering. Biomaterials. 2007;28:441-9.
[114] Chenite A, Chaput C, Wang D, Combes C, Buschmann M, Hoemann C, et al. Novel injectable neutral solutions of chitosan form biodegradable gels in situ. Biomaterials. 2000;21:2155-61.
[115] Comolli N, Neuhuber B, Fischer I, Lowman A. In vitro analysis of PNIPAAm-PEG, a novel, injectable scaffold for spinal cord repair. Acta biomaterialia. 2009;5:1046-55.
[116] Iida S, Yoshida T, Naito K, Sakamoto H, Katoh O, Hirohashi S, et al. Human hst-2 (FGF-6) oncogene: cDNA cloning and characterization. Oncogene. 1992;7:303-9.
[117] Ard MD, Bunge RP. Heparan sulfate proteoglycan and laminin immunoreactivity on cultured astrocytes: relationship to differentiation and neurite growth. J Neurosci. 1988;8:2844-58.
[118] Rowley JA, Madlambayan G, Mooney DJ. Alginate hydrogels as synthetic extracellular matrix materials. Biomaterials. 1999;20:45-53.
[119] Novikova L, Mosahebi A, Wiberg M, Terenghi G. Alginate hydrogel and matrigel as potential cell carriers for neurotransplantation. J Biomed Mater Res A. 2006;77:242-52.
[120] Dhoot N, Tobias C, Fischer I, Wheatley M. Peptide-modified alginate surfaces as a growth permissive substrate for neurite outgrowth. J Biomed Mater Res. 2004;71:191-200.
[121] Janmey P, Winer J, Weisel J. Fibrin gels and their clinical and bioengineering applications. J R Soc Interface. 2009;6:1-10.
[122] Cheng H, Cao Y, Olson L. Spinal Cord Repair in Adult Paraplegic Rats: Partial Restoration of Hind Limb Function. ScienceNew Series. 1996;273:510-3.
[123] Iwaya K, Mizoi K, Tessler A, Itoh Y. Neurotrophic agents in fibrin glue mediate adult dorsal root regeneration into spinal cord. Neurosurgery. 1999;44:589-95; discussion 95-6.
[124] Taylor S, McDonald J, Sakiyama-Elbert S. Controlled release of neurotrophin-3 from fibrin gels for spinal cord injury. Journal of Controlled Release. 2004;98:281-94.
[125] Johnson PJ, Parker SR, Sakiyama-Elbert SE. Controlled release of neurotrophin-3 from fibrin-based tissue engineering scaffolds enhances neural fiber sprouting following subacute spinal cord injury. Biotechnol Bioeng. 2009;104:1207-14.
[126] Johnson PJ, Parker SR, Sakiyama-Elbert SE. Fibrin-based tissue engineering scaffolds enhance neural fiber sprouting and delay the accumulation of reactive astrocytes at the lesion in a subacute model of spinal cord injury. J Biomed Mater Res A. 2010;92:152-63.
[127] Johnson PJ, Tatara A, McCreedy DA, Shiu A, Sakiyama-Elbert SE. Tissue-engineered fibrin scaffolds containing neural progenitors enhance functional recovery in a subacute model of SCI. Soft Matter. 2010;6:5127-37.
[128] King V, Alovskaya A, Wei D, Brown R, Priestley J. The use of injectable forms of fibrin and fibronectin to support axonal ingrowth after spinal cord injury. Biomaterials. 2010;31:4447-56.
[129] Hyatt AJ, Wang D, Kwok JC, Fawcett JW, Martin KR. Controlled release of chondroitinase ABC from fibrin gel reduces the level of inhibitory glycosaminoglycan chains in lesioned spinal cord. J Control Release. 2010;147:24-9.
[130] Uibo R, Laidmaee I, Sawyer ES, Flanagan LA, Georges PC, Winer JP, et al. Soft materials to treat central nervous system injuries: Evaluation of the suitability of non-mammalian fibrin gels. Bba-Mol Cell Res. 2009;1793:924-30.
[131] Semino C. Self-assembling peptides: from bio-inspired materials to bone regeneration. Journal of Dental Research. 2008;87:606-16.
[132] Guo J, Su H, Zeng Y, Liang YX, Wong WM, Ellis-Behnke RG, et al. Reknitting the injured spinal cord by self-assembling peptide nanofiber scaffold. Nanomedicine. 2007;3:311-21.
[133] Silva GA. Selective Differentiation of Neural Progenitor Cells by High-Epitope Density Nanofibers. Science. 2004;303:1352-5.

[134] Ye Z, Zhang H, Luo H, Wang S, Zhou Q, DU X, et al. Temperature and pH effects on biophysical and morphological properties of self-assembling peptide RADA16-I. Journal of Peptide Science. 2008;14:152-62.
[135] Semino C, Kasahara J, Hayashi Y, Zhang S. Entrapment of migrating hippocampal neural cells in three-dimensional peptide nanofiber scaffold. Tissue Engineering. 2004;10:643-55.
[136] Guo J, Leung KK, Su H, Yuan Q, Wang L, Chu TH, et al. Self-assembling peptide nanofiber scaffold promotes the reconstruction of acutely injured brain. Nanomedicine. 2009;5:345-51.
[137] Yang CY, Song B, Ao Y, Nowak AP, Abelowitz RB, Korsak RA, et al. Biocompatibility of amphiphilic diblock copolypeptide hydrogels in the central nervous system. Biomaterials. 2009;30:2881-98.
[138] Foo CTSWP, Lee JS, Mulyasasmita W, Parisi-Amon A, Heilshorn SC. Two-component protein-engineered physical hydrogels for cell encapsulation. Proceedings of the National Academy of Sciences of the United States of America. 2009;106:22067-72.
[139] Williams CG, Malik AN, Kim TK, Manson PN, Elisseeff JH. Variable cytocompatibility of six cell lines with photoinitiators used for polymerizing hydrogels and cell encapsulation. Biomaterials. 2005;26:1211-8.
[140] Royce Hynes S, McGregor LM, Ford Rauch M, Lavik EB. Photopolymerized poly(ethylene glycol)/poly(L-lysine) hydrogels for the delivery of neural progenitor cells. Journal of biomaterials science Polymer edition. 2007;18:1017-30.
[141] Piantino J, Burdick JA, Goldberg D, Langer R, Benowitz LI. An injectable, biodegradable hydrogel for trophic factor delivery enhances axonal rewiring and improves performance after spinal cord injury. Exp Neurol. 2006;201:359-67.
[142] Khaing ZZ, Milman BD, Vanscoy JE, Seidlits SK, Grill RJ, Schmidt CE. High molecular weight hyaluronic acid limits astrocyte activation and scar formation after spinal cord injury. J Neural Eng. 2011;8:046033.
[143] Sarig-Nadir O, Seliktar D. Compositional alterations of fibrin-based materials for regulating in vitro neural outgrowth. Tissue Engineering Part A. 2008;14:401-11.
[144] Nishi C, Nakajima N, Ikada Y. In vitro evaluation of cytotoxicity of diepoxy compounds used for biomaterial modification. Journal of Biomedical Materials Research. 1995;29:829-34.
[145] Sung HW, Huang RN, Huang LL, Tsai CC, Chiu CT. Feasibility study of a natural crosslinking reagent for biological tissue fixation. J Biomed Mater Res. 1998;42:560-7.
[146] Sung H, Chang W, Ma C, Lee M. Crosslinking of biological tissues using genipin and/or carbodiimide. J Biomed Mater Res A. 2003;64:427-38.
[147] Siegel R, Fu J. Collagen cross-linking - purification and substrate-specificity of lysyl oxidase J Biol Chem. 1976;251:5779-85.
[148] Orban JM, Wilson LB, Kofroth JA, El-Kurdi MS, Maul TM, Vorp DA. Crosslinking of collagen gels by transglutaminase. J Biomed Mater Res A. 2004;68:756-62.
[149] Macaya D, Ng KK, Spector M. Injectable Collagen-Genipin Gel for the Treatment of Spinal Cord Injury: In Vitro Studies. Adv Funct Mater. 2011;21:4788-97.
[150] Sundararaghavan H, Monteiro G, Lapin N. Genipin-induced changes in collagen gels: Correlation of mechanical properties to fluorescence. Journal of Biomedical Materials Research Part A. 2008;87A:308-20.
[151] Freudenberg U, Hermann A, Welzel PB, Stirl K, Schwarz SC, Grimmer M, et al. A star-PEG-heparin hydrogel platform to aid cell replacement therapies for neurodegenerative diseases. Biomaterials. 2009;30:5049-60.
[152] Marchand R, Woerly S. Transected spinal cords grafted with insitu self-assembled collagen matrices. Neuroscience. 1990;36:45-60.
[153] de la Torre JC, Hill PK, Gonzalez-Carvajal M, Parker JC, Jr. Evaluation of transected spinal cord regeneration in the rat. Exp Neurol. 1984;84:188-206.
[154] Gelderd JB. Evaluation of blood vessel and neurite growth into a collagen matrix placed within a surgically created gap in rat spinal cord. Brain Res. 1990;511:80-92.

[155] Joosten E, Bar P, Gispen W. Collagen implants and cortico-spinal axonal growth after mid-thoracic spinal cord lesion in the adult rat. J Neurosci Res. 1995;41:481-90.
[156] Marchand R, Woerly S, Bertrand L, Valdes N. Evaluation of two cross-linked collagen gels implanted in the transected spinal cord. Brain Res Bull. 1993;30:415-22.
[157] Jimenez Hamann MC, Tator CH, Shoichet MS. Injectable intrathecal delivery system for localized administration of EGF and FGF-2 to the injured rat spinal cord. Exp Neurol. 2005;194:106-19.
[158] Baumann MD, Kang CE, Tator CH, Shoichet MS. Intrathecal delivery of a polymeric nanocomposite hydrogel after spinal cord injury. Biomaterials. 2010;31:7631-9.
[159] Steward O, Zheng B, Tessier-Lavigne M. False resurrections: distinguishing regenerated from spared axons in the injured central nervous system. J Comp Neurol. 2003;459:1-8.
[160] Wang Y-C, Wu Y-T, Huang H-Y, Lin H-I, Lo L-W, Tzeng S-F, et al. Sustained intraspinal delivery of neurotrophic factor encapsulated in biodegradable nanoparticles following contusive spinal cord injury. Biomaterials. 2008;29:4546-53.
[161] Burdick JA, Ward M, Liang E, Young MJ, Langer R. Stimulation of neurite outgrowth by neurotrophins delivered from degradable hydrogels. Biomaterials. 2006;27:452-9.
[162] Eccleston P, Mirsky R, Jessen K. Type I collagen preparations inhibit DNA synthesis in glial cells of the peripheral nervous system. Experimental cell research. 1989.
[163] Talac R, Friedman J, Moore M, Lu L, Jabbari E, Windebank A, et al. Animal models of spinal cord injury for evaluation of tissue engineering treatment strategies. Biomaterials. 2004;25:1505-10.

Chapter 3:

Development and characterization of an injectable collagen-genipin gel

3.1. Introduction

As highlighted in the background and motivation, minimally invasive therapies are attractive treatment options for SCI due to their ability to conform to heterogeneous lesions and limit the extent of damage associated with the implantation of a pre-formed scaffold. In this chapter, I evaluate an injectable thermo-responsive soluble collagen gel incorporating genipin, an amine reactive covalent cross-linker with low cytotoxicity and fluorogenic attributes. Unlike previous studies, genipin is being investigated as an *in situ* covalent cross-linker that will continue to act on the gel after injection. Physical characterization studies show that the addition of genipin provides control over the mechanical and degradative behavior of the gel, to meet design specifications of an injectable material for neural tissues. Additionally, an improved *in situ* assay to predict the extent of cross-linking reaction is investigated. Encapsulation of mesenchymal stem cells (MSCs) and neural stem cells (NSCs) within collagen-genipin gels was performed to show the gels support cell viability and proliferation, and thus serve as a cyto-compatible material.

3.2. Background and Motivation

While there have been many injectable scaffolds reported in the literature for a wide range of tissues, only a few have been injected into the spinal cord.[1] Several injectable polymeric scaffolds that have been proposed for SCI include: agarose, polyethylene glycol (PEG) conjugates, self-assembling peptides, hyaluronic acid/ methylcellulose, and collagen.[2-6] Natural polymers (biopolymers) are advantageous because they contain intrinsic motifs for cell adhesion and are readily degraded *in vivo*.[7, 8] Biopolymer gels also mimic the morphology and mechanical properties of the native extracellular matrix (ECM).

Collagen is commended as an injectable biomaterial because of its inverse gelation property, which enables it to be applied as a chilled solution that undergoes a gelation reaction upon warming to body temperature.[9, 10] Cells can be mixed into the liquid collagen precursor and the suspension can be injected into a defect. The gelation reaction occurs *in vivo* within minutes to form a fibrillar scaffold that entraps viable, functional cells and therapeutics.

Even though type I collagen is not a principal component of the ECM of the central nervous system (CNS), collagen gels have been widely shown to support the growth and differentiation neural cells, including cortical neurons, astrocytes, and neural progenitor cells.[11] Of importance was that other gel types including a sugar poly(acrylate) hydrogel and agarose were not able to support neural cell growth "as a result of a lack of cell adherence, small pore size and, possibly, harshness of synthesis conditions".[12] Subsequent investigations demonstrated functional synapse formation among neurons grown on collagen gels.[13] Furthermore, collagen gels have been shown to support neural progenitor

proliferative capacity, neuronal differentiation potential as well as and the formation of functional cortical-like networks.[14, 15] Injectable collagen solutions also support rat neural stem/precursor cells migration through the gels, and differentiation into neurons, astrocytes, and oligodendrocytes within the gel culture.[16] Other work demonstrated the capability of chick dorsal root ganglia cells grown in collagen gels to extend neurites within the gels, with the degree of neurite extension related to the concentration (mechanical stiffness) of the gel.[17] Furthermore, collagen can inhibit glial proliferation and thus may decrease glial scar post-spinal cord injury (SCI).[18]

Collagen gels can be fabricated to have mechanical properties similar to the native spinal cord, and thus direct cell behavior. Neurons prefer compliant substrates (0.1-1 kPa) and will elongate along a gradient in mechanical properties, while fibroblasts or scar-forming glial cells prefer stiffer matrices (1-10 kPa) and proliferate in the stiffened ECM after SCI.[17, 19-21]

Despite the advantageous biochemical properties of collagen, the material itself is intrinsically weak and requires additional modifications to improve its stability especially when implanted *in vivo*. While collagen has been applied as a gel scaffold *in vivo,* no cross-linkers have yet been employed to safely covalently cross-link collagen *in vivo*.[5] A novel and critical aspect of the current work is the *in vivo* cross-linking of the *in situ*-forming collagen gel using genipin, a plant extracted iridoid compound which reacts with primary amines in collagen to produce intrahelical, interhelical, and intermicrofibrilliar cross-links (**Figure 3-1**).[22] Genipin is 3000-fold less cytotoxic than glutaraldehyde, and has anti-inflammatory, anti-fibrotic, neurogenic, and neuroprotective properties, which make it not only a cross-linker but a therapeutic agent on its own.[23-29]

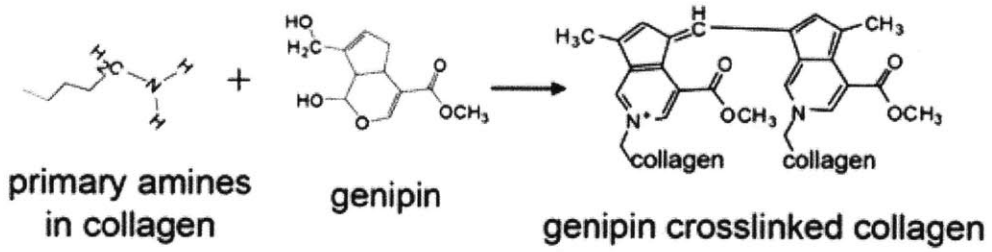

Figure 3-1: Cross-linking of genipin and collagen. From H. Sundararaghavan et al.

Genipin cross-linked collagen is absorbent at 595 nm and fluoresces at 630 nm.[30] This absorbance and fluorescence (590 nm excitation and 630 nm emission filters) thus provides a convenient tool for following the cross-linking and degradation of genipin cross-linked collagen gels. While collagen-genipin fluorescence has been correlated to its mechanical properties, few studies have looked

kinetics of the cross-linking reaction, and none have accounted for the effects of gel absorbance on the observed fluorescence.[30] Specifically, the inner filter effect, which causes a loss in proportionality between the observed intensity and concentration of the flourophore, was not accounted for.[31]

3.3. Overall Goal and Hypotheses

The **goal** of this study was to evaluate the use of genipin as an *in vivo* cross-linker for an injectable collagen gel scaffold. Fluorometric, rheology, and degradation assays were used to evaluate the kinetics of genipin cross-linking, the effects of cross-linking on the gelation time, modulus of elasticity and enzymatic degradation resistance. Unlike previous studies, genipin was being investigated as an *in vivo* cross-linking agent that would not be rinsed out prior to use and would continue to act on the scaffold after gelation. The effect of genipin on select stem cell populations was also investigated.

The **hypotheses** for this chapter are:

1.) The addition of genipin to collagen gels will result in increases in cross-link dependent properties of degradation resistance and shear modulus.

2.) The kinetics of genipin crosslinking of collagen gels is reflected in the absorbance and fluorescence changes of the material.

3.) The viability of cells exposed to genipin will be dependent on cell type, concentration of genipin, and whether they are exposed during the in situ formation of the gel.

3.4. Methods

3.4.1 Materials: Soluble rat-tail type I collagen (3.91 mg/ml) in acetic acid (BD Biosciences, Franklin Lakes, NJ), genipin (Wako Pure Chemical, Japan), type I collagenase (163 U/mg) (Invitrogen, Carlsbad, CA). Buffers were purchased from Invitrogen and were cell-culture grade.

Collagen Gels: Ice cold 1x phosphate buffered saline (PBS), 5x PBS, 1N NaOH and soluble rat tail collagen were combined in that order to obtain 2 mg/ml collagen solutions at pH 7.5 with 1x ionic strength. For gels containing genipin, a stock solution of genipin in 5x PBS (3 mg/ml), made immediately before mixing, was used in place of a volume of 5x PBS to obtain the desired genipin concentration (0-1mM). Thermal gelation of the collagen solutions was induced by warming to 37°C in an incubator.

3.4.2 Absorbance & Fluorescence Measurements: Measurements were taken using a PerkinElmer Wallac 1420 multilabel plate reader with fluorescence technology (Waltham, MA) at 595 & 630 nm (absorbance) or excitation 595 nm, emission 630 nm (fluorescence). Collagen solutions were plated into 96 well plates (100 µl/well) and placed in a 37°C incubator (n=12 independent wells). At regular time

intervals, the plates were taken out of the incubator and measured. Well plates were kept covered and at 100% RH to reduce evaporation. The plates were allowed to cool to RT for 20 min to avoid the effects of temperature variation on the fluorescence intensity.

The fluorescence was corrected for the internal filter effect as described by Palmier, *et al.* **[32]**

$$F_{corrected} = F_{observed} * 10^{\frac{Aex+Aem}{2}} \quad (1)$$

where A_{ex} and A_{em} are the measured absorbance at the excitation and emission wavelengths respectively. The fluorescence data corresponding to varying collagen concentrations with a fixed genipin concentration of 0.5 mM were normalized to the t=1 h value to eliminate the baseline variation in fluorescence due to the differences in collagen matrix density.

3.4.3 Rheological Testing A rheometer (TA instruments AR-G2, New Castle, DE) with a cone and plate geometry (40 mm 2°), was used to determine the gelation time and the storage and loss moduli of the gels (n=3-4). The test conditions employed a constant stress of 0.1 Pa at a frequency of 1 rad/s. Based on our pilot tests, these conditions were chosen to be in the linear viscoelastic regime of the gelled materials and did not interfere with the gelation process. The bottom plate was held at 8°C before the materials were tested at 37°C to prevent premature gelation. A light mineral oil, with a lower viscosity than collagen, was applied around the edges of the cone to reduce evaporation. The gelation time, or gel point, was defined as the time at which the shear storage (G') and loss modulus (G") were equal.

For pre-formed scaffolds, a parallel-plate geometry (8 mm plate) was used to apply a constant shear stress of 1 Pa at a frequency of 1 rad/s. Rheology was performed at a fixed gap of 1044 μm at ~35% compression based on heights of collagen 0 mM gels that best recapitulated the modulus at 1 hour. Sandpaper (400 grit) was applied to both top and bottom platens to avoid gel slippage. Collagen-genipin gels (2 ml) were cast into a 12 well plates and an 8 mm biopsy punch was used to obtain samples for testing. The samples were swollen for 1 hour in 1x PBS and transferred to the stage of the rheometer.

3.4.4 1-D Degradation Assay Collagen gels (0.5 ml, n=3) containing varying amounts of genipin (0-1 mM) were pipetted into a 2 ml cryotube and allowed to gel for a defined amount of time at 37 °C between 1-27 h. Type I collagenase (0.1%, 1 ml, 163U/mg) in 1x PBS with $CaCl_2$, was added on top of the gel and the vial was placed on a shaker table in a 37°C warm room at 150 rpm. After 5 h, the degradation medium was removed, the gels were rinsed with deionized water, frozen, lyophilized overnight, and weighed. The removal time was set by the degradation time for non-cross-linked collagen gels. The dry weights of the scaffolds were compared to the weights of identical gels exposed to 1x PBS buffer for the same amount of time; data are reported as % weight remaining.

The collagenase concentration (0.1 wt%, 163 U/mg) was chosen to provide a standardized, accelerated assay for gel degradation, in order to compare the effect of genipin concentration on gel robustness. The concentration is much greater than what would be found in an inflamed body setting.

An additional degradation assay was conducted with modifications to account for the greater robustness of the gels allowed to cross-link for longer times (*i.e.*, 24 h or greater). Collagen-genipin gels (0.5 ml) were plated in a 24-well plate and allowed to cross-link for 24, 44, or 72 h. Subsequently, 0.5 % collagenase (1 ml) was added for two hours before gels (n=3) were processed and measured as above.

3.4.5 3-D Degradation Assay Collagen-genipin gels (0.5 ml, n=3) with varying genipin concentrations (0-1mM) were cast in 2-ml cryotubes and incubated at 37°C for 1 or 24 h. The gels were transferred from the cryotubes into 24-well plates and swollen in PBS for 1 h. The gels were then exposed to collagenase I (0.1%) on a shaker table (150 rpm); control gels were exposed to PBS instead of collagenase. After 30, 60, 90, or 120 minutes, the collagenase was removed and the gels were washed with PBS on a shaker table for 20 min. The remaining gel samples were collected, lyophilized overnight, and weighed. The dry weights of the gels were compared to the weights of control gels; data are reported as % weight remaining.

3.4.6 Swelling Ratio Collagen-genipin gels (1 ml, 16-mm diameter, 3-4-mm thick, n=43) with varying genipin concentrations (0-1mM) were cast in 24-well plates for 1 or 7 d and then swollen in PBS for 24 h at RT. The disks were scooped up using tweezers and weighed immediately afterwards to obtain the swollen weight. After lyophilization, the disks were weighed to obtain the dry weight. The swelling ratio was calculated using the following equation:

$$Swelling\ ratio = \frac{W_s}{W_d} \tag{2}$$

where W_s is the swollen weight and W_d is the dry weight.

Linear or polynomial regression lines were fit to the data to achieve an R-squared of 0.95 or higher. Half-life times were calculated as the amount of time required to enzymatically degrade the gel to 50% of its original mass.

3.4.7 Gel morphology Environmental scanning electron microscopy (ESEM) was used to observe gel morphology and pore architecture. Hydrogel samples were fixed in 4% paraformaldehyde and 2% glutaradehyde in a buffered solution for 1 h at room temperature. After three 10-min washes in PBS and two 10-min washes in diH_2O, the samples were then dehydrated for 15 min in a series of graded ethanol of 50, 75, 90, 95, 100, 100, 100% concentration respectively. Dehydrated specimens were then critical point dried from ethanol in CO_2 (Autosamdri – 815, Tousimis (Rockville, MD)). The dried gels were

mounted on aluminum stubs using carbon tape, and examined under ESEM (FEI/Philips XL30 FEG ESEM) in low-vacuum conditions with an accelerating voltage of 12-15 kV.

3.4.8 Stem Cell Seeding Marrow-derived pig mesenchymal stem cells (MSCs), prepared as previously described at 400,000 cells/ml, were encapsulated within collagen hydrogels containing various amounts of genipin.[33] Complete medium (DMEM-LG, 10% FBS, 1% penicillin-streptomycin) was pre-warmed in 24-well plates prior to gel plating. Gel solution (0.5 ml) containing MSCs was carefully added to each well to ensure the gel settled to the bottom of the well. This plating technique was done to simulate an environment where the genipin could leach out of the system and react with the surrounding environment (i.e., in the case of cerebrospinal fluid). Media were replaced at 4, 24, and every 48 h thereafter. Additional viability assays configurations were conducted as follows. Gel solution without genipin (0.4 ml) containing MSCs was carefully added to each well as above. After allowing the gel to set overnight, a 6 mm biopsy punch was taken from the center of each 24 well plate and transferred to a new well containing 0.5 ml of media spiked with genipin (gel disk assay). The media was then removed from the center of the original gel and 100 µl of collagen genipin gel was pipetted in and allowed to set for 2 h before adding 0.4 ml cell culture media (peneumbra and edge assay). The effective genipin concentration in each assay is given by:

$$C_{assay} = C_{col-gen\cdot gel}\frac{V_{col-gen\cdot gel}}{V_{media} + V_{cell\cdot gel} + V_{col-gen\cdot gel}} \quad (3)$$

Neural stem cells (F. Gage, Salk Institute, La Jolla, CA) were plated at 90,000 or 400,000 cells/ml. The media were supplemented with 1% penicillin-streptomycin, N2 supplement, and 20 nm/ml FGF to prevent differentiation.[34] Media was replaced after 3 h.

3.4.9 Cell viability Live/dead staining was performed using Calcein AM and Ethidium homodimer (Invitrogen). Cell-encapsulated gels were stained and imaged using a fluorescent microscope. Three random sections of each gel were measured, totaling 500-1500 cells/gel. The cell count was analyzed using Image J software (NIH, Bethesda, MD).

3.4.10 Cell proliferation Cell-seeded gels were collected after 1 and 7 d post-seeding. The samples were first washed in PBS and stored at -20°C until assayed. After lyophilization, samples were digested overnight with Proteinase K (100µg/ml; Sigma) in Tris-HCl-buffer (50 mM Tris, 1mM $CaCl_2$, pH 8.0) at 60°C. Fluorometric quantification of DNA content in the digests was performed using a Quant-iT PicoGreen dsDNA Assay Kit (Invitrogen, Carlsbad, CA). Aliquots of pellet digest were diluted 1:10 in Tris-EDTA buffer (TE, 10mM Tris, 1 mM EDTA, pH 8.0) and processed according to the kit protocol with fluorescence read at 485nm/535nm for 1.0s against a lambda DNA standard on a microplate reader

(Wallac Victor2 1420 Multilabel Counter, PerkinElmer Life and Analytical Sciences, Inc., Wellesley, MA).

3.5 Results

3.5.1 Absorbance and fluorescence

The cross-linking of collagen and genipin molecules induced a blue/purple color change, which could be measured by absorbance at 595 nm as well as a strong fluorescence at the excitation wavelength of 595 nm and emission of 630nm, which served as a unique measure of cross-linking.

For a fixed concentration of collagen, the rate of increase and saturation value of fluorescence intensity was dependent on genipin concentrations (**Figure 3-2a**). Lower genipin concentrations continued to increase in fluorescence for a longer period of time, up to 165 hours (h), most likely due to the decreased frequency of molecular collisions. Further analysis showed the fluorescence intensities were linearly proportional to the log of genipin concentration for all times. The fluorescence of collagen gels without genipin was relatively constant after the onset of gelation. The absorbance of 2 mg/ml collagen gels increased dramatically with genipin concentration (**Figure 3-2b**). This difference was much greater than for fluorescence data on the same gels. The rate of increase and final optical density was dependent on genipin concentration and higher concentrations reached a saturation point more quickly. Little or no change in absorbance occurred with collagen gels alone after the first hour when the gelation was complete.

For a fixed concentration of genipin, the rate of increase for fluorescence intensity as well as the saturation fluorescence, was proportional to the collagen concentration due to the higher density of free amines (**Figure 3-2c**). The fluorescence intensity began to plateau at about 24, 48 and 78 h for 1-3 mg/ml collagen respectively, again due to the density of free-amines. Further analysis showed the fluorescence intensities were linearly proportional to collagen concentration for all times. The initial absorbance of the fixed genipin gels was dependent on the collagen concentration since denser matrices had a higher opacity, however the kinetics of absorbance increase was similar between all gels and reached a saturation value at approximately 97 h (**Figure 3-2d**). A linear dependence of absorbance with collagen concentration is clearly seen when the data were re-plotted with absorbance versus collagen concentration **(Figure 3-3).**

To further elucidate the reaction kinetics of the genipin cross-linked collagen gels, an assay was used to detect genipin released to medium (**Figure 3-4**). Collagen-genipin gels were incubated in equal volumes of Dulbecco's modified Eagle's Medium (DMEM) containing amino acids. The DMEM

contained phenol red, which can interfere with certain fluorescence measurements, but had no effect on the absorbance recorded in this experiment.

DMEM reacted with free genipin within the gels leading to an intense blue/purple color and an increase in absorbance at 595 nm, but little change in fluorescence of the DMEM. At each time point, the difference in absorbance before and after removing the media from on top of the gels was measured. The difference in absorption represented the amount of genipin reacting with the DMEM. After 196 h it was observed that no further genipin could be removed from the gels at all concentrations measured.

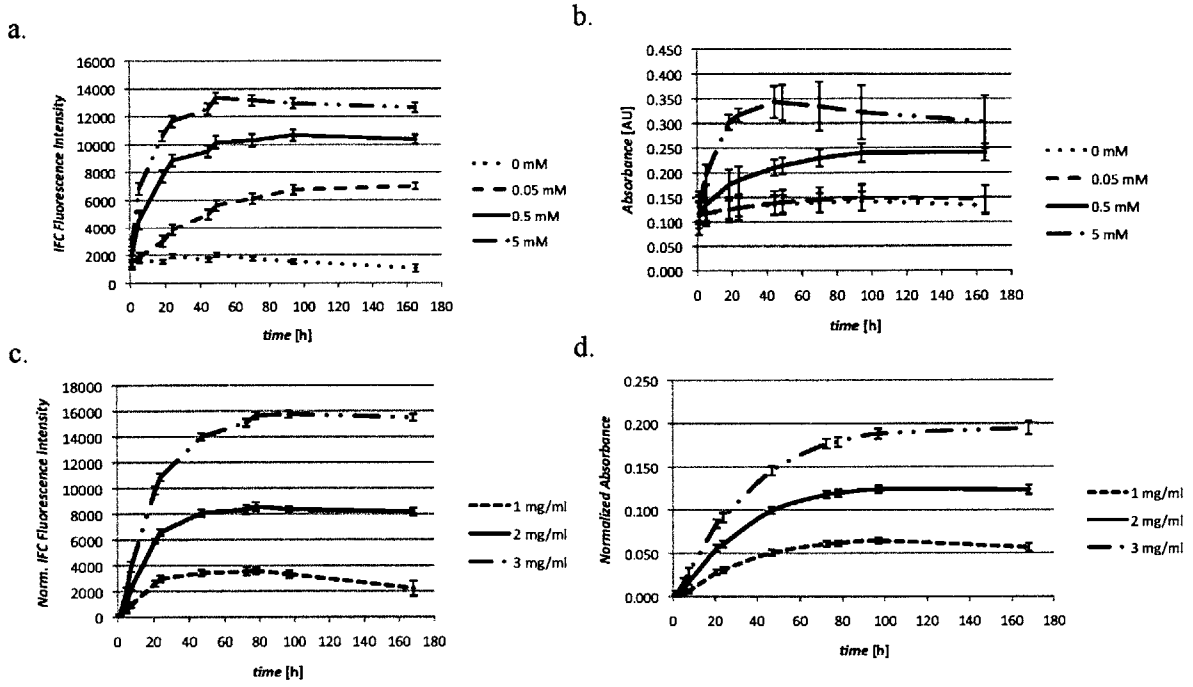

Figure 3-2. a.) Fluorescence measurements (excitation 595 nm/ emission 630 nm) of 2 mg/ml rat tail (type I) collagen gels containing 0-5 mM genipin, n=12 mean ± stdev **b.)** Absorbance (595 nm) measurements of the samples in (a) **c.)** Fluorescence measurements (ex. 595 nm/ em. 630 nm) of 1-3 mg/ml rat tail (type I) collagen gels containing 0.5 mM genipin, n=12 mean ± stdev **d.)** Absorbance (595 nm) measurements of the samples in (c). The internal filter correction was used in fluorescence measurements to account for overlap of ex and em spectra. Figures c & d were normalized to t=1 h to remove optical density differences with collagen concentration.

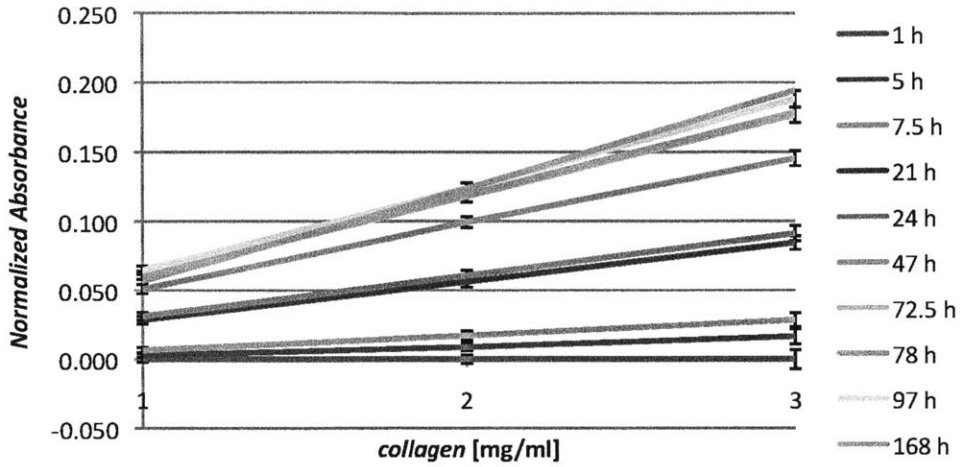

Figure 3-3: Re-plot of figure 1d with absorbance versus collagen concentration for all times. Of note is the linear dependence between absorbance and collagen concentration.

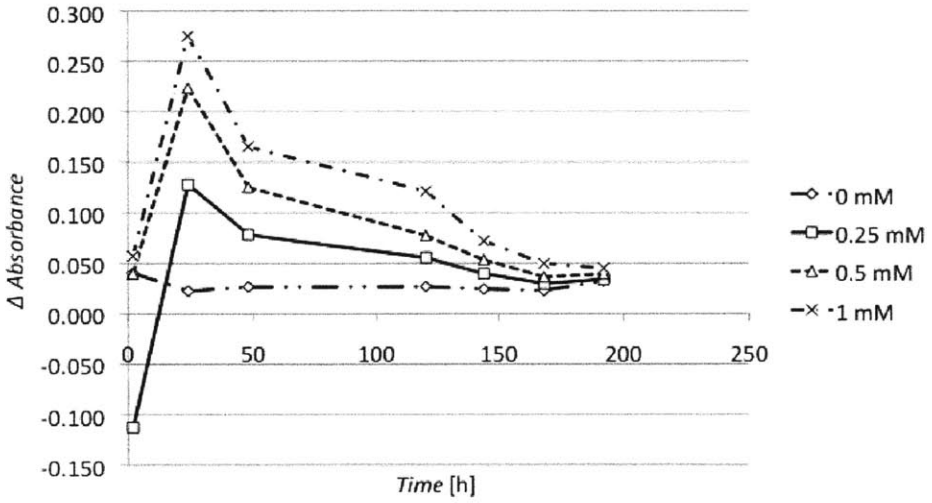

Figure 3-4: Genipin leaching assay where the difference between the gel absorbance with and without cell-media on top was used as a surrogate for how much free genipin was available to react with the amino acid rich media.

3.5.2 Mechanical and gelation studies

The principal metrics derived from the rheological testing were: gel point (time at which the shear storage modulus G' = the shear loss modulus G"); G' at 1500 seconds; and rate of shear storage modulus, G' increase (**Table 3-1**). The rate of increase was taken in the linear approximation of the G' versus time curve ($R^2 > 0.99$). Examples of the rheological data at 37°C are shown in (**Figure 3-5**).

Table 3-1. Rheological evaluation of initial gelation kinetics of rat-tail collagen- genipin gels at 37°C. n=3-4, mean ± SD

Genipin [mM]	Gel point [s]	G' [Pa] at 1500 s	Rate of increase G' [Pa/s]
0	51.1 ± 1.5	20.8 ± 0.9	$2.9 \times 10^{-3} \pm 0.4 \times 10^{-3}$
0.25	50.4 ± 0.9	31.5 ± 5.7	$8.5 \times 10^{-3} \pm 2.5 \times 10^{-3}$
0.5	49.4 ± 0.7	33.8 ± 4.7	$10.2 \times 10^{-3} \pm 2.8 \times 10^{-3}$
1.0	47.0 ± 4.6	45.1 ± 6.0	$17.4 \times 10^{-3} \pm 3.1 \times 10^{-3}$

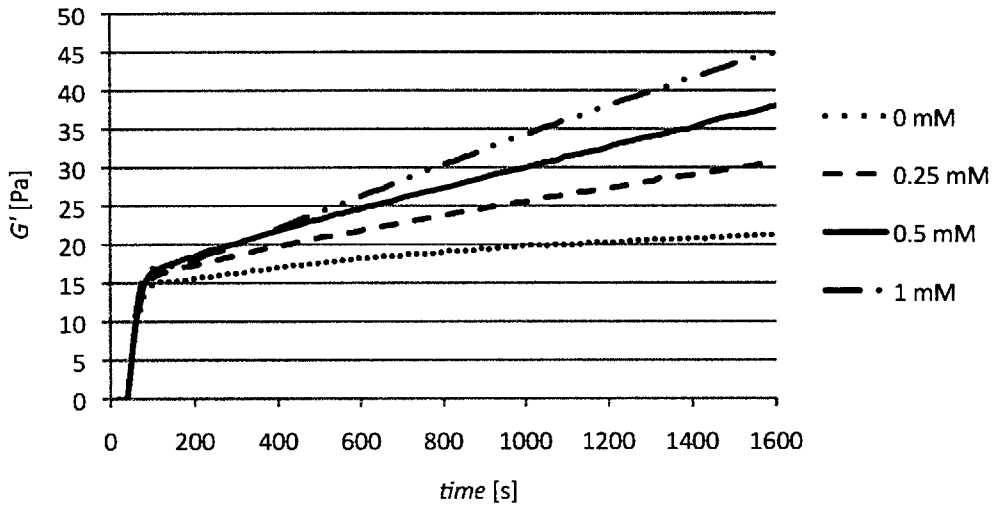

Figure 3-5. Example of rheological data showing the immediate effect genipin has on strengthening collagen gels.

The gel point for the non-cross-linked collagen gel was 51 s. There was an 8% decrease in the gel time for the gels cross-linked with the highest concentration of genipin (1mM; Table 1). There was no significant effect of genipin concentration in gel point by 1-factor ANOVA (p=0.22). G' for the collagen gels cross-linked with 0.25 mM genipin was 50% higher than the value for the non-cross-linked gel, and

the modulus for the samples cross-linked with 1mM was over 2-fold higher than the non-cross-linked G' value (**Table 3-1**). One-factor ANOVA demonstrated a statistically significant effect of genipin concentration on storage modulus ($p=0.022$; power=0.99). Fisher's PLSD post hoc testing showed that all group comparisons were statistically significant except for 0.25 versus 0.5 mM genipin. The rate of increase in G' increased from 3-fold to about 6-fold higher for the 0.25 and 1 mM genipin concentrations, compared to the non-cross-linked gels (**Table 3-1**). One-factor ANOVA demonstrated a statistically significant effect of genipin concentration on the rate of increase of the storage modulus ($p=0.001$; power=1). Fisher's PLSD post hoc testing showed that all group comparisons were statistically significant except for 0.25 versus 0.5 mM genipin.

In order to fine tune of the gel time and shear modulus of the gels, the pH and ionic strength of the gel were varied. Additionally, the interference of cell culture media and lipid microtubules with the gelation processes was explored. The shear modulus of the collagen and collagen-genipin gels at 600 s were directly proportional to the amount of NaOH added to the sample (increasing pH) (**Figure 3.6**). The modulus peaked at pH 8-8.5 for collagen gels and 9-9.5 for collagen genipin gels (2mg/ml, 0.5 mM), after which the modulus sharply declined (**Figure 3-6**). For all gels tested, the gel time remained constant with pH up till approximately pH 9 where it began to increase. Unlike changes in pH, the moduli of the collagen-genipin gels was not significantly affected by the ionic strength of the gel (**Figure 3-7a**), however the gel time was strongly proportional on ionic strength (**Figure 3-7b**). Combining a decreased ionic strength with increased pH produced stiffer gels with shorter gelation times (**Figure 3-7a,b**). The addition of cell medium to collagen-genipin gels in place of PBS buffer did not have an effect on the gel time or short-term modulus as compared to using PBS buffer (**Figure 3-8**). This relation held true for the pH range of 7-8.5. The addition of LMTs to the gels had no significant effect on the gel time or modulus at 0.1 mg/ml, however at 0.4 mg/ml the LMTs began to interfere with the gel causing a decrease in modulus and increase in gelation time (**Figure 3-8**).

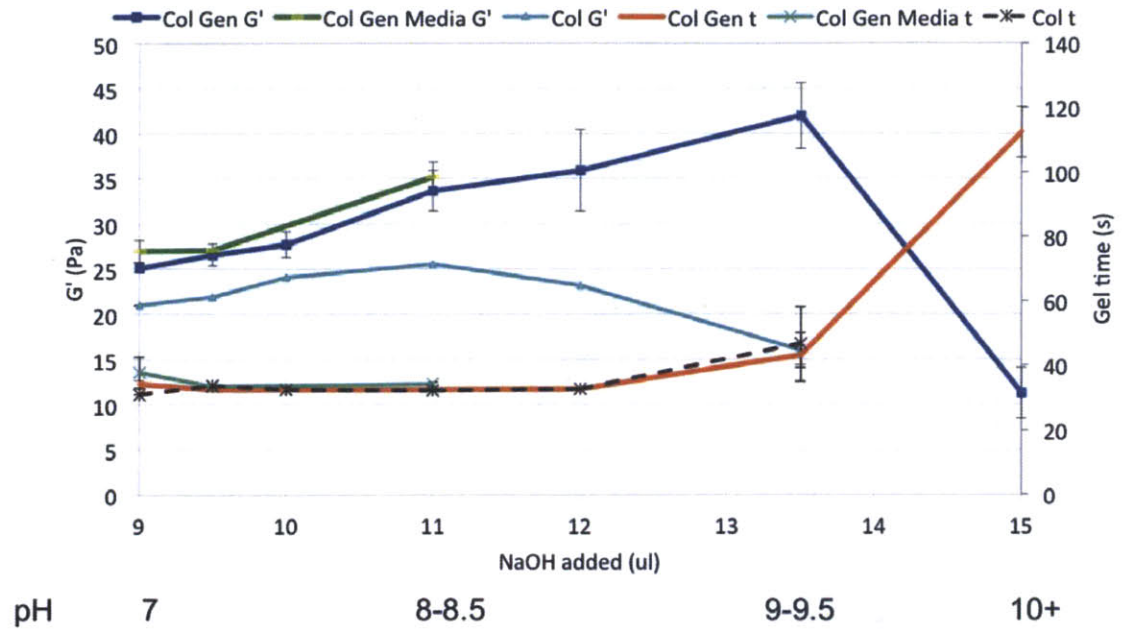

Figure 3-6: Dependence of rheological properties on pH of collagen (2mg/ml) and collagen (2mg/ml)-genipin (0.5 mM) ± cell culture media gels, Left axis (top 3 curves) shear modulus at 600s. Right axis (bottom 3 curves gel time. All gels were at 1x ionic strength. n=3 mean ± stdev.

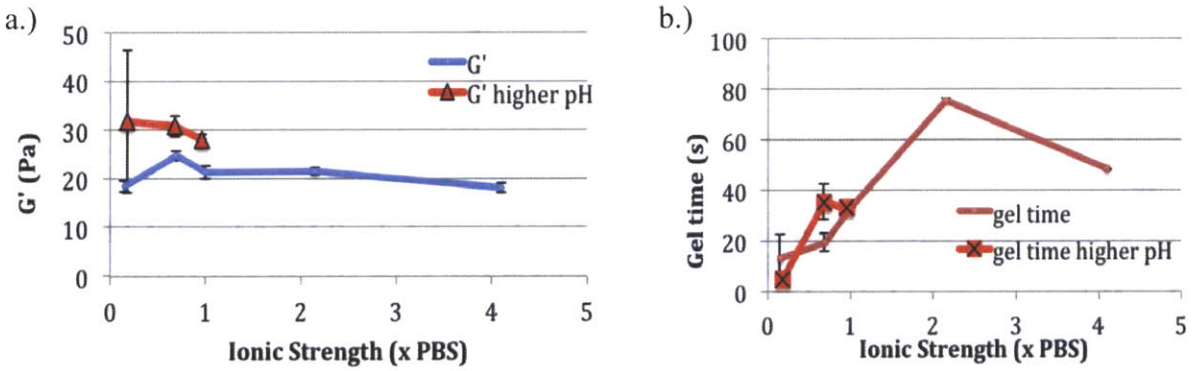

Figure 3-7: Dependence of rheological properties on ionic strength of collagen (2mg/ml)-genipin (0.5 mM) gels **a.)** Shear modulus at 600 s, blue line= pH 7, red line= pH 8 **b.)** Gel time, redline no marker= pH 7, red line black marker= pH 8. n=2-3 mean ± stdev.

The G' of collagen-genipin gels over a longer cross-linking period was determined by rheological testing of preformed samples, tested 24, 48, and 72 h after gelation (**Figure 3-9**). The time required for G' to reach a plateau value was dependent on the amount of genipin, with 1 mM samples saturating in properties within the first 24 h and the samples cross-linked with 0.5mM genipin saturating at 48 h (**Figure 3-9**). The gels cross-linked with the lowest genipin concentration appeared to continue to increase in modulus through 72 h. The 72 h modulus for the gels cross-linked with 1 mM genipin concentrations was 220 ± 33 Pa, compared to approximately 28 ± 0.6 Pa for the non-cross linked gel (**Figure 3-9**). Two–factor ANOVA revealed statistically significant effects of time and genipin concentration on the modulus (for both, p=0.0001; power=1). Fisher's PLSD post hoc testing showed that all group comparisons were statistically significant.

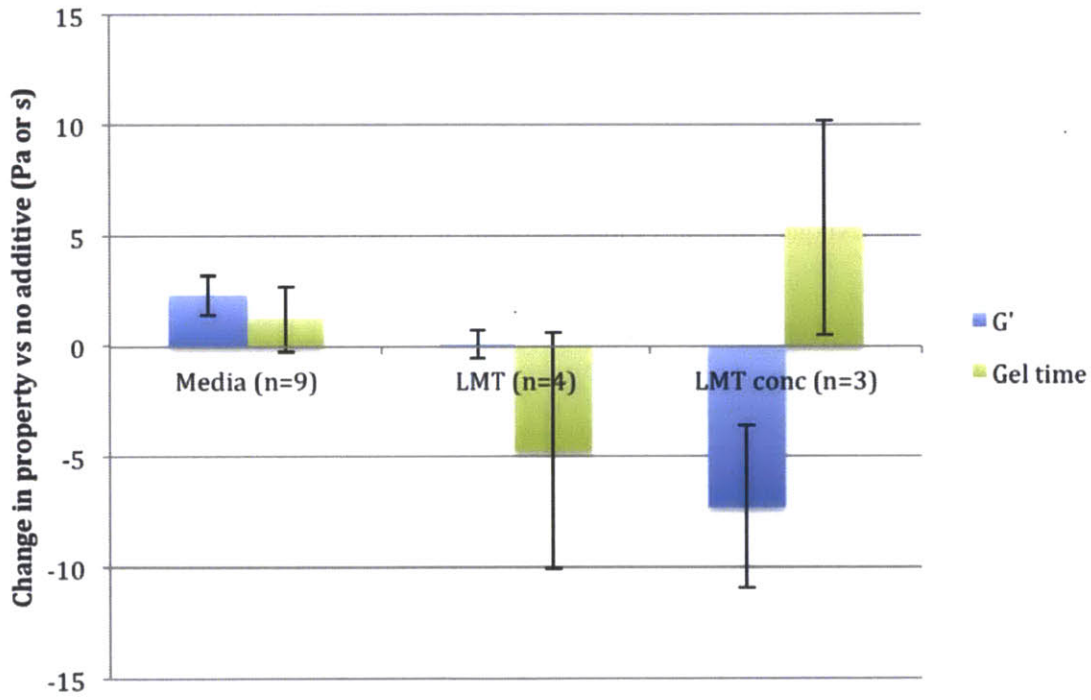

Figure 3-8: Interference effects of cell culture media and lipid microtubules (LMT 0.1 mg/ml, LMT conc 0.4mg/ml) on the rheologic properties of collagen-genipin gels. Shear modluls blue bar, gel time green bar. Values represent relative changes in property as compared to an identical sample without the specified additive. n=3-9 mean ± stdev.

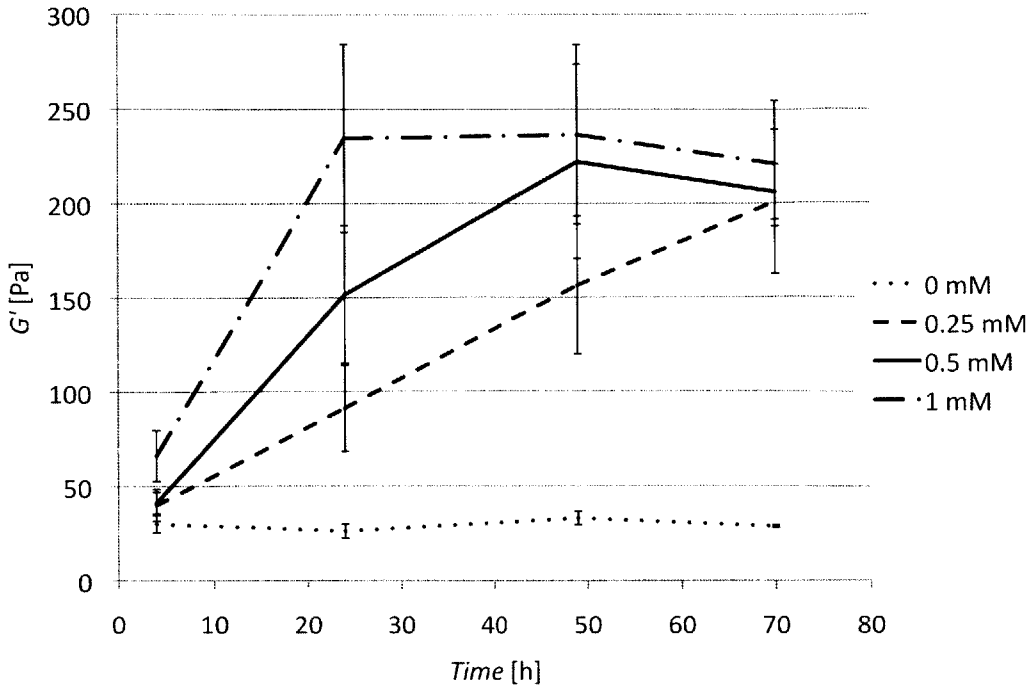

Figure 3-9: Long term rheology studies on preformed scaffolds, elucidating the saturation in gel properties. N=3-4 mean ± stdev.

3.5.3 Degradation studies

To complement the photometric, fluorometric, and mechanical testing data, a series of 1-D and 3-D degradation studies were performed to assess the effects of the degree of cross-linking imparted by genipin (**Figures 3-10, 3-11**).

a.)

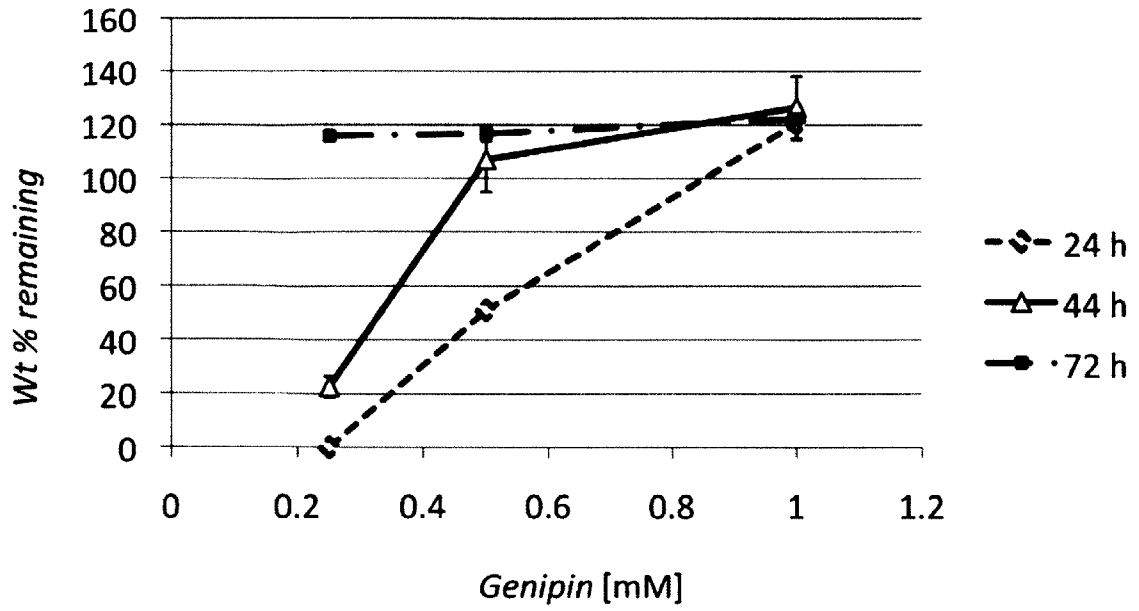

b.)

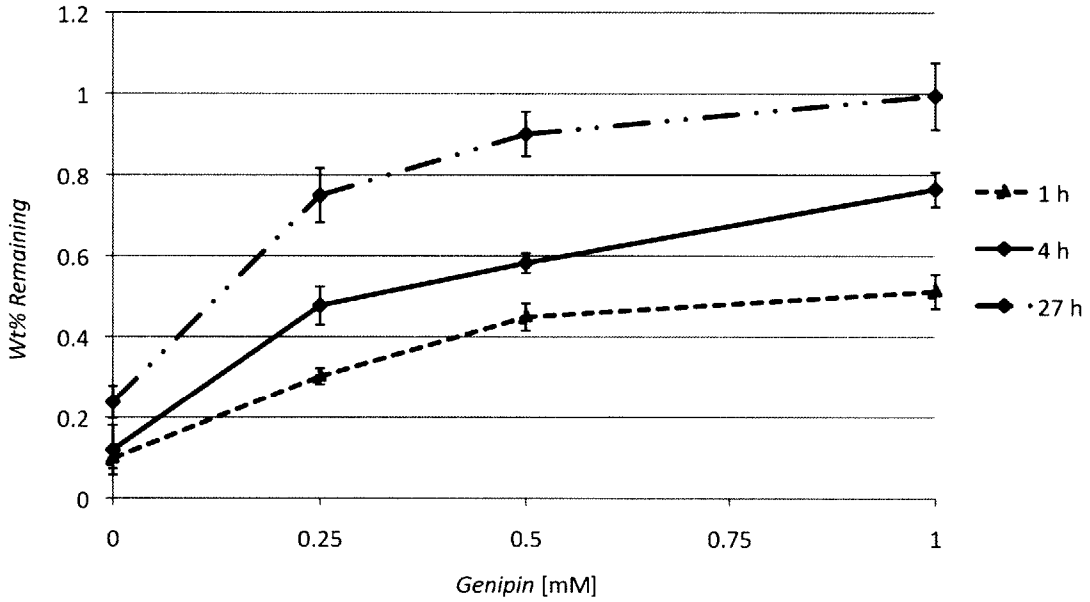

Figure 3-10. a.) 1-D degradation assay of collagen-genipin gels showing the immediate effect of adding genipin on the robustness of the gels. n=3 mean ± stdev **b.)** Longer term degradation assay of collagen gels.

The 1-D degradation curves for the % weight remaining after 5 h of exposure to 0.1 % collagenase, reflecting the degradation resistance of the gels, increased with genipin concentration and maturation time (*i.e.*, 1, 4, and 27 h of incubation; **Figure 3-10a**). Of note was the 3-fold increase in % weight remaining of 0.25 mM genipin gels matured for only one hour as compared to non-cross linked gels. The degradation resistance of the gels cross-linked with the lowest genipin concentration was

almost 4-fold higher for the samples, which were allowed to mature for 27 h prior to exposure to collagenase (**Figure 3-10a**). Two–factor ANOVA revealed statistically significant effects of the maturation time prior to the degradation assay and genipin concentration on the % weight remaining (for both, $p=0.0001$; power=1). Fisher's PLSD post hoc testing showed that all group comparisons were statistically significant.

Degradation experiments were also conducted on gels allowed to cross-link for 24, 44, and 72 h (**Figure 3-10b**). The gel cross-linked with the lowest genipin concentration (0.25mM) for 72 h did not undergo a weight loss, under the collagenase exposure of the test. Virtually no weight loss was similarly detected for the gel cross-linked for the shorter time period of 44 h, when cross-linked with 0.5mM genipin. The samples allowed to gel for 24 h demonstrated no weight loss when cross-linked with 1 mM genipin. A % weight remaining greater than 100%, was due to the entrapment of high concentration collagenase within the gel.

A 3-D model for degradation was used to further investigate the gel's resistance to degradation. Collagen-genipin gels were incubated for 1 and 24 h, Gels matured for 24 h showed greater resistance to degradation than those matured for 1 h (**Figure 3-11**). Furthermore, an increase in genipin concentration increased the gel's resistance to degradation, reflected in a higher % weight remaining. Half-life calculations (**Table 3-2**) showed that gels matured for 1 h exhibited half-life times from 23.3 ± 7.2 min for collagen-only gels to 90 ± 11 min for 1.0 mM genipin gels. Gels matured for 24 h exhibited half-life times up to 260 ± 40 min for 1.0 mM genipin gels. ANOVA testing revealed a significant effect of maturation time ($p<0.001$) and genipin concentration ($p<0.001$) on half-life.

a.)

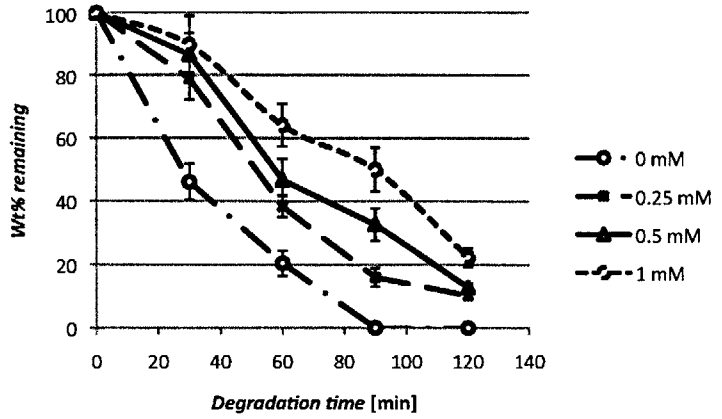

b.)

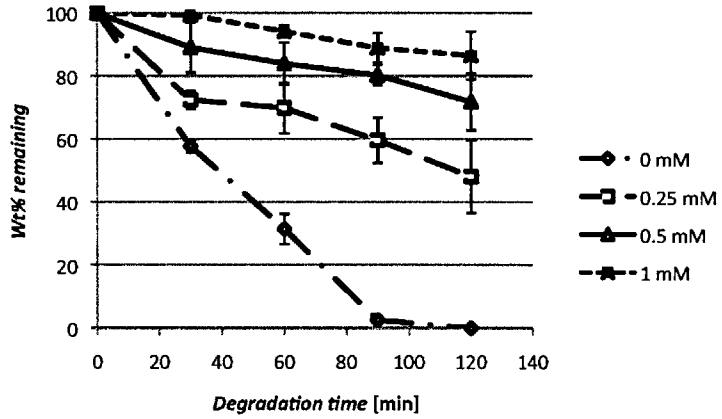

Figure 3-11: a.) 3-D degradation assay, collagen-genipin gel that has been matured for 1 h, degraded for 30, 60, 90, 120 min **b.)** 3-D degradation assay, collagen-genipin gel that has been matured for 24 h, degraded for 30, 60, 90, 120 min. *Data in collaboration with Dr. Karen Ng

Table 3-2: Half-life calculation of collagen-genipin gels after degradation in 0.1% type I collagenase, from figure 4. n=3, mean ± SD. *Data in collaboration with Dr. Karen Ng.

Genipin [mM]	Half-life [min]	
	1 h maturation	24 h maturation
0	23.3 ± 7.2	38.8 ± 1.4
0.25	54.6 ± 1.5	94 ± 11.4
0.5	66.1 ± 2.7	181.1 ± 47.2
1	89.5 ± 10.7	260 ± 40

3.5.4. Swelling ratio and gel morphology

The swelling ratio of collagen-genipin gels formed with different concentrations of genipin was calculated (**Figure 3-12**). The swelling ratio of collagen alone is 77.2 ± 1.5 and 89.7 ± 22.8 at 1 and 7 days (d), respectively. With the addition of 0.25mM genipin, the swelling ratio increases to 109.6 ± 17.4 and 117.6 ± 9.2 at 1 and 7 d, respectively. With the further addition of genipin, the swelling ratio decreases, indicating that the swelling capacity was reduced due to more cross-links.

Collagen-genipin gels exhibited fibrillar network of collagen fibers with diameter of about 75 nm (**Figure 3-13**). Furthermore environmental scanning electronmicroscopy (ESEM) imaging revealed that

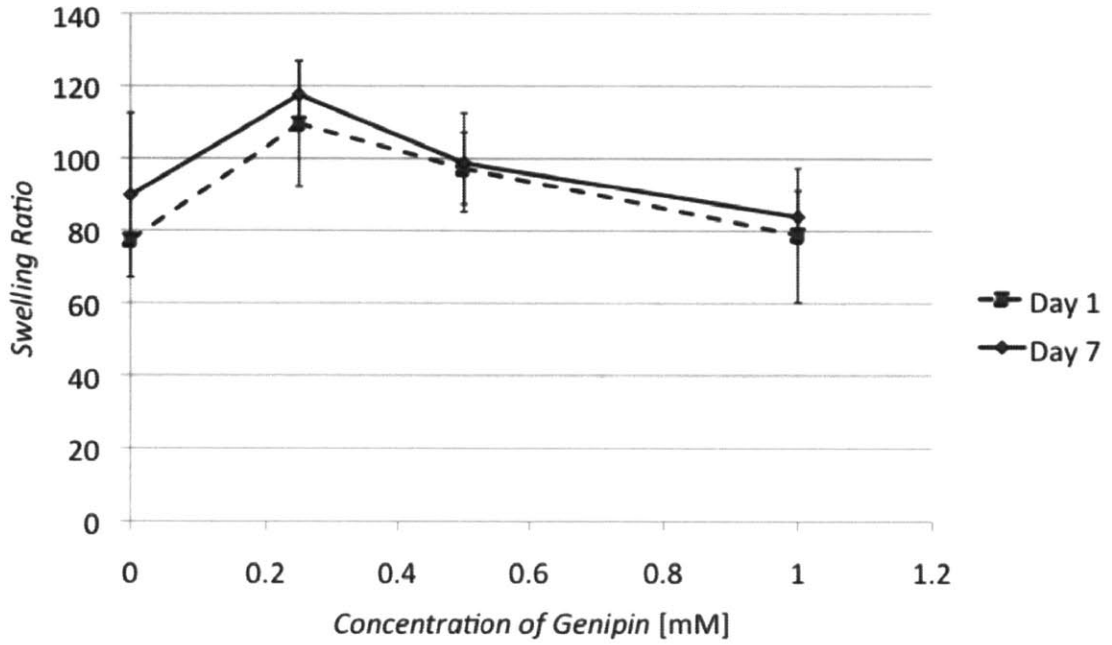

Figure 3-12: Swelling ratio of non-cell-seeded gels (n=3) *Data in collaboration with Dr. Karen Ng.

pore size decreased with increasing genipin concentration, supporting the swelling ratio results.

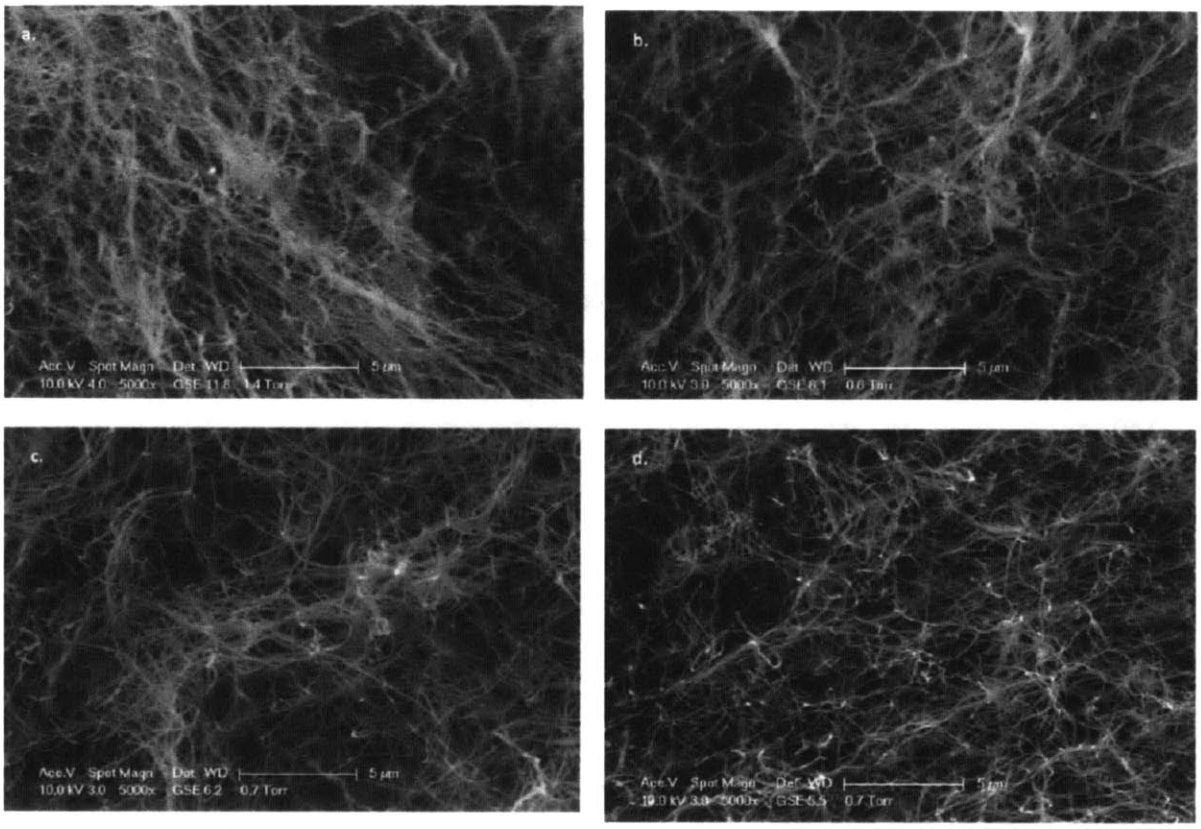

Figure 3-13. ESEM images (gels critically point dried)A: collagen only B: collagen + 0.25 mM genipin C: collagen + 0.5 mM genipin D: collagen + 1.0 mM genipin. *Data in collaboration with Dr. Karen Ng.

3.5.5 Stem cell-seeded collagen gels

Goat and pig MSCs could be incorporated into the collagen-genipin gels and survive the gelation process. These cells could also be incorporated in the gel after being injected with the gel solution into an equal volume of media. Live-dead staining was used to assess cell viability at 1,3,7, and 10 d post gelation (**Figure 3-14a**). Viability was maintained at similar levels to the control (0 mM genipin group) up to concentrations of 0.5 mM at 10 d. Also of note was that unlike non-cross-linked gels, genipin-containing gels did not undergo contraction by MSCs.

Proliferation studies on MSC-encapsulated collagen-genipin gels (**Figure 3-14b)** shows that there was a significant increase in DNA content for MSCs encapsulated in collagen-only and 0.25mM genipin gels. Specifically, DNA content increased from 0.053 ± 0.006 μg to 0.278 ± 0.028 μg (a 6-fold increase) for collagen-only gels and increased from 0.057 ± 0.011 μg to 0.383 ± 0.022 μg (a 6-7-fold increase) for 0.25mM genipin gels. For genipin concentrations 0.5 mM or greater, DNA content levels were

maintained or decreased from 1 to 7 d. The morphology of of MSCs within the gel is shown in (**Figure 3-15)**

a.)

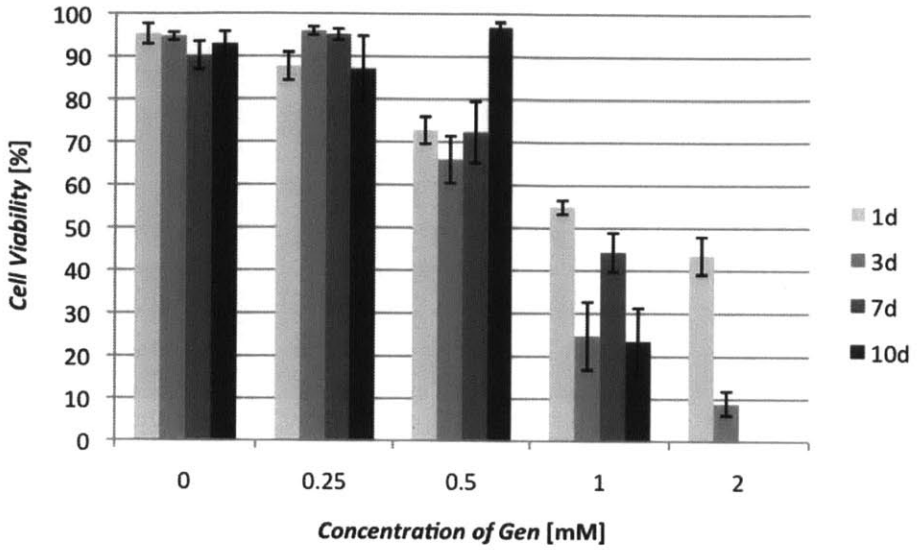

b.)

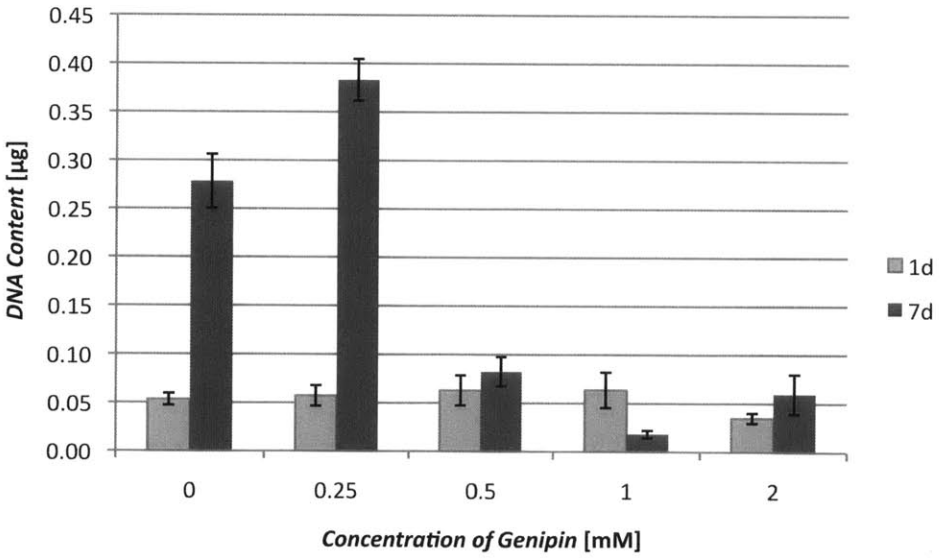

Figure 3-14. a.) Porcine mesenchymal stem cell viability assay using a live/dead stain at up to 10 days post encapsulation in collagen-genipin gels (n= 6 gels) **b.)** pMSC proliferation (n=6).

*Data in collaboration with Dr. Karen Ng.

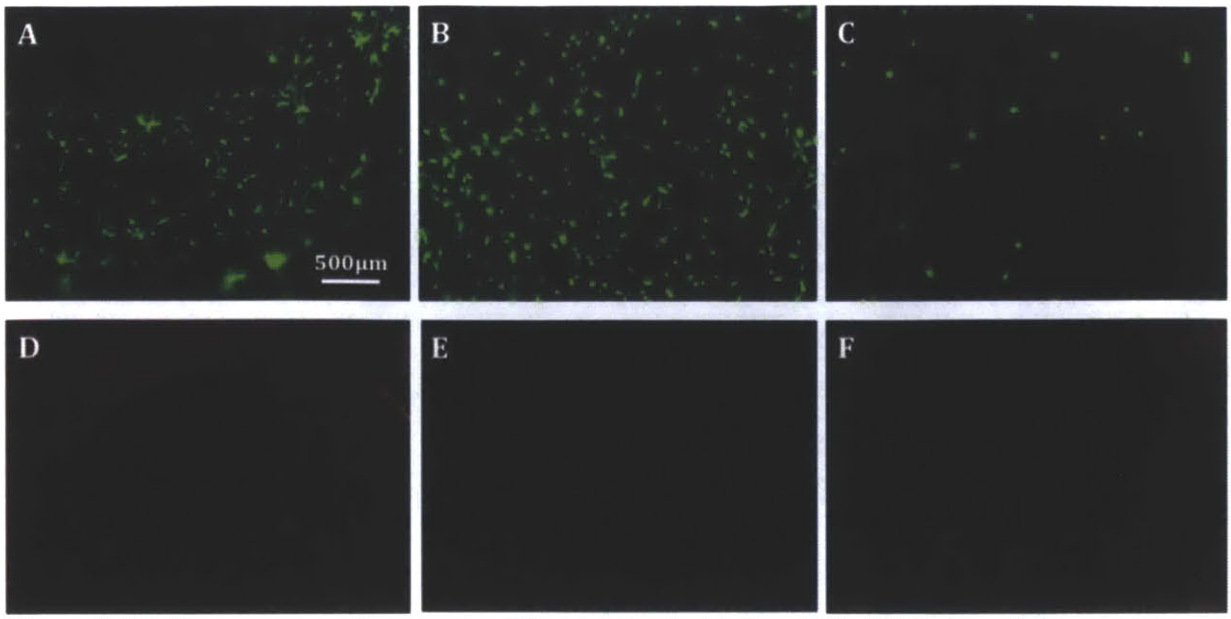

Figure 3-15: Fluorescence micrographs of live-dead cell staining of pig MSCs in collagen-genipin gels at 7 days. A. Live: collagen-only B. Live: 0.25mM genipin C: Live: 0.5mM genipin D: Dead: collagen-only E: Dead: 0.25mM genipin F: Dead: 0.5mM genipin

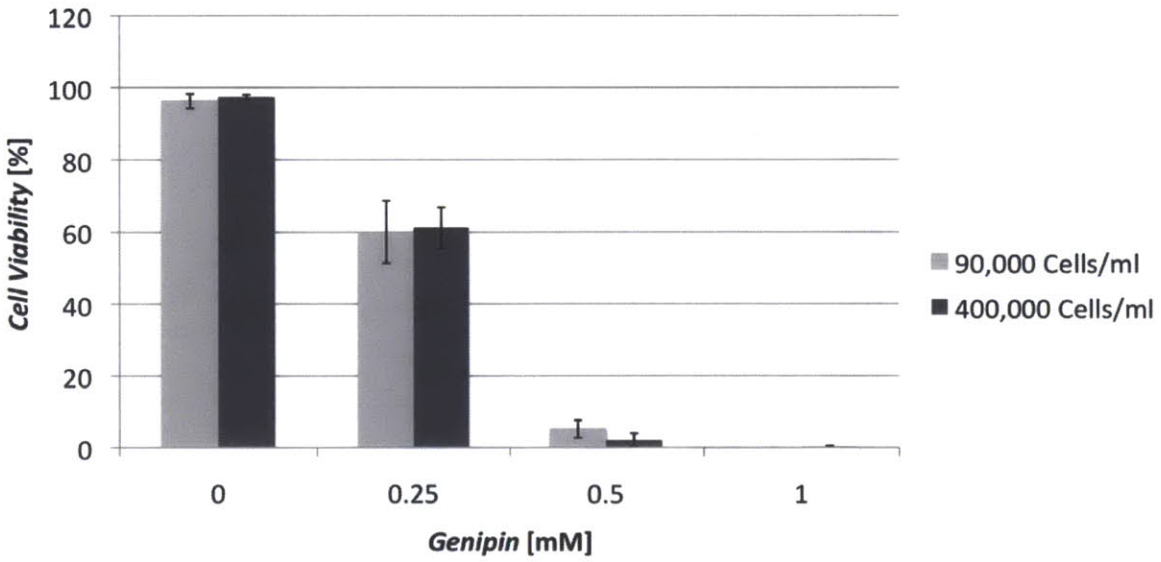

Figure 3-16. NSC viability assay using live dead stain at 24 hours using 2 cell seeding densities. (n= 4 gels) mean ± stdev.

Neural stem cells were more sensitive to the genipin contained within the gel solutions. At genipin concentrations of greater than 0.25 mM there was a significant decrease in the viability of NSCs (**Figure 3-16**). Higher cell seeding densities were not beneficial for enhancing cell viability.

a.) Penumbra

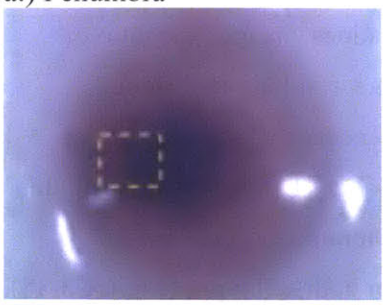

disk in media

b.)

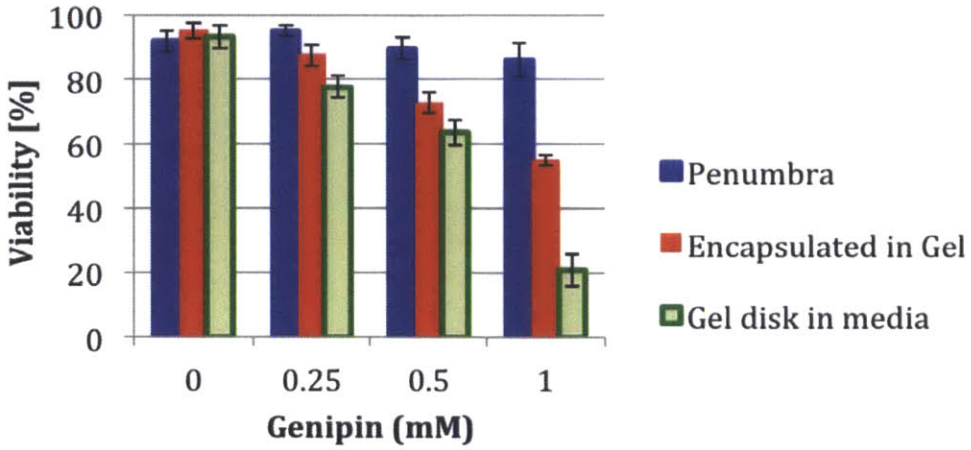

c.)

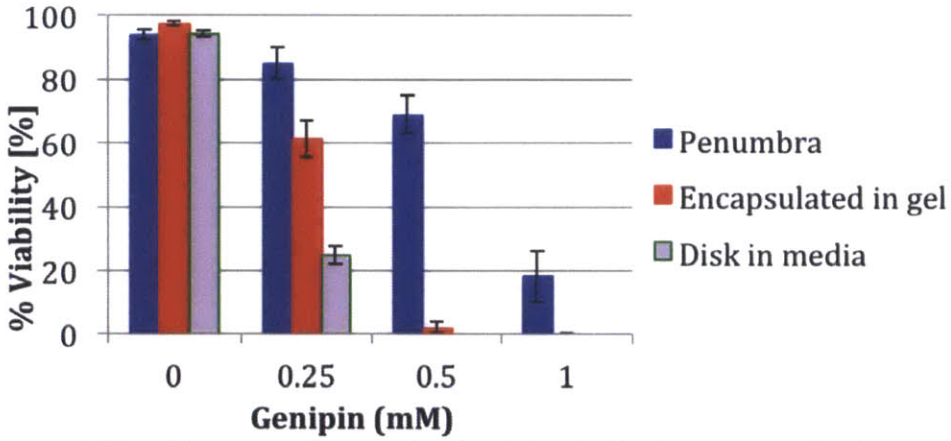

Figure 3-17: a.) Pictures of peneumbra (with box indicating region of evaluation) and disk in media cell viability assay configurations. Encapsulated in gel data is from figures 2-14, 2-16 **b.)** MSC viability assay using live dead stain at 24 hours using a several assay configurations. N=4-6 mean mean ± stdev. **c.)** NSC viability assay using live dead stain at 24 hours using a several assay configurations. N=4-6 mean mean ± stdev.

To further elucidate the effect a collagen-genipin gel would have on cell populations *in vivo*, several configurations of the viability assay were examined. The configurations changed the ratio of genipin containing volume (in media or in the gel) to cell seeded gel volume, resulting in different effective genipin concentrations seen by the cells. There was a strong dependence of cell viability on assay configuration for both mesenchymal and neural stem cells (**Figure 3-17**). To further elucidate this phenomena, the effective concentration of genipin seen by the cells was determined (**equation 3**). Plotting the viability vs effective concentration resulted in a linear trend for both cell types (**Figure 3-18**).

a.)

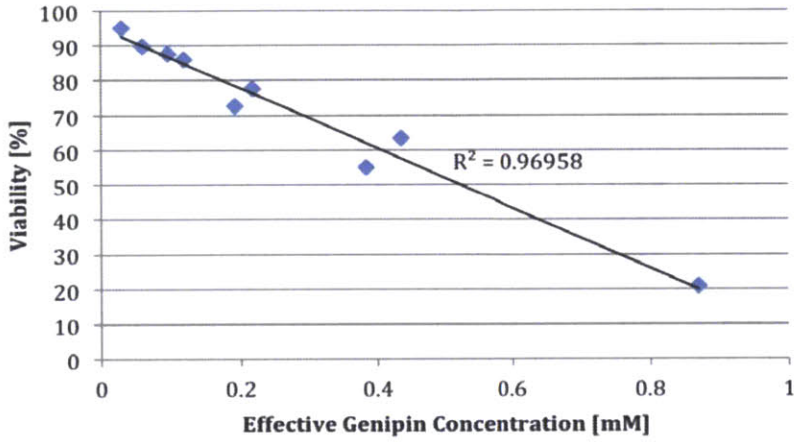

b.)

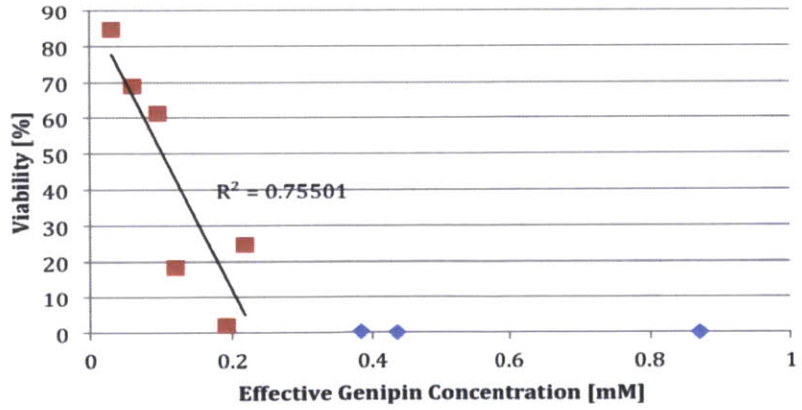

Figure 3-18. a.) Figure 2-17 b plotted as a function of viability vs. effective genipin concetration within the assay as determined by equation **b.)** Figure 2-17 c plotted as a function of viability vs. effective genipin concetration within the assay as determined by equation 3. Linear regression was taken on the values in red which represent viabilies >0.

3.6. Discussion

3.6.1. Cross-linking of collagen and genipin:

Acid solubilized collagen is a thermogelling material, which undergoes a sol-gel transition upon warming above 4°C, when brought to physiologic pH and ionic strength, to form a fibrillar gel network.[35] The reaction kinetics are temperature-dependent, occurring on the order of seconds to minutes close to 37°C.[36] The telopeptide regions among triple helices play an important role in the formation and stabilization of the collagen fibrills.[37] Collagen has approximately 90 amine groups per collagen molecule, dispersed throughout the triple helical and telopeptide regions.[38] These primary amine groups provide cross-linking sites for genipin.

Genipin reacts non-specifically with primary amine groups to produce a secondary activated form of genipin, which can subsequently polymerize with other genipin molecules.[39] The ability of genipin to polymerize allows for the formation of intrahelical, interhelical, and intermicrofibrillar cross-links throughout the fibrillar collagen gel. The wide variety of covalent cross-links gives genipin-cross-linked collagen gels a high resistance to collagenase degradation as multiple parts of the collagen molecule and collagen fibrils can be linked together.[40]

In our study, swelling studies and scanning electron microscopy (SEM) images showed decreasing pore size and swelling ability with increased genipin concentration and maturation time. These findings are consistent with previous results that examined the pore morphology of collagen/chitosan-genipin gels.[41] The exception was 0.25 mM genipin, which exhibited a higher swelling ratio. This observation may be attributed to the increased strength of the gel, which allowed the gel to stand under its own weight and entrap water as opposed to the collagen-only gels, which sagged under their own weight. After 1 day there was little change in swelling properties of the gels, which reflects that most cross-linking occurs over the first 24 hours.

3.6.2. Absorbance and fluorescence properties

In the presence of oxygen, genipin-bound amines turned blue in color and increased in absorbance at 590 nm.[39] The blue pigment is believed to be composed of polymerized genipin molecules containing up to 44 monomer units of genipin with more highly absorbent pigments consisting of higher molecular weight chains.[42] Therefore, the confounding factor of genipin polymerization makes it difficult to use absorbance as an absolute indicator of the extent of cross-linking of collagen gels.

The cross-linking of collagen molecules with genipin also fluoresces at 630 nm.[30] This is a unique marker for collagen cross-linking and does not occur strongly with amino acids alone despite high absorbance at 590 nm (data not shown). Similarly, the reaction of genipin with amines on chitosan

polymers, induces a characteristic peak fluorescence at 470 nm with an absorbance maximum at 369 nm.[43] The fluorescence of collagen-genipin gels can therefore be used as a surrogate *in situ* measurement of cross-link dependent gel properties such as stiffness and degradation resistance. However, since the absorbance and fluorescence spectra of the gel overlapped, there were effects of *a.)* the absorbance of incident light before it reached the point at which luminescence was observed and *b.)* re-absorption of emitted light before it left the gel.[31] Therefore a correction for the interference caused by the internal filter effect as described by was used to restore the fluorescence-concentration proportionality.[32]

Exploration of absorbance and fluorescence characteristics over a broad range of genipin concentrations from 0-5 mM with a fixed collagen concentration of 2 mg/ml, yielded a linear relationship between fluorescence and log (genipin concentration) for all times. A linear relationship between fluorescence and collagen concentration existed from 1-3 mg/ml, using a fixed concentration of 0.5 mM genipin, for all times. As the genipin concentration increases, the equilibrium number of reacted amines increases, but must saturate as the potential number of free-amines remaining decreases. As collagen concentration is increased using a constant genipin concentration, the equilibrium is shifted and a greater total number of amines can be reacted.

There was a direct relationship between both genipin and collagen concentration and rate of fluorescence increase, and higher genipin concentrations or lower collagen concentrations caused a more rapid plateau in fluorescence intensity. Together, these results show that the reaction rate is dependent on the concentration of both free amines and genipin, which affects the frequency of molecular collisions. The saturation time of gel fluorescence is decreased as the concentration of genipin increased, thus increasing the collision frequency, or density of free-amines decreased at a constant genipin, thus increasing the ratio of genipin:collagen.

Of particular interest to our study, the saturation of fluorescence in gels containing 0.5 mM gels occurred at approximately 48 h, corresponding with the saturation of both mechanical properties (via rheological measurements of pre-formed gels) and degradation resistance (via long term degradation assay) of the gel. There was also a large increase in fluorescence of the gels over the first 24 h, which mirrored the results of mechanical and degradation experiments. The saturation point of absorbance for the same gels was almost twice as long, as 96 h, potentially due to the additional absorbance gained from polymerizing genipin.

The absorbance of genipin proved useful as a metric of genipin leaching from the gel. Overall, genipin was a slowly acting cross-linker, taking days to lose its activity. While most of the cross-linking appeared to happen over the first 24-48 h, active genipin remained within the system for up to a week. To

further elucidate the reaction kinetics of genipin and collagen gels, an assay for the leaching of genipin from the gels was created (see Experimental section). After 196 h it was evident that all samples returned to baseline collagen values (**Figure 3-4**). These results confirmed that genipin remained in the gel for an extended period of time to resist degradation and could act as a therapeutic itself after implantation.

3.6.3. Mechanical and degradation properties

For *in vivo* applications, the properties of an injectable material will be difficult to predict shortly after implantation. Therefore, *in situ* rheology and short-term degradation studies were conducted to explore the immediate effect of genipin on gel properties. The concentrations explored in these experiments were based upon the cell viability data presented in this paper.

The addition of genipin to solutions of collagen resulted in a slight decreasing trend in the gel point (G'=G") at 37°C. While a difference in gel point for collagen-genipin gels of varying genipin concentration could not be determined by the testing setup at 37°C, a lower temperature above the LCST of collagen (28°C) was employed to observe the improvement in setting properties with genipin (data not shown) although this would not correlate to the actual application of the gel.

A more substantial dose dependent effect was noted in the rate of increase in shear storage modulus (G'). After the initial gelation period, the moduli of collagen-genipin gels exhibited a linear rate of increase in modulus, proportional to the concentration of genipin cross-linker **(Figure 3-5)**. G' at 1500 seconds served as a comparison point between gels that relates to the time at which the surgical procedure would be complete and the gel properties will begin to be affected by endogenous effects. By 1500 seconds (~23 minutes) 0.5 and 1 mM genipin containing gels were ~50 and 100% stiffer than non-cross-linked collagen gels respectively. While the G' of the collagen-only gel saturated by 1 h, gels containing various concentrations of genipin were still increasing in modulus signifying that the cross-linking reactions were still taking place.

The gelation of soluble collagen is primarily dependent on three factors, temperature, ionic strength of the solution, and pH. Since the gelation temperature of an injectable gel is fixed, the pH and ionic strength of the solution can be tuned. Lowering the ionic strength of the solution favors a more rapid gelation as noted in **Figure 3-7**. A low ionic strength, there is a decrease in the driving force for "salting in" (solubilizing) of collagen monomers. Additionally, fewer electrolytes in the solution increase the interaction between charged amino acids on collagen, leading to aggregation and gelation.[44] At higher pH, there is less lateral aggregation resulting in slender tightly packed fibers (decreased fiber diameter, decreased pore size, and increased fiber length), which would lead to stiffer gels as noted in **Figure 3-6** but no change in gelation speed.[44] The effects of pH on collagen gels containing genipin

were more profound than collagen gels alone **Figure 3-6**. Genipin has an optimum cross-linking reaction rate at pH of 8-9 and at higher pH; there is an induction of self-polymerization of genipin monomers to form long bridges between cross-linking sites.[45-47]

The saturation of G' as determined by pre-formed rheology studies, indicated that all gels treated with 0.25-1 mM genipin reached a similar modulus but the time course to reach the final modulus was dependent on genipin concentration. The modulus of all gels at 72 h (saturation modulus) was in the range of moduli for spinal cord parenchyma tissue.[48]

Standardized degradation assays can provide simple metrics to predict an important *in vivo* property of the gel; its persistence to provide a provisional stroma for axons and supportive cell populations. It also provides a reliable high-throughput method for comparing the extent of cross-linking in collagen gels with respect to both genipin concentration and maturation time.

3-D degradation experiments were conducted at 1 and 24 h and for degradation times of 30-120 min to establish a kinetic profile for gel degradation, from which a half-life was obtained as a comparative metric for each gel. Significant increases in gel strength were obtained with 0.25 mM genipin even after a maturation time of 1 h. The degradation resistance increased with genipin concentration due to the increased rate of reaction at higher concentrations. This trend was also observed in gels that were matured for 24 h.

Linear 1-D degradation experiments were used to explore the effect of cross-linking on gel stability in a controlled manner by only exposing a single constant area surface to the degradation medium. Due to the significant differences in gel strength with time, two linear degradation assays were conducted for short (<1 day) and long (> 1 day) maturation times. Consistent with the 3-D degradation experiment, the short term 1-D degradation assay (**Figure 3-10a)** showed that even after a maturation time of 1 h, gels of all genipin concentrations provided substantial resistance to collagenase-associated degradation, with 3, 4.5, and 5 times the dry gel weight remaining as compared to non-cross-linked gels for 0.25, 0.5, and 1 mM genipin respectively. Longer maturation times or increasing genipin concentration led to more robust gels. The long-term degradation assay (**Figure 3-10b**) was used to determine an approximate saturation point for cross-linking of the material. The saturation in gel properties closely followed the pre-formed gel rheology data. After 72 h maturation time, all gels showed very little degradation even after exposure to collagenase for 24 h.

Overall, genipin has a more substantial impact on the degradation properties of the collagen gel compared to its impact on the gel's mechanical properties. Since genipin has the ability to form cross-links of multiple lengths, it is possible that the combination of short- and long-range cross-links provide

more substantial degradation resistance to the gels but not as much stiffness because stiffness is more dependent on the number of shorter links to oppose collagen fiber motion.

3.6.4. Correlation of fluorescence, mechanical, and degradation properties (long term behavior of collagen-genipin)

Correlation between mechanical, degradation, and fluorescence studies over 72 h showed the long term action of genipin in collagen. In each of the experiments, free genipin molecules were not flushed out of the system and were allowed to react with the collagen throughout the full time course of the experiment. By 72 h, all genipin concentrations tested (0.25-1 mM) reached a similar saturation point in modulus, degradation resistance, and fluorescence. The main difference between concentrations was the time it took to reach the plateau value G'. Therefore one can focus on tuning the properties of the system based on the amount of genipin required to obtain the desired properties before excess genipin diffuses out of the gel. The point at which they saturated in these properties was dependent on the concentration of genipin and was consistent across assay methods.

3.6.5. Cell-biomaterial interactions

Our studies showed that genipin is well tolerated in many stem cell types at concentrations capable of producing robust gels. Mesenchymal and neural stem cells have the potential to provide therapeutic benefit after SCI by reducing inflammation, modulating the wound environment, and replacing lost cell populations.[49] Pig MSCs were capable of being encapsulated within the gel scaffolds, surviving the gelation process, and remaining viable for 10 days within the gel (**Figure 3-14a**). Substantial numbers of MSCs survived at genipin concentrations up to 0.5 mM. The morphology of cells at genipin concentrations of 0.25 mM was also similar to the control collagen gels, exhibiting an elongated spindle-like shape (**Figure 3-15**). Short-term experiments using NSCs (**Figure 3-16**) showed that these cell types are less tolerant of higher genipin concentrations and survived in gels containing up to 0.25 mM genipin. One potential reason for this observation was the sensitivity of the cells to medium conditions which are changed as the genipin reacted with amino acids and proteins within the media.

Since the cytotoxicity of a biomaterial is highly dependent on its application (i e. cell encapsulating vs. acellular construct adjacent to healthy tissue), a more detailed investigation of cytotoxicity from genipin exposure was conducted. The relative volume of genipin, contained in a gel or in the media, compared to the volume of cells showed a strong correlation to cell viability for both MSCs and NSCs **Figures 3-17, 3-18**. This type of response allows for the determination of a tolerable level for genipin in the gels based on the intended application of the gel and was used as the rationale for choosing genipin concentrations for experiments in this thesis. For example, 1 mM genipin was used to create a

stiffer more robust gel for injection into a spinal cord defect (chapter 6) where the volume of genipin containing gel is low compared to the surrounding cell/tissue volume, while 0.25 mM genipin was used in the astrocyte outgrowth assay (chapter 4) due to the relatively high genipin:cell volume.

Genipin at 5 μg/ml (22 μM) has neurotrophic properties similar to nerve growth factor (1 ng/ml) via the neural nitric oxide synthase pathway.[24, 26] Genipin interacts with fibroblasts to inhibit their differentiation into myofibroblasts above 25 μg/ml (0.11mM) and decreases their expression of collagen I, α-SMA, and TGF-β.[29] Similar effects have been noted with hepatic stellate cells. [28, 50] The similarity of stellate cells to astrocytes may be beneficial to reduce glial scarring after SCI. Additionally, genipin has known anti-inflammatory properties.[27] Together these properties make genipin not only a cross-linking agent for collagen but a therapeutic agent itself.

3.7. References:

[1] Macaya D, Spector M. Injectable hydrogel materials for spinal cord regeneration: a review. Biomed Mater. 2012;7:012001.

[2] Comolli N, Neuhuber B, Fischer I, Lowman A. In vitro analysis of PNIPAAm-PEG, a novel, injectable scaffold for spinal cord repair. Acta biomaterialia. 2009;5:1046-55.

[3] Jain A, Kim Y, McKeon R, Bellamkonda R. In situ gelling hydrogels for conformal repair of spinal cord defects, and local delivery of BDNF after spinal cord injury. Biomaterials. 2006;27:497-504.

[4] Gupta D, Tator CH, Shoichet MS. Fast-gelling injectable blend of hyaluronan and methylcellulose for intrathecal, localized delivery to the injured spinal cord. Biomaterials. 2006;27:2370-9.

[5] Joosten E, Bar P, Gispen W. Collagen implants and cortico-spinal axonal growth after mid-thoracic spinal cord lesion in the adult rat. J Neurosci Res. 1995;41:481-90.

[6] Tysseling-Mattiace VM, Sahni V, Niece KL, Birch D, Czeisler C, Fehlings MG, et al. Self-assembling nanofibers inhibit glial scar formation and promote axon elongation after spinal cord injury. Journal of Neuroscience. 2008;28:3814-23.

[7] Mano JF, Silva GA, Azevedo HS, Malafaya PB, Sousa RA, Silva SS, et al. Natural origin biodegradable systems in tissue engineering and regenerative medicine: present status and some moving trends. Journal of the Royal Society, Interface / the Royal Society. 2007;4:999-1030.

[8] Willerth S, Sakiyama-Elbert S. Approaches to neural tissue engineering using scaffolds for drug delivery. Advanced Drug Delivery Reviews. 2007;59:325-38.

[9] EHRMANN R, GEY G. The growth of cells on a transparent gel of reconstituted rat-tail collagen. J Natl Cancer Inst. 1956.

[10] Elsdale T, Bard J. Collagen substrata for studies on cell behavior. J Cell Biol. 1972;54:626-37.

[11] O'Connor S, Stenger D, Shaffer K, Ma W. Survival and neurite outgrowth of rat cortical neurons in three-dimensional agarose and collagen gel matrices. Neuroscience Letters. 2001;304:189-93.

[12] O'Connor SM, Andreadis JD, Shaffer KM, Ma W, Pancrazio JJ, Stenger DA. Immobilization of neural cells in three-dimensional matrices for biosensor applications. Biosensors and Bioelectronics. 2000;14:871-81.

[13] O'Shaughnessy TJ, Lin HJ, Ma W. Functional synapse formation among rat cortical neurons grown on three-dimensional collagen gels. Neuroscience Letters. 2003;340:169-72.

[14] Ma W, Tavakoli T, Chen S, Maric D, Liu JL, O'shaughnessy TJ, et al. Reconstruction of Functional Cortical-like Tissues from Neural Stem and Progenitor Cells. Tissue Engineering Part A. 2008;14:1673-86.

[15] Ma W, Fitzgerald W, Liu Q-Y, O'Shaughnessy TJ, Maric D, Lin HJ, et al. CNS stem and progenitor cell differentiation into functional neuronal circuits in three-dimensional collagen gels. Experimental Neurology. 2004;190:276-88.

[16] Watanabe K, Nakamura M, Okano H, Toyama Y. Establishment of three-dimensional culture of neural stem/progenitor cells in collagen Type-I Gel. Restorative Neurology and Neuroscience. 2007;25:109-17.

[17] Willits R, Skornia S. Effect of collagen gel stiffness on neurite extension. Journal of Biomaterials Science, Polymer Edition. 2004;15:1521-31.

[18] Eccleston P, Mirsky R, Jessen K. Type I collagen preparations inhibit DNA synthesis in glial cells of the peripheral nervous system. Experimental Cell Research. 1989;182:173-85.

[19] Sundararaghavan HG, Monteiro GA, Firestein BL, Shreiber DI. Neurite Growth in 3D Collagen Gels With Gradients of Mechanical Properties. Biotechnol Bioeng. 2009;102:632-43.

[20] Georges P, Janmey P. Cell type-specific response to growth on soft materials. Journal of Applied Physiology. 2005;98:1547-53.

[21] Georges P, Miller W, Meaney D, Sawyer E. Matrices with compliance comparable to that of brain tissue select neuronal over glial growth in mixed cortical cultures. Biophysical journal. 2006;90:3012-8.

[22] Sung H, Chang W, Ma C, Lee M. Crosslinking of biological tissues using genipin and/or carbodiimide. J Biomed Mater Res A. 2003;64:427-38.

[23] Sung HW, Huang RN, Huang LL, Tsai CC. In vitro evaluation of cytotoxicity of a naturally occurring cross-linking reagent for biological tissue fixation. J Biomater Sci Polym Ed. 1999;10:63-78.
[24] Suzuki H, Yamazaki M, Chiba K, Sawanishi H. Characteristic properties of genipin as an activator in neuronal nitric oxide synthase. J Health Sci. 2007;53:730-3.
[25] Yamazaki M, Chiba K. Neurotrophic effects of genipin on Neuro2a cells. J Health Sci. 2005;51:687-92.
[26] Yamazaki M, Chiba K, Mohri T, Hatanaka H. Cyclic GMP-dependent neurite outgrowth by genipin and nerve growth factor in PC12h cells. European journal of pharmacology. 2004;488:35-43.
[27] Koo H, Lim K, Jung H, Park E. Anti-inflammatory evaluation of gardenia extract, geniposide and genipin. Journal of ethnopharmacology. 2006;103:496-500.
[28] Imanishi Y, Maeda N, Otogawa K, Seki S, Matsui H, Kawada N, et al. Herb medicine Inchin-ko-to (TJ-135) regulates PDGF-BB-dependent signaling pathways of hepatic stellate cells in primary culture and attenuates development of liver fibrosis induced by thioacetamide administration in rats. J Hepatol. 2004;41:242-50.
[29] Kitano A, Saika S, Yamanaka O, Ikeda K, Reinach PS, Nakajima Y, et al. Genipin suppresses subconjunctival fibroblast migration, proliferation and myofibroblast transdifferentiation. Ophthalmic Res. 2006;38:355-60.
[30] Sundararaghavan H, Monteiro G, Lapin N. Genipin-induced changes in collagen gels: Correlation of mechanical properties to fluorescence. Journal of Biomedical Materials Research Part A. 2008;87A:308-20.
[31] Kubista M, Sjoback R, Eriksson S, Albinsson B. Experimental correction for the inner-filter effect in fluorescence spectra. Analyst. 1994;119:417-9.
[32] Palmier MO, Van Doren SR. Rapid determination of enzyme kinetics from fluorescence: Overcoming the inner filter effect. Analytical Biochemistry. 2007;371:43-51.
[33] Sun X-D, Jeng L, Bolliet C, Olsen BR, Spector M. Non-viral endostatin plasmid transfection of mesenchymal stem cells via collagen scaffolds. Biomaterials. 2009;30:1222-31.
[34] Palmer TD, Takahashi J, Gage FH. The Adult Rat Hippocampus Contains Primordial Neural Stem Cells. Molecular and Cellular Neuroscience. 1997;8:389-404.
[35] Forgacs G, Newman SA, Hinner B, Maier CW, Sackmann E. Assembly of Collagen Matrices as a Phase Transition Revealed by Structural and Rheologic Studies. Biophysical journal. 2003;84:1272-80.
[36] Palmer MP, Abreu EL, Mastrangelo A, Murray MM. Injection Temperature Significantly Affects In Vitro and In Vivo Performance of Collagen-Platelet Scaffolds. Journal of Orthopaedic Research. 2009;27:964-71.
[37] Sato K. Possible Involvement of Aminotelopeptide in Self-assembly and Thermal Stability of Collagen I as Revealed by Its Removal with Proteases. Journal of Biological Chemistry. 2000;275:25870-5.
[38] Pieper JS, Hafmans T, Veerkamp JH, van Kuppevelt TH. Development of tailor-made collagen-glycosaminoglycan matrices: EDC/NHS crosslinking, and ultrastructural aspects. Biomaterials. 2000;21:581-93.
[39] Touyama R, Takeda Y, Inoue K, Kawamura I, Yatsuzuka M, Ikumoto T, et al. Studies on the blue pigments produced from genipin and methylamine .1. structures of the brownish-red pigments, intermediates leading to the blue pigments. Chem Pharm Bull. 1994;42:668-73.
[40] Ma L, Gao C, Mao Z, Zhou J, Shen J. Enhanced biological stability of collagen porous scaffolds by using amino acids as novel cross-linking bridges. Biomaterials. 2004;25:2997-3004.
[41] Yan L-P, Wang Y-J, Ren L, Wu G, Caridade SG, Fan J-B, et al. Genipin-cross-linked collagen/chitosan biomimetic scaffolds for articular cartilage tissue engineering applications. Journal of Biomedical Materials Research Part A. 2010;95A:465-75.
[42] Park J, Lee J, Kim H, Hahn T, Paik Y. Isolation and characterization of water-soluble intermediates of blue pigments transformed from geniposide of Gardenia jasminoides. J Agr Food Chem. 2002;50:6511-4.

[43] Chen H, Wei O, Bisi L, Martoni C, Prakash S. Reaction of chitosan with genipin and its fluorogenic attributes for potential microcapsule membrane characterization. Journal of Biomedical Materials Research Part A. 2005;75A:917-27.
[44] Achilli M, Mantovani D. Tailoring Mechanical Properties of Collagen-Based Scaffolds for Vascular Tissue Engineering: The Effects of pH, Temperature and Ionic Strength on Gelation. Polymers. 2010;2:664-80.
[45] Slusarewicz P, Zhu K, Hedman T. Kinetic characterization and comparison of various protein crosslinking reagents for matrix modification. Journal of materials science Materials in medicine. 2010;21:1175-81.
[46] Mi F, Shyu S, Peng C. Characterization of ring-opening polymerization of genipin and pH-dependent cross-linking reactions between chitosan and genipin. Journal of Polymer Science Part A: Polymer Chemistry. 2005;43:1985-2000.
[47] Mi F, Sung H, Shyu S. Synthesis and characterization of a novel chitosan-based network prepared using naturally occurring crosslinker. J Polym Sci Pol Chem. 2000;38:2804-14.
[48] Flanagan LA, Ju YE, Marg B, Osterfield M, Janmey PA. Neurite branching on deformable substrates. Neuroreport. 2002;13:2411-5.
[49] Barnabe-Heider F, Frisen J. Stem cells for spinal cord repair. Cell Stem Cell. 2008;3:16-24.
[50] Imanishi Y, Maeda N, Matsui H, Takashima T, Seki S, Arakawa T, et al. Suppression of Rat Stellate Cell Activation and Liver Fibrosis by a Japanese Herbal Medicine, Inchinko-to (TJ135). Comp Hepatol. 2004;3 Suppl 1:S11.

Chapter 4

Permissiveness of Collagen-Genipin gels Containing FGF-2 to Infiltration by Primary Astrocytes using an *In Vitro* Cellular Outgrowth Assay

4.1 Introduction

In this chapter, the permissiveness of genipin-cross-linked collagen hydrogels to infiltration by primary cortical astrocytes was investigated using a 3-D cellular outgrowth assay. The ability of FGF-2 either freely loaded within the gel or encapsulated within LMTs to alter the cell-biomaterial interaction and facilitate the population of the gels with astrocytes was analyzed in detail. That the astrocyte infiltration of the gel may be due to the combined processes of migration and proliferation is compatible with the intended use of the gel and would demonstrate that the gel is permissive of both processes. The effect of genipin on astrocyte viability and movement into the gel was examined to better understand how these cells would react to the use of this collagen cross-linking agent. The *in vitro* studies presented in this chapter of the thesis helped to guide the selection of materials and growth factors to best enhance astrocyte ingrowth and framework formation *in vivo*.

4.2. Background and motivation

The astrocyte is one of the main endogenous cell types modulating the native response to SCI. Following injury, astrocytes undergo many phenotypic changes including: hypertrophy; proliferation; increased expression of glial fibrillary acidic protein (GFAP) and α-smooth muscle actin; and release of numerous growth factors, cytokines, and ECM molecules including axon growth inhibitory chondroitin sulfate proteoglycans (CSPGs) [1, 2]. The onset of glial scarring occurs approximately 3 days post injury and begins to stabilize by about 28 days [3]. The scar serves to separate the viable nerve tissue from the necrotic damaged tissue as well as from the invading inflammatory and mesenchymal cells, but has the drawback of preventing axon regeneration through the damaged areas of the cord. Astrocytes may extend a few processes into the defect area but are primarily localized to the border zone.

Despite their growth inhibitory phenotype after injury, astrocytes also hold a highly important role after SCI to limit the extent of secondary damage by providing trophic support to for neurons and oligodendrocytes: restoring a homeostatic environment; limiting the accumulation of toxic metabolites such as glutamate from damaged neural tissue; restoring the blood brain barrier; and limiting the infiltration of inflammatory and mesenchymal cells [4-6]. Perhaps even more valuable is the potential for astrocytes to facilitate regeneration after SCI by forming a framework necessary for axon growth and guidance [7-9]. Prior work has shown that transplanted dorsal root ganglion cells have been able to send processes down both intact and degenerating white matter *in vivo*, seemly guided by astrocytic processes [9, 10]. The many roles that the astrocyte can play in supporting a regenerative response make the case for facilitating its infiltration into the SCI defect, by providing a lesion-filling matrix permissive of astrocyte infiltration capable of delivering a pro-migratory factor and permissive of astrocyte migration.

Fibroblast growth factor-2 (FGF-2) is a promising molecule to consider for increasing the population of astrocytes within a biomaterial matrix after injury. FGF-2 is a potent growth factor released by astrocytes after injury to the CNS, which is both a mitogen and chemoattractant for astrocytes [11, 12] and may contribute to the limitation of injury and induction of progenitor cells after SCI [13]. In addition to its action on astrocytes, FGF-2 has many other positive effects on neural cell populations. FGF-2 increases the survival of mature neurons *in vitro* [14, 15], and promotes the survival and proliferation of NSCs and maintains them in an undifferentiated state [15, 16]. FGF-2 can prevent oligodendrocyte apoptosis after injury and can induce mature oligodendrocytes to dedifferentiate and proliferate [13, 14]. It is also a mitogen and chemoattractant for oligodendrocyte precursor cells [13, 14, 17]. Together these results suggest that FGF-2 can promote remyelination of spared axons after injury. Furthermore, FGF-2 is a potent angiogenic factor and accelerates revascularization of the injury site, which is critical for repair of injured tissue [18].

However, the use of FGF-2 in spinal cord injury necessitates the use of controlled delivery system to mitigate the detrimental effects of FGF-2 overstimulation. FGF-2 has been implicated in stimulating astrogliosis both *in vitro* [12, 19] and *in vivo* [20-24]. FGF-2 has also been shown to disrupt myelin production in mature oligodendrocytes, cause reactive changes in oligodendrocyte progenitor cells, and increase accumulation of microglia at high concentrations *in vivo* [21]. In prior studies FGF-2 has been delivered to the spinal cord through a variety of means including: direct injections into the parenchyma; sub-dural osmotic mini-pumps; and intrathecal polymer-drug implants [25-29]. However, the penetration of FGF-2 into the cord is very limited, potentially due to its sequestration in the ECM [28, 30], and such methods do not deal with the creation of a provisional stroma to allow for the repopulation of the cavitary defect, which occurs after SCI. To this end, an injectable gel conducive to cellular ingrowth, could provide a useful treatment for SCI due to its ability to serve both as a scaffold and as a medium for delivery of therapeutic agents.

In order to provide additional control over the release of FGF-2 from the scaffold, a secondary release vehicle, lipid microtubules (LMTs), was commended for this study. LMTs are self-assembled structures with high drug loading capacity, can serve to protect FGF-2 during *in situ* cross-linking of the gel. LMTs, which can sustain controlled delivery of proteins for weeks by varying the average length of the tubules via the self-assembly conditions [31], have been used in prior models of SCI to deliver brain-derived neurotrophic factor and chondroitinase ABC [32, 33]. These studies reported sustained release and preserved bioactivity of proteins over a period of two weeks. Additionally, the LMTs were non-cytotoxic and non-inflammatory at concentrations of 8.3 mg/ml.

4.3. Overall Goal and Hypotheses:

The **overall goal** of this study is to develop an injectable collagen-genipin hydrogel capable of being infiltrated with astrocytes, in order to ultimately test the hypothesis *in vivo* that astrocyte infiltration of a gel-filled defect in SCI will stimulate neurite ingrowth into the defect and reduce the astrocyte scarring around the defect.

The **hypotheses** of this chapter are:

1.) Infiltration and population of collagen gels with astrocytes will be enhanced through the use of FGF-2 incorporated within the gels.

2.) The action of genipin on both the cross-linking of the collagen gel and directly on the astrocytes will impede their growth into the gels.

3.) Encapsulation of FGF-2 within LMTs will enhance the infiltration of astrocytes into the gels particularly at low FGF-2 concentrations and in the presence of genipin.

4.4. Methods

4.4.1 Experimental design

The effects of genipin cross-linking of collagen gels and the effects of 2 concentrations of FGF-2 as freely incorporated and LMT-contained protein on cell infiltration into various gel formulations and on cell proliferation were evaluated. Using an outgrowth assay the following metrics were evaluated: the total number of cells penetrating into the gel (which may include proliferating cells), the number of cells present at various distances within the gel, and the average distance to the furthest penetrating cell within the gel. In order to begin to assess the relative contribution of proliferation versus migration on the number of cells infiltrating the gels, two experiments were performed: 1) a proliferation assay to evaluate the mitogenic effects of FGF-2 dose on the astrocytes, in monolayer culture; and 2) staining of astrocyte-infiltrated gels with Ki-67 to provide an indication of the percentage of cells in the gels undergoing mitosis Given that the morphology of astrocytes may reflect their reactivity, the percentage of cells infiltrating the gels with select morphologies was determined.

4.4.2 Materials

Soluble rat-tail type I collagen (3.54-3.91 mg/mL) in acetic acid (BD Biosciences, Franklin Lakes, NJ, USA), genipin (Wako Pure Chemical, Japan), 1,2-bis-(triscosa-10,12-diynoyl)-sn-glycero-3-phosphocholine ($DC_{8,9}PC$) (Avanti Polar lipids, Alabaster, AL, USA), human fibroblast growth factor-2 (Peprotec, Rocky Hill, NJ, USA). Buffers were purchased from Invitrogen (Grand Island, NY, USA) and were cell-culture grade.

4.4.3 Collagen gels

Ice cold 1x phosphate buffered saline (PBS), 5x PBS, 1N NaOH, and soluble rat tail type I collagen were combined in that order to obtain 2 mg/mL collagen solutions at pH 7.5 with 1x ionic strength. For gels containing genipin, a stock solution of genipin in 5x PBS (3 mg/mL), made immediately before mixing, was used in place of a volume of 5x PBS to obtain the desired genipin concentration of 0.25mM. This genipin concentration was employed based on its favorable gelation time, modulus and degradation rate for central nervous system applications, and the lack of cytotoxicity.[34]

FGF-2 was loaded into the gels by adding the appropriate volume of 100 μg/ml FGF-2 or 1 mg/ml FGF-2-LMTs in 1x PBS. Thermal gelation of the collagen solutions was induced by warming to 37 °C in an incubator.

4.4.4 Lipid microtubules

LMTs were prepared using a self-assembly method as previously described [31]. $DC_{8,9}PC$ lipid was dissolved in 55°C ethanol. 55°C DI water was then added to bring the final lipid concentration to 1 mg/ml in 70% ethanol. The lipid solution was held at 55°C for 6 h and then slowly cooled to 25°C, heated to 33°C, and finally cooled back down to 25°C at 1°C/hr in a microprocessor-controlled circulating water bath (Cole-Palmer, Vernon hills, IL, USA). The LMTs were then stored at room temperature for two weeks in the dark. Before usage, 50 mM trehalose (Sigma, St. Louis, MO, USA) was added to the LMT solution overnight to preserve the tubular structure during lyophilization. The LMTs were then centrifuged (1500 g, 10 min) and the supernatant was removed. LMTs were re-suspended in DI water and lyophilized overnight. LMTs were loaded with recombinant human FGF-2 in 5% trehalose by rehydrating the dried LMTs overnight in 40 μl of FGF-2 solution with one of 2 concentrations: 0.11 or 1 mg/ml per mg of lipid, referred to as "Low" and "High," respectively. Un-encapsulated growth factor was removed by diluting the LMTs to 0.5 mg/ml with 1x PBS, centrifuging (1500 g, 10 min), and removing the supernatant. LMTs were re-suspended in 1x PBS at 1 mg/ml prior to loading into the gel.

The amount of protein encapsulated within the LMTs was estimated as previously described via the total internal volume of the LMTs and the concentration of loading solution [31]. High levels of fluorescently labeled protein can be seen within the LMTs immediately after loading and following 6 days of release after being encapsulated within a collagen gel (**Figure 4-1**). The amount of FGF-2 contained in the Col-FGF gels corresponded to approximately the maximum theoretical amount encapsulated within the LMT-FGF containing gels.

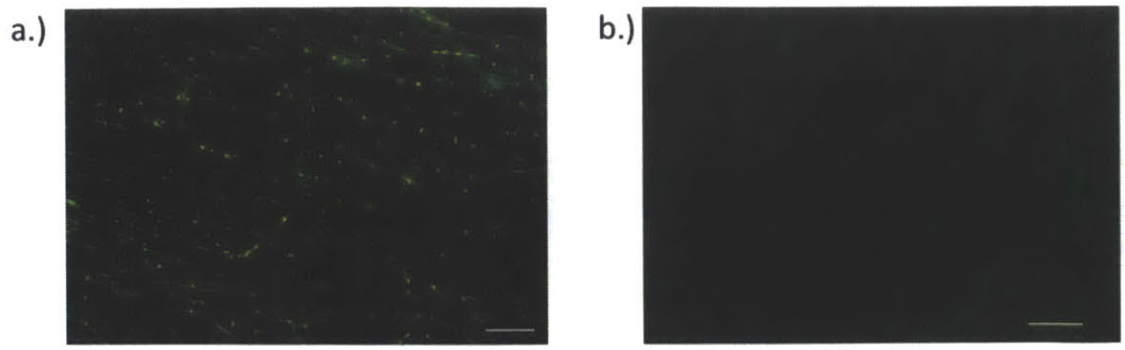

Figure 4-1: 40x fluorescent images of LMTs loaded with fluorescein isothiocyanate conjugated BSA. a.) immediately after loading and rinsing steps b.) After 6 days embedded in a collagen gel submerged in 1x PBS. Scale bar= 20 micrometers

4.4.5 Astrocyte culture

Cortical astrocytes were harvested from post-natal day 2 Sprague Dawley rats according to prior published procedures yielding a >95% pure population of cortical astrocytes [35]. The astrocytes were seeded into 2 mg/ml type I collagen gels at 1 million cells/ml. 1 ml of the gel was poured into each well of a 12 well plate and allowed to set for 15 min at 37°C. 1 ml of cell culture media: DMEM high glucose with glutamate, 10% fetal bovine serum (FBS), and 1% Penicillin/Streptomycin antibiotics, was then added and the astrocytes were cultured overnight. A 6 mm biopsy punch was used to create the core cell-seeded disks for the outgrowth assay.

For the cell priming experimental groups, astrocyte-collagen gels were incubated for 24 hours in either genipin or FGF-2 before being cut into 6 mm disks and used as the core of the outgrowth assay setup. In these experiments, the encapsulating gel was the same as the Col group. The purpose of these groups was to explore if either Gen or FGF-2 could alter the outgrowth response of astrocytes even if it was not contained within the encapsulating gel.

4.4.6 Outgrowth assay

The outgrowth assay setup is illustrated in **Figure 4-2**. 200 μl of 2% agarose at 60°C was used to coat the bottom of a 24 well plate to prevent astrocytes from moving along the bottom of the well plate. After 2 hours of gelation, 200 μl of 2mg/ml type I collagen was added on top of the agarose to act as an interface layer and was allowed to gel for 1 hour at 37°C. 6 mm disks of the astrocyte-seeded gels were then gently placed into the center of the 24 well plates containing the agarose and collagen. Once in place, 400 ul of the gel to be tested in the outgrowth experiment "encapsulating gel" was added and the constructs were allowed to gel for 15 min at 37°C before adding 0.5 ml of cell culture media. The

medium was changed the following day and every 48 hours thereafter. Each group (**Table 4-1**) contained 4-8 gels, results were pooled from three independent experiments.

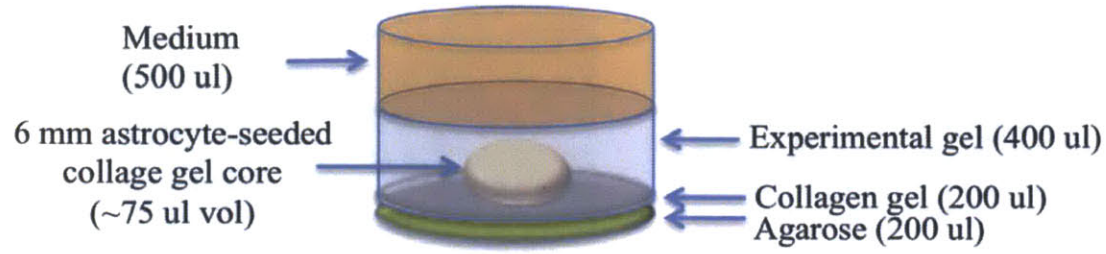

Figure 4-2: Outgrowth assay setup consisting of a core astrocyte seeded collagen gel encapsulated within a collagen gel containing the experimental factors (Genipin, LMTs, FGF-2). The outgrowth/infiltration of cells into the encapsulating gel was examined at 10 days.

Table 4-1: Experimental groups for migration assay. Col, collagen; Gen, genipin.

n	Group	
5	Col	2 mg/ml collagen
4	Col + FGF primed cells	Col + Astrocytes exposed to 150 ng/ml FGF-2 for 24 hr
5	Col FGF Low	Col + 15 ng/ml FGF-2
6	Col FGF High	Col + 150 ng/ml FGF-2
6	Col-Gen	Col + 0.25 mM Genipin
4	Col + Gen primed cells	Col + Astrocytes exposed to 0.25 mM genipin for 24 hr
8	Col-Gen FGF High	Col + 0.25 mM Genipin + 150 ng/ml FGF-2
6	Col LMT PBS	Col + 0.1 mg/ml LMT loaded with PBS
6	Col LMT FGF low	Col + 0.1 mg/ml LMTs loaded with 0.11 mg/ml FGF-2
4	Col LMT FGF high	Col + 0.1 mg/ml LMTs loaded with 1 mg/ml FGF-2
4	Col-Gen LMT FGF Low	Col + 0.25 mM genipin + 0.1 mg/ml LMT loaded with 0.11 mg/ FGF-2
4	Col-Gen LMT FGF High	Col + 0.25 mM genipin + 0.1 mg/ml LMT loaded with 1 mg/ml FGF-2

4.4.7 Quantification of the number of cells infiltrating the gels, migration distance, and cell morphology

The constructs were imaged from days 0 to 10 (principal quantification time-point). At day 10, the gels were stained with calcein AM (20 μg/ml) in 1x PBS for 60 min at 37°C to visualize the live cells. Gels were carefully removed from the 24 well plate, placed on glass slides, blotted dry, and imaged at 4x

exposure on a epifluorescence microscope (Olympus BX-60, Center valley, PA, USA). 5-6 images were taken around the perimeter of each gel. Each image was classified into one of four categories (short isolated, spread, chain-like , and chain-like with clustering) based on the outgrowth pattern of the astrocytes. For each image, the number of cell bodies crossing the interface into the encapsulating gel was manually counted using the Image J cell counting software (NIH, Bethesda, MD). The number of cells in the encapsulating gel was normalized to the interface length from which the analyzed imaged were taken.

The distance from the interface to the furthest cell (via perpendicular line segment) was also measured. Only cells in reasonable focus were counted. The average distance to the furthest cell was then calculated for each group. The image with the furthest cell was then further quantified by measuring the distance of each cell from the interface, creating an outgrowth distance histogram.

Following the calcein AM imaging, the gels were then fixed in 4% paraformaldehyde in PBS for 1 hour and permeabilized with 0.5% Triton-x 100 containing 5% serum for 40 min. The gels were stained with 1 μg/ml 4',6-diamidino-2-phenylindole (DAPI) for 1 hour and rinsed 3x with 1x PBS. The DAPI-labeled gels were evaluated for the number of penetrating cells and the outgrowth distance to validate the findings from the calcein AM-stained constructs. The high cell resolution in the DAPI images enabled calculation of the outgrowth distance histogram using the Image J cell counter application. The X-Y coordinates of the nucleus of the cell were subtracted from the X-Y coordinates of the gel interface to determine the outgrowth distance (images were scaled to 62 pixels= 100 micrometers).

Given that the morphology of astrocytes can provide an indication of their reactivity, the percentages of images with cells displaying the following morphologies was evaluated: isolated short, highly spread, chain-like, and chain-like with clustering.

4.4.8 Cell viability and proliferation

Live/dead cell staining was performed using Calcein AM and Ethidium homodimer (Invitrogen, Grand Island, NY, USA) in an assay simulating the conditions of the outgrowth assay. Constructs in the same configuration as the outgrowth assay were used, except that astrocytes were seeded at 300,000 cells/ml in order to facilitate visualization. Genipin and/or FGF-2 were mixed into the encapsulating gel at the defined concentrations. After 15 min of gelation, 500 μL of astrocyte medium was added on top of the construct. The gels were incubated for 24 hr and then stained and imaged using an epifluorescence microscope at 4x objective. Three to four random sections of each gel were measured, totaling 500–1500 cells/gel. The cell count was analyzed using Image J software (NIH, Bethesda, MD). Percentage viability was calculated as the number of viable cells divided by the total number of cells measured per

gel, multiplied by 100.

To assess the proliferation of primary cortical astrocytes in response to FGF-2, astrocytes in monolayer culture were stimulated with $5x10^{-5}$ μg/ml to 50 μg/ml FGF-2. Forty-eight hours after FGF-2 stimulation, cell proliferation was assessed by WST reduction assay (Dojindo, Rockville, MD, USA), which detects dehydrogenase activity of viable cells. The cells were incubated with 10% WST solution for 1 h at 37°C. Then the absorbance of the culture medium was measured with a microplate reader at a test wavelength of 450 nm and a reference wavelength of 630 nm.

To evaluate the effect of proliferation under assay conditions, astrocyte outgrowth assay gels (after 10 days culture) were fixed in 4% paraformaldehyde in PBS for 1 hour and permeabilized with 0.5% Triton-x 100 containing 5% serum for 40 min. The gels were embedded in paraffin, sectioned on a microtome at 6 micrometers, and mounted on glass slides. A heat induced epitope retrieval was performed with Tris/EDTA buffer at 95°C for 25 minutes. The gels were stained for the proliferation marker Ki-67 using anti-rabbit Ki-67 sp6 clone (Abcam, Cambridge, MA, USA) at 1:100 dilution. Detection was achieved through the EnVision kit anti rabbit HRP AEC+ (Dako, Carpinteria, CA). Nuclei were counterstained using Mayer's hematoxylin.

4.4.9 Statistical analysis

One-way analysis of variance (ANOVA) with a Fishers PLSD *post hoc* test was used to determine the statistical significance of the cellular outgrowth and viability data. Pair-wise comparisons were performed using a Student's *t*-test assuming equal variances (α=0.05).

4.5. Results

4.5.1 Number of cells infiltrating into the gels

As early as 1 day, cell processes could be seen crossing the interface into the encapsulating gel for FGF containing groups. By 2 days, several cells in the FGF-2 containing groups could be found across the interface while process extension began in the collagen only group. No cells could be seen crossing the interface in the genipin containing gels until day 3. By day 4 there were significant numbers of cells crossing the interface for all groups. In a comparison of FGF-2 containing groups there was a significant difference between the number of cells crossing the interface between days 4 and 6 but not between days 6 and 10 suggesting a decrease in the rate of cells crossing the interface after 6 days. However, the cells continued to migrate further into the encapsulating gel through day 10.

By 10 days, there was more than a 10-fold difference in the number of cells within the encapsulating gel between the groups with the greatest (**Figure 4-3**; Col-FGF High) and least amount (**Figure. 4-3**; Col-Gen) of outgrowth. The collagen hydrogels without chemokine (groups labeled Col, Col-Gen) or with PBS loaded LMTs induced minimal astrocyte recruitment. In contrast, collagen hydrogels with FGF-2 loaded freely or within LMTs at 2 concentrations each dramatically increased cell recruitment (**Figure 4-3**).

One-factor ANOVA with Fishers PLSD *post hoc* testing over all groups (**Figure 4-3**) showed a statistically significant increase in the number of cells/mm interface present within the encapsulating gel

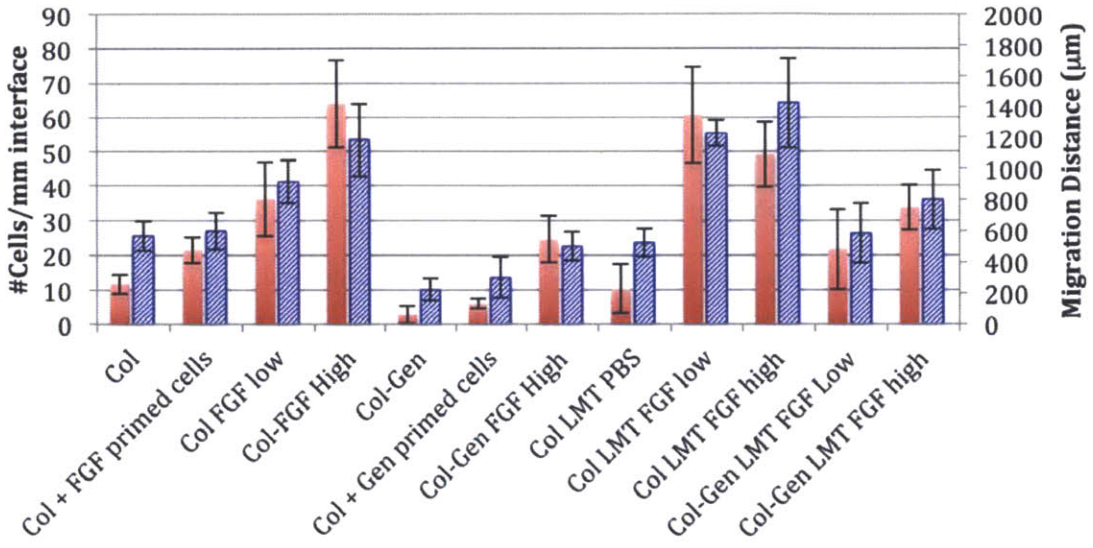

Figure 4-3: Number of cells infiltrating into the encapsulating collagen gel normalized by the total mm of gel interface imaged (solid, primary axis) and the average infiltration distance from the interface to the furthest cell body for all gels (stripes, secondary axis). n= 4-8 gels, 5-6 images/gel (45-50% of interface). Mean ± stdev (number) Mean ± SEM (length). Images used for examination were taken at 4x using an epifluoresence microscope on calcein AM stained cells.

between the control Col gel and: Col FGF Low ($p=0.00004$), Col FGF High ($p=1.159 \times 10^{-13}$), Col LMT FGF Low ($p=9.51 \times 10^{-13}$), Col LMT FGF High ($p=3.6 \times 10^{-8}$), and Col Gen LMT FGF High ($p=0.00037$). There was a statistically significant difference in outgrowth number for FGF-2 concentration with Col FGF High/Low groups ($p=2.51 \times 10^{-6}$), but not for Col-Gen LMT High/low or Col LMT High/Low groups. There was no statistically significant difference between Col FGF High, Col LMT FGF High, or Col LMT FGF Low. There was also no statistical significance between Col Gen LMT FGF High and Col LMT FGF High. There was also no statistically significant difference between Col Gen LMT FGF High

and Col Gen FGF High. While there was no significance between Col and Col Gen in the ANOVA analysis, pair-wise comparison using a Student's *t* test showed a significant difference ($p=0.00034$).

The addition of genipin dramatically decreased the number of cells within the encapsulating gel when no FGF-2 was present, however this effect was mitigated with the addition of FGF-2 either freely or within LMTs such that the number of cells within the encapsulating gel approached non-genipin containing gels. In the presence of genipin, FGF-2 within LMTs appeared to enhance outgrowth slightly better than un-encapsulated FGF-2.

Priming cells with genipin prior to the outgrowth assay decreased the number of cells that penetrated into the encapsulating collagen gel as well as their penetration distance as compared to untreated cells. Conversely, priming cells with FGF-2 increased the number of cells within the encapsulating gel as well as their penetration distance. However, the effect of priming the cells in either case was not as dramatic as when collagen or FGF-2 was present within the encapsulating gel.

4.5.2 Infiltration distance and morphology of infiltrating cells

The average distance to the furthest cell in each image at 10 days showed a correlation ($R^2=0.877$) to the number of cells crossing the interface **(comparing the data in Figure 4-3)**. In some groups, cells could be found a distance of 1-2 mm in the gels. Generally, higher levels of FGF within the encapsulating gel led to deeper penetration. Of special note is the presence of FGF-2 within LMTs (but not blank LMTs) appeared to increase the infiltration distance of astrocytes into the gel over free FGF-2. Col-Gen LMT FGF high also yielded longer infiltration distances than Col Gen FGF high.

One-factor ANOVA with Fishers PLSD *post hoc* testing over all groups in **Figure 4-3** showed a statistically significant increase in infiltration distance between the control Col gel and: Col FGF Low ($p=3.67\times10^{-3}$), Col FGF High ($p=7.92\times 10^{-7}$), Col LMT FGF Low ($p=1.66\times10^{-7}$), and Col LMT FGF High ($p=4.22\times10^{-9}$). There was a statistically significant decrease in infiltration distance between Col and Col Gen ($p=0.3.14\times10^{-3}$). There was no statistically significant difference with FGF-2 concentration for Col LMT High/Low, Col Gen LMT High/Low, or Col FGF High/Low.

The distribution of cells within the encapsulating gel in select groups was further elucidated by a distance histogram noting the position of each cell relative to the interface (**Figure 4-4a**). Non FGF containing groups (Col, LMT PBS, and Col-Gen), had a high percentage of cells close to the interface which rapidly decreased by 500-1000 μm. Col FGF high, Col LMT FGF low and Col LMT FGF high all had a more gradual decrease in the distribution of cells with distance, which tapered off between 1700-2500 μm. Interestingly, they all showed approximately the same linearly decreasing trend in the percentage of cells within the encapsulating gel as distance increased (**Figure 4-4b**). The histogram of

gels containing Genipin and FGF-2 (Col Gen FGF High and Col Gen LMT FGF High) had characteristics in between control and FGF-2 containing gels, with a greater % of cells close to the interface and only growing out to about half of the distance of other FGF containing gels. Histograms of the remaining gels can be found in **Figure 4-5**.

a.)

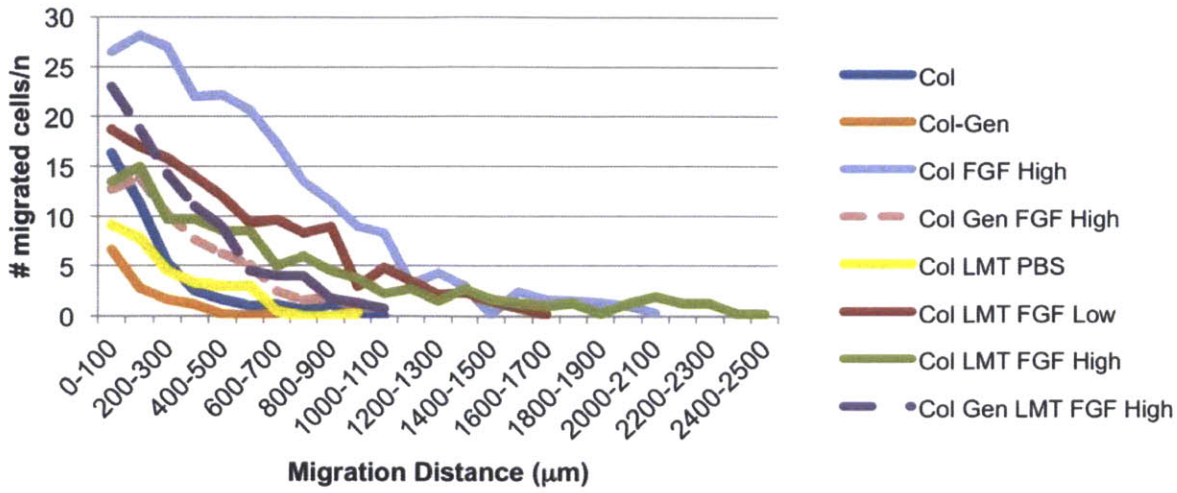

b.)

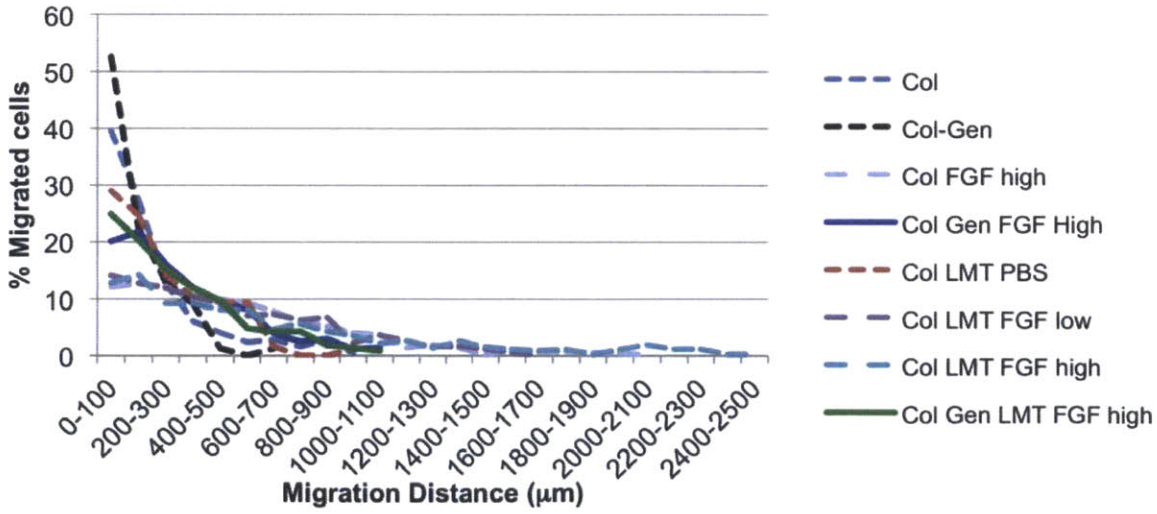

Figure 4-4: a.) Histogram of the total number of infiltrating cells at 100 μm intervals for select control and outgrowth promoting gels. The image with the furthest infiltration distance in each gel was used n=4-8. The count represents the sum total of infiltrating cells at the specified distance normalized by the number of gels examined. b.) Distance histogram as in b, showing the percentage of cells at 100 μm intervals. n= 4-8.

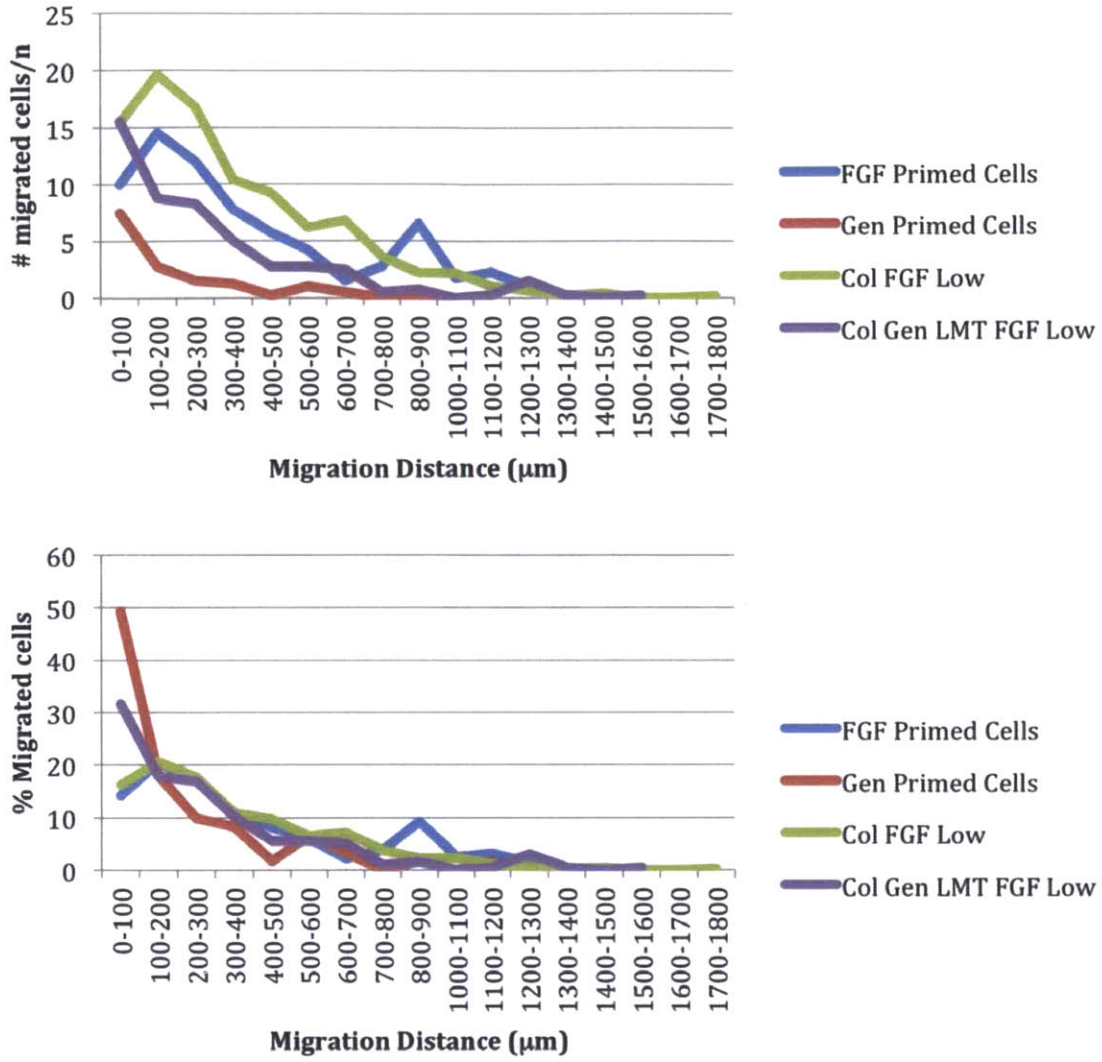

Figure 4-5 a.) Histogram of the total number of migrating cells at 100 μm intervals for groups not shown in figure 4-4. The image with the furthest migration distance in each gel was used n=4-5. The count represents the sum total of migrating cells at the specified distance normalized by the number of gels examined. b.) Distance histogram as in b, showing the percentage of cells at 100 μm intervals. n=4-5.

Of specific note was the morphology of the astrocytes within the encapsulating the test gels **(Figure 4-6).** In non- FGF containing gels, several isolated cells per field of view could be seen crossing the interface from the core gel into the encapsulating gel with little nearest neighbor interaction. However, all of the FGF-2 containing gels exhibited instances of the chain-like outgrowth of astrocytes similar to a network/framework. **Figure 4-7** further quantifies the distinct cell outgrowth patterns noted in the images taken including isolated short, highly spread, chain-like, and chain-like with clustering.

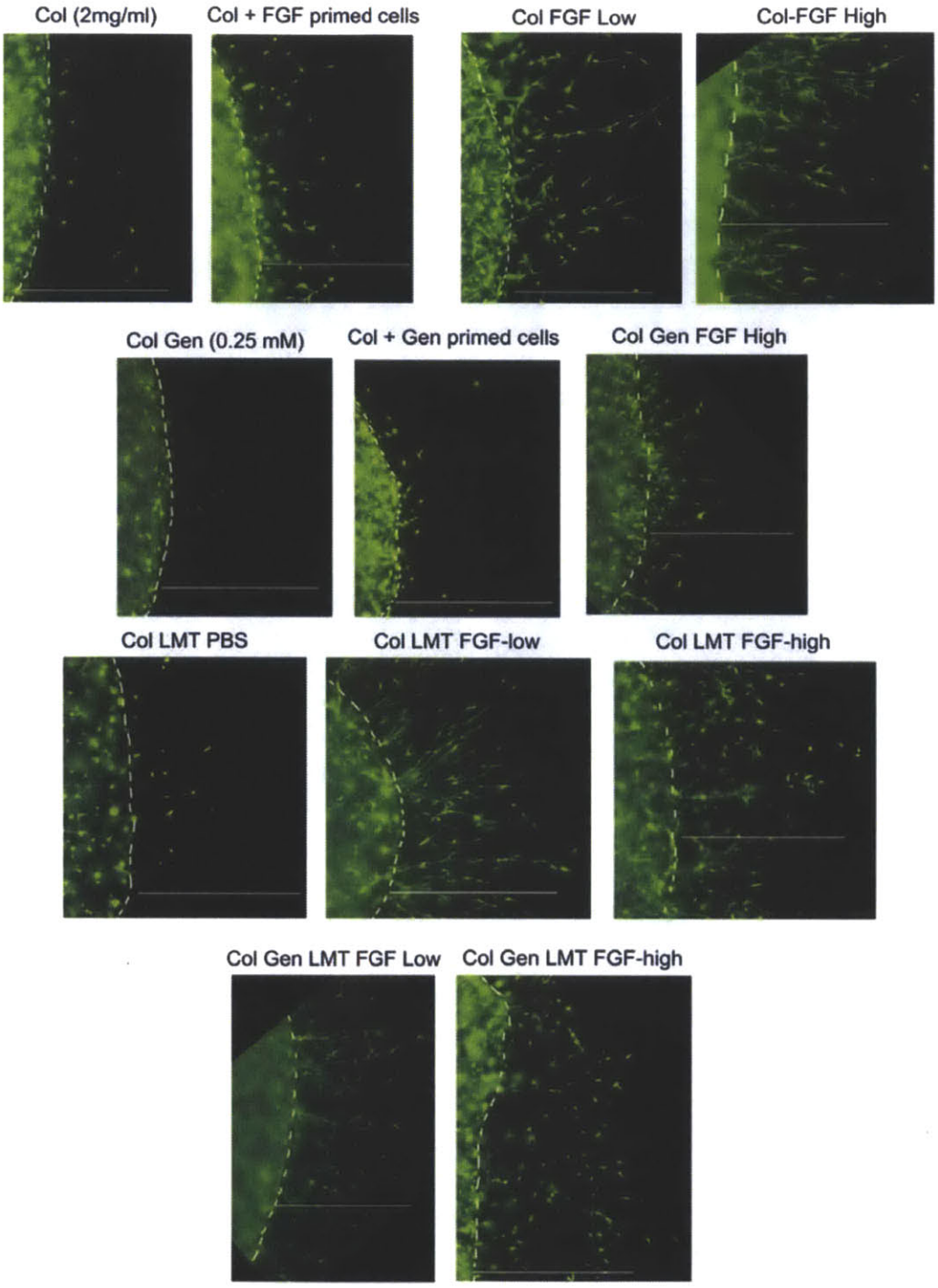

Figure 4-6: Representative long distance outgrowth images of the interface between astrocyte seeded and encapsulating gels for each group. T=10 days. Taken under a 4x objective using a calcein AM viable cell stain and epifluorescence microscopy. The dotted line signifies the interface. Scale marker= 1000 micrometers. Col= collagen (2 mg/ml), FGF primed cells= astrocytes exposed to 150 ng/ml FGF-2 prior to assay setup, FGF low = 15 ng/ml FGF-2 freely loaded in the gel, FGF High = 150 ng/ml FGF-2 freely loaded in the gel, Gen= genipin (0.25 mM), Gen primed cells= astrocytes exposed to 0.25 mM prior to assay setup, LMT PBS= 0.1 mg/ml LMTs loaded with PBS, LMT FGF low= 0.1 mg/ml LMTs loaded with 0.11 mg/ml FGF-2, LMT FGF High= 0.1 mg/ml LMTs loaded with 1 mg/ml FGF-2.

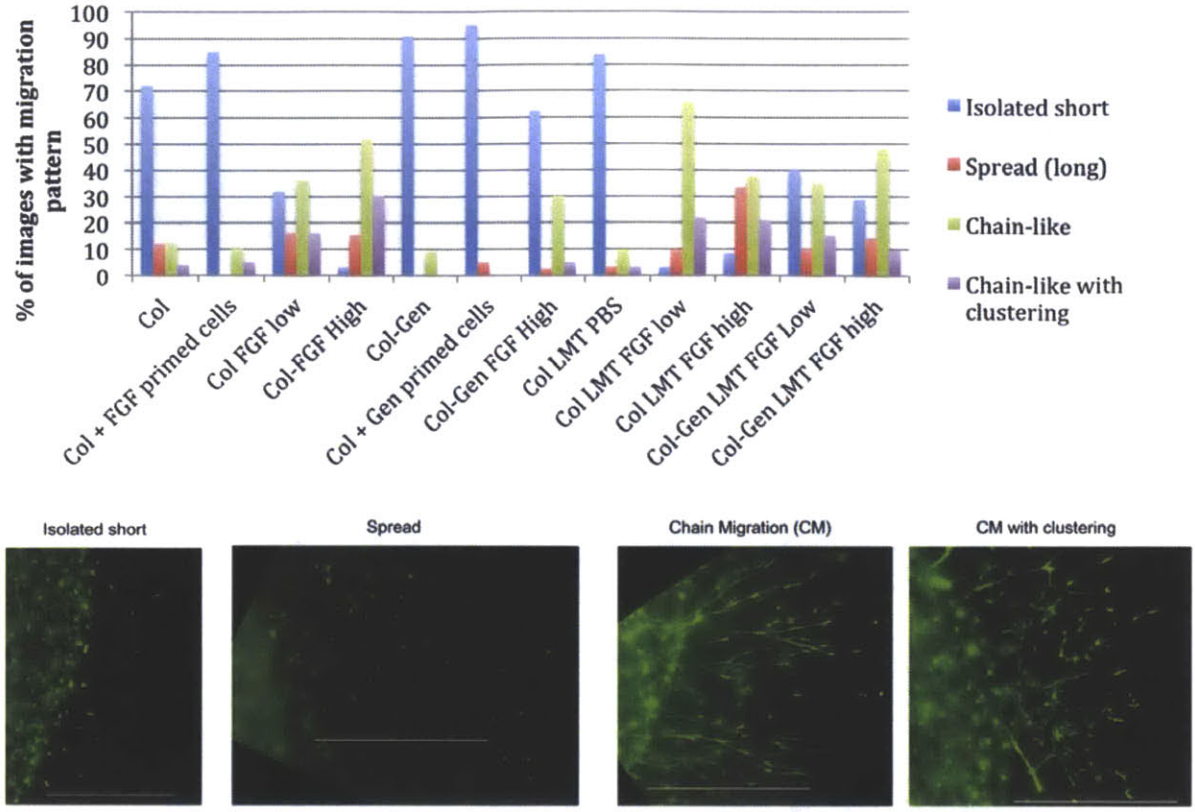

Figure 4-7: Quantification of the four main astrocyte outgrowth patterns observed in the outgrowth assay. The percentage of images with each of the morphologies was calculated based on the total images of each group (5-6 images/gel 4-8 gels/group). b.) Example images of each type of morphology. Scale bar = 1000 μm

4.5.3 Proliferation and viability

Analysis of the cellular density within the core astrocyte seeded gel was performed on select control and high growth gels to determine the effect cellular overcrowding due to proliferation might have played a role in the outgrowth phenomena (**Figure 4-8**). One-factor ANOVA with Fishers PLSD *post hoc* testing of DAPI stained images of the center of the astrocyte seeded gels at 10 days showed no significant difference in cell number between Col and any other group examined. Statistical significance was only reached between Col FGF High and Col Gen (p=.0007), LMT PBS (p=.00339), and Col Gen LMT FGF High (p=.0013). Overall, there was also a trend towards a higher average number in the Col

FGF High group and lower average number in Genipin containing groups. Cell counts at the edges of the gel showed no statistically significant difference in the number of cells within the gel between Col and any other groups.

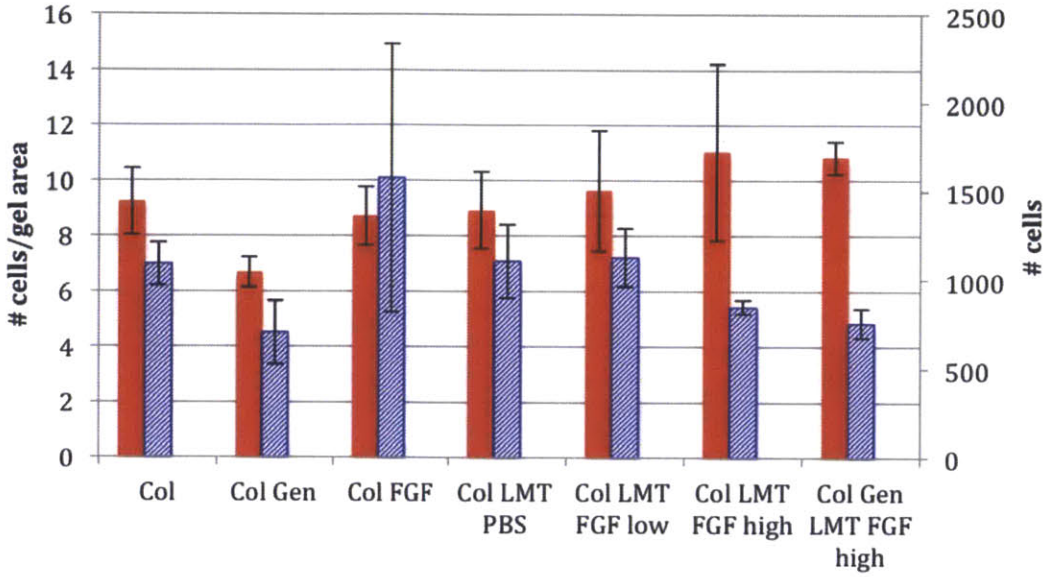

Figure 4-8: Number of DAPI stained cells in the center (solid, primary axis) and edge (stripes, secondary axis) of select control and pro-outgrowth gels at day 10. 4x objective n=4 gels (center) 3-4 gels (edge) mean ± stdev. Number of DAPI stained cells at the edge was normalized by the area of core gel measured.

Further analysis of the proliferation of cells in the gels was performed on microtomed sections from several astrocyte outgrowth assay gels embedded in paraffin using Ki-67 staining. Images taken at 10x in the center of the astrocyte-seeded constructs revealed that only a small percentage of astrocytes (estimated to be less than 15%) were proliferating after 10 days in culture. There were comparable percentages of proliferating cells in control and FGF-2 containing gels (**Figure 4-9**).

It was noted that in monolayer culture, astrocytes increased in number by almost two-fold in response to 48 hours of FGF-2 stimulation as measured by WST reduction assay. Interestingly, the effect was relatively independent of concentration over several orders of magnitude and began to decrease by 50 μg/ml (**Figure 4-10**). One-factor ANOVA with Fishers PLSD post hoc testing over all FGF-2 concentrations showed a statistically significant difference in proliferation between control 0 μg/ml and all other concentrations examined except 50 μg/ml. There was no significant difference between proliferation of astrocytes exposed to FGF-2 concentrations between $5x10^{-5}$ μg/ml and 5 μg/ml. Additionally, the encapsulation of astrocytes within 0.25 mM genipin gels did not alter the viability

(**Figure 4-11**).

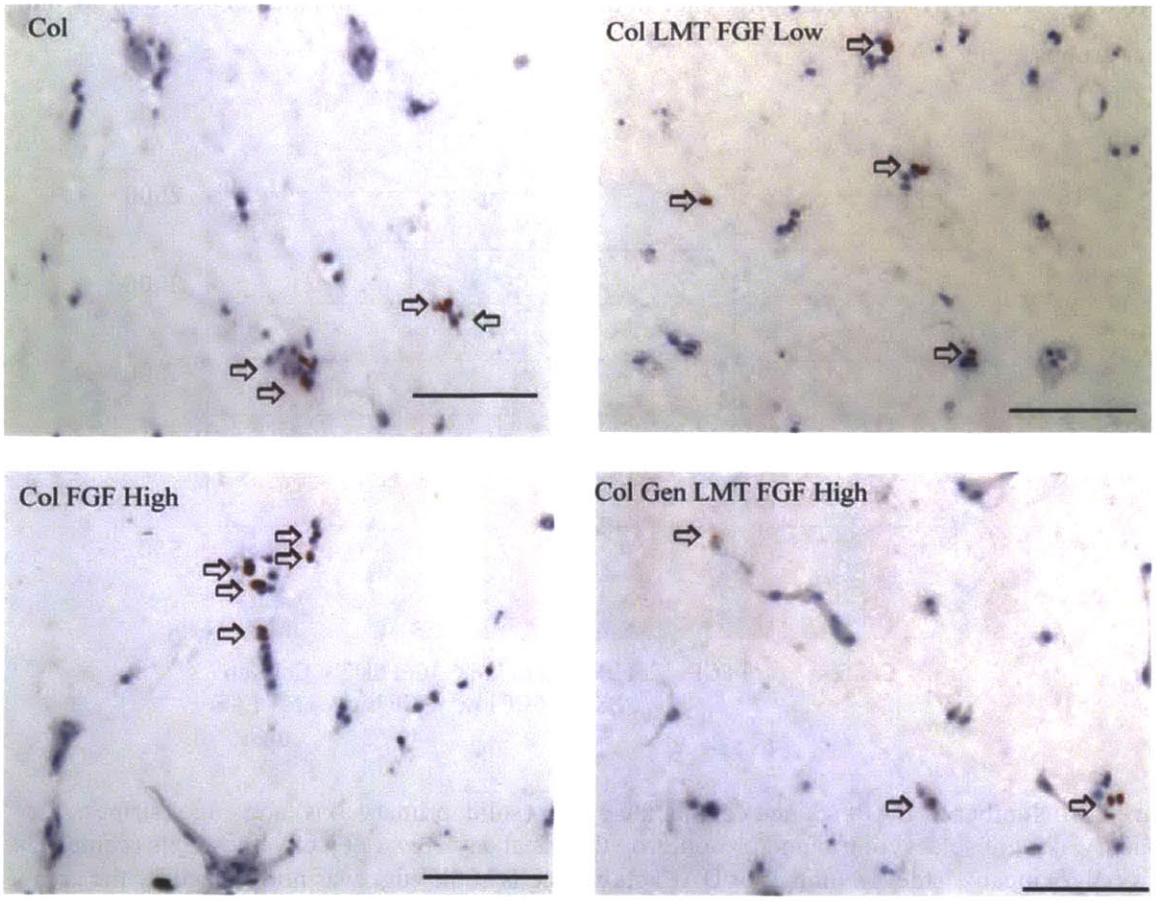

Figure 4-9: Ki-67 proliferation marker immunohistochemistry on select paraffin embedded astrocyte outgrowth assay gels at 10 days. Images were taken at 10x in the center of the astrocyte seeded core gel. Arrows highlight positive staining within the cell nucleus. Scale bar= 100 μm.

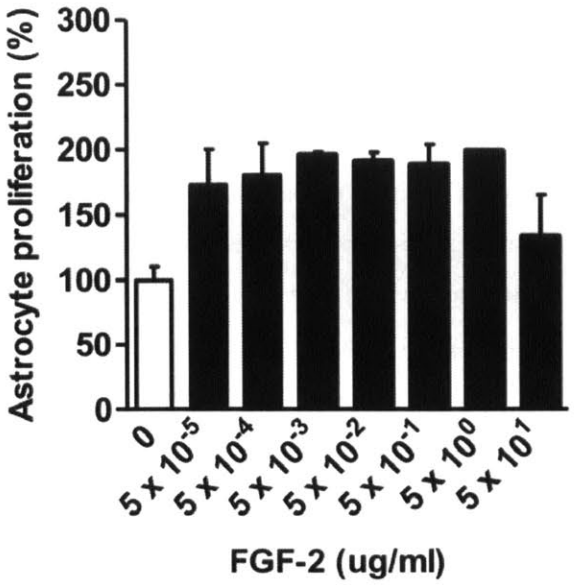

Figure 4-10: Proliferation assay of astrocytes in monolayer culture in response to FGF-2. Forty-eight hours after FGF-2 stimulation, cell proliferation was assessed by WST reduction assay, which detects dehydrogenase activity of viable cells. The cells were incubated with 10% WST solution for 1 h at 37°C. Then the absorbance of the culture medium was measured with a microplate reader at a test wavelength of 450 nm and a reference wavelength of 630 nm. n=3, mean +/- stdev. *Data in collaboration with Dr. Kazuhide Hayakawa.

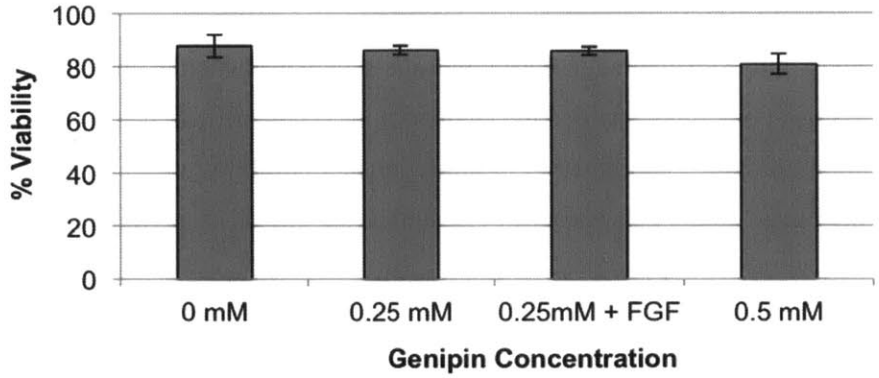

Figure 4-11: 24 hour viability assay for genipin toxicity. Constructs were made in the same configuration as the migration assay. Genipin (0-0.5 mM) and/or FGF-2 (150 ng/ml) were added to the gels. After 24 hours, the constructs were stained with calcein AM and ethidium homodimer and visualized at 4x with an epifluorescent microscope. Three independent fields of view were taken at random for each gel. Percentage viability was calculated based on the ratio of live to total (live+dead) cell count. n=4 gels mean ± stdev

4.6. Discussion

4.6.1 Rationale for scaffolding to enable astrocyte infiltration after SCI

The microenvironment of the damaged spinal cord is unfavorable for the re-growth of axons. Necrosis and the influx of inflammatory cells within the lesion core leads to the formation of a cystic cavity which is walled off from viable neural tissue by a dense glial scar. Depending on the extent of damage to the surrounding dura, a fibrous scar containing meningeal fibroblast and Schwann cell infiltration may also be present within the defect. As a result, in addition to the barrier imposed by the glial scar, the cavitary nature of the defect itself provides no framework for axonal growth. Therefore, regeneration likely requires replacement of the lesioned area with a tissue regenerative matrix.

Endogenous astrocytes may be a promising candidate cell to target after injury since their native response is to proliferate and migrate towards the damaged tissue and they have the capability to form the framework for subsequent axon ingrowth. Renault-Mihara, *et al.*, showed that enhancement of astrocyte migration may be beneficial to regeneration. The group investigated systemic administration of a glycogen synthase kinase-3 (GSK-3) inhibitor Ro3303544 for 5 days after SCI in mice in order to promote astrocyte migration [36]. The inhibitor resulted in accelerated migration of reactive astrocytes, which restricted inflammatory cell infiltration, spared myelinated axons, decreased scarring, and promoted functional recovery.

4.6.2 Gel permissiveness of astrocyte infiltration

In the present study, injectable collagen-based hydrogels were evaluated in an astrocyte cell outgrowth assay. The assay, at one time, enabled the evaluation of: 1) the permissiveness of the collagen gels to astrocyte infiltration, through a combination of migration and proliferation; 2) the release and retained bioactivity of the FGF-2 in the gels and in LMTs; and 3) the effects of genipin on cell motility.

All of the collagen gels containing FGF-2 elicited a pro-outgrowth effect on the astrocytes while the collagen hydrogels without chemokine (group labeled Col, Col-Gen, or Col LMT PBS) induced minimal astrocyte recruitment (**Figure 4-3**). Specifically, the groups Col FGF High, Col LMT FGF High, Col LMT FGF Low, and Col Gen LMT FGF High all had substantial increases in infiltration over control gels. Despite the wide range of FGF-2 concentrations and release rates, there was only a small difference among the outgrowth inductive properties of the FGF-2 containing gels.

For the FGF-2 containing groups—Col LMT FGF low, Col LMT FGF High, and Col FGF High—the distance histograms (**Figure 4-4a)** demonstrated a linear decrease in the number of cells as the distance from the interface increased. Moreover, the plot of the percentage of cells versus distance (**Figure 4-4b)** showed a fairly even distribution of cells as distance increased suggesting that cells

exposed to FGF continued to penetrate deeply into the gel in contrast to groups without FGF-2, which stayed clustered at the interface.

In groups without FGF-2, the distance histograms (**Figure 4-4a)** showed an almost exponential drop off in the number of cells with increasing distance. The plot of the percentage of cells versus distance (**Figure 4-4b)** revealed a high percentage of cells very close to the interface. The presence of 0.1 mg/ml LMTs was enough to slightly inhibit cell outgrowth from the astrocyte-seeded gel.

It was noted that the number of cells infiltrating the gels tapered off after 6 days (**data not shown)** suggesting a decreased driving force for outgrowth. The deep penetration (>1 mm, and up to 2 mm in some gels) of astrocytes into the gel over 10 days shows that these gels hold potential to fully bridge SCI defects *in vivo* of up to 4 mm if astrocytes are infiltrating from both ends. These distances are also promising cases of human SCI, which typically have defects smaller than a spinal segment [37]. Early repopulation of the defect will be important for forming the regenerative template for axon growth.

4.6.3 Effects of genipin

Genipin had a significant effect on preventing cellular outgrowth from the astrocyte core gel. This finding is supported by several studies noting the anti-proliferative, anti-migratory, anti-fibrotic, and anti-contraction effects genipin on other cell types such as fibroblasts and endothelial cells [38, 39].

A genipin concentration of 0.25 mM was chosen for this study in order to lessen potential confounding effects on outgrowth due to cytotoxicity. As seen in **Figure 4-6** there was a high density of viable cells in the genipin-containing groups. Viability assays conducted on Col-Gen gels in the same configuration as the outgrowth assay, showed minimal toxicity with genipin concentrations of 0.25mM and 0.5 mM (**Figure 4-11**), suggesting that the cytotoxicity of the surrounding gel was not a major factor in the observed results. Additionally, the presence of FGF either within LMTs or freely in the gel did not significantly impact the viability suggesting that FGF-2 did not have any additional protective effect against genipin induced toxicity.

It is also possible that the additional strength and degradation resistance imparted by genipin on the gels prevented cellular outgrowth, however at the concentration used especially in the presence of amine rich media which readily reacts with free genipin, the increases would only be mild and would not account for the dramatic decrease in cell outgrowth seen [34]. Further evidence that the genipin induces a decrease in cellular infiltration primarily through its actions on the cells as opposed to its effects on the physical properties of the collagen gel includes: a) priming cells with genipin decreased the outgrowth even though there were only trace amounts of genipin in the encapsulating gel due to diffusion from the

core; b) the addition of FGF-2 dramatically enhanced cellular outgrowth although genipin was still present; and c) genipin decreased the proliferation of astrocytes as noted in **Figure 4-10**.

One of the most dramatic increases (~1200%) in cell outgrowth among groups occurred when FGF-2 LMTs were added to Col-Gen gels. The effect of FGF-2 still exhibited a lag period with cells emerging from the gel after 3-4 days corresponding to a timeframe when the genipin was most likely fully reacted with collagen and amines in the media and the cells could also degrade the cross-linked collagen fibers. From the distance histogram and percentage of cells **(Figure 4-4a,b)** the groups containing both genipin and FGF-2 group had a higher percentage of cells closer to the interface that the corresponding FGF-2 group without genipin. This was most likely due to the early inhibition of outgrowth by genipin. It is also important to note that adding free FGF-2 directly to Col-Gen gels was less effective in promoting outgrowth than if it was loaded within LMTs, suggesting that may react with FGF-2 reducing its bioactivity. These results suggest that the use of growth factors such as FGF-2 protected within a secondary release vehicle such as LMTs, would be required to maintain an early cell permissive environment within the Col-Gen gels.

Of note is that the concentration of genipin used in this study was lower than would be proposed in an *in vivo* study. Since the volume of cell-seeded gel was much smaller than the volume of genipin containing gel there was a large amount of free genipin relative to the volume of cells. *In vivo* the reverse would be true and the volume of injected collagen-genipin gel would be much lower than the surrounding tissue, thus mitigating the cytotoxicity of higher genipin concentrations while still allowing for substantial increases in gel strength.

4.6.4 Cell phenotype

In groups without FGF-2, there was little to no chain-like outgrowth phenomena and only a few isolated cells left the gels. However, in many instances for gels containing FGF-2, astrocytes moved in a chain-like outgrowth fashion traveling in multiple straight lines out of the gel **(Figures 4-6, 4-7)**. Of specific note is the cells undergoing chain-like outgrowth had an elongated bipolar morphology similar to radial glia, the immature cells that are supportive of axon growth during development [40]. With increasing concentrations of FGF-2, the cells became more clustered as they left the gel forming more disorganized clumps of stellate cells in addition to directed projections (chain-like with clustering) which more resembled astrogliosis. The formation of directed growth is also a profound finding as it may create an organized framework for axon migration in an otherwise non-oriented gel.

In animals capable of spinal cord regeneration, such as the newt [41] and zebrafish [42], GFAP-positive glia serve as a bridge to facilitate axons crossing the injury site. Goldshmit, *et al.*, showed that

FGF signaling regulates the regenerative behavior of zebrafish glia post injury causing them to dedifferentiate, proliferate, and migrate towards the injury site, then differentiate to adopt an elongated bipolar morphology, and form axon growth permissive bridges across the lesion. Primate astrocytes activated by FGF-2 adopted a similar morphology to that induced in the zebrafish glia and were able to accelerate the defect closure in a scratch wound assay [42].

Similarly, transforming growth factor-a (TGF-a) has been show to induce the proliferation, migration, and transformation towards a radial glia-like bipolar morphology of astrocytes and glial progenitors, which allowing them to be highly permissive of axonal growth [43]. Intrathecal delivery or endogenous overproduction of TGF-a (via adeno-associated virus injection) in mice was able to enhance astrocyte infiltration and axonal growth within the injury site [43, 44].

While FGF-2 stimulates many pro-regenerative effects, it also has the potential to negatively affect the injury site, especially at higher concentrations, which may induce gliosis or fibrosis. Many studies support the astrogliotic effects of FGF-2 *in vivo* [20-24]. For example, normal brain astrocytes exposed to high dosages of FGF-2 at 10 μg/ml (administered to the cerebrospinal fluid) underwent astrogliosis, while exposure to 0.5 μg/ml in CSF did not induce such changes [21]. In the same study, the high FGF-2 dosage disrupted myelin production in mature oligodendrocytes, caused reactive changes in oligodentrocyte progenitor cells (OPCs), and increase accumulation and activation of microglia [21]. The lower dosage did not induce such effects and actually increased recruitment of oligodendrocytes. While FGF-2 promotes the survival and proliferation of OPCs, it can also prevent their maturation; therefore, high dosages could be detrimental to remyelination of newly growing and spared fibers [45]. Interestingly, injection of FGF-2 after an electrolytic injury in the brain of adult rats did not significantly increase the level of reactive gliosis induced by the injury alone but rather accelerated the actions of the astrocytes [20]. FGF-2 can also lead to fibroblast proliferation, which may increase the formation of scar tissue in and around the cord [46] however, FGF-2 appears to have a positive effect on reducing scar formation in skin wounds [47]. FGF-2 can also lead to an increased expression of endothelial cell adhesion molecules, which could enhance the recruitment of monocytes, T cells, and neutrophils [48].

While in the present study it is unclear if the astrocytes in the encapsulating gels containing FGF-2 will be beneficial towards regeneration *in vivo*, the observed chain-like outgrowth phenotype of many astrocytes within the gels is promising. Future work should be done to best understand the phenotype of the cells including growth factor (*viz.*, brain-derived neurotrophic factor and neurotrophic growth factor) and chondroitin sulfate proteoglycan production and expression of immature cell markers including nestin, vimentin, and brain lipid binding protein.

4.6.5 Sustained delivery and dosage of FGF-2

The FGF-2 concentrations investigated in this study showed that a wide range of dosages over which FGF-2 may elicit pro-outgrowth effects. The range of FGF-2 concentrations investigated in this study are appropriate for translation into an *in vivo* study. From our predictions the low FGF-2 LMT group in total contained approximately 20 ng FGF-2 while the high FGF-2 group had up to 200 ng (included encapsulated and the approximately 1% of un-removed protein from the rinse step). Prior *in vitro* studies report migratory effects with as low as 20 ng/ml FGF-2 in media [11], which is comparable to the results of this study. Literature reports of *In vivo* dosages of FGF-2 in models of SCI were used in the in the range 168 ng- 21 μg total, released over 7-14 days [26, 27, 29, 49].

In the present study, it was difficult to distinguish the importance of a sustained release of FGF-2 as both free and encapsulated FGF-2 produced similar effects on the cells. There are several explanations for this observation. Since, FGF-2 induces the expression of its own mRNA, exposure to FGF-2 may trigger an autocrine response, within the astrocytes leading to sustained production of the growth factor [50]. Astrocytes have been shown to secrete heparin sulfate proteoglycans (HSPGs) *in vitro,* particularly when exposed to serum containing media [51]. HSPGs are essential to FGF-2 dimerization and FGF receptor activation [52]. FGF-2 is known to strongly bind to HSPGs, so it is feasible that FGF-2 is sequestered in the ECM surrounding the astrocytes [11]. Additionally, due to the set-up of the outgrowth assay, it was not possible to create an "infinite sink" environment in which the growth factor could dissipate into. At most, the growth factor concentration was decreased by ½ with each media change, which occurred at 48-hour intervals. This could have given an effective sustained release in the group containing free FGF-2 without a delivery vehicle.

Priming the astrocytes with a high concentration of FGF-2 prior to encapsulating them within a collagen gel gave enhanced growth over non-primed cells, but did not stimulate the same degree of infiltration, cell elongation, or chain-like outgrowth as an equivalent or 10-fold less concentration within the encapsulating gel. This experiment suggests that even a short exposure to FGF-2 is enough to stimulate an increased outgrowth of astrocytes however; a more sustained external source of FGF-2 is required for a more robust response and chain-like outgrowth.

Moving forward towards an *in vivo* study, there are several advantages of using a separate delivery vehicle for FGF-2 within the collagen gels. The presence of FGF-2 LMTs appeared to increase the penetration distance of astrocytes into the gel over groups containing free FGF (**Figure 4-3**), suggesting that sustained release is important for enhancing continued movement into the gel. LMTs also serve to protect the bioactivity of FGF-2 especially during the collagen-genipin cross-linking process. Both the number of cells crossing the interface and their penetration distance in Col-Gen groups containing FGF was enhanced when the FGF-2 was contained within LMTs (**Figure 4-3**). This also

becomes more important as the concentration of genipin is increased. LMTs can prevent a bolus release of FGF-2, which can have an adverse effect on gliosis and fibrosis and mentioned above. FGF-2 will also have the potential to remain localized long enough to have a neuroprotective effects. For example, several studies have investigated the benefits of administering FGF-2 to rodents after SCI. The delivery of FGF-2 to moderate and severe contusion SCI via an infusion pump both rostral and caudal to the injury resulted in enhanced functional recovery and tissue sparing [26, 49]. The authors suggested that the beneficial effects of acute FGF-2 treatment are manifested over a 2-3 week time period after SCI. The neuroprotective effect of FGF-2 can also be seen by enhanced tissue sparing 1-week post contusive injury and a two-fold increase in surviving ventral horn neurons adjacent to the injury site, which, attenuated respiratory deficits due to the injury [27, 29].

4.6.6 Proliferation

The proliferation and cellular localization data of the gel suggest that the outgrowth phenomenon of the astrocytes was not principally due to proliferation. DAPI staining of the center of the gels showed no significant difference in the cell number among groups, except for Col-Gen groups (**Figure 4-8**). The number of cells at the edge of the gel was also fairly constant among groups with a slight increase in number for FGF-2 containing groups. These findings are consistent with the Ki-67 immunostaining that revealed that only a small percentage of astrocytes in the core of the outgrowth assay gel were proliferating at 10 days, and that the number of proliferating cells was similar between control collagen and FGF-2-containing gels (**Figure 4-9**). In monolayer culture, FGF-2 significantly stimulated astrocyte proliferation in a 48-hour cell proliferation assay (**Figure 4-10**). Interestingly, the proliferation assay exhibited an insignificant dose dependency over several orders of magnitude in FGF-2 concentration, particularly in the ng/ml range relevant to the current study, and actually decreased proliferation at 50 μg/ml. Taken together these data suggest that the FGF-2-containing gels may have experienced a similar initial burst in proliferation, with the subsequent outgrowth behavior dictated by non-proliferative FGF-2-induced cell migration and changes in cell phenotype.

Faber-Elman, *et al.*, previously explored the migration of astrocytes in response to the presence of FGF-2, using a 1D scratch wound assay [11]. The study showed that in response to 20 ng/ml FGF-2 in the media, astrocytes repopulated the "wounded" area 800% more control cultures. They also demonstrated that proliferation was not a key element of astrocyte migration in this assay as only 21-31% of the repopulating cells in all cultures (FGF-2, control, or other growth factors) were proliferating cells. Recently Lichtenstein, *et al.*, showed that FGF-2 induces astrocyte migration through the activation of the JNK and ERK or FAK signaling pathways [53]. Using a scratch wound assay, this group also showed that FGF-2 accelerated defect closure whether or not a proliferation inhibitor cytosine arabinoside was

added. They suggested that the acceleration was due to increased cellular polarity and migration as opposed to proliferation.

The outgrowth assay set-up did not allow for the detection of a specific chemotactic effect because the concentration of growth factor quickly equilibrated throughout the system In the current work, the assay was not employed for the definitive differentiation contributing effects of proliferation and migration on astrocyte infiltration of the gels. Future studies may be directed towards separating these individual contributions by adding an anti-mitotic compound such as aphidicolin, demecolcin or nocodazole to the assay. In the present study, the presence of FGF-2 had a profound effect on stimulating infiltration of the gel, which *in vivo* could translate to robust repopulation of the gel-filled defect.

4.7 References:

[1] Kalman M. Glial reaction and reactive glia. In: Leif H, editor. Advances in Molecular and Cell Biology: Elsevier; 2003. p. 787-835.

[2] Sofroniew MV. Molecular dissection of reactive astrogliosis and glial scar formation. Trends Neurosci. 2009;32:638-47.

[3] Robel S, Berninger B, Gotz M. The stem cell potential of glia: lessons from reactive gliosis. Nat Rev Neurosci. 2011;12:88-104.

[4] Faulkner JR, Herrmann JE, Woo MJ, Tansey KE, Doan NB, Sofroniew MV. Reactive astrocytes protect tissue and preserve function after spinal cord injury. J Neurosci. 2004;24:2143-55.

[5] Sofroniew MV. Reactive astrocytes in neural repair and protection. Neuroscientist. 2005;11:400-7.

[6] Buffo A, Rolando C, Ceruti S. Astrocytes in the damaged brain: molecular and cellular insights into their reactive response and healing potential. Biochemical pharmacology. 2010;79:77-89.

[7] Rolls A, Shechter R, Schwartz M. The bright side of the glial scar in CNS repair. Nat Rev Neurosci. 2009;10:235-41.

[8] Davies JE, Proschel C, Zhang N, Noble M, Mayer-Proschel M, Davies SJ. Transplanted astrocytes derived from BMP- or CNTF-treated glial-restricted precursors have opposite effects on recovery and allodynia after spinal cord injury. J Biol. 2008;7:24.

[9] Davies SJ, Goucher DR, Doller C, Silver J. Robust regeneration of adult sensory axons in degenerating white matter of the adult rat spinal cord. J Neurosci. 1999;19:5810-22.

[10] Davies SJ, Fitch MT, Memberg SP, Hall AK, Raisman G, Silver J. Regeneration of adult axons in white matter tracts of the central nervous system. Nature. 1997;390:680-3.

[11] Faber-Elman A, Solomon A, Abraham JA, Marikovsky M, Schwartz M. Involvement of wound-associated factors in rat brain astrocyte migratory response to axonal injury: in vitro simulation. J Clin Invest. 1996;97:162-71.

[12] Hou YJ, Yu AC, Garcia JM, Aotaki-Keen A, Lee YL, Eng LF, et al. Astrogliosis in culture. IV. Effects of basic fibroblast growth factor. J Neurosci Res. 1995;40:359-70.

[13] Zai LJ, Yoo S, Wrathall JR. Increased growth factor expression and cell proliferation after contusive spinal cord injury. Brain Res. 2005;1052:147-55.

[14] Bikfalvi A, Klein S, Pintucci G, Rifkin DB. Biological roles of fibroblast growth factor-2. Endocr Rev. 1997;18:26-45.

[15] Freudenberg U, Hermann A, Welzel PB, Stirl K, Schwarz SC, Grimmer M, et al. A star-PEG-heparin hydrogel platform to aid cell replacement therapies for neurodegenerative diseases. Biomaterials. 2009;30:5049-60.

[16] Mahoney MJ, Anseth KS. Contrasting effects of collagen and bFGF-2 on neural cell function in degradable synthetic PEG hydrogels. J Biomed Mater Res A. 2007;81:269-78.

[17] Bribian A, Barallobre MJ, Soussi-Yanicostas N, de Castro F. Anosmin-1 modulates the FGF-2-dependent migration of oligodendrocyte precursors in the developing optic nerve. Mol Cell Neurosci. 2006;33:2-14.

[18] Yun YR, Won JE, Jeon E, Lee S, Kang W, Jo H, et al. Fibroblast growth factors: biology, function, and application for tissue regeneration. J Tissue Eng. 2010;2010:218142.

[19] Polikov VS, Su EC, Ball MA, Hong JS, Reichert WM. Control protocol for robust in vitro glial scar formation around microwires: essential roles of bFGF and serum in gliosis. Journal of neuroscience methods. 2009;181:170-7.

[20] Eclancher F, Kehrli P, Labourdette G, Sensenbrenner M. Basic fibroblast growth factor (bFGF) injection activates the glial reaction in the injured adult rat brain. Brain Res. 1996;737:201-14.

[21] Goddard DR, Berry M, Kirvell SL, Butt AM. Fibroblast growth factor-2 induces astroglial and microglial reactivity in vivo. J Anat. 2002;200:57-67.

[22] Reilly JF, Bair L, Kumari V. Heparan sulfate modifies the effects of basic fibroblast growth factor on glial reactivity. Brain Res. 1997;759:277-84.

[23] Silver J, Miller JH. Regeneration beyond the glial scar. Nat Rev Neurosci. 2004;5:146-56.

[24] Menon VK, Landerholm TE. Intralesion injection of basic fibroblast growth factor alters glial reactivity to neural trauma. Exp Neurol. 1994;129:142-54.

[25] Baumann MD, Kang CE, Tator CH, Shoichet MS. Intrathecal delivery of a polymeric nanocomposite hydrogel after spinal cord injury. Biomaterials. 2010;31:7631-9.

[26] Rabchevsky AG, Fugaccia I, Turner AF, Blades DA, Mattson MP, Scheff SW. Basic fibroblast growth factor (bFGF) enhances functional recovery following severe spinal cord injury to the rat. Exp Neurol. 2000;164:280-91.

[27] Lee TT, Green BA, Dietrich WD, Yezierski RP. Neuroprotective effects of basic fibroblast growth factor following spinal cord contusion injury in the rat. J Neurotrauma. 1999;16:347-56.

[28] Jimenez Hamann MC, Tator CH, Shoichet MS. Injectable intrathecal delivery system for localized administration of EGF and FGF-2 to the injured rat spinal cord. Exp Neurol. 2005;194:106-19.

[29] Teng YD, Mocchetti I, Taveira-DaSilva AM, Gillis RA, Wrathall JR. Basic fibroblast growth factor increases long-term survival of spinal motor neurons and improves respiratory function after experimental spinal cord injury. J Neurosci. 1999;19:7037-47.

[30] Kang CE, Tator CH, Shoichet MS. Poly(ethylene glycol) modification enhances penetration of fibroblast growth factor 2 to injured spinal cord tissue from an intrathecal delivery system. J Control Release. 2010;144:25-31.

[31] Meilander NJ, Yu X, Ziats NP, Bellamkonda RV. Lipid-based microtubular drug delivery vehicles. J Control Release. 2001;71:141-52.

[32] Jain A, Kim Y, McKeon R, Bellamkonda R. In situ gelling hydrogels for conformal repair of spinal cord defects, and local delivery of BDNF after spinal cord injury. Biomaterials. 2006;27:497-504.

[33] Lee H, McKeon RJ, Bellamkonda RV. Sustained delivery of thermostabilized chABC enhances axonal sprouting and functional recovery after spinal cord injury. Proc Natl Acad Sci U S A. 2010;107:3340-5.

[34] Macaya D, Ng KK, Spector M. Injectable Collagen-Genipin Gel for the Treatment of Spinal Cord Injury: In Vitro Studies. Adv Funct Mater. 2011;21:4788-97.

[35] Hayakawa K, Arai K, Lo EH. Role of ERK map kinase and CRM1 in IL-1beta-stimulated release of HMGB1 from cortical astrocytes. Glia. 2010;58:1007-15.

[36] Renault-Mihara F, Katoh H, Ikegami T, Iwanami A, Mukaino M, Yasuda A, et al. Beneficial compaction of spinal cord lesion by migrating astrocytes through glycogen synthase kinase-3 inhibition. EMBO molecular medicine. 2011;3:682-96.

[37] Norenberg MD, Smith J, Marcillo A. The pathology of human spinal cord injury: defining the problems. J Neurotrauma. 2004;21:429-40.

[38] Kitano A, Saika S, Yamanaka O, Ikeda K, Reinach PS, Nakajima Y, et al. Genipin suppresses subconjunctival fibroblast migration, proliferation and myofibroblast transdifferentiation. Ophthalmic Res. 2006;38:355-60.

[39] Kitano A, Saika S, Yamanaka O, Reinach PS, Ikeda K, Okada Y, et al. Genipin suppression of fibrogenic behaviors of the alpha-TN4 lens epithelial cell line. J Cataract Refract Surg. 2006;32:1727-35.

[40] Vaccarino FM, Fagel DM, Ganat Y, Maragnoli ME, Ment LR, Ohkubo Y, et al. Astroglial cells in development, regeneration, and repair. Neuroscientist. 2007;13:173-85.

[41] Zukor KA, Kent DT, Odelberg SJ. Meningeal cells and glia establish a permissive environment for axon regeneration after spinal cord injury in newts. Neural development. 2011;6:1.

[42] Goldshmit Y, Sztal TE, Jusuf PR, Hall TE, Nguyen-Chi M, Currie PD. Fgf-dependent glial cell bridges facilitate spinal cord regeneration in zebrafish. J Neurosci. 2012;32:7477-92.

[43] White RE, Rao M, Gensel JC, McTigue DM, Kaspar BK, Jakeman LB. Transforming growth factor alpha transforms astrocytes to a growth-supportive phenotype after spinal cord injury. J Neurosci. 2011;31:15173-87.

[44] White RE, Yin FQ, Jakeman LB. TGF-alpha increases astrocyte invasion and promotes axonal growth into the lesion following spinal cord injury in mice. Exp Neurol. 2008;214:10-24.

[45] Nair A, Frederick TJ, Miller SD. Astrocytes in multiple sclerosis: a product of their environment. Cell Mol Life Sci. 2008;65:2702-20.

[46] Parr AM, Tator CH. Intrathecal epidermal growth factor and fibroblast growth factor-2 exacerbate meningeal proliferative lesions associated with intrathecal catheters. Neurosurgery. 2007;60:926-33; discussion -33.

[47] Spyrou GE, Naylor IL. The effect of basic fibroblast growth factor on scarring. Br J Plast Surg. 2002;55:275-82.

[48] Zittermann SI, Issekutz AC. Basic fibroblast growth factor (bFGF, FGF-2) potentiates leukocyte recruitment to inflammation by enhancing endothelial adhesion molecule expression. Am J Pathol. 2006;168:835-46.

[49] Rabchevsky AG, Fugaccia I, Fletcher-Turner A, Blades DA, Mattson MP, Scheff SW. Basic fibroblast growth factor (bFGF) enhances tissue sparing and functional recovery following moderate spinal cord injury. J Neurotrauma. 1999;16:817-30.

[50] Gomez-Pinilla F, Lee JW, Cotman CW. Distribution of basic fibroblast growth factor in the developing rat brain. Neuroscience. 1994;61:911-23.

[51] Ard MD, Bunge RP. Heparan sulfate proteoglycan and laminin immunoreactivity on cultured astrocytes: relationship to differentiation and neurite growth. J Neurosci. 1988;8:2844-58.

[52] Zhang Z, Coomans C, David G. Membrane heparan sulfate proteoglycan-supported FGF2-FGFR1 signaling: evidence in support of the "cooperative end structures" model. J Biol Chem. 2001;276:41921-9.

[53] Lichtenstein MP, Madrigal JL, Pujol A, Galea E. JNK/ERK/FAK mediate promigratory actions of basic fibroblast growth factor in astrocytes via CCL2 and COX2. Neuro-Signals. 2012;20:86-102.

Chapter 5:

Qualitative biocompatibility pilot study of injectable collagen-genipin gels in spinal cord injury

5.1 Introduction and motivation

This chapter describes the early *in vivo* pilot tests of the injectable collagen-genipin gel in a rodent hemi-resection model of SCI. The two formulations of gel used in this study were best guided by the *in vitro* mechanical, cytotoxicity, and astrocyte outgrowth studies presented in chapters 3 and 4. Evaluation was performed at 1 and 4 weeks post injury. It should be noted that the results in this chapter are qualitative due to the low yield of acceptable samples for analysis due to issues with histological processing. Nevertheless, the work presented here gave valuable insight into the feasibility of delivering the gel into the defect and the biomaterial-tissue interaction of collagen-genipin gels with and without and FGF-2 with spinal cord tissue. These results were later used to design a second-generation gel, which was investigated in a complete detailed *in vivo* study using the same animal model (**chapter 6**).

5.2 Overall goal and hypotheses

The **overall goal** of this chapter is to investigate the feasibility and biocompatibility of injectable collagen-genipin gels in a rodent hemi-resection model of SCI.

The **hypotheses** are:

1.) Collagen-genipin gels will undergo gelation sufficiently rapid enough to localize within the defect.

2.) Collagen-genipin gels are permissive to cellular infiltration

3.) A genipin concentration of 0.5 mM will not provoke a severe inflammatory response

4.) Cellular infiltration of the collagen-genipin gel will be enhanced by adding FGF-2 containing LMTs into the gel.

5.3 Methods

5.3.1 Collagen gel fabrication Col-Gen and Col-Gen LMT FGF-2 gels were fabricated as described in chapter 4. Briefly, ice cold 1x phosphate buffered saline (PBS), 5x PBS, 1N NaOH, a stock solution of genipin in 5x PBS (3 mg/mL), and soluble rat tail type I collagen were combined in that order to obtain 2 mg/mL collagen solutions with 0.5 mM genipin at pH 7.5 with 1x ionic strength. LMTs loaded overnight with 1 mg/ml FGF-2 were added to the Col-Gen LMT FGF-2 gels at 0.1 mg/ml.

5.3.2 Animal procedure Adult female Lewis rats (Charles River Laboratories, Wilmington MA) weighing 200-220 grams were used in this study. Animal care and surgical procedures were performed at the Veterans Administration Medical Center Animal Research Facility (Jamaica Plain, MA) and were

approved by the VA Boston Healthcare System Institutional Animal Care and Use Committee (IACUC). Protocol number 188-J.

The hemi-resection injury model is based off of the work performed by Cholas et al.[1] A schematic and images of the injury model and surgical procedure is shown in **Figure 5-1**. The hair on the back of the anesthetized rat was shaved and the skin was cleaned with Betadine. The rat was placed on a flat operating board in the prone position and its limbs were gently fixed in an extended position using rubber bands. Oxygen was continuously supplied to the rat during surgery. A longitudinal incision, 2 inches in length was made through the skin above the thoracic spine and the back musculature was incised along the midline and dissected away from the vertebral column. A dorsal laminectomy was performed between T7 and T10 using small bone rongeurs and microscissors. Bleeding from the muscle was controlled by gelfoam or coagulation with a bipolar cautery. A 3 mm plastic template was placed in the center of the exposed spinal cord and a lateral hemi-resection of the spinal cord was created by making two lateral cuts (3 mm apart) on the left side of the spinal cord using ultra fine surgical scissors or a surgical blade. A midline incision was then made between the lateral cuts using the dorsal spinal vein as a midline marker. A 3 mm gap was created by removing the tissue between the two lateral cuts. Bleeding was controlled using gelfoam placed into the defect site. Once hemostasis was achieved the gelfoam was removed from the defect and the treatment was applied. In col-gen treatment groups, 30 microliters of gel (kept on ice) was delivered into the defect using a computer-controlled microsyringe (Harvard apparatus) over two minutes. After visual confirmation of gel filling and remaining localized within the defect, a piece of collagen type I/III membrane (Bio-Gide, Geistlich Biomaterials, Wolhusen, Switzerland). In Col-gen LMT FGF-2 treatment groups, 30 microliters of gel (kept on ice) was pipetted into the defect in two 15 microliter drops spaced 1 minute apart using a micropipette. After visual confirmation of gel filling and remaining localized within the defect, a thin muscle fascia was placed extradurally over the defect site (covering 2 mm past the spinal cord stumps at both ends) to serve as a dorsal barrier. Following treatment and placement of the dorsal barrier, the overlying musculature was closed using 4-0 vicryl sutures (Johnson and Johnson, Sommerville, NJ) and the skin was closed with wound clips.

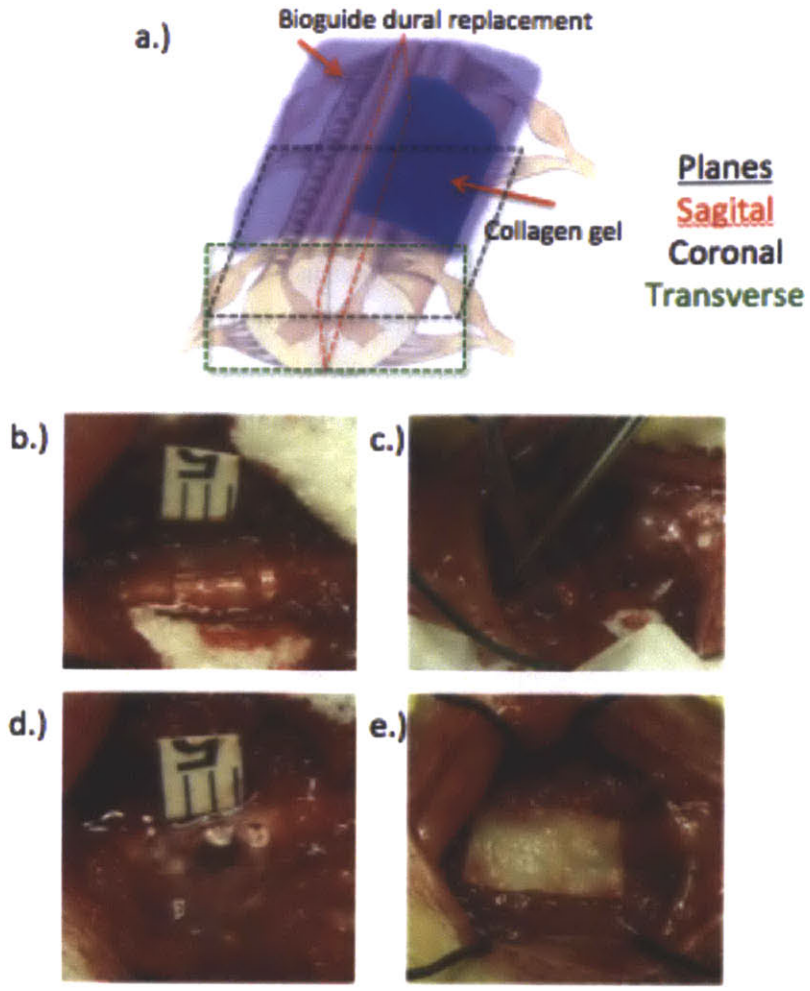

Figure 5-1: a.) Schematic of the left lateral hemi-resection SCI model and planes of sectioning for histology. **b.)**Placement of the 3 mm plastic template on the thoracic spinal cord **c.)** Filling of the defect site with collagen gel via catheter tubing connected to a computer controlled syringe pump **d.)** Gel filling the defect **e.)** Placement of the Bioguide membrane over the defect.

Post-operative care of the animals included placement of the rat on a heating pad to maintain body temperature, subcutaneous injection of 6 ml lactated Ringer's solution to compensate for blood loss during surgery and dehydration, subcutaneous injection of antibiotics (cefazolin sodium 100 mg, 35 mg/kg, Abbot Laboratories, North Chicago, IL), subcutaneous injection of an analgesic, Ketofen (5 mg/kg) and a continuous supply of oxygen until the animals regained consciousness 4-6 hours later. After regaining consciousness, the rats were transferred to their original plastic cage with wood chip bedding and free access to food and water.

Analgesic (ketofen 5 mg/kg) was administered once a day for an additional 3 days post surgery for pain relief, and antibiotics (ceftazolin, 35 mg/kg) was administered twice a day for 1 week post surgery to

prevent bladder infection. Post operatively, the animals lacked a normal micturition reflex and their bladders had to be manually emptied every 12 hours using Crede's maneuver until bladder function recovered.

5.3.3 Animal sacrifice, transcardial perfusion

Animal sacrifice was performed by transcardial perfusion. Rats were administered a dose of 150 mg/kg of sodium pentobarbital and secured to a surgical board. A thoracotomy was performed to expose the heart, after which a needle attached to a peristaltic pump was inserted into the left ventricle and into the ascending aorta. 100 ml of heparinized saline was circulated through the animal, followed by 150 ml 4% paraformaldehyde. Following sacrifice, the spine was removed and placed in 60 ml 4% PFA at 4°C overnight. The following day, for the Col-Gen treatment group, the spine was trimmed of the overlying musculature while leaving the vertebral bone and fascia over the defect intact. For the Col-Gen LMT FGF-2 group, the vertebral bone surrounding the spinal cord was carefully and completely removed from the surrounding vertebra using bone rongeurs, surgical scissors, and a scalpel. All of the spinal cords were then immersion fixed in 4% PFA an additional 3 days at 4°C.

5.3.4 Histology and immunohistochemistry: Samples from the Col-Gen treatment group with the vertebral bone still intact were decalcified in a 15% EDTA at 4°C for 20 days prior to tissue processing. The whole spinal column was then embedded in paraffin using a tissue processor (HypercenterXP, Tissue Processor, ThermoShandon, Houston, TX). Serial sections of the defect were cut at 6 μm with a microtome and mounted on glass slides.

Samples from the Col-Gen LMT FGF-2 treatment group were processed in two ways. For the one-week time point, spinal cords removed from the surrounding vertebrae snap frozen in isobutene at -30°c and embedded in OCT compound (Tissue-Tek, Sakura, The Netherlands). Serial sections were cut at 20 μm on a cryostat (Leica Biosystems, IL, USA). For the four-week time point, spinal cords removed from the surrounding vertebra were cut in half transversely through the center of the defect, one of these halves was then cut coronally through the center of the tissue **Figure 5-2**. The samples were then paraffin processed and sectioned as above.

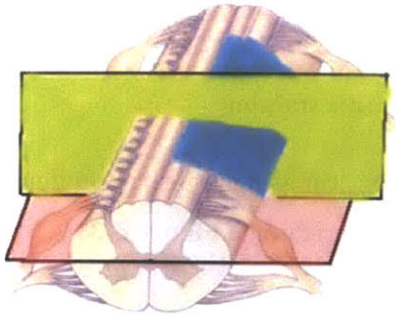

Figure 5-2: Schematic of the multi-plane sectioning technique for four-week Col-Gen LMT FGF-2 samples. Prior to paraffin embedding, the spinal cords were cut in half transversely through the center of the defect and then one of those halves was cut again coronally. The tissue was embedded in a single block to yield two coronal and one transverse plane per section.

Sections were stained with Masson's trichrome, hematoxylin and eosin, or IHC antibody. For IHC staining, a labeled polymer HRP system (AEC+ system, Dako) was used to detect the presence of antibody. Some sections were also counterstained with Mayer's Hematoxylin.

The following antibodies were used in the IHC staining of the paraffin sections containing the defect.

Stain (dilution) Incubation	Antigen retrieval	Company (cat#) Species	Staining color	Cells/ECM Identified
Masson's Trichrome	None	Sigma HT15	Nuclei-black Cytoplasm-red Collagen-blue	Viable tissue Fibrous Scar Gel
Hematoxylin & Eosin	None	Sigma GHS216 HT110232	Nuclei- blue Cytoplastm-pink Col gel-pink	Cellular infiltrate
GFAP (1:1000) 45 min	Protease XIV 20 min	Dako Z0334 Rabbit	Red	Astrocytes
CD68 (1:200) 45 min	Citrate AR 95°C 20 min	AbD serotec MCA341R Mouse	Red	Macrophages (MΦ)
VWF (1:100) 60 min	Protease XIV 40 min	Dako A0082 Rabbit	Red	Endothelial cells/blood vessels
GAP-43 (1:1000) 45 min	Citrate AR 95°C 20 min	Abcam AB12274 Rabbit	Red Blue	Regenerating Axons Nuclear counterstain

5.4 Results:

5.4.1 Appearance of the Col-Gen gel via Masson's trichrome staining

Paraffin embedded Col-Gen gels (both *in vitro* and *in vivo*) appear as light blue amorphous areas with a few noticeable fiber like structures when stained with Masson's trichrome **Figure 5-3**.

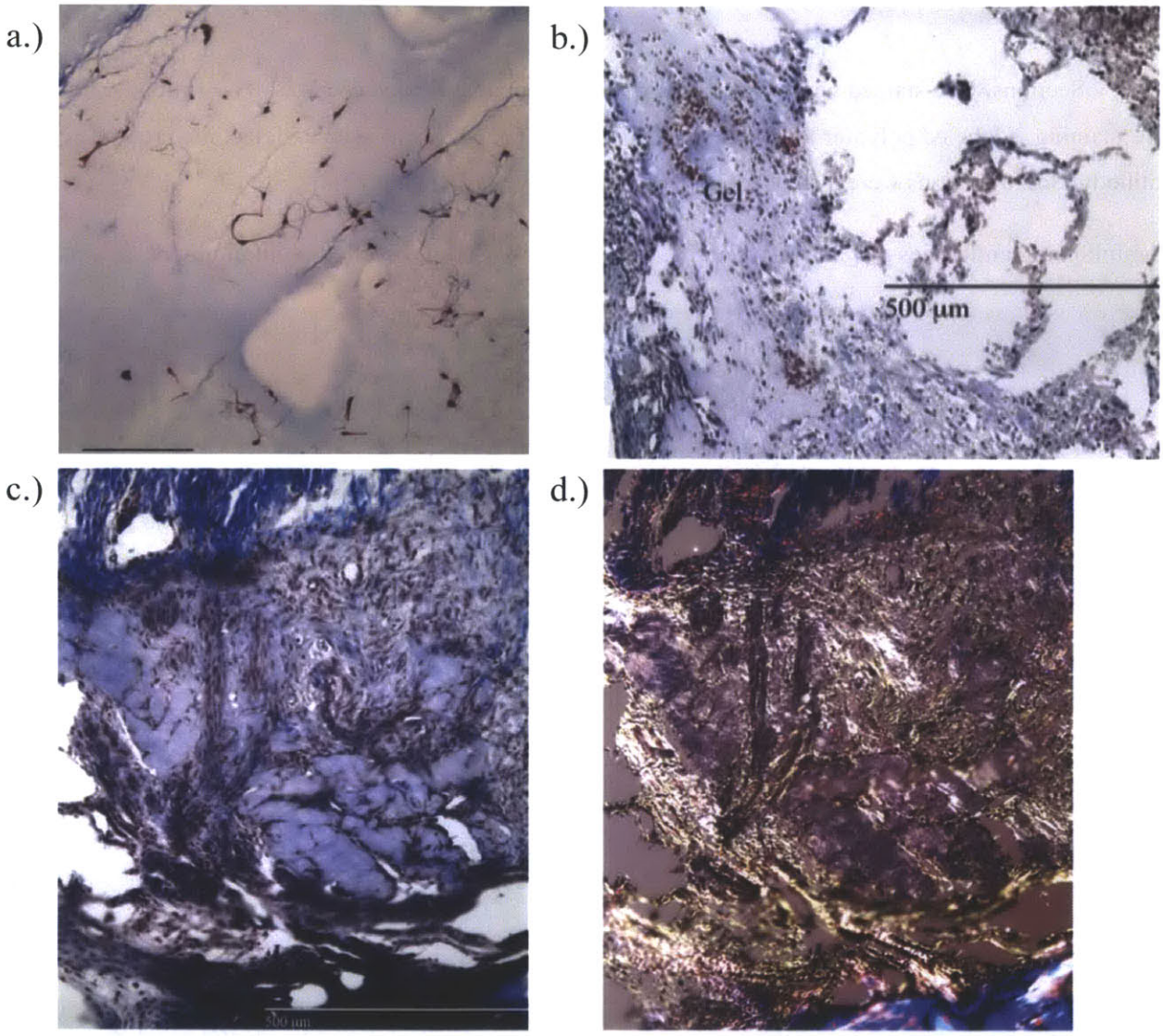

Figure 5-3: Appearance of the Col-Gen gel in Masson's trichrome stained paraffin sections **a.)** *In vitro* containing primary astrocytes. Scale bar 200 µm. **b.)** *In vivo* at one-week post injury. Coronal section. Pale blue area is col-gen gel. **c.)** *In vivo* at four weeks. Sagital section, scale bar 1000 µm. **d.)** Polorized light microscopy of the same image in c.) showing the high birefrigence of the endogenously produced collagen matrix and relative lack of birefrigence in the col-gen gel. Of note is the reasonable amount of amout un-degraded gel (light blue) within the defect of this animal at four weeks. Bands of elongated fibroblast-like cells can be seen traversing through the gel in some areas while in others the gel is largely unpopulated by cells.

5.4.2 Response at one-week Col-Gen treated animals

The success of the surgery (proper anesthesia, controlled bleeding), was noted to have a substantial impact on the severity of the spinal cord injury noted at one week **Figure 5-4**. At one extreme, in one animal the bleeding was so extensive that it resulted in a hematoma encompassing the entire width of the spinal cord. On the other extreme, one animal had a hemi-section injury with no damage to the contralateral white matter.

a.)

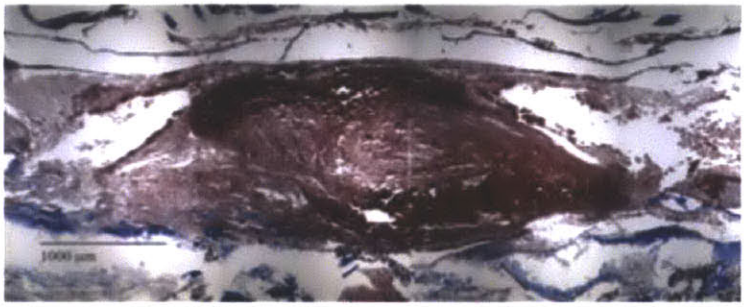

b.)

Figure 5-4: Masson's trichrome stained coronal sections showing the extremes in injury severity at one week **a.)** Complete destruction of the spinal cord and large hematoma formation **b.)** Hemi-resection injury with full sparing of contralateral white matter.

At this time point, there is an expansion in defect area depending on the degree of secondary damage after creation of the primary lesion. The lesion site is filled with cellular debris, red blood cells, and foamy macrophages. There is a substantial degree of infiltration by connective tissue cells with a fibroblast-like appearance that secrete a collagenous ECM. Varying amounts of non-degraded gel can be found in the defect. Within the non-degraded gel, a low density of cells can be observed. Astrocytes are localized to the border of the spared tissue. **Figure 5-5**.

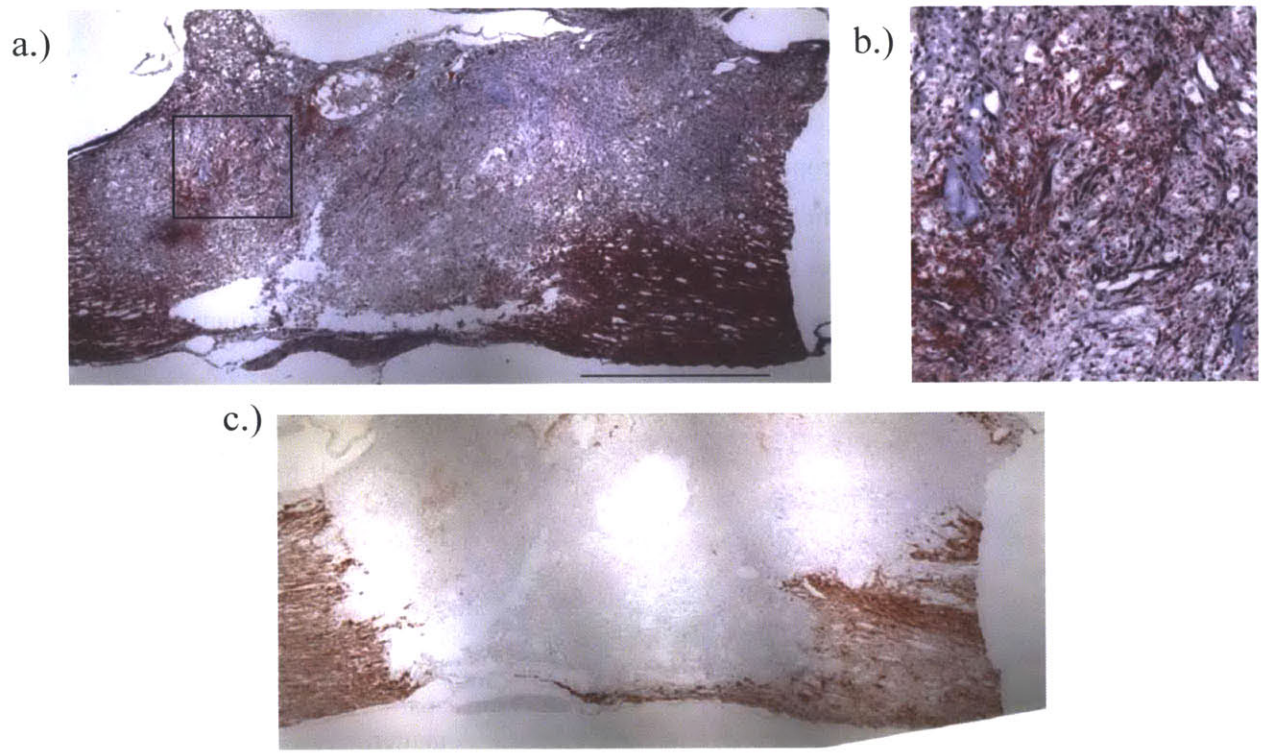

Figure 5-5: Coronal section of the defect in Col-Gen treated animals at 1 week **a.)** Masson's trichrome staining showing a heavy infiltration of cells and the presence of a small amount of un-infiltrated gel. Scale bar 1000 μm **b.)** Magnification of the inset in a.) **c.)** GFAP staining showing astrocytes localized at the border of the lesion. Astrocytes did not survive in areas of secondary damage.

The defect site and any areas of secondary damage/degeneration are heavily infiltrated by CD68+ macrophages. There is a significant amount of angiogenesis occurring by one week as noted by the population of VWF+ endothelial cells within the defect, forming noticeable blood vessels. Several GAP-43+ axons can be seen at the white matter bordering of the defect, however these cells do not enter the defect **Figure 5-6**.

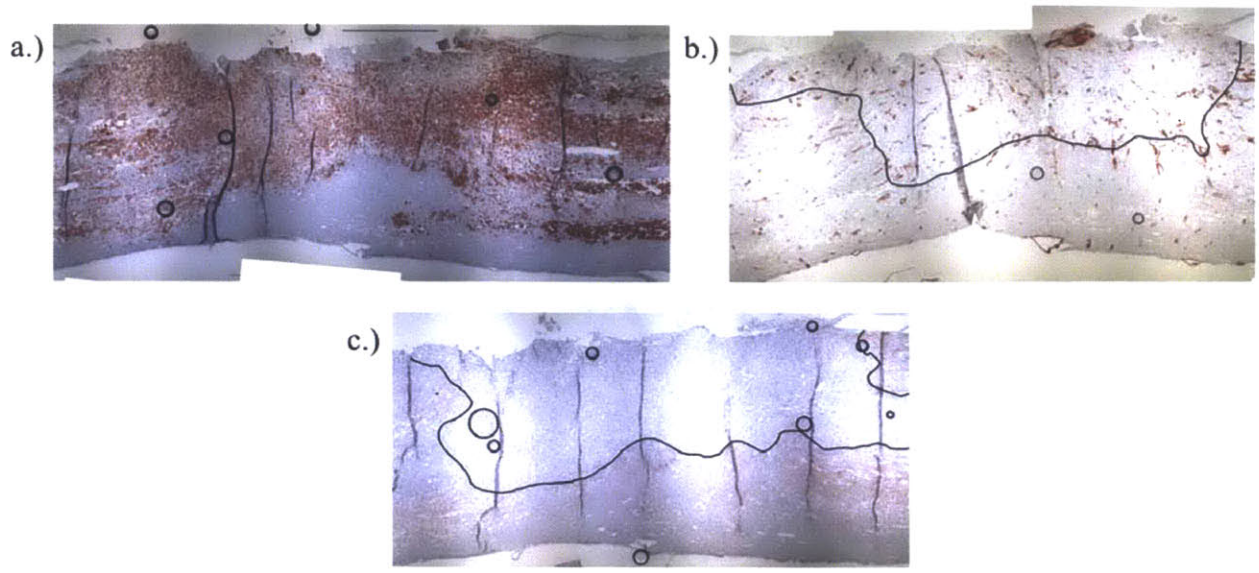

Figure 5-6: Coronal IHC stained sections for **a.)** CD68 (macrophages) **b.)** VWF (endotheial cells/blood vessels) **c.)** GAP-43 regenerating axons. By one-week the defect and areas of secondary damage are heavily infiltrated by macrophages. There is a substantial degree of angiogenesis occurring within the injury site but no regenerating axons can be found within the defect. Scale bar 1000 μm

5.4.3 Response at four-weeks Col-Gen treated animals

Hematoxlin and eosin staining of Col-Gen gel within the defect at four-weeks showed a normal wound healing inflammatory response to injury. Connective tissue can be seen forming around the gel and no atypical inflammatory cells (eosinophils, basophils, plasma cells) could be identified **Figure 5-7.**

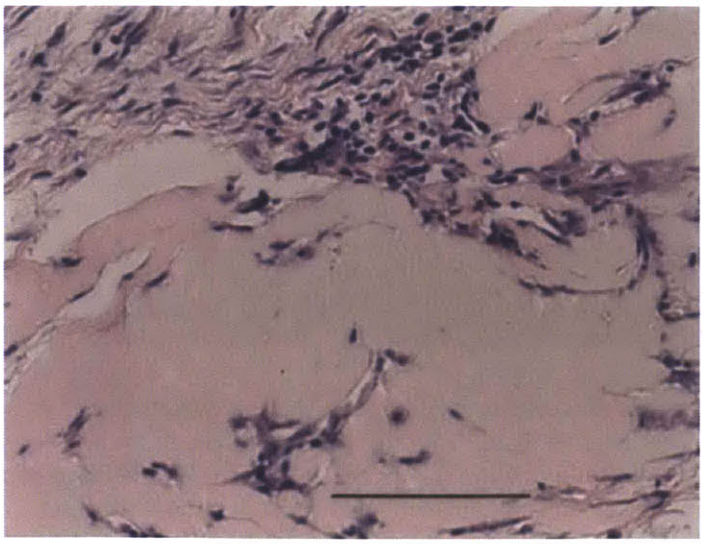

Figure 5-7: Hematoxylin & eosin image of the col-gen gel at 4 weeks post injury. Endogenous connective tissue can be seen adjacent to the gel. Few cells can be seen within the non-degraded gel. There is no noticeable presence of atypical inflammatory cells (eosinophils, basophils, or plasma cells). Scale bar 100 μm

At four-weeks the defect was filled with connective tissue and contained several cavitary areas. Ingrowth of fibrous connective tissue was noted from the veterbra adjacent to the defect. A small amount of non-degraded gel can also still be identified within the defect. Astrocytes could be seen growing into the fibrous tissue on the lateral border of the defect. and a small number of blood vessels could be found in the fibrous tissue of the defect. **Figure 5-8.**

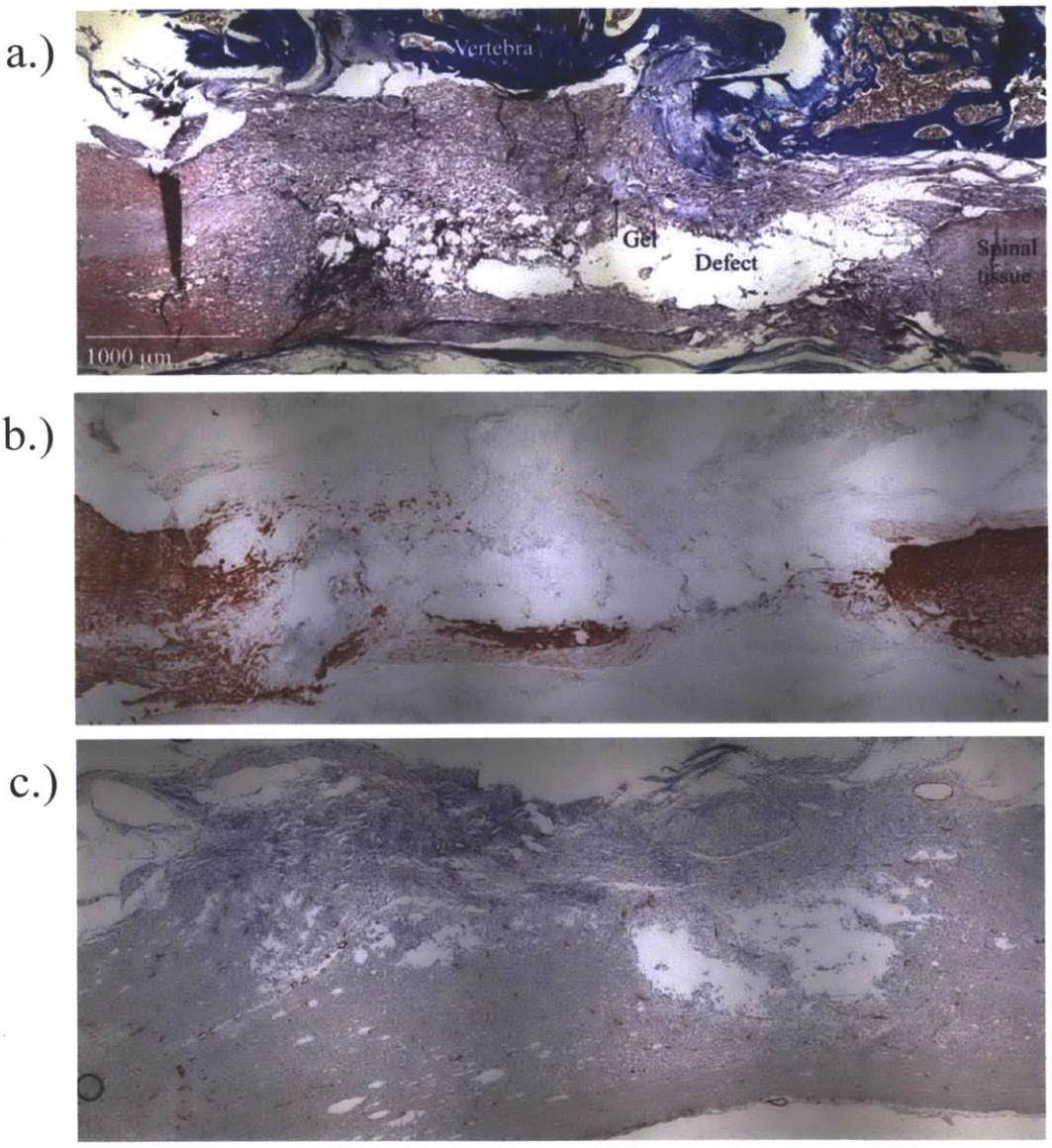

Figure 5-8: Coronal sections of Col-Gen treated animal 4 weeks post injury. **a.)** Masson's trichrome stained section illustrating the ingrowth of fibrous connective tissue from the vertebra adjacent to the defect. A small amount of non-degraded gel can still be found within the defect. **b.)** GFAP IHC section of defect showing a small band of contralateral spared tissue and an ingrowth of astrocytes into the fibrous tissue on the lateral border of the defect. **c.)** VWF IHC section further into the defect showing a small number of blood vessels within the defect. This sectional also shows region of greater tissue sparing

5.4.4 Response at one-week Col-Gen LMT-FGF-2 treated animals

Analysis of Col-Gen LMT FGF-2 treated animals at one-week was limited to Masson's trichrome staining. At one-week there is noticeable disruption to the tissue architecture around the defect area and varying extents of dense connective tissue infiltration **Figure 5-9.** In one sample, a central region of blood clot-gel mixture was found within the defect.

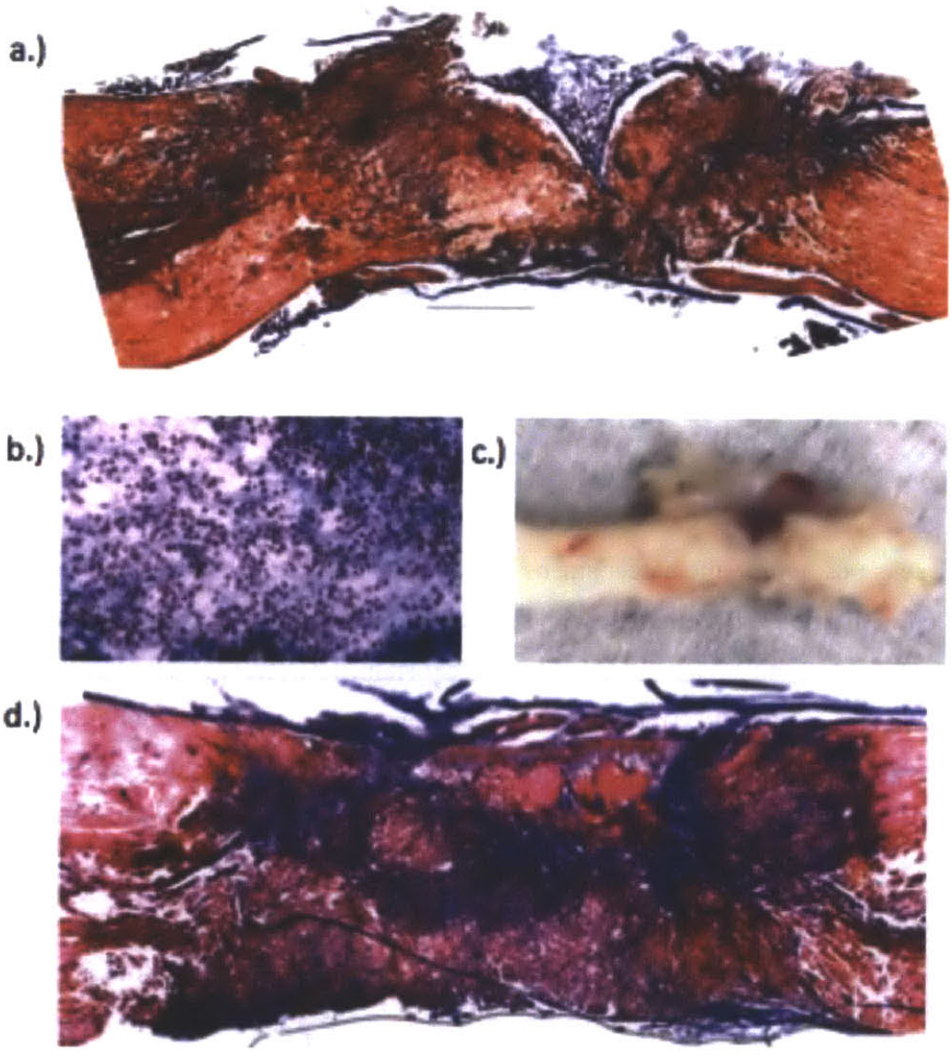

Figure 5-9: a.) Coronal section through the defect at one week for a Col-Gen LMT FGF-2 treated animal. There is noticeable disruption to the tissue architecture around the defect area. There is a central region of un-degraded gel/clot. Frozen section, Masson's trichrome, scale bar 1000 μm. **b.)** Higher magnification image of the tissue inside the un-degraded gel/clot in a.) There is a fibrillar collagenous matrix inclusive of many cells. **c.)** Gross-image of the spinal cord corresponding to the image in a.) the central region appears to contain substantial blood. **d.)** Coronal section through the defect of another animal from the same treatment group showing substantially more fibrous tissue infiltration than the animal in a.)

5.4.5 Response at four-weeks Col-Gen LMT-FGF-2 treated animals

At 4 weeks, the gross appearance of the spinal cord in several animals was severely stenotic and histology analysis of the defect revealed the lesion consisted of dense collagen scar tissue **Figure 5-10**.

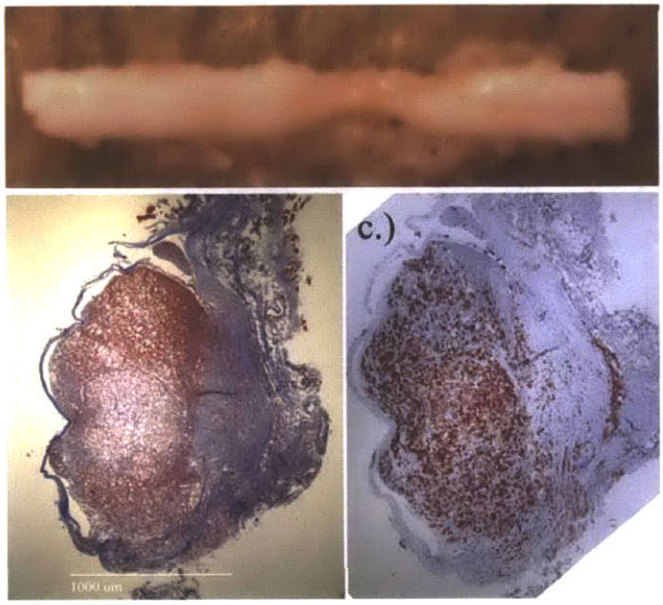

Figure 5-10: a.) Gross image of a spinal cord for a Col-Gen LMT FGF-2 treated animal at four-weeks displaying severe stenosis. Corresponding **b.)** Masson's trichrome **c.)** CD68 stained transverse sections through the defect. The defect has been filled with dense connective tissue which adhered to the overlying fascia, pulling it into the defect. There is substantial macrophage infiltration and tissue destruction of the contralateral white matter.

Four-weeks post injury, the defect site of all most animals (n=5/6) treated with col-gen LMT FGF-2 was filled with a dense fibrotic scar with severe contralateral tissue destruction and fibrous tissue infiltration **Figure 5-11**. Some areas of dense fibrous scar stained positive for GFAP indicating that astrocytes were present in the newly formed tissue. The fibrous scar stained for numerous VWF positive endothelial cells suggesting significant angiogenesis was taking place. Macrophages were present throughout the areas of secondary damage and fibrous infiltration of the spinal cord tissue adjacent to the defect. Macrophages were generally excluded from the areas of dense fibrous tissue formation within the defect. Only one animal showed a half-width injury without significant fibrous/inflammatory infiltration of the contralateral tissue. Within the defect of that animal, there was a dense fibrous scar surrounding a cystic cavity with little astrocyte infiltration of the defect **Figure 5-12**.

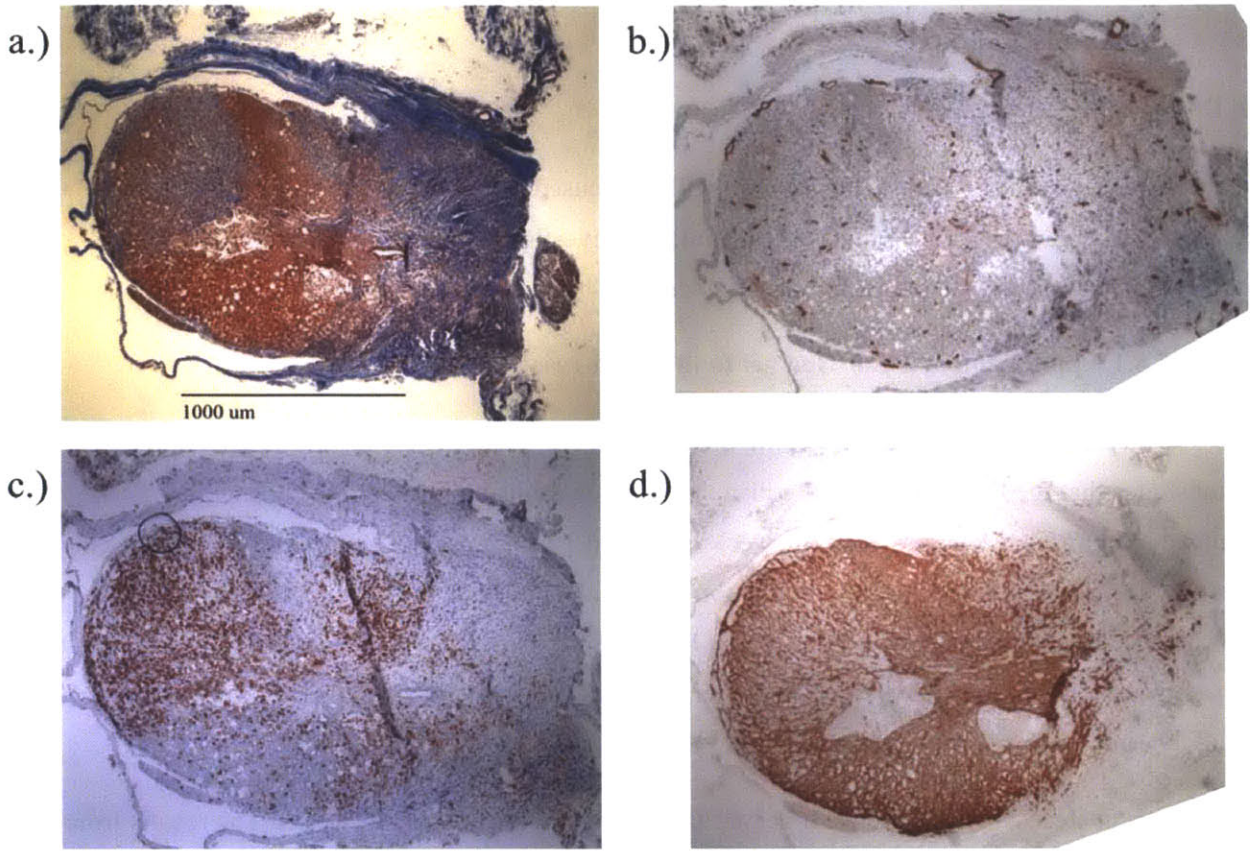

Figure 5-11: Transverse sections through the center the defect of an animal treated with Col-Gen LMT FGF-2 which did not have a large degree of stenosis at the level of the defect. a.) Masson's trichrome staining showing dense collagenous scarring on the defect side as well as fibrous infiltration of contralateral white matter. b.) VWF staining demonstrating the high degree of vascularity in the fibrous and spared tissue. c.) CD68 staining noting the heavy macrophage infiltration of the contralateral white matter (note the correlation to the areas of fibrous infiltration in a.) very few macrophages can be seen in the dense fibrous tissue of the defect. d.) GFAP staining showing growth of astrocytes into the fibrous defect tissue. Also of note is the disruption of normal astrocyte morphology in the areas of macrophage/fibrous infiltration.

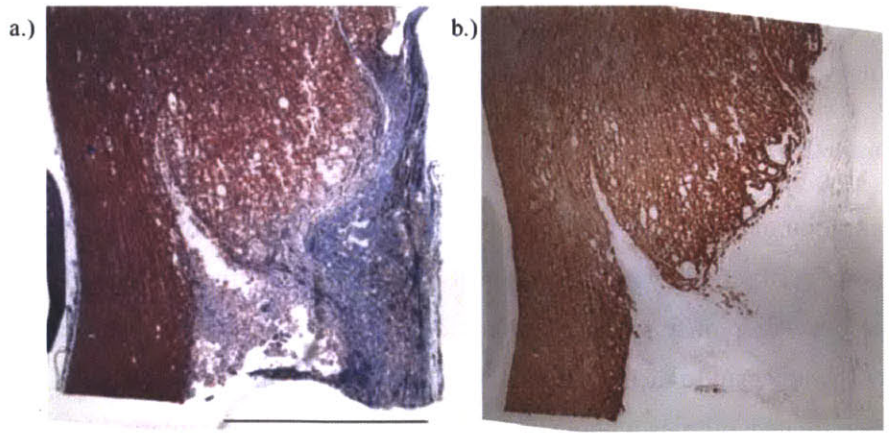

Figure 5-12: Coronal sections of a Col-Gen LMT FGF-2 treated animal with limited secondary damage. **a.)** Masson's trichrome stained section showing dense a lateral dense collagenous scar and cystic center. Scale bar 1000 μm **b.)** GFAP stained section noting limited astrocyte infiltration into the defect.

5.5 Discussion:

The discussion section of this chapter will be focused on the optimization of procedure and methods for the *in vivo* study. A thorough quantitative investigation of the cellular response to gel implantation and the associated functional recovery will be presented in chapter 6.

5.5.1 Application of a Col-Gen gel to the hemi-resection defect:

The presence of Col-Gen gel within the defect at one and four weeks post injury **Figure 5-3b,c** demonstrates that the liquid solution of collagen can successfully gel inside of the defect and remain localized to this area throughout the four-week survival period. Areas of un-degraded gel could easily be identified from endogenous collagen production by its pale blue amorphous appearance and low birefringence under polarized light microscopy **Figure 5-3d.** Areas of non-degraded gel could be found in 2/6 samples at one week and 3/8 samples at four weeks. As illustrated by **Figure 5-7** there was a lack of significant inflammatory infiltrate in or around the gel itself.

It is unclear why some areas of gel are largely devoid of cells at four weeks. The results from chapter 4 suggest these gels are permissive of cell migration so it is possible that the areas of non-degraded gel were walled off by infiltrating connective tissue cells and subsequently contracted making them isolated from the rest of the infiltrating tissue and too dense for cells to penetrate. The bands of cells in Figure 5-3b suggest that imperfections in the gel created by mixing with blood (noticeable in **figure 5-2b**), which are more heavily infiltrated by cells then the original collagen gel.

By four-weeks, the defect evolves into a mixture of connective tissue and cavitary/cystic areas with limited astrocyte in-growth **Figure 5-8**. This type of response is characteristic of an "open" lesion where there is no longer an intact dura to prevent surrounding connective tissue cells from infiltrating the defect.[2] While the Bioguide membrane provided some barrier to infiltrating cells, it did not prevent their entry into the defect, particularly from the adjacent vertebrae **Figure 5-8a**.

5.5.2. Addition LMTs loaded with 1 mg/ml FGF-2 to the Col-Gen gel

Unexpectedly, the concentration of FGF-used in this study resulted in substantial fibrosis, spinal cord stenosis, and contralateral tissue destruction by four-weeks post implantation **Figures 5-10, 5-11**. One likely basis for this is an overstimulation of fibroblast proliferation, migration, and matrix production in the meninges and connective tissue adjacent to the spinal cord. [3] Since a substantial amount of fibrous tissue was found in Col-Gen treated animals without additional FGF-2, further stimulation of

fibroblasts could lead to the observed results. FGF-2 can also lead to an increased expression of endothelial cell adhesion molecules, which could enhance the recruitment of monocytes, T cells, and neutrophils. [4] FGF-2 has also been reported to increase the accumulation of microglia *in vivo* [5] An intensification of the inflammatory response due to this increased recruitment of cells could explain the substantial destruction and macrophage infiltration of the contralateral tissue.

Also of note was the homogeneity in astrocyte infiltration of the defect **Figures 5-11d, 5-12a**. One source of this variation could be the presence of physical barriers, which would block astrocyte migration into the defect such as dense scar tissue and necrotic cavities **Figure 5-12a**. It is also possible that the concentration of FGF-2 used caused significant astrogliosis resulting in the formation of a more robust glial scar at the border of the defect. FGF-2 has been implicated in stimulating astrogliosis both *in vitro* [6, 7] and *in vivo* [5, 8-11]. However, this effect is concentration dependent. Normal brain astrocytes exposed to FGF-2 at 10 μg/ml (administered to the cerebrospinal fluid) underwent astrogliosis, while exposure to 0.5 μg/ml in CSF did not induce such changes [5] In the same study, the higher FGF-2 dosage also disrupted myelin production in mature oligodendrocytes, caused reactive changes in oligodentrocyte progenitor cells (OPCs), and increase accumulation and activation of microglia [5].

From our predictions the Col-Gen LMT FGF-2 gels contained approximately 200 ng/ml FGF-2 (including encapsulated and the approximately 1% of un-removed protein from the rinse step) equivalent to 6 ng total in the injected volume. This amount is much lower than Prior *in vivo* dosages of FGF-2 in models of SCI, which ranged from 168 ng- 21 μg total, released over 7-14 days. [12-15] The discrepancy between the observed and reported results suggest that either a much higher concentration of FGF-2 was actually loaded into the LMTs or the nature of the hemi-resection defect (unlike the previously reported contusion injuries) is substantially more prone to fibrosis.

5.5.3 Optimization of the procedure and methods for the animal study

In addition to the formulations of the Col-Gen gel treatments, several different procedures and methods were tested in this study to determine the optimum way to conduct the remainder of the animal studies. They included a.) Choice of dorsal barrier to cover the injury b.) Method of delivering the gel to the defect site c.) Histological plane of sectioning d.) Frozen vs. paraffin sections e.) Decalcifying vs. removing the spinal cord from the bone

In terms of selecting a dorsal barrier to cover the spinal cord after surgery, the Bio-Gide collagen membrane used in the Col-Gen group was replaced by autologous fascia in the Col-Gen LMT FGF-2 group. The Bio-Gide membrane was replaced for two main reasons. Firstly, the thickness and weight of

the membrane sometimes caused it to collapse into the defect thus impinging on the gel. Secondly, the membrane was an additional biomaterial being placed within the defect and had the potential to cause an inflammatory reaction separate from the collagen gel itself. The Bio-Gide membrane also did not appear to prevent connective tissue infiltration of the injury site. Autologous fascia was chosen as a replacement to the membrane because it is a thin, lightweight, non-reactive layer to cover the injury.

Using a computer-controlled syringe pump for the controlled delivery of the gel was effective but was cumbersome to use during surgery and the large open nature of the hemi-resection defect did not require precise delivery. The length of plastic tubing needed to operate the pump required it to be filled with a much large volume of gel compared to the amount delivered to the defect. It also encountered difficulty extruding the gel if an air bubble was caught within the line. Pipetting the gel directly into the defect using a micropipette proved to be a simple and effective way to ensure proper filling and localization of the gel. To provide some temporal control over the administration of the gel, the solution was delivered in 2 equal boluses, which allowed some time for the gel to set within the defect. As noted in **Figure 5-9a** the gel was still able to localize within the defect.

A coronal (also known as longitudinal) histological plane of sectioning was used in the Col-Gen group while a multi-plane sectioning modality (transverse and two half longitudinal) was attempted in the Col-Gen LMT-FGF-2 group. The multi-plane modality involved cutting the spinal cord in half through the center of the defect and then cutting one of the halves in half, creating two pieces through the center of the defect **Figure 5-2**. The longitudinal plane allowed for a top-down view of both spared and injured sides of the spinal cord tissue, while the multi-plane sectioning allowed for simultaneous viewing of a transverse and two longitudinal sections. While useful in theory, in practice the multi-plane sectioning proved difficult to interpret as gross cutting of the spinal cord tissue resulted in off-angle planes and un-even amounts of defect tissue contained in each half, which made comparisons between animals difficult.

All of the spinal cord tissues were embedded in paraffin except for the 1-week col-gen LMT FGF-2 group. Frozen sections were employed to try and better preserve the gel at early time points however, the low quality of cellular detail compared to paraffin sections limited the usefulness of this method and it was not used further.

Most of the samples in the col-gen group were sectioned with the spinal cord still encased by the decalcified vertebrae. Two of the 1-week col-gen group samples as well as all of the Col-Gen LMT FGF-2 samples had the spinal cord removed from the bone before embedding in paraffin. Keeping the bone around the spinal cord had the advantage of not disrupting the defect site prior to sectioning but due to the differences in modulus between bone and spinal cord/defect tissue and areas of incomplete decalcification,

many rips and tears occurred in the tissue, which made it difficult to interpret the contents of the defect area in most samples. Removing the tissue from the bone prior to embedding carried the risk of damaging or destroying the delicate tissue within the defect. However, given the high quality of the sections obtained from spinal cords without the surrounding bone and success of preserving tissue during removal from the bone, it was decided that all further samples were to be removed from the bone before sectioning. Interestingly, samples which contained the vertebra were able to be sectioned much more effectively if the paraffin blocks were melted, the tissue removed from the bone, and the sample re-embedded.

Overall, the various processing and surgical methods used in this study, as well as the observed tissue responses to Col-Gen and Col-Gen LMT FGF-2 treatments were very useful in guiding the subsequent animal experiments and gel formulations. For the next set of animal experiments, specific changes to the gel formulation were employed. They included increasing the concentrations of both collagen and genipin to 3mg/ml and 1 mM respectively, in order to enhance their resistance to early cellular infiltrate, and decreasing the FGF-2 concentration within LMTs by 50 fold to prevent the massive fibrotic and inflammatory response seen in this study.

5.6 References

[1] Cholas R, Hsu HP, Spector M. Collagen scaffolds incorporating select therapeutic agents to facilitate a reparative response in a standardized hemiresection defect in the rat spinal cord. Tissue Eng Part A. 2012;18:2158-72.
[2] Iannotti C, Zhang Y, Shields L, Han Y, Burke ... D. Dural repair reduces connective tissue scar invasion and cystic cavity formation after acute spinal cord lasceration in adult rats. J Neurotrauma. 2006;23:853-65.
[3] Parr AM, Tator CH. Intrathecal epidermal growth factor and fibroblast growth factor-2 exacerbate meningeal proliferative lesions associated with intrathecal catheters. Neurosurgery. 2007;60:926-33; discussion -33.
[4] Zittermann SI, Issekutz AC. Basic fibroblast growth factor (bFGF, FGF-2) potentiates leukocyte recruitment to inflammation by enhancing endothelial adhesion molecule expression. Am J Pathol. 2006;168:835-46.
[5] Goddard DR, Berry M, Kirvell SL, Butt AM. Fibroblast growth factor-2 induces astroglial and microglial reactivity in vivo. J Anat. 2002;200:57-67.
[6] Polikov VS, Su EC, Ball MA, Hong JS, Reichert WM. Control protocol for robust in vitro glial scar formation around microwires: essential roles of bFGF and serum in gliosis. Journal of neuroscience methods. 2009;181:170-7.
[7] Hou YJ, Yu AC, Garcia JM, Aotaki-Keen A, Lee YL, Eng LF, et al. Astrogliosis in culture. IV. Effects of basic fibroblast growth factor. J Neurosci Res. 1995;40:359-70.
[8] Eclancher F, Kehrli P, Labourdette G, Sensenbrenner M. Basic fibroblast growth factor (bFGF) injection activates the glial reaction in the injured adult rat brain. Brain Res. 1996;737:201-14.
[9] Reilly JF, Bair L, Kumari V. Heparan sulfate modifies the effects of basic fibroblast growth factor on glial reactivity. Brain Res. 1997;759:277-84.
[10] Silver J, Miller JH. Regeneration beyond the glial scar. Nat Rev Neurosci. 2004;5:146-56.
[11] Menon VK, Landerholm TE. Intralesion injection of basic fibroblast growth factor alters glial reactivity to neural trauma. Exp Neurol. 1994;129:142-54.
[12] Lee TT, Green BA, Dietrich WD, Yezierski RP. Neuroprotective effects of basic fibroblast growth factor following spinal cord contusion injury in the rat. J Neurotrauma. 1999;16:347-56.
[13] Rabchevsky AG, Fugaccia I, Fletcher-Turner A, Blades DA, Mattson MP, Scheff SW. Basic fibroblast growth factor (bFGF) enhances tissue sparing and functional recovery following moderate spinal cord injury. J Neurotrauma. 1999;16:817-30.
[14] Rabchevsky AG, Fugaccia I, Turner AF, Blades DA, Mattson MP, Scheff SW. Basic fibroblast growth factor (bFGF) enhances functional recovery following severe spinal cord injury to the rat. Exp Neurol. 2000;164:280-91.
[15] Teng YD, Mocchetti I, Taveira-DaSilva AM, Gillis RA, Wrathall JR. Basic fibroblast growth factor increases long-term survival of spinal motor neurons and improves respiratory function after experimental spinal cord injury. J Neurosci. 1999;19:7037-47.

Chapter 6:

Biomaterials-tissue interaction of a second-generation collagen-genipin gel containing FGF-2 in a rodent hemi-resection model of SCI

6.1 Introduction and motivation

Building upon the *in vitro* studies presented in chapters 3 and 4, as well as the pilot *in vivo* study in chapter 5, this chapter investigates the use of an improved second generation collagen-genipin gel in the hemi-resection model of SCI. Based on the biocompatibility of the 2mg/ml collagen 0.5 mM genipin gel, it was determined that a higher concentration of genipin will be well tolerated. To this extent, a more robust 3mg/ml 1 mM genipin gel was used to increase resistance to early connective tissue infiltration of the gel and defect. Additionally, a 50 fold lower concentration of FGF-2 was employed to mitigate the robust fibrous scarring and tissue destruction, which occurred in the pilot FGF-2 containing gel. Four weeks was chosen as the principal investigation time for this study since it correlates to stabilization in functional recovery, inflammatory response, and glial scar.[1] Therefore, the tissue matrix formed within the defect at 28 days allows for a good comparison of the regenerative response between the groups.

6.2 Overall goal and hypotheses

The **overall goal** of this chapter is to provide an *in vivo* histological study of the early chronic tissue response to injection of Col-Gen gels in a standardized hemi-resection defect in the rat spinal cord. Specifically, the work in this chapter is aimed at elucidating how the presence of Col-Gen gels with and without FGF-2 changes the extent of damage which occurs after a hemi-resection SCI, as well as the composition of the tissue formation (cellular and extracellular) within the defect.

The **hypotheses** for this chapter are:

1.) The injectable Col-Gen gel cross-linked in vivo, will re-create a continuous tissue matrix after hemi-resection SCI thus allowing for cellular population of the defect site after injury.

2.) The presence of FGF-2 containing LMTs within Col-Gen gels will have a neuroprotective effect, resulting in an increased amount of tissue sparing after injury as compared to control animals.

3.) The presence of FGF-2 containing LMTs within Col-Gen gels will alter astrocyte localization after injury and increase the number astrocytes within the defect

4.) The presence of FGF-2 containing LMTs within Col-Gen gels will result in an increased number of endothelial cells and blood vessels within the defect

5.) Tissue bridges created via cellular infiltration and extracellular matrix deposition within the lesion site will allow for the growth of regenerating axons into the defect.

6.3 Methods

6.3.1 Collagen gel fabrication: Col-Gen and Col-Gen LMT FGF-2 gels were fabricated as described in chapter 4. Briefly, ice cold 1x phosphate buffered saline (PBS), 5x PBS, 1N NaOH, a stock solution of genipin in 5x PBS (3 mg/mL), and soluble rat tail type I collagen were combined in that order to obtain 3 mg/mL collagen solutions with 1 mM genipin at pH 7.5 with 1x ionic strength. LMTs loaded overnight with 0.02 mg/ml FGF-2 were added to the Col-Gen LMT FGF-2 gels at 0.1 mg/ml.

6.3.2 Animal procedure: Adult female Lewis rats (Charles River Laboratories, Wilmington MA) weighing 200-230 grams were used in this study. Animal care and surgical procedures were performed at the Veterans Administration Medical Center Animal Research Facility (Jamaica Plain, MA) and were approved by the VA Boston Healthcare System Institutional Animal Care and Use Committee (IACUC). Protocol number 188-J.

The hemi-resection model used in this study was based on the work of Cholas et al.[2] The hair on the back of the anesthetized rat was shaved and the skin was cleaned with Betadine. The rat was placed on a flat operating board in the prone position and its limbs were gently fixed in an extended position using rubber bands. Oxygen was continuously supplied to the rat during surgery. A longitudinal incision, 2 inches in length was made through the skin above the thoracic spine and the back musculature was incised along the midline and dissected away from the vertebral column. A dorsal laminectomy was performed between T7 and T10 using small bone rongeurs and micro-scissors. Bleeding from the muscle was controlled by gelfoam or coagulation with a bipolar cautery. A 3 mm plastic template was placed in the center of the exposed spinal cord and a lateral hemi-resection of the spinal cord was created by making two lateral cuts (3 mm apart) on the left side of the spinal cord using ultra fine surgical scissors or a surgical blade. A midline incision was then made between the lateral cuts using the dorsal spinal vein as a midline marker. A 3 mm gap was created by removing the tissue between the two lateral cuts. Bleeding was controlled using gelfoam placed into the defect site. Once hemostasis was achieved the gelfoam was removed from the defect and the treatment was applied. In gel treatment groups, 30 microliters of gel (kept on ice) was pipetted into the defect in two 15 microliter drops spaced 1 minute apart using a micropipette. After visual confirmation of gel filling and remaining localized within the defect, a piece of thin muscle fascia was placed extradurally over the defect site (covering 2 mm past the spinal cord stumps at both ends) to serve as a dorsal barrier. For the control group, the fascia was applied after hemostasis was achieved.

Following treatment and placement of the dorsal barrier, the overlying musculature was closed using 4-0 vicryl sutures (Johnson and Johnson, Sommerville, NJ) and the skin was closed with wound clips.

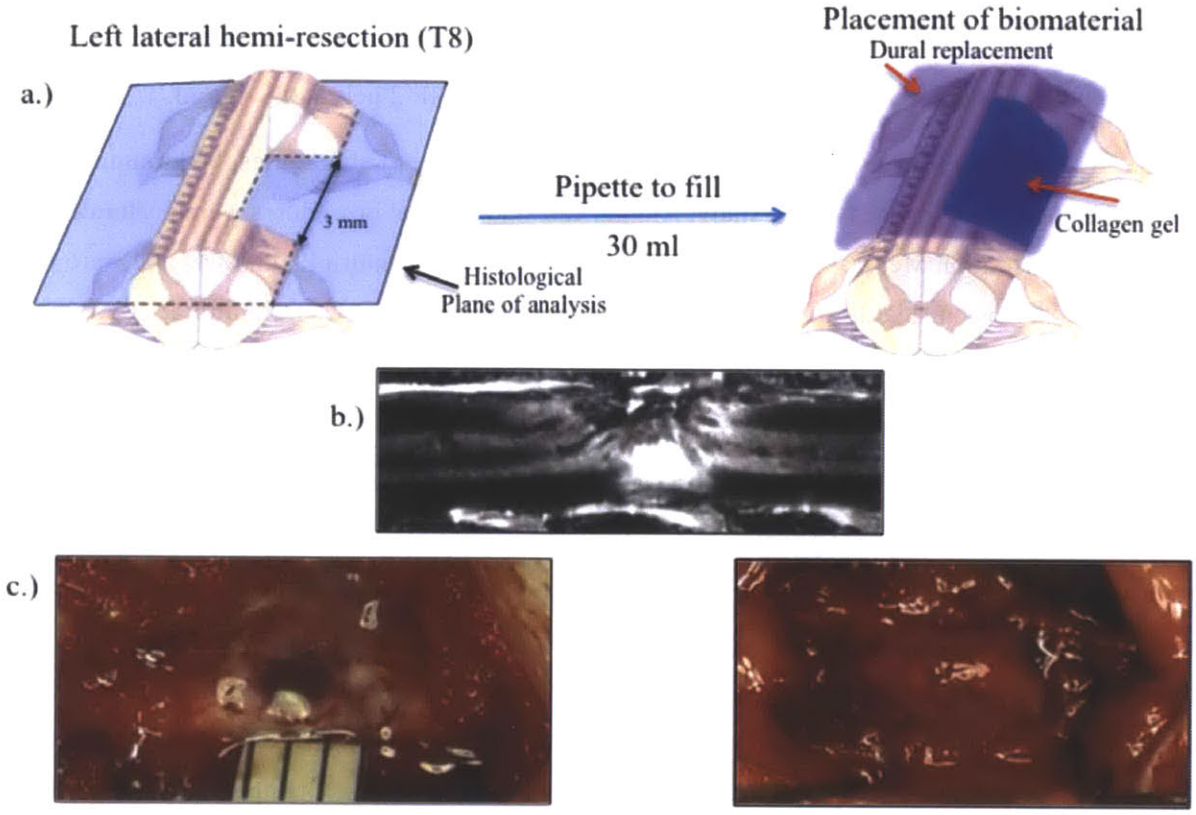

Figure 6-1: a.) (**Left**) Schematic of the 3 mm T8 left lateral hemi-resection spinal cord injury noting the histological plane of analysis (longitudinal section). (**Right**) Schematic of the biomaterial and autologous fascia (dural replacement) position within the defect. **b.)** T2 weighted MRI of the histological plane of analysis, showing the orientation histology sections will be presented in this chapter. **c.)** Surgical pictures of gel implantation showing (**Left**) filling of the defect and **(Right**) dural replacement using a piece of autologous fascia.

Post-operative care of the animals included placement of the rat on a heating pad to maintain body temperature, subcutaneous injection of 6 ml lactated Ringer's solution to compensate for blood loss during surgery and dehydration, subcutaneous injection of antibiotics (cefazolin sodium 100 mg, 35 mg/kg, Abbot Laboratories, North Chicago, IL), subcutaneous injection of an analgesic, Ketofen (5 mg/kg) and a continuous supply of oxygen until the animals regained consciousness 4-6 hours later. After regaining consciousness, the rats were transferred to their original plastic cage with wood chip bedding and free access to food and water.

Analgesic (ketofen 5 mg/kg) was administered once a day for an additional 3 days post surgery for pain relief, and antibiotics (ceftazolin, 35 mg/kg) was administered twice a day for 1 week post surgery to prevent bladder infection. Post operatively, the animals lacked a normal micturition reflex and their bladders had to be manually emptied every 12 hours using Crede's maneuver until bladder function recovered.

6.3.3 Animal sacrifice, transcardial perfusion: Animal sacrifice was performed by transcardial perfusion. Rats were administered a dose of 150 mg/kg of sodium pentobarbital and secured to a surgical board. A thoracotomy was performed to expose the heart, after which a needle attached to a peristaltic pump was inserted into the left ventricle and into the ascending aorta. 100 ml of heparinized saline was circulated through the animal, followed by 150 ml 4% paraformaldehyde. Following sacrifice, the spine was removed and placed in 60 ml 4% PFA at 4°C overnight. The following day, the bone overlying the spinal cord was removed to enhance the exposure of the spinal cord to fixative while still maintaining a straight configuration, and the cords were allowed to fix for another 2 days at 4°C. Alternatively, after perfusion, the spine was trimmed of the overlying musculature while leaving the fascia over the defect intact and drop fixed in 4% PFA at 4°C for four days.

6.3.4 Histology and immunohistochemistry (IHC): Prior to tissue processing, the spinal cord tissue was carefully and completely removed from the surrounding vertebra using bone rongeurs, surgical scissors, and a scalpel. The spinal cord parenchyma was embedded in paraffin using a tissue processor (HypercenterXP, Tissue Processor, ThermoShandon, Houston, TX). Serial longitudinal sections of the defect were cut at 6 μm with a microtome and mounted on glass slides.

Adjacent tissue sections were stained with Masson's Trichrome for general observation of the cellular and extracellular matrix features of the defect, particularly the presence of collagenous tissue within the defect. Sections from approximately the same level of cord (middle of the defect) were used for trichrome and IHC analysis. A labeled polymer HRP system (AEC+ system, Dako) was used to detect the presence of antibody. Some sections were also counterstained with Mayer's Hematoxylin.

The following antibodies were used in the IHC staining of the paraffin sections containing the defect.

Stain (dilution) Incubation	Antigen retrieval	Company (cat#) Species	Staining color	Cells/ECM Identified
Masson's Trichrome	None	Sigma HT15	Nuclei- black Cytoplasm- red Collagen- blue	Viable tissue Fibrous Scar Gel
GFAP (1:1000) 45 min	Protease XIV 20 min	Dako Z0334 Rabbit	Red	Astrocytes
CD68 (1:200) 45 min	Citrate AR 95°C 20 min	AbD serotec MCA341R Mouse	Red	Macrophages (MΦ)
a-SMA (1:400) 45 min	Citrate AR 95°C 20 min	Sigma A2547 Mouse	Red	Contractile fibroblasts, pericytes
VWF (1:100) 60 min	Protease XIV 40 min	Dako A0082 Rabbit	Red	Endothelial cells/blood vessels
GAP-43 (1:1000) 45 min	Citrate AR 95°C 20 min	Abcam AB12274 Rabbit	Red Blue	Regenerating Axons Nuclear counterstain
Laminin (1:100) 30 min	Protease XIV 40 min	Abcam 11575 Rabbit	Red	ECM molecule Basement membrane
Fibronectin (1:100) 30 min	Protease XIV 40 min	Abcam Ab6328 Mouse	Red	ECM molecule, Blood clot
CS-56 (1:200) 60 min	High pH AR 95°C 20 min	Abcam Ab11570 Mouse	Red	ECM (Chondroitin sulfate proteoglycans)
P75 (1:200) 60 min	High pH AR 95°C 20 min	Millipore AB1554 Rabbit	Red	NGF receptor (Schwann cells)
(AR) Antigen retrieval solutions: Protease XIV (0.1% in tris buffered saline), Citrate (10 mM sodium citratre, 0.05% tween 20, pH 6.0), High pH (Vector labs cat# H3301 pH 9.0)				

6.3.5 Image quantification: Images were imported into Photoshop CS5 and processed to isolate the areas of staining within the defect and obtain the area of the defect.[3] Positively stained cells were

either counted manually or the percentage staining area was calculated using ImageJ 1.45s. (see appendix for more detailed procedure of image analysis and validation of area-cell count relationship). This procedure is similar to previously published studies on cell quantification after SCI.[4] For GAP-43 analysis, a grid (63784 pixels^2) was placed over the image, which broke the defect up into 20-30 sections depending on its size. The number of boxes containing positive GAP-43 staining was counted for each animal.

6.3.6 Functional Evaluation: Animals were evaluated each week until sacrifice using an open field locomotor test. The rats were removed from their cages and videotaped walking in an open space. Hind-limb function was evaluated using a scoring system modified from Wrathall et al. [5] The time required for each animal to recover bladder function, defined by the time till the animal had a completely empty or very small (few drops of urine) bladder upon manual expression, was recorded.

Score	Behavior
0	No hind limb movement, flaccid paralysis
1	Non-weight bearing, spastic uncontrolled hind-limb movement
2	Non-weight bearing, controlled hind-limb movement
3	Partial weight bearing, wide gait, can get hind-limb under body once in a while
4	Partial weight bearing, more frequent stepping still has a wide gait
5	Full weight bearing, hind-limb under body most of the time, movement is slow/jagged
6	Full weight bearing, fast hind-limb movement but has some limp
7	Full weight bearing, normal gait

6.3.7 Statistical analysis and sample size determination

Our power calculation for sample size determination is based on the desire to determine significant a 30% difference in a selected outcome variable with a 15% standard deviation, and with α=0.05 and β=0.05.

The statistical significance of treatment on histomorphometric and IHC staining results were determined by one-way ANOVA analysis using Fishers Post Hoc testing. Non-parametric data such as functional score was analyzed for statistical significance using the Mann-Whitney U test, Wilcoxon signed rank test, or Chi squared test.

6.4 Results

6.4.1 Functional Evaluation

Wilcoxon matched pairs test showed a significant improvement in left leg functional score between 1 and 4 week for Col-Gen ($p=0.0277$) and Col-Gen LMT FGF-2 ($p=0.0431$) groups but not for the control group. While there was a trend in increasing functional score for right and left hind-limbs with Col-Gen and Col-Gen LMT FGF-2 treatment as compared to control, no statistical significance was found in the scores between treatment groups for either leg at 1 or 4 weeks **Figure 6-2a,b**. To account for differences in baseline functional score, each animal was used as its own control and the number difference in functional score between one and four weeks was tabulated **Figure 6-2c**. There was an increase but no statistical difference between animals improving by 2 more points on the functional scale between control and Col-Gen LMT FGF-2 animals for both left and right legs.

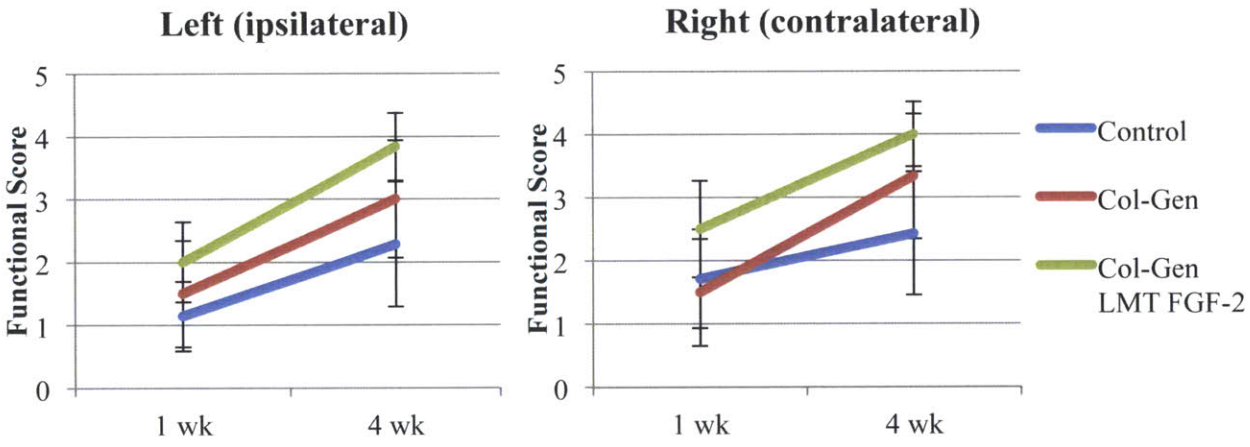

LEFT	-1	0	1	2+
Control	1	2	1	3
Col-Gen	0	0	4	2
Col-Gen LMT FGF-2	0	1	0	5
RIGHT				
Control	0	3	3	1
Col-Gen	0	1	1	4
Col-Gen LMT FGF-2	1	0	1	4

Figure 6-2: Top: functional evaluation of left and right hind-limbs at 1 and 4 weeks post injury. **Bottom**: Tabulation of the improvement in functional score from week 1 to week 4 on the left and right hind-limbs of each animal. N=6-7 Mean ± SEM.

A reasonable correlation between the average of the left and right hind-limb functional scores of each

animal and the percentage of spared tissue in the peri-lesional area **Figure 6-3a**, width of the spared contralateral white matter at its most narrow point **Figure 6-3b**, and time to the return of bladder function **Figure 6-3c**. There was no notable correlation between the functional score and any other histomorphologic or IHC staining metric. It should be noted that the R^2 of Figure **6-3a** increases to 0.713 if the outlying animal (74% spared tissue 3 functional score), which had a small half width injury in the middle plane of the defect but extensive fibrous tissue infiltration of the dorsal columns and adjacent gray matter, is removed.

Bladder function returned for 3/7 control, 4/6 Col-Gen treated, and 5/6 Col-Gen LMT FGF-2 treated animals during the 28 day survival period. Of note, one of the Col-Gen LMT FGF-2 animals, which recovered bladder function at 3 days, lost the ability to void on its own at day 16 and continued to have some degree of urine retention for the remainder of the study period. The average time to return of bladder function for those animals, which did recover the ability to void was not significant between the groups.

a.)

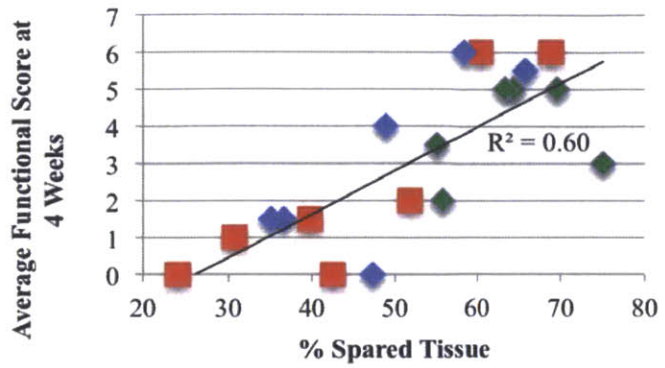

b.)

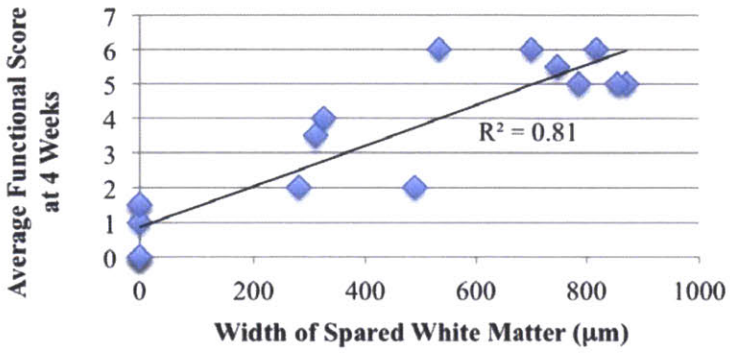

c.)

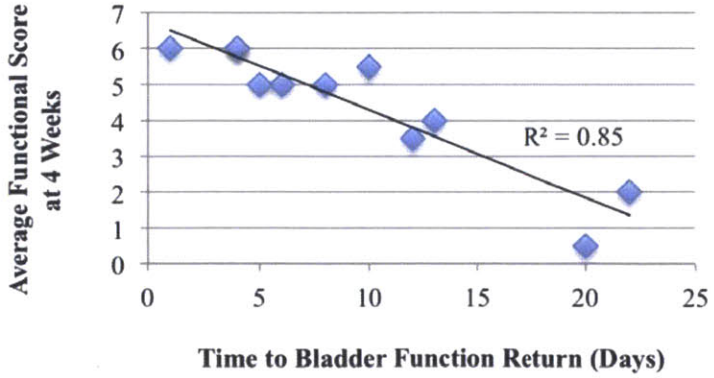

Figure 6-3: Correlation of average functional score (right & left hind-limbs) with **a.)** Percentage of spared tissue in the peri-lesional area (R^2=0.713 with removal of the outlying animal). Red= control, Blue=col-gen, Green= col-gen LMT FGF-2 **b.)** Width of the contralateral spared white matter at its most narrow point from Masson's trichrome stained sections in the middle of the defect (omitted two samples which had substantial connective tissue infiltration of the contralateral tissue making it difficult to analyze) **c.)** Time to the return of bladder function- includes only animals, which recovered this ability during the four-week survival period.

6.4.2 Early analysis of the defect at one day and one week post injury

Several animals were sacrificed at one day and one-week post injury to provide a qualitative assessment of the acute injury phase and integration of the Col-Gen gel with the surrounding tissue. After one day, the Col-Gen gel can be localized within the hemi-resection defect and is mixed to varying degrees with blood from the hemorrhage within the spinal cord parenchyma or bleeding into the defect from the surrounding musculature **Figure 6-4a**. Notably, the gel is able to conform to the defect and bond directly to the tissue **Figure 6-4b**.

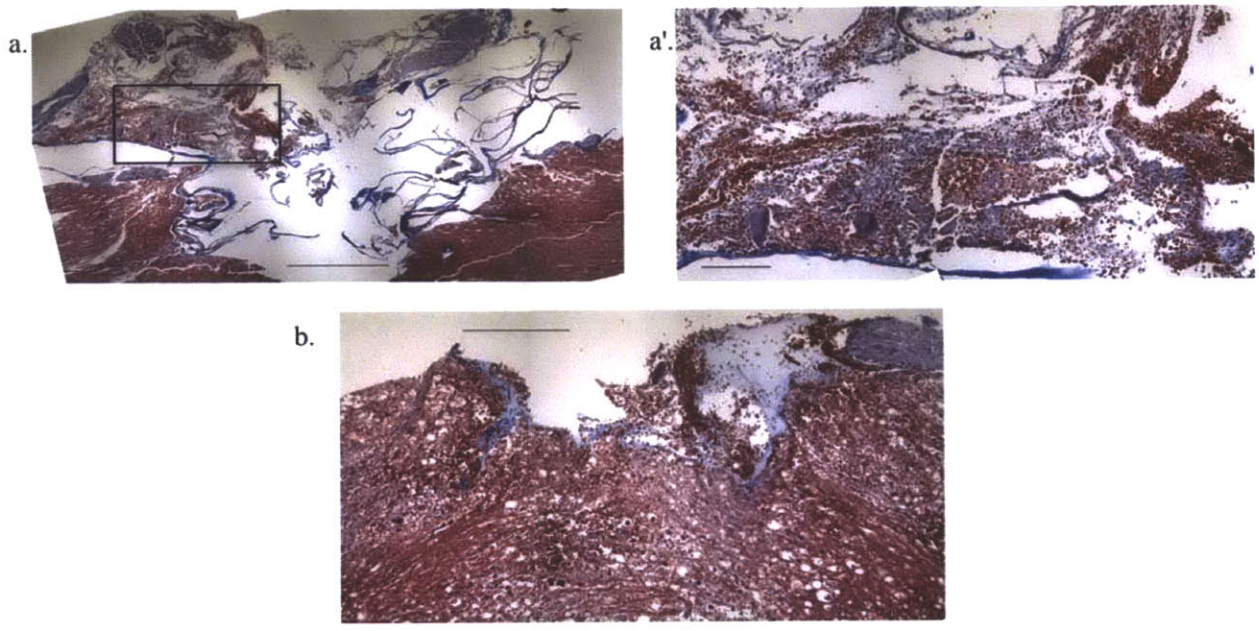

Figure 6-4: Masson's trichrome images of the defect site one-day post injury and injection of the Col-Gen gel. **a.)** Image of a section towards the ventral aspect of the spinal cord showing blood (red) mixing with collagen gel (blue) in the defect cavity. Contents of the defect cavity were pushed out during histological sectioning. Scale bar 1000 μm **a'.)** Magnified image of the inset in a. Scale bar 500 μm **b.)** Image of the section in the middle of the spinal cord demonstrating the close bonding of the tissue with the implanted col-gen gel. Scale bar 400 μm. Most of the gel in the defect was lost during removal of the spinal cord from the vertebra after sacrifice. Images taken at a 4x or 10x objective.

Histology of the lesion site at one week reveals the varying degrees of secondary damage, which occur after the initial hemi-resection injury **Figure 6-5**. At this time-point in both control and Col-Gen treatment groups, the defect area is heavily infiltrated by cells, many of which appear to be of connective tissue origin and appear to be synthesizing a collagenous ECM (noted by the light blue staining in Masson's trichrome). At one week, most of the Col-Gen has been degraded/remodeled and a few areas of un-degraded gel can be found (insets **Figures 6-5 b',c'**).

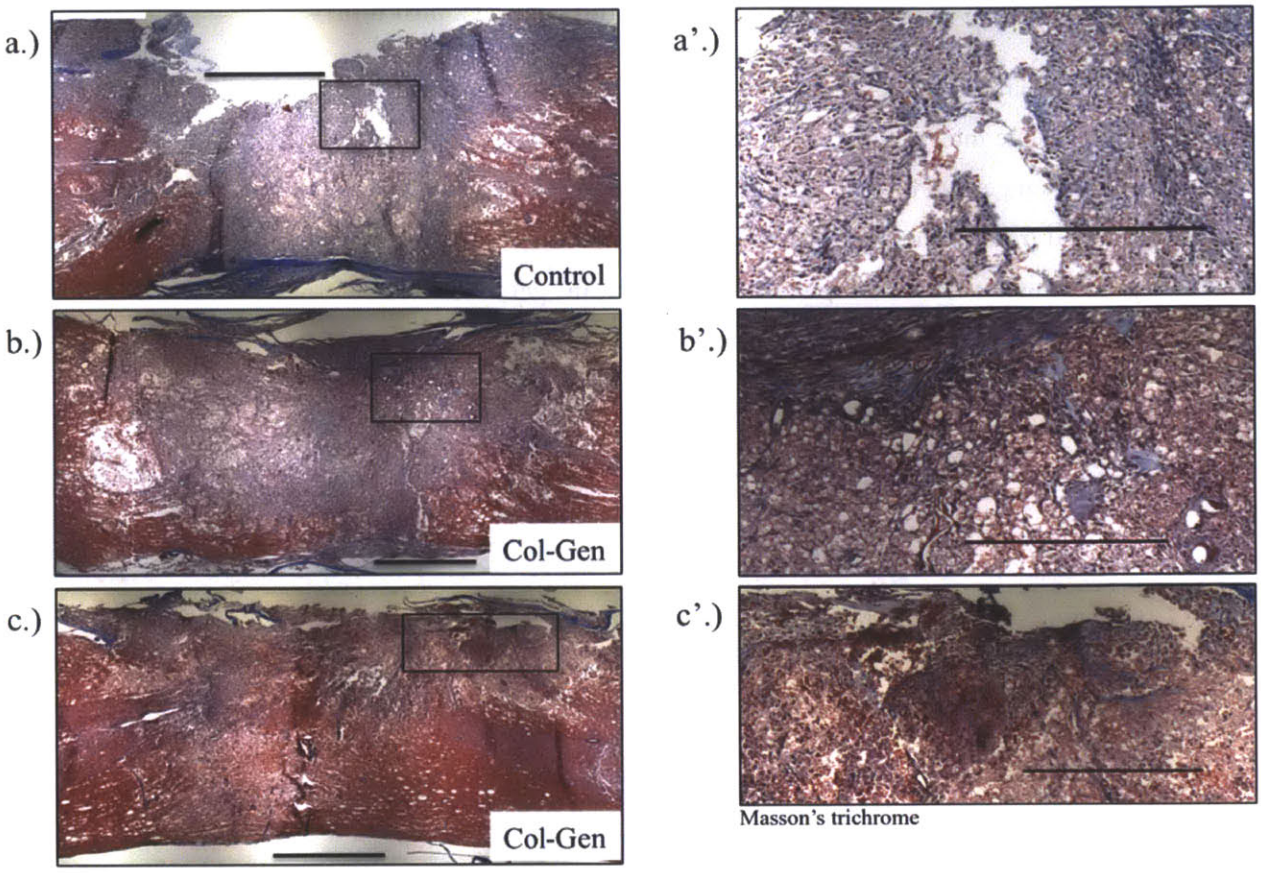

Figure 6-5: Masson's trichrome images of the defect at one week of control and Col-Gen treated animals. **a.)** Longitudinal section of a control animal showing extensive secondary damage and infiltration of connective tissue cells within the defect and the deposition of a collagenous ECM **a'.)** Magnified image of the inset in a. showing a heterogeneous cell infiltrate **b.)** Longitudinal section of an animal treated with Col-Gen gel showing extensive secondary damage and cellular infiltration **b'.)** Magnified image of the inset in b. demonstrating a small amount of un-degraded Col-Gen gel (light blue amorphous deposits) **c.)** Longitudinal section of an animal treated with Col-Gen gel with little secondary damage to the contralateral tissue **c')** Magnified image of the inset in c. demonstrating un-degraded gel and gel blood mix. Images taken at 4x objective. Scale bar (a,b,c) 1000 μm (a',b',c') 500 μm.

To further elucidate the composition of the defect at one week, sections of Col-Gen animals were stained with CD68, fibronectin, and laminin **Figure 6-6**. Agreeing with the hypercellularity noted at one week, the defect is rich in fibronectin (component of blood clotting and matrix for cellular infiltration), laminin (major component of the basal lamina), and macrophages (inflammatory cells and mediators of tissue remodeling). VWF+ endothelial cells can be seen migrating in from the viable tissue. GFAP+ astrocytes are absent from the defect. Interestingly, the fibronectin staining is most dense in the center while the laminin, VWF, and CD68 staining is most dense at the edges of the defect.

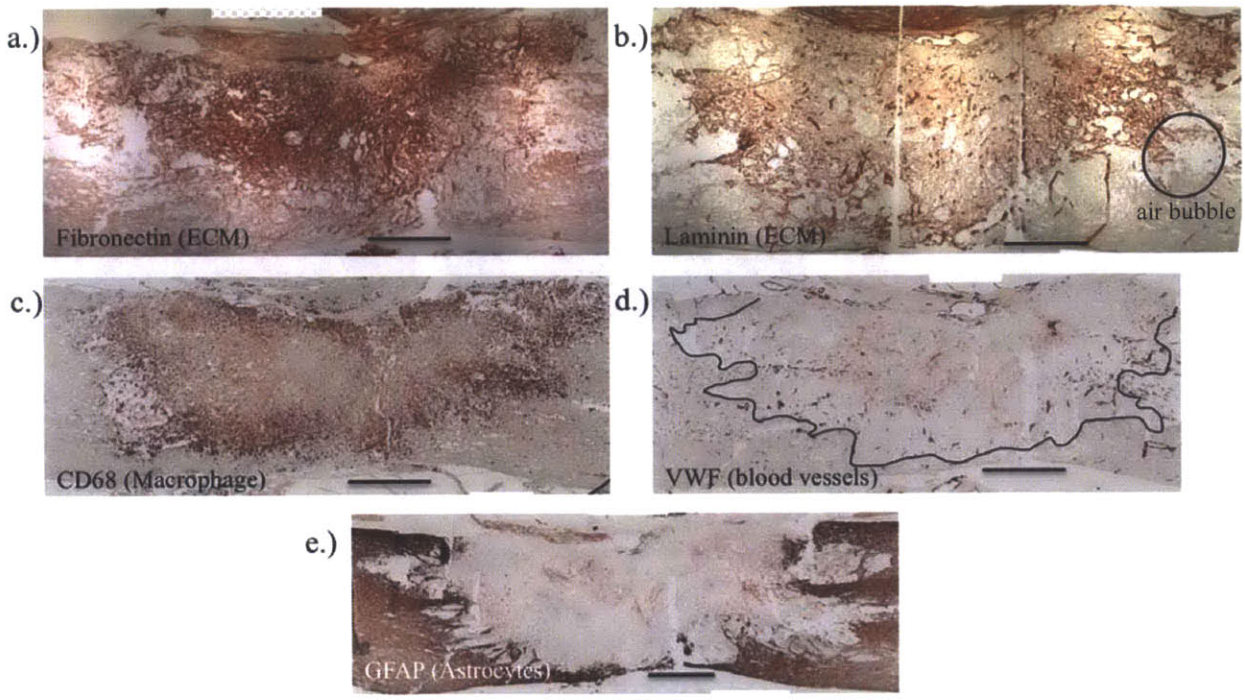

Figure 6-6: IHC staining for **a.** fibronectin **b.** laminin **c.** CD68 d. VWF and e. GFAP in sections of Col-Gen gel treated animals corresponding to the section in figure 6-3b. Of note is the dense fibronectin matrix significant of a blood clotting within the defect. Laminin reactivity is most prominent in endothelial cells within the defect and cellular infiltration at the borders of the viable tissue. Macrophages can be seen through the defect and increase in density towards the edge of the defect. VWF+ endothelial cells can be seen migrating in from the viable tissue. GFAP+ astrocytes are absent from the defect. Images taken at 4x objective, scale bar = 1000 μm

6.4.3 Histomorphologic assessment of the extent of injury and new tissue formation within the defect at 4 weeks

Depending on the degree of secondary damage occurring after the primary hemi-resection injury, each of the animals in this study can be classified as having one of three major responses to injury (**Figure 6-7**). The exact composition of new tissue formation within the defect (i e. percentage of dense collagenous scar, loose granular matrix, cavitary macrophage filled) varied between animals and between treatments. There was also a difference in the number of animals exhibiting each response depending on treatment group, although the sample size was too small find statistical significance.

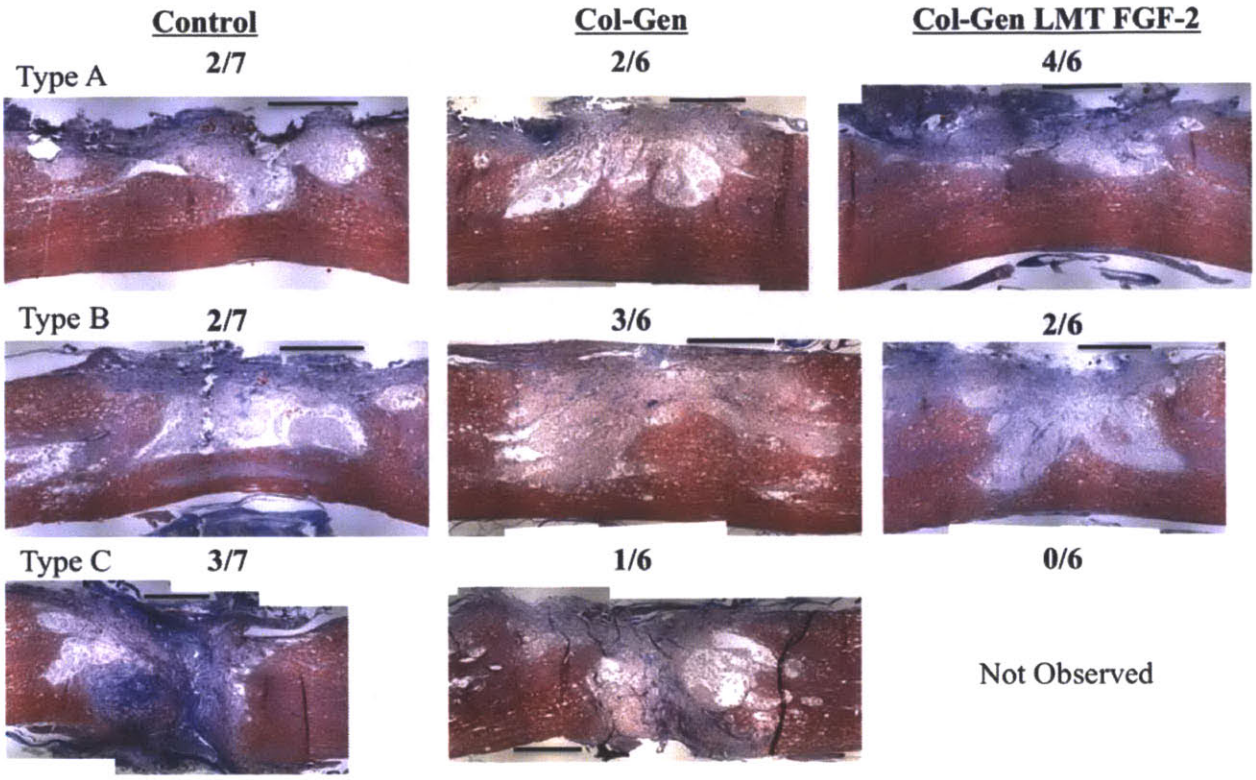

Figure 6-7: Representative longitudinal Masson's Trichrome stained sections through the center of the spinal cord defect for each treatment group (columns) 4 weeks post injury demonstrating the three main responses to injury (rows). Type A: half width defect; Type B: greater than half width with some tissue sparing; Type C: full width defect. The number of animals in each treatment group exhibiting the specific response type is listed above the image. 4x objective, scale bar =1000 μm

Type A: Half width defect (Control n=2, Col-Gen n=2, Col-Gen LMT FGF-2 n=4). This injury consists of a dense collagenous fibrous scar localized to the lateral border of the defect and a cavitary/granular tissue core containing a high density of foamy looking cells varying degrees of non-inflammatory cell infiltration and associated ECM. The dense tissue was usually aligned parallel to the long axis of the spinal cord. The core area of Col-Gen LMT FGF-2 treated animals tended to have more dense collagenous tissue and granular matrix than control or Col-Gen treatment groups, which displayed a more cavitary inflammatory cell filled core.

Type B: Greater than half width defect with varying degree of tissue sparing (Control n=2, Col-Gen n=3, Col-Gen LMT FGF-2 n=2). Animals exhibiting this response had significant but typically incomplete destruction of the contralateral white and gray matter. The areas of additional tissue destruction consisted predominantly of inflammatory cells and contained fewer infiltrating connective tissue/glial cells than the tissue within the original defect. In the case of one control animal with this type

of injury (not shown), the lesion site and areas of secondary degeneration were heavily infiltrated by connective tissue cells and contained a dense collagenous tissue matrix.

Type C: Full width defect with substantial connective tissue infiltration (Control n=3, Col-Gen n=1, Col-Gen LMT FGF-2 n=0). Animals with this response to injury had a defect, which spread to encompass the entire width of the spinal cord and consisted of fibrous scar tissue in the center with cystic/cavitary lesions on either side. In some cases, the collagenous tissue in the center was oriented such that it "capped" off the distal and proximal ends of the spinal cord

At four weeks, the center of the defect was evaluated using Masson's trichrome staining to assess the area of the defect, nature of the new tissue formation within the defect, and amount of viable tissue in the peri-lesional area (**Figure 6-8**). Between treatment groups, there was a statistically significant difference in the percentage spared tissue around the defect between control and Col-Gen LMT FGF-2 groups ($p=0.018$). There was no statistically significant difference found in absolute defect size, percentage of scar tissue, or percentage of cavitary/granular tissue within the defect between treatment groups.

a.)

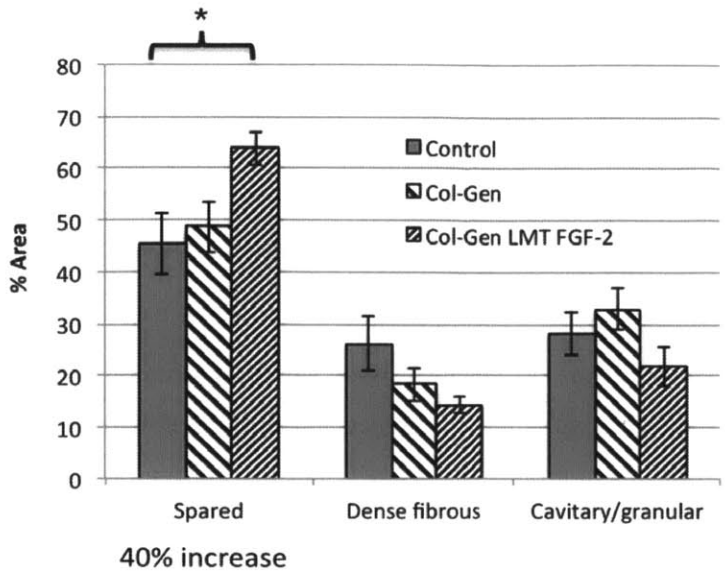

b.)

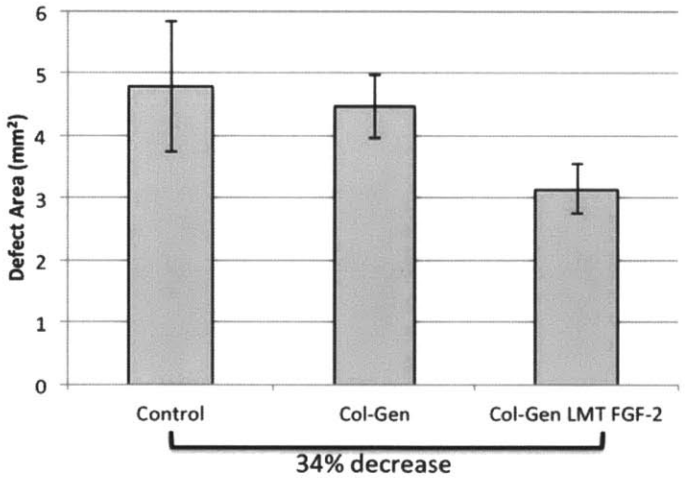

Figure 6-8: a.) Histomorphological characterization of the spinal cord defect and peri-lesional area using Masson's trichrome stained longitudinal sections from the middle of the defect at 4 weeks post injury. Spared tissue is defined as parenchyma, which appears viable, without fibrous infiltration or significant edema. Dense fibrous tissue is an area staining strongly for collagenous tissue (blue). The cavitary/granular tissue is defined as as an area of moderate cellular ingrowth within the defect without the presence of a dense collagenous ECM or an edematous area occupied of foamy-looking cells. b.) Absolute defect area (dense fibrous + cavitary/granular tissue) determined from Masson's trichrome stained sections. N=6-7 mean ± SEM

6.4.4 Immunohistochemical analysis of the cellular and extracellular composition of the defect

6.4.4.1 α-SMA:

The areas containing dense fibrous scar tissue within the defect largely stained negative for α-SMA positive cells at 4 weeks (**Figure 6-9**) suggesting that myofibroblasts were not actively contracting the matrix within the defect at this point.

Figure 6-9: a-SMA stained IHC image of the control Type C injury response shown in Figure 6-2. Of note is the sparse distribution of positive staining cells in the center of the defect where there is a dense collagenous ECM. A thin band of a-SMA positive cells can be seen at the lateral border of the defect. Black lines were traced along the border of the defect with viable parenchyma. 4x objective, scale bar =1000 μm

6.4.4.2 Laminin:

Laminin staining was performed to assess the cellular infiltration of the lesion site and presence of a growth supportive matrix for axon elongation into the defect (**Figure 6-10**). In all treatment groups, laminin could be found on the border of and scattered throughout the defect and co-localized with the presence of cellular infiltration and connective tissue formation. The density of laminin staining was decreased in areas of dense collagenous scar and absent in purely cavitary areas. There was a statistically significant increase in the amount of laminin within the defect area for the Col-Gen LMT FGF-2 treatment group as compared to control ($p=0.005$) **Figure 6-10d**.

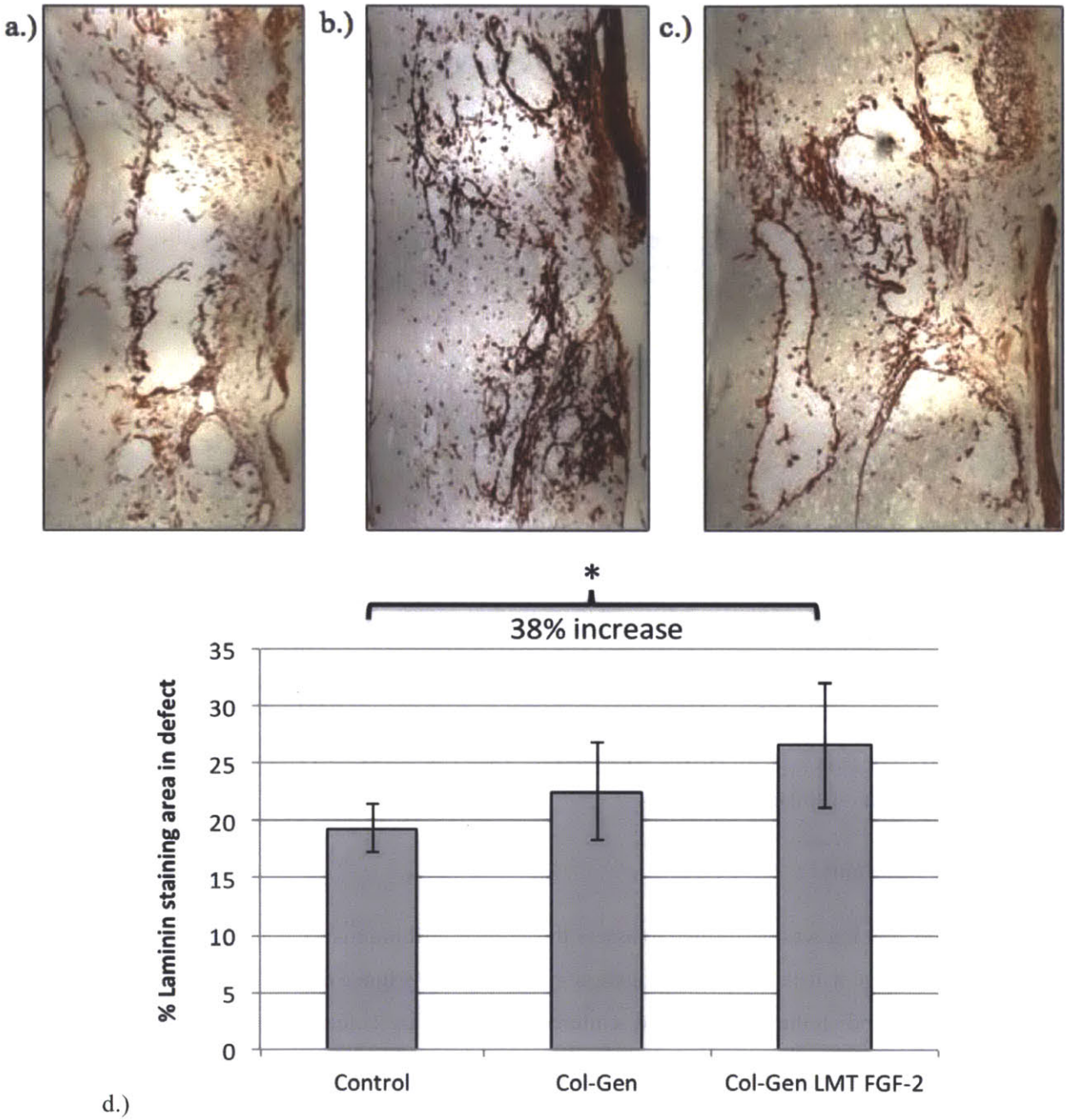

Figure 6-10: Longitudinal laminin IHC stained sections through the middle of the defect (corresponding to the animal with a Type B response in figure 6-7) for a.) Control b.) Col-Gen c.) Col-Gen LMT FGF-2 treatment groups. 4x objective, scale bar 1000 μm. d.) Quantitative analysis of laminin staining within the defect. N=6-7 mean ± SEM.

6.4.4.3 Astrocytes

In the control group **Figure 6-11a**, astrocytes could be found bordering the defect and sparsely within the defect. In some cases astrocytes grew into the defect directly adjacent to the parallel oriented fibrous scar on the lateral border of the defect. In the cases where the center of the defect was filled with dense collagenous tissue, astrocytes could be seen growing into the less dense fibrous tissue but were impeded from growing into the more dense tissue. Astrocytes were rarely present in the cystic/cavitary areas of the lesion.

Similar to the control group, astrocytes in Col-Gen treated animals (**Figure 6-11b**) were predominantly found at the borders, however the cells appeared to extend further into the defect than in control animals. In one of the Type A response animals, astrocytes were observed growing out in substantial number right below the fibrous scar on the lateral border of the defect from either side (image shown in section 6.4.3.7).

In animals treated with Col-Gen LMT-FGF-2 (**Figure 6-11c**), astrocytes entered the defect extensively within the granular tissue matrix of the defect site. Astrocytes grew out and extended processes into the defect forming what appeared to be a network-like structure with other cells in the defect. Few if any cells could be found in the dense fibrous scar tissue, even if it was adjacent to viable tissue. Populations of astrocytes within the defect could be found mixing with fibroblast-like cells, which stained positive for collagen in Masson's trichrome.

There was a statistically significant increase in the percentage of defect tissue staining for GFAP was significantly higher in Col-Gen LMT FGF-2 treatment groups as compared to control ($p=0.000055$) or Col-Gen ($p=0.0455$) groups (**Figure 6-11d**).

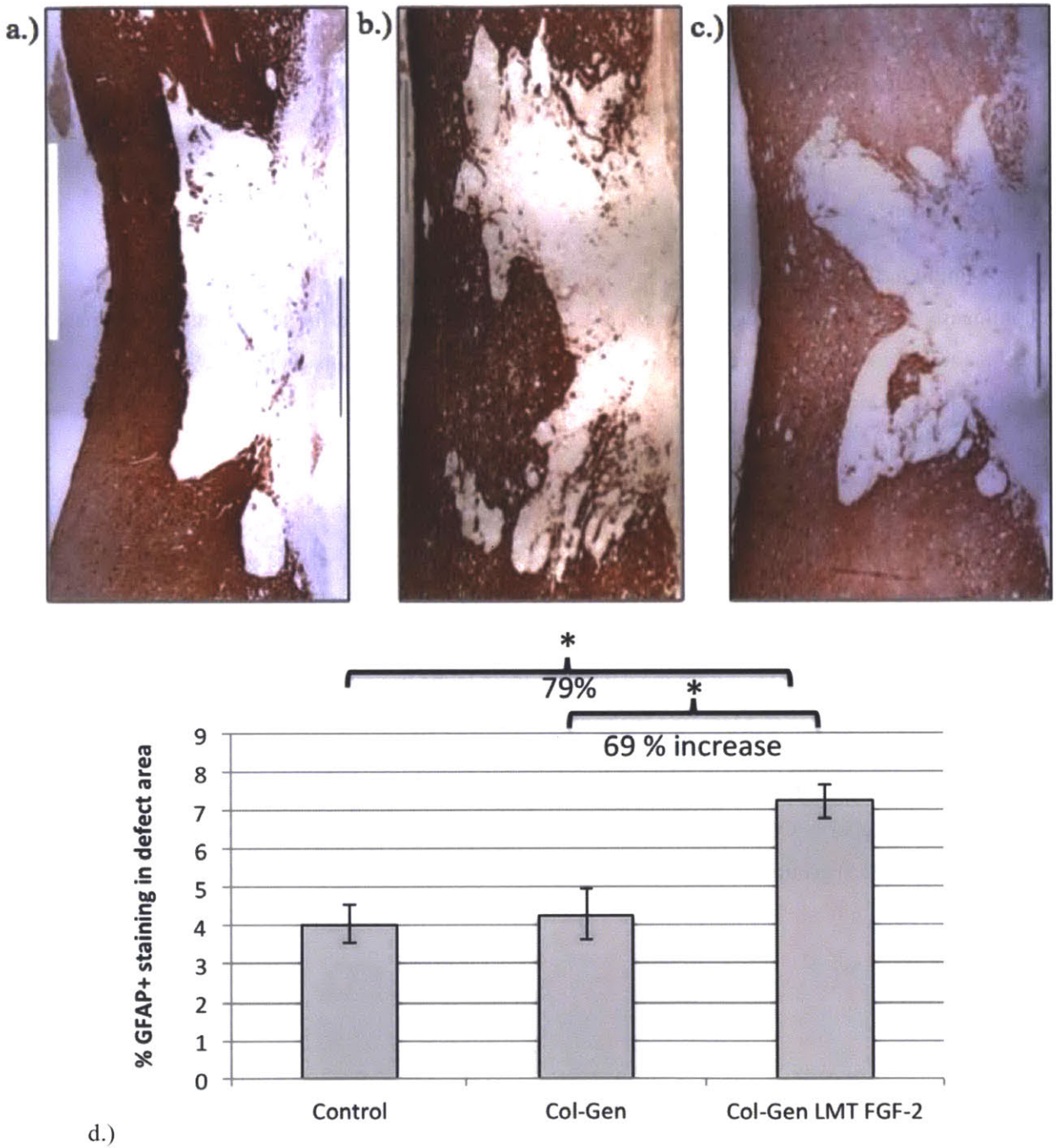

Figure 6-11: Longitudinal GFAP IHC stained sections through the middle of the defect (corresponding to the animal with a Type B response in figure 6-7) for a.) Control b.) Col-Gen c.) Col-Gen LMT FGF-2 treatment groups demonstrating the ingrowth of astrocytes into the lesion site . 4x objective, scale bar 1000 μm. d.) Quantitative analysis of GFAP staining within the defect. N=6-7 mean ± SEM.

6.4.4.4 Endothelial cells/angiogenesis

VWF positive endothelial cells were distributed throughout the entirety of the defect area (**Figure 6-12**). The cells were present at a higher density in the more densely packed connective tissue areas as compared to the cavitary/granular tissue regions. There was no statistical difference in the number of VWF+ cells in the more dense fibrous tissue areas between the control and treatment groups. However, animals treated with Col-Gen LMT FGF-2 gels has a substantial and increase in the number of VWF+ cells within the cavitary/granular tissue as compared to control ($p= 0.00032$) and Col-Gen ($p=0.0056$) groups. There was also a statistically significant difference in the number of VWF+ cells over the entire defect between control and Col-Gen LMT FGF-2 groups ($p=0.0023$) (**Figure 6-12d**).

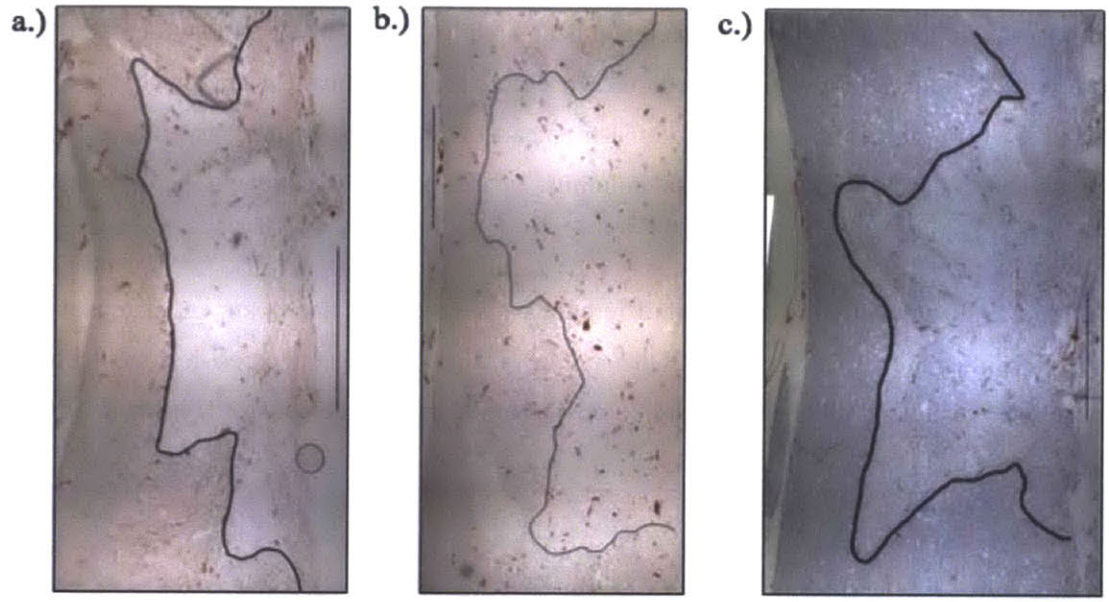

d.)

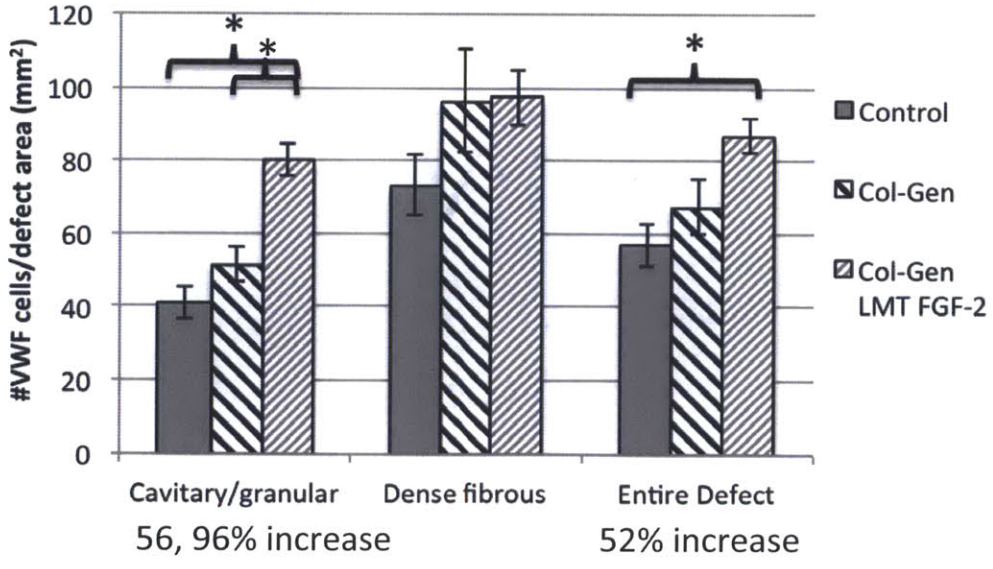

Figure 6-12: Longitudinal VWF IHC stained sections through the middle of the defect (corresponding to the animal with a Type B response in figure 6-7) for.) Control b.) Col-Gen c.) Col-Gen LMT FGF-2 treatment groups, demonstrating the presence of endothelial cells and blood vessel formation within the lesion. The edges of the defect are outlined for clarity. 4x objective, scale bar 1000 μm. d.) Quantitative analysis of VWF staining within the defect. N=6-7 mean ± SEM.

6.4.4.5 Inflammatory response: macrophages

Macrophages dominated the lesion site at 28 days post injury, localizing at high density within the loose tissue matrix or cavitary/cystic areas and decreased with distance rostral and caudal to the defect (**Figure 6-13**). Macrophages were largely excluded from areas of dense fibrous scar and could only be seen sparsely throughout the dense tissue. It should be noted that macrophages were present in all areas of the spinal cord, which were infiltrated by fibroblasts as part of the secondary damage process. This was particularly evident in the degenerating dorsal columns; an area particularly prone to hemorrhage after injury (**figure not shown**).

There was no statistically significant difference between control and treatment groups with respect to the absolute area of unregulated CD68 staining within the defect and peri-lesional area at 4 weeks or the relative area of CD68 staining as compared to the original defect size (**Figure 6-13d**).

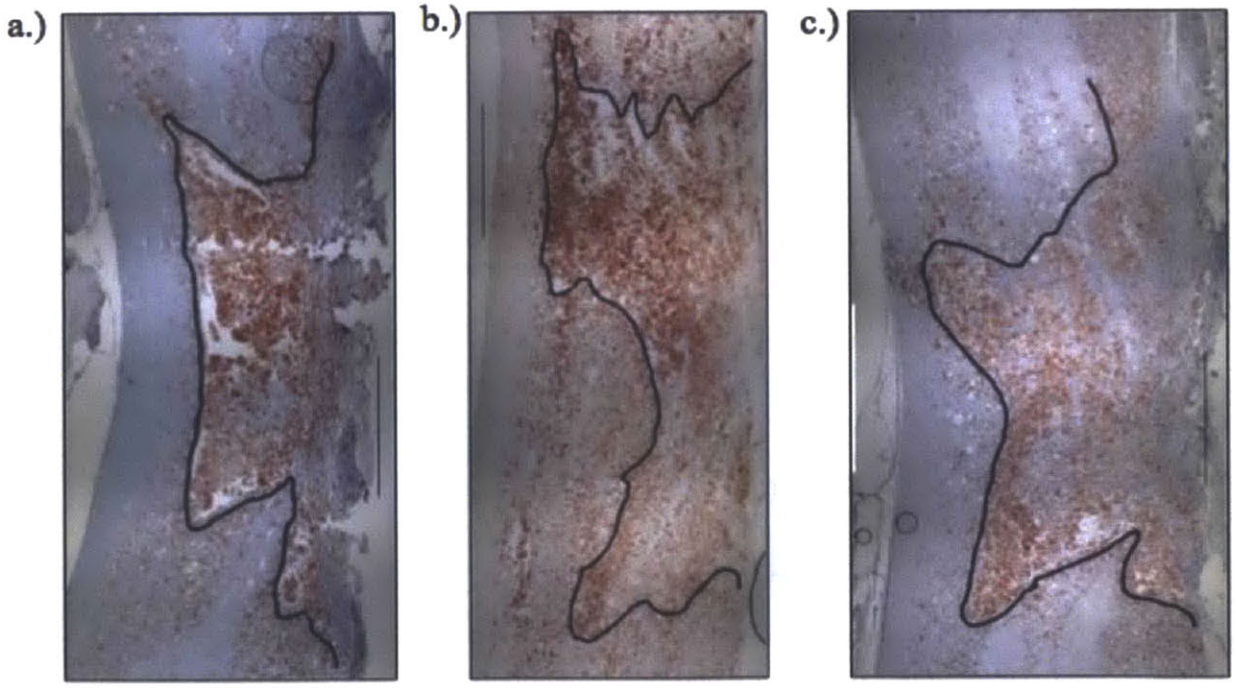

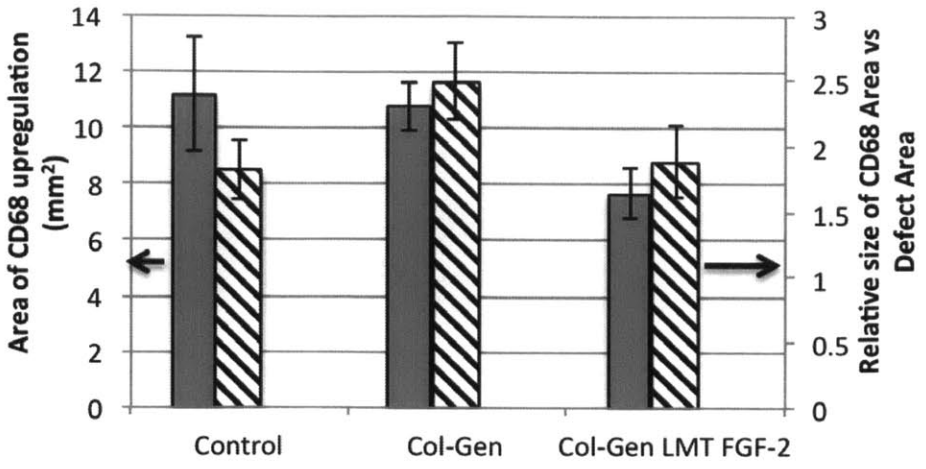

d.)

Figure 6-13: Longitudinal CD68 IHC stained sections through the middle of the defect (corresponding to the animal with a Type B response in figure 6-7) for a.) Control b.) Col-Gen c.) Col-Gen LMT FGF-2 treatment groups, demonstrating the presence of macrophages within the defect and peri-lesional area. The edges of the defect are outlined for clarity. 4x objective, scale bar 1000 μm. d.) Quantitative analysis of CD68 staining within the defect, area of upregulation (primary axis solid bar), relative size of upregulated area vs original defect area (secondary axis striped bar). N=6-7 mean ± SEM.

6.4.4.6 Regenerating axons

GAP-43 positive regenerating axons could be seen coursing into the defect from the edges of the viable tissue **Figure 6-14**. The axons were closely associated with collections of non-inflammatory cells, which infiltrated into the defect and could not be found alone in the cavitary macrophage filled regions of the defect. No statistical difference could be found in either the percentage of the defect staining for GAP-43+ axons or the number of fields of view within the defect containing GAP-43 axons (**Figure 6-14d**).

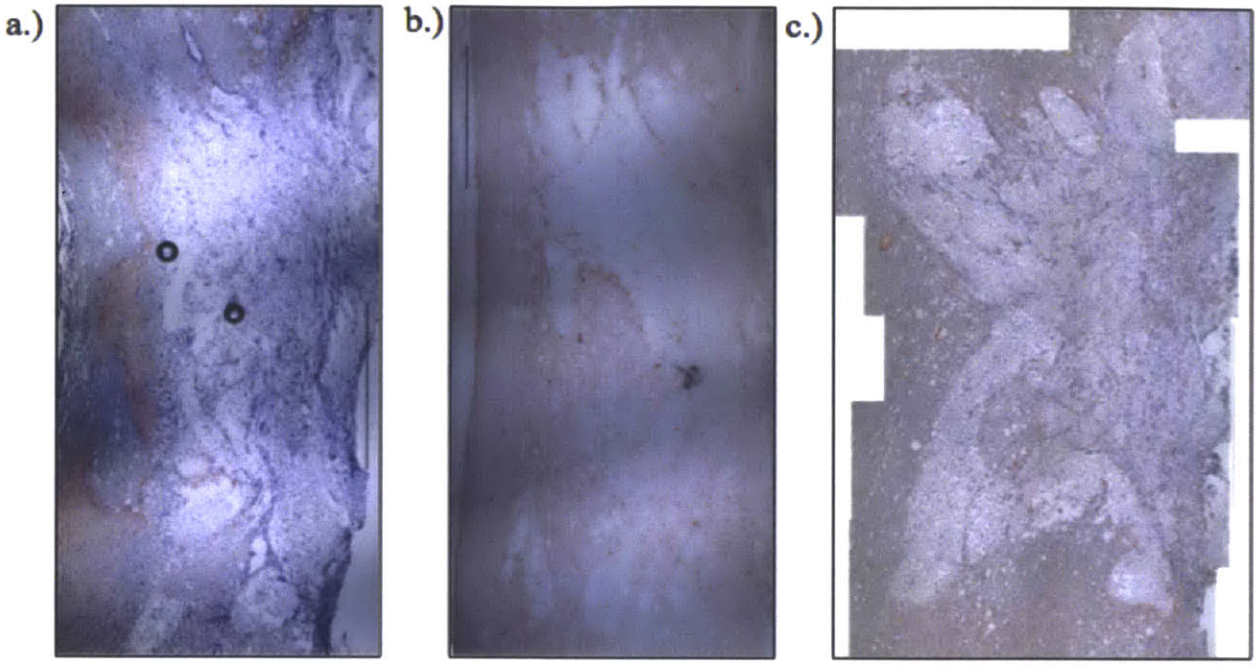

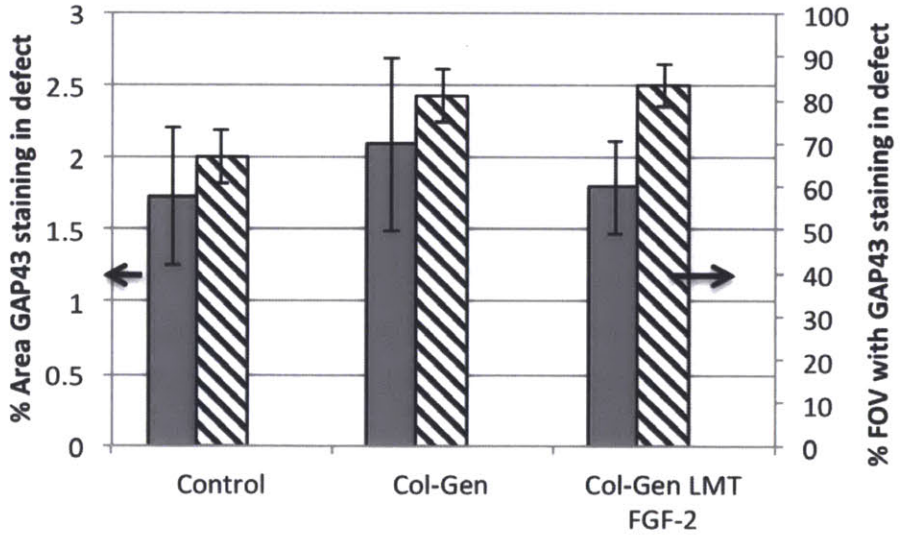

d.)

Figure 6-14: Longitudinal GAP-43 IHC stained sections through the middle of the defect (corresponding to the animal with a Type B response in figure 6-7) for a.) Control b.) Col-Gen c.) Col-Gen LMT FGF-2 treatment groups, demonstrating the presences of regenerating axons with the defect. Of note is the high number of regenerating axons streaming into the lesion for the Col-Gen LMT FGF-2 animal in c. 4x objective, scale bar 1000 μm. d.) Quantitative analysis of GAP-43 staining within the defect. Percentage of area staining within defect (primary axis, solid bars), Percentage of fields of view within the defect with GAP-43 staining (secondary axis, striped bars). N=6-7 mean ± SEM.

6.4.4.7 Overview of marker co-localization in animals exhibiting a Type A response to injury

For the purposes of facilitating the co-localization of IHC markers, a region of interest with active neurovascular regeneration into the lesion was chosen for a Type A response animal in each treatment group (control **Figure 6-15**, Col-Gen **Figure 6-16, 6-17**, Col-Gen LMT FGF-2 **Figure 6-18**). Serial sections stained for Masson's trichrome and IHC antigens laminin, GFAP, GAP-43, VWF, and CD68 were combined into single figure for each group. Additionally, Col-Gen treatment group was stained for CS-56, P75, and fibronectin **Figure 6-17.**

Regenerating GAP-43+ axons can be seen growing directly into the defect in close association with cellular bridges. These areas are rich in laminin, astrocytes, fibroblast-like cells, and VWF positive endothelial cells. While regenerating axons could be seen associating with astrocytes, they did not appear to be the only cell able to support the axon growth. Fibroblast-like cells staining positive for collagen on Masson's tricrhome were also commonly found in association with the axons. Axon growth was not observed in the cavitary macrophage filled regions within the defect unless these tissue bridges were present. Interestingly, the cellular bridges in the area directly below the parallel oriented fibrous scar tissue on the lateral border of the defect created a niche for regenerating axons growth into the defect.

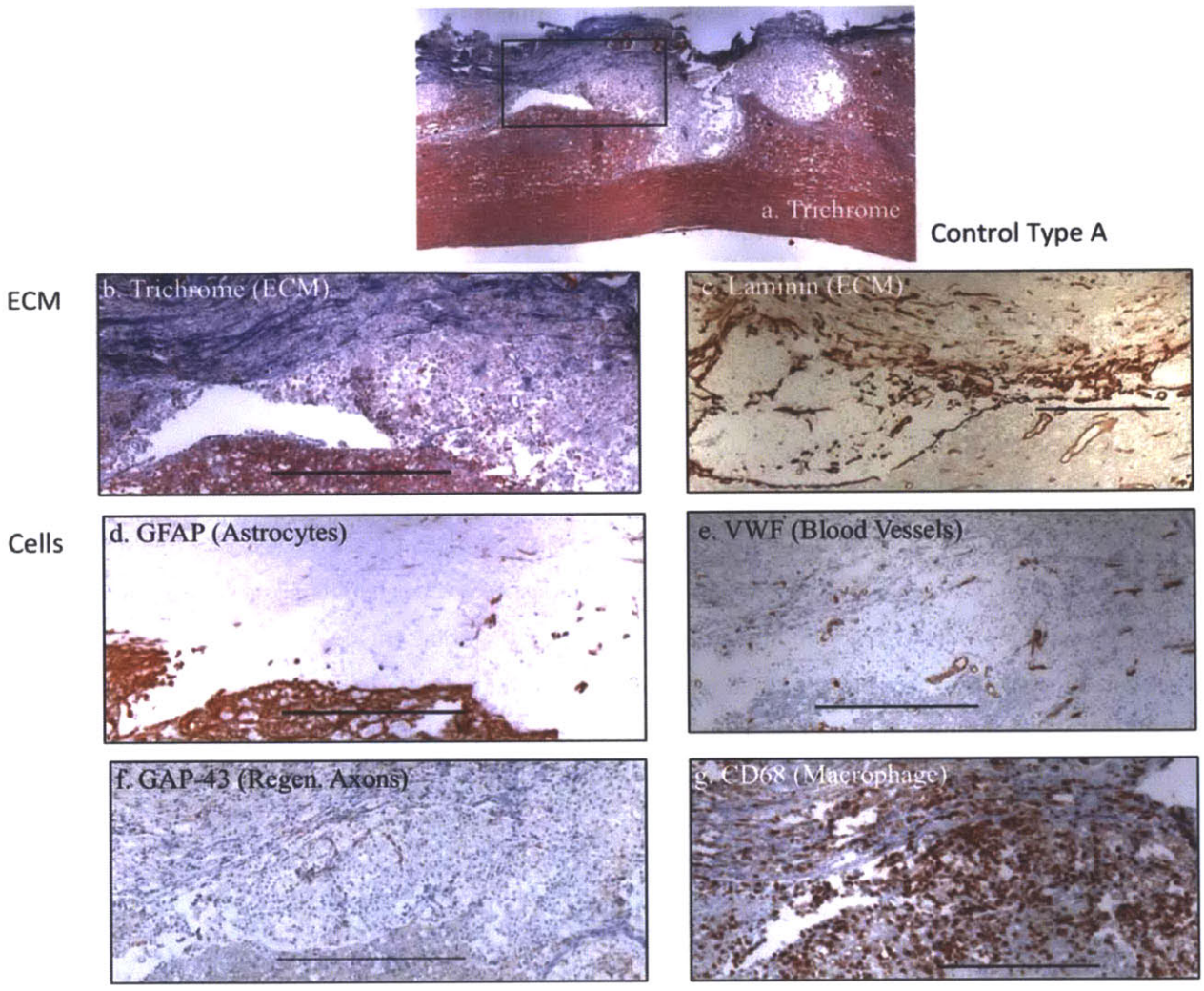

Figure 6-15: Histological/IHC images of a control animal exhibiting a Type A response. **a.)** Longitudinal Masson's trichrome image with a boxed region of interest. Scale bar 1000 μm. **b-g.)** IHC of serial sections of the region of interest. Active growth of GAP-43+ regenerating axons can be seen occurring on cellular bridges directly below the parallel oriented fibrous scar tissue on the lateral border of the defect. The bridges are largely devoid of astrocytes but have a high density of VWF+ capillaries and stain positive for laminin. Axon growth is not observed in the cavitary macrophage filled regions within the defect. Images taken at 4x objective, scale bar 500 μm.

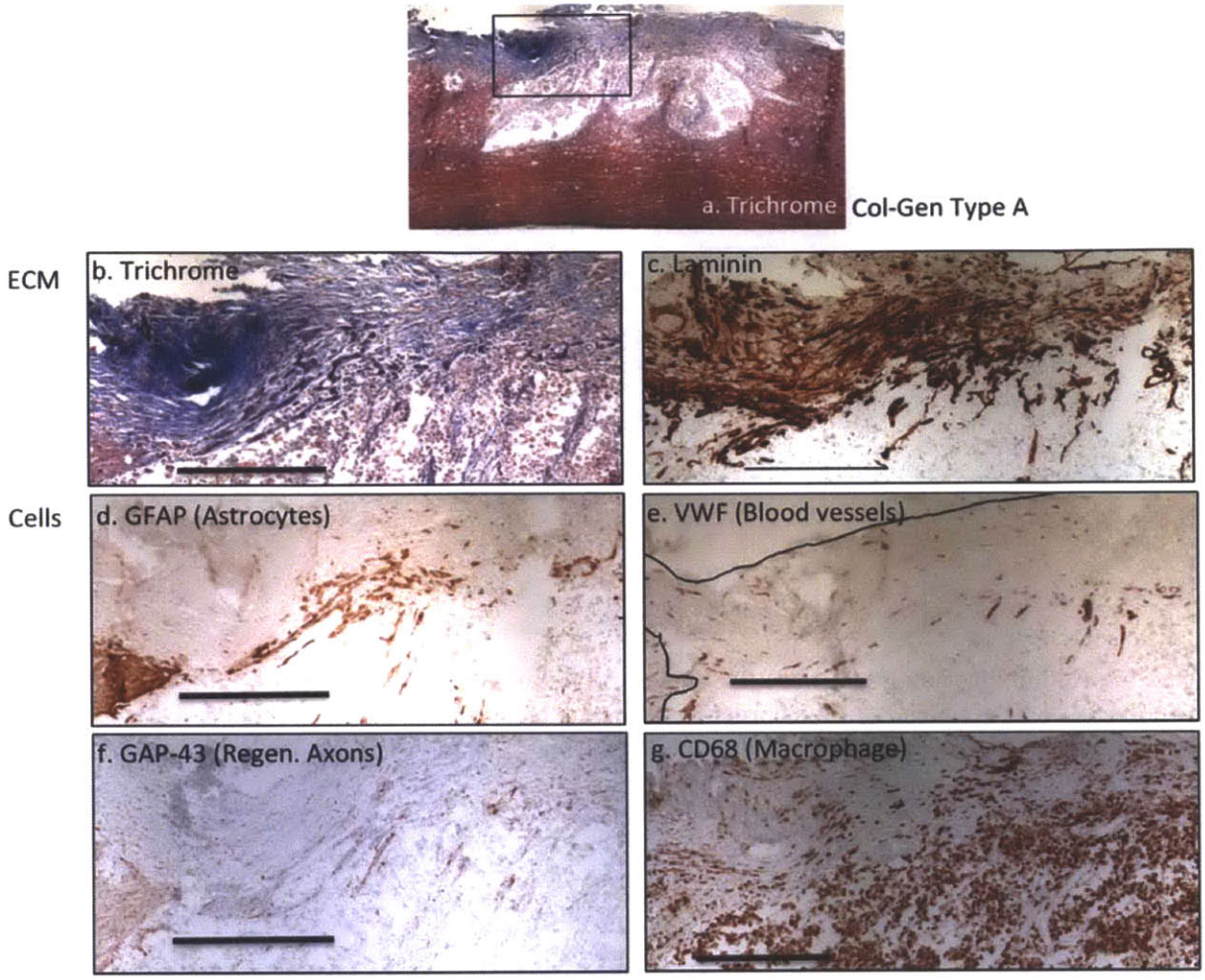

Figure 6-16: Histological/IHC images of a Col-Gen animal exhibiting a Type A response. **a.)** Longitudinal Masson's trichrome image with a boxed region of interest. Scale bar 1000 μm **b-g**.) IHC of serial sections of the region of interest. Active growth of GAP-43+ regenerating axons can be seen occurring on cellular bridges directly below the parallel oriented fibrous scar tissue on the lateral border of the defect. The bridges are highly populated of astrocytes and have a high density of VWF+ capillaries and stain positive for laminin. Axon growth is not observed in the cavitary macrophage filled regions within the defect. 4x objective, scale bar 500 μm

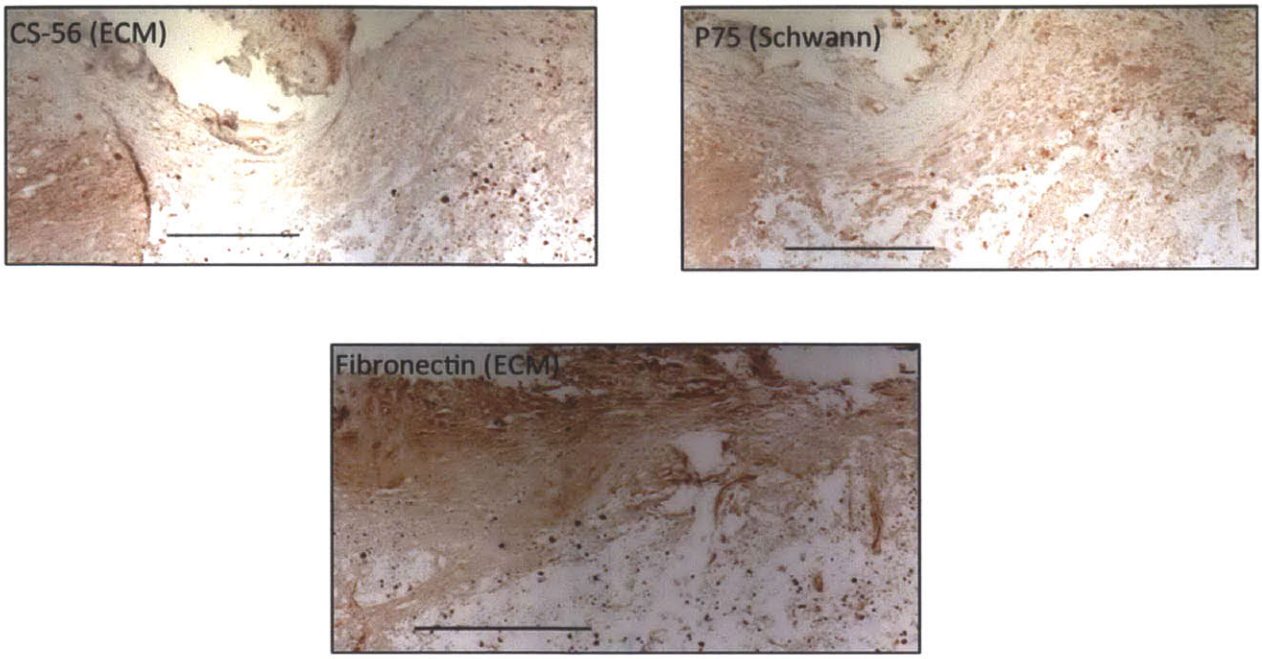

Figure 6-17: Additional (non-quantified) IHC stains of the Col-Gen animal in Figure 6-14. Chondroitin sulfate proteoglycans are present at the border of the defect but are not found within the defect itself. Schwann cells and fibroblasts can be seen scattered through the defect.

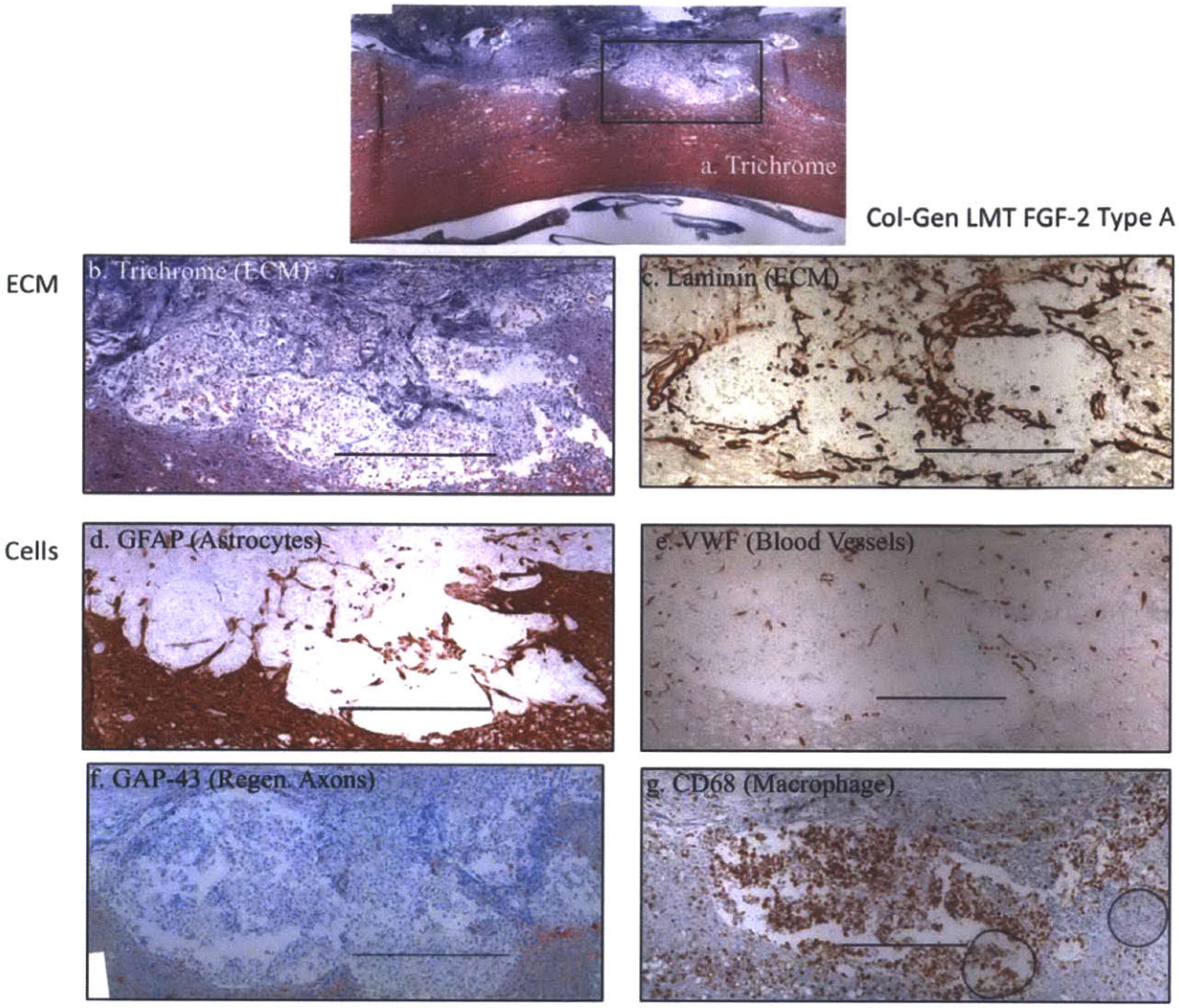

Figure 6-18: Histological/IHC images of a Col-Gen LMT FGF-2 animal exhibiting a Type A response. **a.)** Longitudinal Masson's trichrome image with a boxed region of interest. Scale bar 1000 μm. **b-g.)** IHC of serial sections of the region of interest. Active growth of GAP-43+ regenerating axons can be seen occurring on cellular bridges directly into the defect . The bridges populated by astrocytes and have a high density of VWF+ capillaries and laminin. Axon growth is not observed in the cavitary macrophage filled regions within the defect. 4x objective, scale bar 500 μm

6.5 Discussion

6.5.1 Functional evaluation

Despite having a hemi-resection injury, the many of the rodents exhibited some level of functional ability as early as a few days after injury. By four weeks several animals showed significant ability to bear weight and walk on their impaired hind limb. It is well know that animals receiving lateral hemi-section injuries can regain substantial recovery of their impaired side.[6, 7] However, there are several deficits, mostly observed on the side of the lesion, which can persist including transiently impaired body equilibrium, inter-limb coupling, and impaired skilled locomotion.[6] The observed recovery from hemi-section injuries can occur through a multitude of mechanisms.[6] Un-injured pathways can sprout connections capable of accessing spinal circuits distal to the lesion such as central pattern generators (CPGs). Intrinsic changes in the existing spinal circuitry including the formation of new or modified anatomical circuits, may allow for these sprouted axons to exert voluntary control over them. In rodents, limited sprouting of the spared corticospinal and corticobulbar fibers have been shown to establish new connections from the cortex to downstream targets.[8] Additionally, in non-human primates, the ability to extensively use their impaired hand after cervical hemisection is attributed to the pre-existing "cross-over" CST projections within the spared contralateral side of the spinal cord.[9, 10] While the regeneration of lesioned axons through the defect site is limited, these axons can play a triggering rather than controlling role by activating propriospinal pathways in more rostral segments which can then organize the rhythmic output of the spinal cord generated by more caudal segments.[6] Finally, the reorganization of local spinal circuitry and input from sensory afferents alone may be enough to elicit rhythmic movement of limbs through CPGs.[11] Hence, it is difficult to tell what mechanism is causing the increase in functional score seen in this study. Nevertheless, functional outcome and functional improvement are important outcome metrics in the treatment of spinal cord injury.

The functional score of the animals in this study **Figure 6-2** appeared to be more correlated with the success of the surgery (degree of secondary damage caused by bleeding and trauma in the peri-operative timeframe) than the treatment group. Of all the metrics analyzed, percentage of spared tissue in the peri-lesional area and the width of the contralateral white matter at its most narrow point was the best predictor of functional ability at 4 weeks (**Figure 6-3b**). To account for differences in the extent of injury (baseline functional score), and to focus on the recovery from injury due to treatment, each animal was used as its own control by comparing functional scores at 1 and 4 weeks post injury (**Figure 6-2 bottom**). One week was used as a more stable platform to assess the recovery since it is after the acute inflammatory phase.[1] The number of animals which improved by 2 or more points was greater in the

col-gen LMT FGF-2 group but not statistically significant. Wilcoxon matched pairs test showed a significant improvement in left leg functional score between 1 and 4 week for Col-Gen ($p=0.0277$) and Col-Gen LMT FGF-2 ($p=0.0431$) groups but not for the control group. This early beneficial effect of the gel would seem to be related to its function in ameliorating the initial response to injury, perhaps by aiding hemostasis or by preventing inflammatory cells from entering the defect. Cholas et al. also found significant increases in one to four week hind limb score for animals treated with pre-formed scaffolds containing mesenchymal stem cells or chondrotinase ABC but not for control animals [2]. This was potentially due to their immunomodulatory and neuroplasticity effects respectively.

Main limitation of these comparisons is that the metric is non-linear so a 2-point increase from 0-2 (translating to the shift from flaccid paralysis to significant but non-weight bearing hind limb movement) cannot be equated to an increase from 3-5 (translating to a shift from partial to full weight bearing). The number and diversity of metrics used for behavioral recovery after SCI including endpoint measures, kinematic measures, kinetic measurements, and electrophysiological measurements make it difficult to compare results between studies.[12] The usefulness of the metric is also dependent on the type of SCI for which it was developed for since the deficits caused by each type of injury model are unique. For the purposes of this study, a slightly more complex version of an established simpler scoring metric [2], which did not require advanced training or specialized equipment was used to provide a reasonable estimate of functional recovery between treatment groups. Future studies aimed at parsing out more minute differences between animals should take advantage of more complex scoring metrics or electrophysiological studies.

Closely related to the functional score, was the time it took for animals to recover bladder function after injury. Although not all animals were able to recovered bladder function, the ones that were able to had a recovery time, which ranged from under 1 day to 22 days suggesting that the mechanism of recovery was due to either white matter sparing (early recovery) or re-wiring of neural pathways (later recovery). Interestingly, one of the animals in the Col-Gen LMT FGF-2 group which recovered the ability to void at 3 days post injury, lost that ability at day 16 suggesting a second event which caused destruction of this pathway. This animal was noted to have a half-width injury in the middle of the defect but extensive fibrous tissue infiltration of the dorsal columns and adjacent white matter, both of which are involved in the micturition pathway.[13] This animal was also noted to have a decrease in functional score of the right leg and no change in functional score of the left leg from one to four weeks.

Given the multitude of recovery mechanisms and the time course of axon regeneration as mentioned above, it is not surprising that no correlation was found between the density of regenerating

axons or tissue composition within the defect. The permissive composition of the defect in Col-Gen LMT FGF-2 animals however, is promising towards the future regeneration of axons through the defect and is an important area of future work to follow up on by looking at longer survival time points.

6.5.2 Histological evaluation

Defect and ECM

The present study compares the response to tissue response to injury in a hemi-resection model of SCI. Although the control group did not have a therapy applied, the blood clot, which forms in the defect after injury, provides a provisional matrix for cellular ingrowth. The "open" nature of a hemi-resection injury facilitates the entry of inflammatory and connective tissue cells into the lesion site, which is unlike "closed" contusion injuries that do not breach the dura mater. Consequently, the control groups in this study also had significant tissue formation within the defect. However, the matrix formed by the blood clot in control animals predominantly resolved into either a cavitary region filled with macrophages and little tissue matrix or a highly dense collagenous scar filling the entire defect, both of which are not favorable for nerve tissue regeneration. Therefore, the goal of the study was to examine if the presence of a collagen-genipin hydrogel and the growth factor FGF-2 could facilitate the creation of a tissue matrix within the defect containing elements that are more conducive towards axon regeneration.

Histology of the defect at 1 day **Figure 6-4** shows that the collagen gel mixes to various degrees with the blood that fills the defect after injury due to hemorrhage from the spinal cord parenchyma or bleeding from the overlying musculature. This means that pipetting the gel directly into the defect did not allow the gel to form rapidly or stiff enough to displace the continued bleeding into the defect. Indeed, the dense staining of fibronectin **Figure 6-6a** within the defect at one week suggests the gel was substantially mixed with blood, as soluble plasma fibronectin is deposited in areas of blood clotting to allow for the attachment of cells.[14]The mixing of gel with blood is not necessarily an unwanted event. Blood can create more pores and imperfections in the gel, which can facilitate cellular migration into the scaffold. The formation of a fibrin-fibronectin clot in the areas of hemorrhage and blood-gel mixing serves as an additional cell permissive scaffold. Finally, nucleated blood cells (leukocytes) contained within the gel, have the capability to release pro-regenerative growth factors.[15]

By one week, connective tissue and inflammatory cells heavily infiltrated the defect of the Col-Gen treated animals and little un-degraded gel could be found. Even though the gel contained 1 mM genipin, the low weight percentage of collagen in the gel (0.3%) and the ability of the invading cell populations to secrete proteases, caused the gel to be almost completely re-modeled/degraded by this

point **Figure 6-5b,c**. It is also likely that genipin reacted with proteins in the blood thereby decreasing the concentration available to cross-link the collagen gel.

By four weeks post injury, there was a noticeable stratification in the injury severity and degree of collagenous scar formation within the defect between animals within the same group (especially in control and Col-Gen groups) **Figure 6-7**. One hypothesis for this is the amount of bleeding into the defect post injury. Blood forms a fibrin clot and platelets embedded within the clot release growth factors such as PDGF, which enhance fibroblast infiltration and connective tissue formation. Blood also contains peripheral leukocytes, which can cause substantial secondary damage [15], the presence of blood also introduces secondary damage to the spinal cord through lipid peroxidation and ischemia from vasospasm.[16] The hyper-cellularity of control or gel treatment groups noted at one-week post injury, greatly changed by four-weeks. Largely evolved to a macrophage core with few cells and connective tissue deposition. The dense fibronectin staining at one week largely disappeared **Figure 6-17** and much higher density of collagen was noted suggesting a remodeling of the defect area with an endogenous ECM. Areas adjacent to the defect were also prone to invasion by connective tissue cells most likely fibroblasts. The areas of fibroblast invasion, especially in the dorsal columns also co-localized with macrophage staining suggesting that the population of macrophages in these areas released factors to attract fibroblasts such as FGF-2. Given the discussion about the initial matrix present in control and treatment groups, it is not surprising that the col-gen gel treatment group did not differ substantially (histologically and functionally) from control groups since the matrix which formed within the defect was largely the same except with the addition of the collagen and possible less direct initial exposure to invading inflammatory cells. However, as described in more detail below, animals treated with Col-Gen LMT FGF-2 gels had a lesion site, which was populated to a greater extent with astrocytes and endothelial cells and contained a tissue matrix rich in laminin, thus creating an environment conducive to future axonal regeneration. The addition of FGF-2 also had a neuroprotective effect as noted by the increase in viable tissue around the defect and the absence of any animals exhibiting a full width defect, thus supporting our working hypothesis (2).

Laminin is an extracellular matrix protein produced by fibroblasts, endothelial cells, Schwann cells and astrocytes, most commonly found in the basement membrane of these cells or as membrane independent isoforms important for cell adhesion and signaling.[17-19] Laminin and particularly its membrane independent laminin γ1 chain is a particularly important substrate for axon growth during development and regeneration.[17, 18, 20] Regenerating axons have been reported in several studies to be in close association with a laminin matrix of Schwann cells and/or astrocytes within a defect area after spinal cord injury.[20-23] Interestingly, axons are capable of regenerating through areas where growth

inhibitory (CSPG) and growth promoting (laminin) molecules are present, suggesting that the axons respond to a balance of attractive and repulsive cues.[21] The enhanced deposition of laminin within the defect of Col-Gen LMT FGF-2 treated animals is reflective of the increased cellular infiltration of the defect, especially by astrocytes and endothelial cells, and is a promising finding towards the creation of an axon regenerative template within the lesion site.

In addition to axon growth promoting substrates, astrocytes and fibroblasts also produce growth-inhibiting substrates after SCI such as chondroitin sulfate proteoglycans (CSPGs).[24] In this study, sections were only preliminarily stained for CSPGs due to a.) Technical difficulty of using this antibody in paraffin sections b.) Unclear interpretation for what the staining would mean in the context of regeneration. Given the correct growth promoting cues such as laminin [21, 22], NT-3, NGF, and BDNF [25], axons can extend past regions of CSPGs deposition within the lesion site. The increase of astrocytes within the defect may result in a corresponding increase the CSPGs reactivity as well as laminin and growth factor secretion which could promote instead of hinder axon regeneration. Interestingly, the astrocytes within the defect do not appear to produce CSPGs, which could potentially indicate a shift towards a less reactive phenotype **Figure 6-17**.

Inflammatory macrophage response

There was no statistical difference between the macrophage response to injury in either the absolute area of macrophage infiltration or the relative area of infiltration as compared to the original defect size suggesting that treatment with the col-gen or col-gen LMT FGF-2 gels neither promoted nor lessened the inflammatory response to injury. This finding is important in showing that the presence of the collagen gel and concentrations of both genipin and FGF-2 were well tolerated by the animals and did not cause a severe inflammatory reaction. In comparison, Cholas et al. found a significant decrease in the density of macrophages within the defect of animals treated with preformed collagen sponges compared to control injuries [2]. This finding is not surprising as preformed scaffolds can greatly hinder cellular infiltration of the defect compared to hydrogel scaffolds due to their persistence in vivo. As mentioned earlier, the presence of macrophages is important for wound healing and regeneration due to their actions in clearing the defect of cellular debris and releasing factors to promote angiogenesis.

Astrocytes

The use of Col-Gen LMT FGF-2 gels resulted in significant increases in GFAP staining within the defect compared to control or Col-Gen groups, supporting our working hypothesis (3) **Figure 6-11**. As a comparison, Cholas et al. reported that no GFAP staining was seen within the defect of animals

treated with pre-formed collagen sponges after four weeks in a similar hemi-resection model of SCI [2].

In other species capable of regenerating their spinal cord such as the newt or zebrafish, GFAP+ glia (astrocytes) play an important role in bridging the defect after injury and templating the growth of axons across the defect.[26, 27] In zebrafish, this process (proliferation and elongation across the defect) is mediated by FGF-2 signaling.[27] Even in mammals, mature astrocytes are capable of supporting axon growth down degenerating white matter tracks[28] and hold an intrinsic capability to support the regeneration of axons.

Using an intrathecal administration TGF-a and an adenovirus induced overexpression of TGF-a in the spinal cord parenchyma, White et al. was able to increase the proliferation and migration of astrocytes into the lesion core after contusion SCI in mice.[22, 29] The astrocytes took on an elongated axon growth supportive phenotype and at the borders of the defect there was a close association of laminin, GFAP, and numerous GAP43+ axons. There was also an increase in NF positive axons within the defect as compared to control groups.

Davies et al. transplanted astrocytes derived from embryonic glial-restricted precursors treated with BMP-4 into dorsal column transection injuries in rats.[30] This study found the cells promoted robust axon growth and restoration of locomotor function after the acute transection injury, promoting growth of over 60% of ascending dorsal column axons into lesion, with 66% of these axons extending beyond the injury sites. These cells formed a tissue bridge across the injury site and interestingly caused astrocytes in the host tissue to orient their processes towards the lesion center.[30] Even more noteworthy is that astrocytes differentiated from glial-restricted precursors treated with CTNF failed to promote axon growth, survival, or functional recovery suggesting the importance of the specific astrocyte subpopulation in the observed response.[31]

In the context of the current study, the elongated astrocyte processes oriented towards the center of the defect (especially noticeable in **Figure 6-11c,6-16d**) are hypothesized to be of the growth supporting phenotype while astrocytes on the border of the lesion with dense interweaved processes are of the inhibitory glial scar phenotype (**Figure 6-15d**). Indeed, these areas of astrocytes are also noted to be associated with GAP-43 axons (**Figure 6-14c, 6-16c**). As described in detail in chapter 4, the exposure of astrocytes to FGF-2 causes them to increase their outgrowth into Col-Gen gels and produces a chain-like movement of these cells similar to the framework described in the studies above. Although not specifically quantified in this study, astrocytes growing into the defect of Col-Gen (especially right below the parallel oriented scar) and Col-Gen LMT FGF-2 groups appeared to have an elongated phenotype, which was not noticeable in control animals.

Endothelial cells

FGF-2 is a potent angiogenic factor [32] and animals treated with Col-Gen LMT FGF-2 gels had a significant increase in the number of VWF+ cells within the defect compared to control or Col-Gen groups, thus supporting our working hypothesis (4) **Figure 6-12.** In contrast, work by Cholas et al. showed that pre-formed scaffolds significantly decreased the density of blood vessels within the defect at four weeks post injury compared to control animals [2].

Blood vessels are highly important for the support of new tissue growth into the defect. Local vasculature is particularly important for axon regeneration. Dray et al. used two photon microscopy to analyze the dynamics of vascular and axonal networks in the injured mouse spinal cord and found the growth kinetics of sensory regenerating axons are strongly enhanced by their vicinity to posttraumatic angiogenic vessels after SCI, however that vessels do not help axons to recover their initial trajectories.[33] Therefore, the enhancement of the vascular network along with a framework of astrocytes within the defects of Col-Gen LMT FGF-2 provides a supportive environment for future axonal growth.

Regenerating axons and additional growth supportive cell types

Regenerating axons were identified using an antibody for GAP-43, a protein in the growth cones of regenerating axons. Tetzlaff et al. showed that another commonly use axonal marker neurofilament (NF) underestimated the extent of axonal regeneration as compared to GAP-43.[34] Therefore due to the sensitivity of axon regeneration required at the relatively early time point of assessment (28 days post injury) GAP-43 staining was chosen over NF.

GAP-43 positive axons closely followed the laminin matrix, astrocytes, and elongated fibroblast like-cells within the defect **Figures 6-15, 6-16, 6-18.** There was also a network of blood vessels in close proximity to areas of axon growth. Axons not found in either the macrophage filled cavitary areas or dense collagenous scar tissue due to the lack of cellular and extracellular matrix support. Regenerating axons were not always associated with astrocytes demonstrating that they were not the only or principal cells responsible for axon growth into the defect. Interestingly, the presence of a dense parallel oriented collagenous scar localized to the lateral border of the defect of control or Col-Gen treatment groups templated the growth of astrocytes, endothelial cells, and axons right below it. In fact, most of the cellular ingrowth into the defect for control or col-gen groups (excluding the full width fibrous defects) happened right below this border unlike col-gen LMT FGF-2 groups where growth took place more distributed throughout the lesion site. It is likely that other infiltrating cell types such as Schwann cells and

fibroblasts provided a growth supportive matrix for axon regeneration **Figure 6-17**.[20, 35] Transplantation of meningeal fibroblasts into spinal cord defects promoted the growth of peptidergic axons from dorsal root afferents and, to a lesser extent, of supraspinal serotonergic fibers at the periphery of the grafts. These fibroblasts were shown to produce multiple neurotrophic factors including beta-NGF, NT3, aFGF and bFGF.[35] Typically, astrocytes exclude fibroblasts from areas of spinal cord tissue[19] which was the case in many areas of collagenous scar within the defect, however there were notable places within the defect where GAP-43 axons were traversing across collections of cells partially staining for GFAP and staining for collagen **Figures 6-15, 6-16, 6-18**. Some of the tissue bridging cells in the defect could also have been Schwann cells. Schwann cells stain strongly for laminin and it is possible that some of the laminin rich areas are due to the presence of these cells. Preliminary staining for Schwann cells using a P75 antibody was employed in this study and warrants future investigation. It should be noted that there are limited good markers for Schwann cells [19] as the commonly used markers S100b is also expressed in astrocyte; P75 a NGF receptor is up-regulated in de-differentiated Schwann cells and is also present in oligodendrocyte progenitors, macrophages and microglia; and peripheral myelin proteins like P0 will not stain non-myelinating Schwann cells. Overall, the findings of this study suggests that not all of the cells in the axon supportive tissue bridges are astrocytes or typical fibroblasts and the identity of these cells needs to be more well characterized in future studies.

Despite the differences in defect composition between control and treatment groups, no statistical difference could be found in two measures of GAP-43 staining within the defect. There are several potential reasons for this finding: Firstly, four weeks post injury represents an early time point of analysis for the regeneration of sensory and motor axons after SCI. For example, cortical spinal tract (CST) axon sprouting occurs between three weeks and three months post injury.[36] Also, the specific GAP-43 antibody used had a heterogeneous pattern of staining between slides, meaning that some sections appeared faintly stained while others appeared heavily stained for the same animal. While the general pattern remained the same, it was possible that areas with GAP-43 staining were missed or incorrectly counted (i e. false staining of connective tissue elements which would look like regenerating axons) during image analysis. Regenerating sensory axons from dorsal root ganglion cells are also known to enter the defect after SCI and were not differentiated our analysis.[19] Finally, GAP-43 immunoreactivity can be found in non-myelinating Schwann cells and Schwann cells in the distal stump of a peripheral nerve four weeks after transection.[37] It is possible that infiltrating Schwann cells are also causing some of the observed GAP-43 staining. Nevertheless, it was quite apparent that GAP-43 fibers could be found within the defect tissue on tissue bridges (especially apparent in **Figures 6-14c, 6-16c**) containing laminin and a network of blood vessels.

6.6 References

[1] Hagg T, Oudega M. Degenerative and spontaneous regenerative processes after spinal cord injury. J Neurotrauma. 2006;23:264-80.
[2] Cholas R, Hsu HP, Spector M. Collagen scaffolds incorporating select therapeutic agents to facilitate a reparative response in a standardized hemiresection defect in the rat spinal cord. Tissue Eng Part A. 2012;18:2158-72.
[3] Brey EM, Lalani Z, Johnston C, Wong M, McIntire LV, Duke PJ, et al. Automated selection of DAB-labeled tissue for immunohistochemical quantification. The journal of histochemistry and cytochemistry : official journal of the Histochemistry Society. 2003;51:575-84.
[4] Salegio EA, Pollard AN, Smith M, Zhou XF. Macrophage presence is essential for the regeneration of ascending afferent fibres following a conditioning sciatic nerve lesion in adult rats. Bmc Neurosci. 2011;12:11.
[5] Wrathall JR, Pettegrew RK, Harvey F. Spinal cord contusion in the rat: Production of graded, reproducible, injury groups. Experimental Neurology. 1985;88:108-22.
[6] Rossignol S, Frigon A. Recovery of locomotion after spinal cord injury: some facts and mechanisms. Annu Rev Neurosci. 2011;34:413-40.
[7] Darian-Smith C. Synaptic plasticity, neurogenesis, and functional recovery after spinal cord injury. Neuroscientist. 2009;15:149-65.
[8] Maier IC, Schwab ME. Sprouting, regeneration and circuit formation in the injured spinal cord: factors and activity. Philosophical transactions of the Royal Society of London Series B, Biological sciences. 2006;361:1611-34.
[9] Rosenzweig ES, Brock JH, Culbertson MD, Lu P, Moseanko R, Edgerton VR, et al. Extensive spinal decussation and bilateral termination of cervical corticospinal projections in rhesus monkeys. J Comp Neurol. 2009;513:151-63.
[10] Darian-Smith C. Primary afferent terminal sprouting after a cervical dorsal rootlet section in the macaque monkey. J Comp Neurol. 2004;470:134-50.
[11] Barriere G, Leblond H, Provencher J, Rossignol S. Prominent role of the spinal central pattern generator in the recovery of locomotion after partial spinal cord injuries. J Neurosci. 2008;28:3976-87.
[12] Muir GD, Webb AA. Mini-review: assessment of behavioural recovery following spinal cord injury in rats. The European journal of neuroscience. 2000;12:3079-86.
[13] Fowler CJ, Griffiths D, de Groat WC. The neural control of micturition. Nat Rev Neurosci. 2008;9:453-66.
[14] Corbett SA, Lee L, Wilson CL, Schwarzbauer JE. Covalent cross-linking of fibronectin to fibrin is required for maximal cell adhesion to a fibronectin-fibrin matrix. J Biol Chem. 1997;272:24999-5005.
[15] Trivedi A, Olivas AD, Noble-Haeusslein LJ. Inflammation and Spinal Cord Injury: Infiltrating Leukocytes as Determinants of Injury and Repair Processes. Clinical neuroscience research. 2006;6:283-92.
[16] Mautes AE, Weinzierl MR, Donovan F, Noble LJ. Vascular events after spinal cord injury: contribution to secondary pathogenesis. Physical therapy. 2000;80:673-87.
[17] Grimpe B, Dong S, Doller C, Temple K, Malouf AT, Silver J. The critical role of basement membrane-independent laminin gamma 1 chain during axon regeneration in the CNS. J Neurosci. 2002;22:3144-60.
[18] Liesi P, Silver J. Is astrocyte laminin involved in axon guidance in the mammalian CNS? Developmental biology. 1988;130:774-85.
[19] Buss A, Pech K, Kakulas B, Martin D, Schoenen J. Growth-modulating molecules are associated with invading Schwann cells and not astrocytes in human traumatic spinal cord injury. Brain. 2007;130:940-53.
[20] Risling M, Fried K, Linda H, Carlstedt T, Cullheim S. Regrowth of motor axons following spinal cord lesions: distribution of laminin and collagen in the CNS scar tissue. Brain Res Bull. 1993;30:405-14.

[21] Jones LL, Sajed D, Tuszynski MH. Axonal regeneration through regions of chondroitin sulfate proteoglycan deposition after spinal cord injury: a balance of permissiveness and inhibition. J Neurosci. 2003;23:9276-88.
[22] White RE, Rao M, Gensel JC, McTigue DM, Kaspar BK, Jakeman LB. Transforming growth factor alpha transforms astrocytes to a growth-supportive phenotype after spinal cord injury. J Neurosci. 2011;31:15173-87.
[23] Frisen J, Haegerstrand A, Risling M, Fried K, Johansson CB, Hammarberg H, et al. Spinal axons in central nervous system scar tissue are closely related to laminin-immunoreactive astrocytes. Neuroscience. 1995;65:293-304.
[24] Rolls A, Shechter R, Schwartz M. The bright side of the glial scar in CNS repair. Nat Rev Neurosci. 2009;10:235-41.
[25] Silver J, Miller JH. Regeneration beyond the glial scar. Nat Rev Neurosci. 2004;5:146-56.
[26] Zukor KA, Kent DT, Odelberg SJ. Meningeal cells and glia establish a permissive environment for axon regeneration after spinal cord injury in newts. Neural development. 2011;6:1.
[27] Goldshmit Y, Sztal TE, Jusuf PR, Hall TE, Nguyen-Chi M, Currie PD. Fgf-dependent glial cell bridges facilitate spinal cord regeneration in zebrafish. J Neurosci. 2012;32:7477-92.
[28] Davies SJ, Goucher DR, Doller C, Silver J. Robust regeneration of adult sensory axons in degenerating white matter of the adult rat spinal cord. J Neurosci. 1999;19:5810-22.
[29] White RE, Yin FQ, Jakeman LB. TGF-alpha increases astrocyte invasion and promotes axonal growth into the lesion following spinal cord injury in mice. Exp Neurol. 2008;214:10-24.
[30] Davies JE, Huang C, Proschele C, Noble M, Mayer-Proschel M, Davies SJA. Astrocytes derived from glial-restricted precursors promote spinal cord repair. Journal of Biology. 2006;5:7.1-7.21.
[31] Davies JE, Proschel C, Zhang N, Noble M, Mayer-Proschel M, Davies SJ. Transplanted astrocytes derived from BMP- or CNTF-treated glial-restricted precursors have opposite effects on recovery and allodynia after spinal cord injury. J Biol. 2008;7:24.
[32] Yun YR, Won JE, Jeon E, Lee S, Kang W, Jo H, et al. Fibroblast growth factors: biology, function, and application for tissue regeneration. J Tissue Eng. 2010;2010:218142.
[33] Dray C, Rougon G, Debarbieux F. Quantitative analysis by in vivo imaging of the dynamics of vascular and axonal networks in injured mouse spinal cord. Proc Natl Acad Sci U S A. 2009;106:9459-64.
[34] Tetzlaff W, Zwiers H, Lederis K, Cassar L, Bisby MA. Axonal transport and localization of B-50/GAP-43-like immunoreactivity in regenerating sciatic and facial nerves of the rat. J Neurosci. 1989;9:1303-13.
[35] Franzen R, Martin D, Daloze A, Moonen G, Schoenen J. Grafts of meningeal fibroblasts in adult rat spinal cord lesion promote axonal regrowth. Neuroreport. 1999;10:1551-6.
[36] Hill CE, Beattie MS, Bresnahan JC. Degeneration and sprouting of identified descending supraspinal axons after contusive spinal cord injury in the rat. Exp Neurol. 2001;171:153-69.
[37] Curtis R, Stewart HJ, Hall SM, Wilkin GP, Mirsky R, Jessen KR. GAP-43 is expressed by nonmyelin-forming Schwann cells of the peripheral nervous system. J Cell Biol. 1992;116:1455-64.

Chapter 7:

Pilot *ex vivo* MRI study of the gel implantation and tissue remodeling after hemi-resection injury in rodents

7.1 Introduction & motivation:

Magnetic resonance imaging (MRI) is a powerful clinical tool used to visualize pathomorphic changes in the spinal cord parenchyma and predict the extent of neurological deficit after spinal cord injury (SCI) in humans.[1] Experimental models show that MRI correlates with histopathologic findings such as edema, hemorrhage, and secondary degenerative changes such as demyelination and cyst formation.[2] Conventional MRI techniques for evaluation of spinal cord injury include the pulse sequences: T1-weighted images, T2-weighted images, T2* susceptibility images, and short tau inversion recovery (STIR) images.[3] For these pulse sequences, contrast is based on intrinsic properties of the tissue (T1 and T2 values). T2-weighted images are particularly useful for imaging the spinal cord parenchyma for their ability to discern white matter, gray matter, edema, and hemorrhage. Another imaging modality, diffusion-weighted MRI (DWI) measures the free diffusion of water molecules and can provide a measure of white matter sparing, axon swelling, and myelin disruption after injury.[3]

Several studies have correlated *in vivo* and *ex vivo* MRI of SCI with its histopathology.[2, 4-7] However, these studies all utilized a contusion type model and followed the natural progression of the injury as opposed to assessing the effect of a treatment on lesion parameters. To these points, Iannotti et al. employed a 1.5T MRI to examine the growth of tissue into Schwann cell bridging transplants in a hemiresection injury and had an 86% success rate of identifying tissue within the cables.[8] Also, Austin et al. utilized MR imaging to assess the lesion volume of a clip compression SCI after treatment with a drug releasing hydrogel implanted into the subarachnoid space.[9] However, both of these studies employed field strengths of <7T, which suffered from low spatial resolution and did not allow them to explore the composition of the defect in detail. There are currently, limited studies monitoring the remodeling of a biomaterial gel after SCI or assessing the progression of a hemi-resection type SCI using high-resolution MR imaging.

Utilizing MRI in the context of experimental SCI gives us the opportunity to non-destructively analyze the extent of the lesion size and features, as well as allowing a single animal to be monitored serially through the time course of regeneration. In this study, MRI was used to provide further insight into the localization of the Col-Gen biomaterial within the spinal cord defect, as well as the extent of secondary damage and progression of tissue remodeling after injury.

7.2 Overall Goal, hypothesis, and rationale:

The **overall goal** of this chapter is to use MR imaging (using a 9.4T MRI) to localize the collagen-genipin hydrogel within the defect soon after injury (1 day) and monitor the remodeling of the

gel at 1 and 4 weeks. The MR results will be correlated to histology of the defect in order to make predictions about the composition of tissue in the defect. This study is meant to be a pilot experiment, showing the feasibility of using the MR imaging modality for analyzing the remodeling of the defect and biomaterial. Therefore, only a small number of samples were used in order to highlight important features (such as gel localization) and allow for comparison between different treatment groups.

The **hypotheses** of this chapter are

1. By setting the T2 parameters based on the signal of the collagen gel, the material can be identified against the contrast of the defect and viable tissue at 1 day post injury.
2. Using the gel based parameters and a surface coil, the MR images of the injury site (edema, hemorrhage, degeneration) will have sufficient contrast and resolution to be correlated to the histopathological features of the injury.
3. Changes in tissue architecture and density will be reflected in the MR imaging at later time points.

7.3 Methods:

7.3.1 Experimental groups:

1-day post injury:

Collagen-genipin gel (3mg/ml col 1 mM gen), n=1

1-week post injury:

Control, n=1

Collagen-genipin gel (3mg/ml col 1 mM gen), n=1

4 weeks post injury:

Control, n=1

Collagen-genipin gel (3mg/ml col 1 mM gen), n=1

Collagen-genipin gel (3mg/ml col 1 mM gen) + LMT-FGF-2, n=1

7.3.2: Surgical procedures: The procedures used in this study were identical to the procedures in chapter 6. Animals used for the MRI study, were also a part of the histomorphologic and functional assessments of chapter 6.

7.3.3 MRI acquisition: Animals were sacrificed after 1 day, 1 week, or 4 weeks by transcardial perfusion as described in chapter 6 (to account for the fragility of the tissue soon after injury, the 1 day sample was perfused with 200 ml of PFA and post-fixed for 5 days at 4°C). The spinal column was

removed and trimmed of the ribs and surrounding musculature leaving the spinal column and fascia intact. The samples were immersed in fomblin oil prior to imaging to increase image contrast. MR imaging was performed at the Beth Israel Deaconess Medical Center preclinical MRI core facility using a Bruker Biospec 9.4T magnet with 20 cm bore horizontal magnet.

Imaging parameters: Sequence: 3D Rare, TR: 3000ms, TE: 80 ms, Matrix 192 x192x 192, FOV 1.3x 1.3 x 1.3 cm, Isotropic voxel 68 μm^3. T2 weighted images were employed in this study to provide good contrast for the features of interest within the defect. The imaging parameters chosen were based on a Col-Gen gel sample alone such that the gel would appear brighter than the gray matter. In general, for T2 weighted images, water (edema, cerebral spinal fluid) appears bright, and hemosiderin (blood) or proton dense tissues: fat (myelin in white matter) and fibrous scar tissue (scar) appear dark.

The RAW data files were reconstructed into a 3D volumetric reconstruction of the spinal cord using OsiriX DICOM viewer version 5.6 (Pixmeo, Switzerland). The volumetric image was then cropped to the correct plane corresponding to the histology sections as determined by the shape and size of the defect and adjacent gray matter.

7.3.4 Histology and immunohistochemistry (IHC): Prior to tissue processing, the spinal cord tissue was carefully and completely removed from the surrounding vertebra using bone rongeurs, surgical scissors, and a scalpel. The spinal cord parenchyma was embedded in paraffin using a tissue processor (HypercenterXP, Tissue Processor, ThermoShandon, Houston, TX). Serial longitudinal sections of the defect were cut at 6 μm with a microtome and mounted on glass slides.

Adjacent tissue sections were stained with Masson's trichrome for general observation of the cellular and extracellular matrix features of the defect, particularly the presence of collagenous tissue within the defect. For IHC labeling of macrophages, a mouse antibody against CD68 was used (AbD serotec MCA341RA). A labeled polymer HRP system (AEC+ system, Dako) was used to detect the presence of the CD68 antibody.

7.4 Results analysis of the defect:

7.4.1 One-day post injury: Col-Gen gel

Ventral aspect (bottom): The ventral aspect of the spinal cord defect (before the presence of gray matter) appeared as a defect comprising half the width of the spinal cord with a jagged border. There was a thin light border around the defect, which was presumably edematous. The inside of the defect was gray

with a few pockets of black. Histology of the bottom of the spinal cord revealed that the defect contained collage gel mostly mixed with blood **Figure 7-1**.

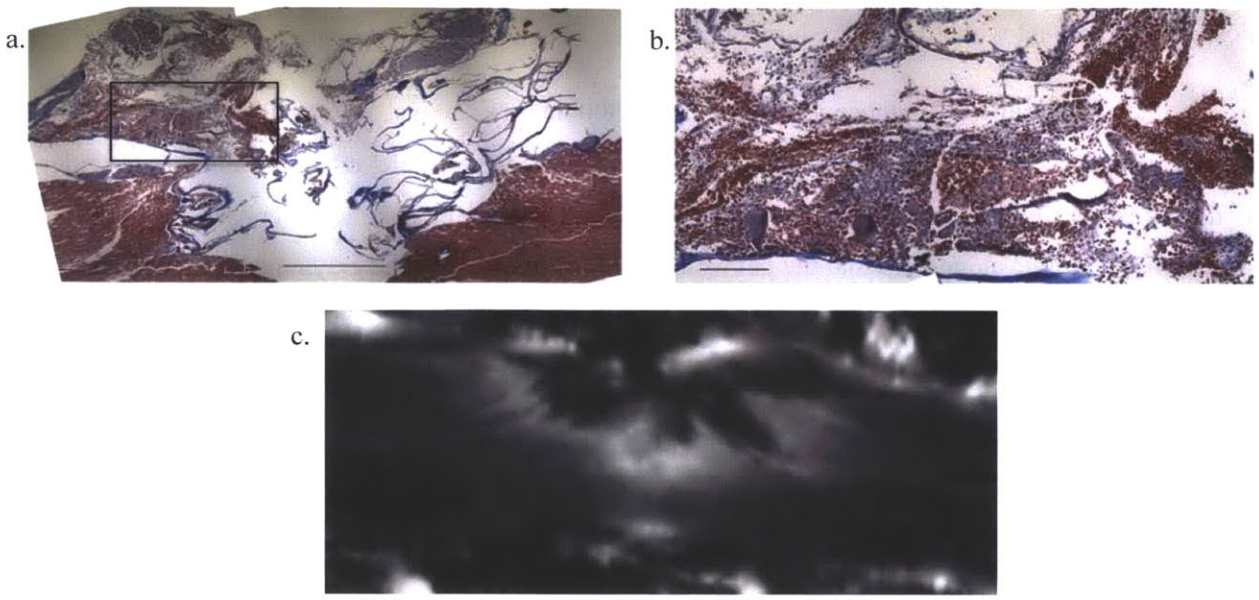

Figure 7-1: Bottom (ventral aspect) of the defect one-day after injury and implantation with a Col-Gen gel. **a.)** Masson's trichrome stained section showing the defect and its contents (pushed out during the sectioning and mounting process), which included gel (light blue) mixed with blood (red). Scale bar 1000 μm **b.)** Higher magnification image of the defect contents. Scale bar 200 μm **c.)** MR image corresponding to the histological section showing the hemi-resection injury. The gel-blood mix appears dark gray within the center of the defect. Areas of mostly blood appear black.

Mid level: One of the most prominent features of the middle of the spinal cord was the highly edematous (bright on MRI and spacious on histology) white matter on the contralateral spared side of the spinal cord immediately adjacent to the defect **Figure 7-2**. The center of the defect has multiple dark areas containing blood, as well as brighter areas indicative of gel not mixed with blood. Un-mixed gel could be found bound to the spared tissue and at the lateral border of the defect both in histology and observed on MRI (hyper intense areas within the defect)

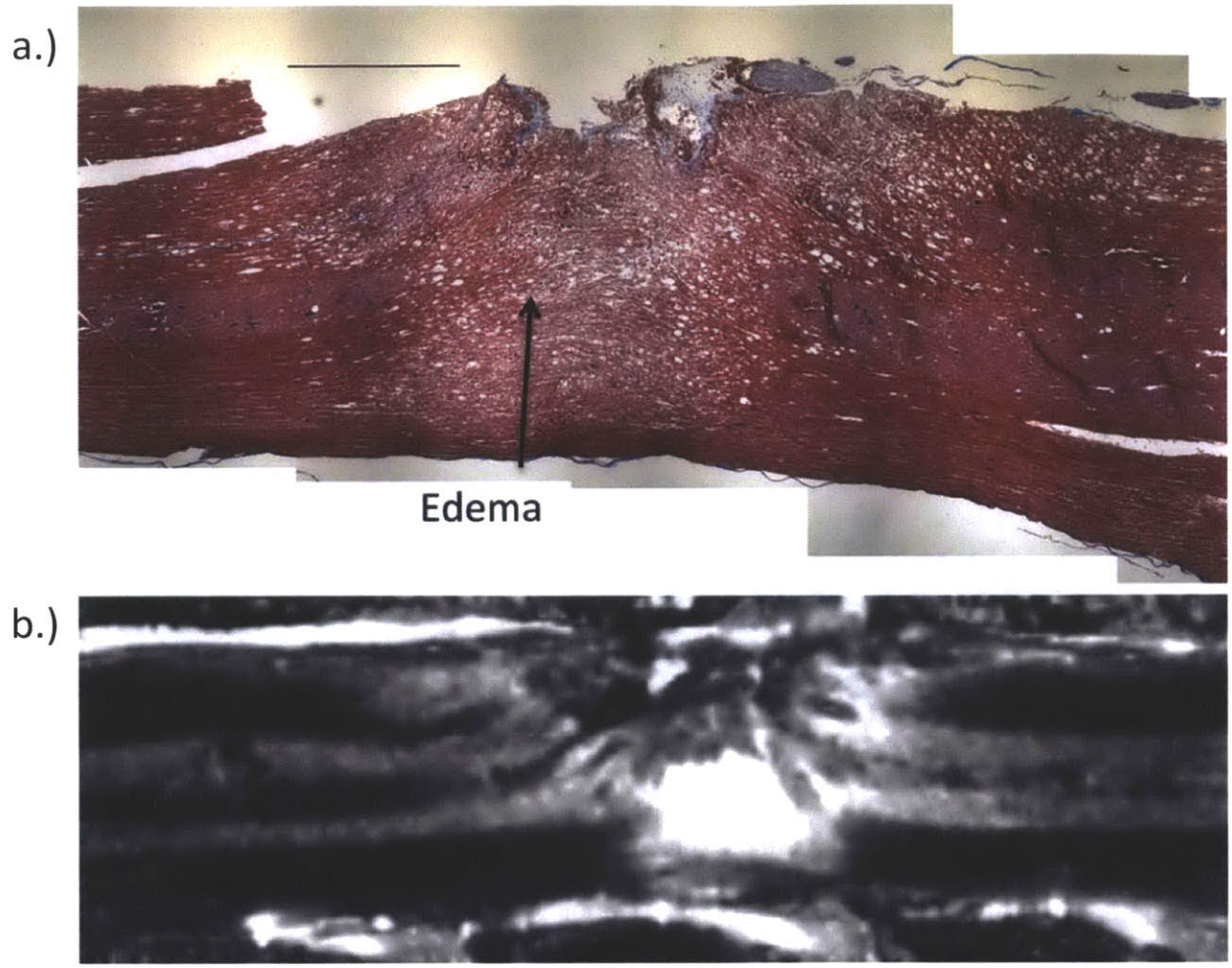

Figure 7-2: Mid level of the defect one-day after injury and implantation with a Col-Gen gel. **a.)** Masson's trichrome stained section exhibiting extensive swelling of the tissue contralateral to the defect. A portion of Col-Gen gel (light blue) can also be seen within the defect, bonded to the edge of the viable tissue and contains pockets of blood (red) **b.)** MR image corresponding to the histological section showing the hemi-resection injury. The area of swelling can be seen as a bright region. Varying contrast intensities can be seen within the defect corresponding to gel and blood. Scale bar 1000 μm

Dorsal aspect (upper): Hemorrhagic areas of white and gray matter were noticeable immediately adjacent to and extending several mm away from the center of the defect **Figure 7-3**. Many of the same features of the mid level of the spinal cord were also apparent at this level. As compared to the mid-level sections, there was a smaller amount of edema in the spared white matter adjacent to the injury and more gel could be found at the lateral border of the defect, in addition to small pockets directly in contact with the spared tissue. The center of the defect was difficult to preserve but showed areas of light and dark gray on MRI, which indicates a mixture of gel and blood.

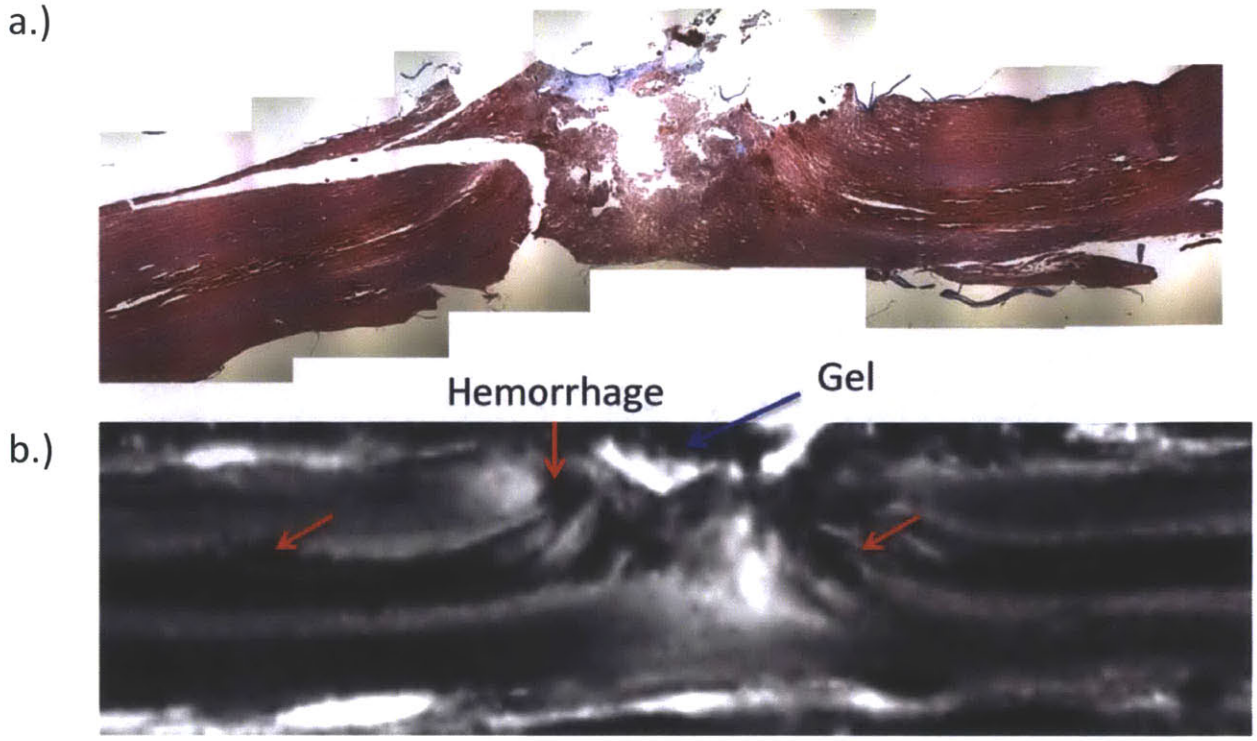

Figure 7-3: Top level (dorsal aspect) of the defect one-day after injury and implantation with a Col-Gen gel. **a.)** Masson's trichrome stained section displaying swelling of the tissue contralateral to the defect. A strip of Col-Gen gel (light blue) is noticeable on the lateral border of the defect. Extensive hemorrhage can be observed in the white and gray matter outside of the defect **b.)** MR image corresponding to the histological section showing the hemi-resection injury. Darker areas in caudal and rostral to the defect in the gray and white matter correspond to hemorrhage. A moderate area of swelling can be seen as a bright region right below the injury. A portion of Col-Gen gel not mixed with blood is observed as a bright band on the lateral border of the defect..

7.4.2 One-week post injury: Control and Col-Gen gel

By 1 week the middle of the defect in both control and Col-Gen treated groups were highly populated by cells and contained a substantial edematous tissue matrix seen as a bright region on MRI **Figure 7-4**. Areas of secondary damage were clearly visible and could encompass up to the entire width of the cord at the level of the defect. Macrophage density is highest at the borders of the defect. Very little remaining gel could be found in the Col-Gen treated animal and it was not possible to distinguish it from the surrounding tissue at this time-point. Darker areas within the defect most likely corresponded to residual blood clots or dense endogenous tissue formation.

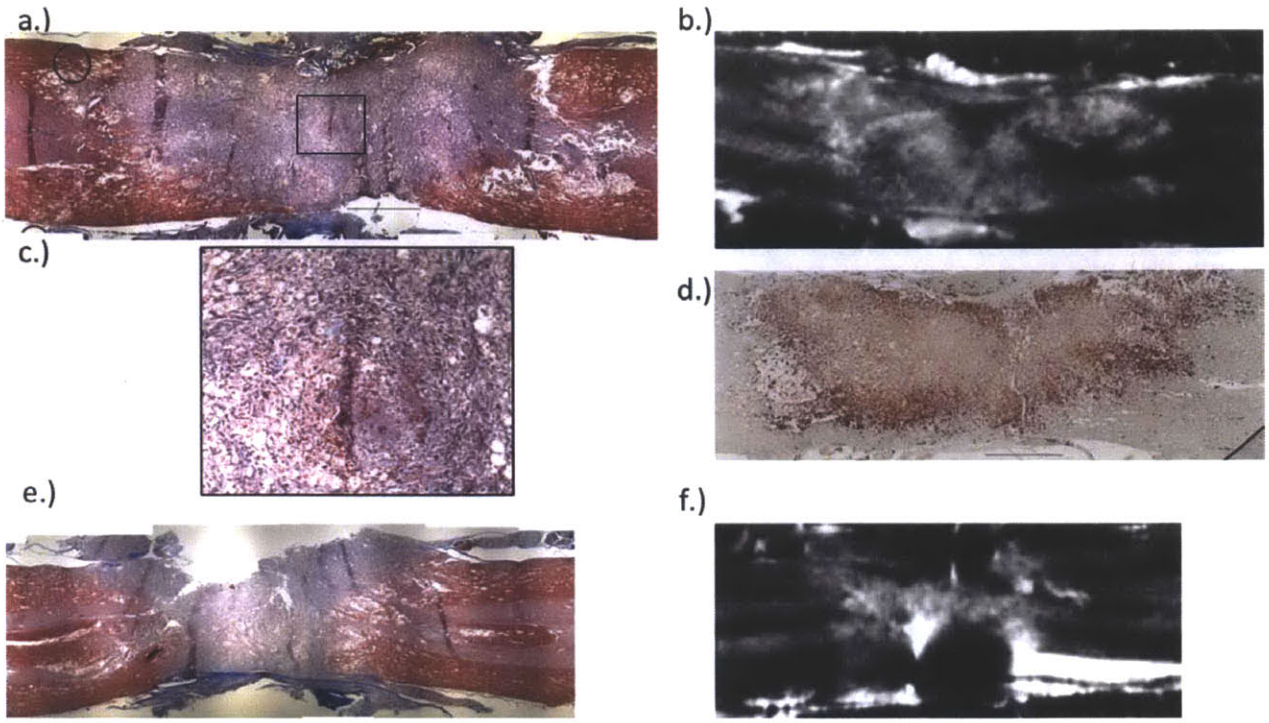

Figure 7-4: a.) Masson's trichrome stained section middle of the defect one-week after injury for a Col-Gen treated animal. **b.)** Corresponding MRI image to a **c.)** Inset of the center of the defect in a. **d.)** CD68 staining of the defect of a Col-Gen treated animal at 1 week post injury. **e.)** Masson's trichrome stained section middle of the defect one-week after injury for a control animal. **f.)** Corresponding MRI image to e. Extensive cellular infiltration can be seen in both control and Col-Gen treated defects. The areas of cellular infiltration are mostly hyper-intense on MRI indicating it is loose/edematous in nature. The black area on the bottom center part of f.) is most likely due to fomblin oil seeping into the tissue. Scale bar 1000 μm.

The dorsal aspect of both control and Col-Gen animals exhibited extensive connective tissue infiltration and collagen deposition as well as destruction of the dorsal column white matter (**Figures 7-5, 7-6**). The density of collagen produced by infiltrating cells appeared to be greater in the control animal as compared to the Col-Gen animal. A portion of the fascia overlying the defect could also be seen within the defect of the Col-Gen animal **Figure 7-5**.

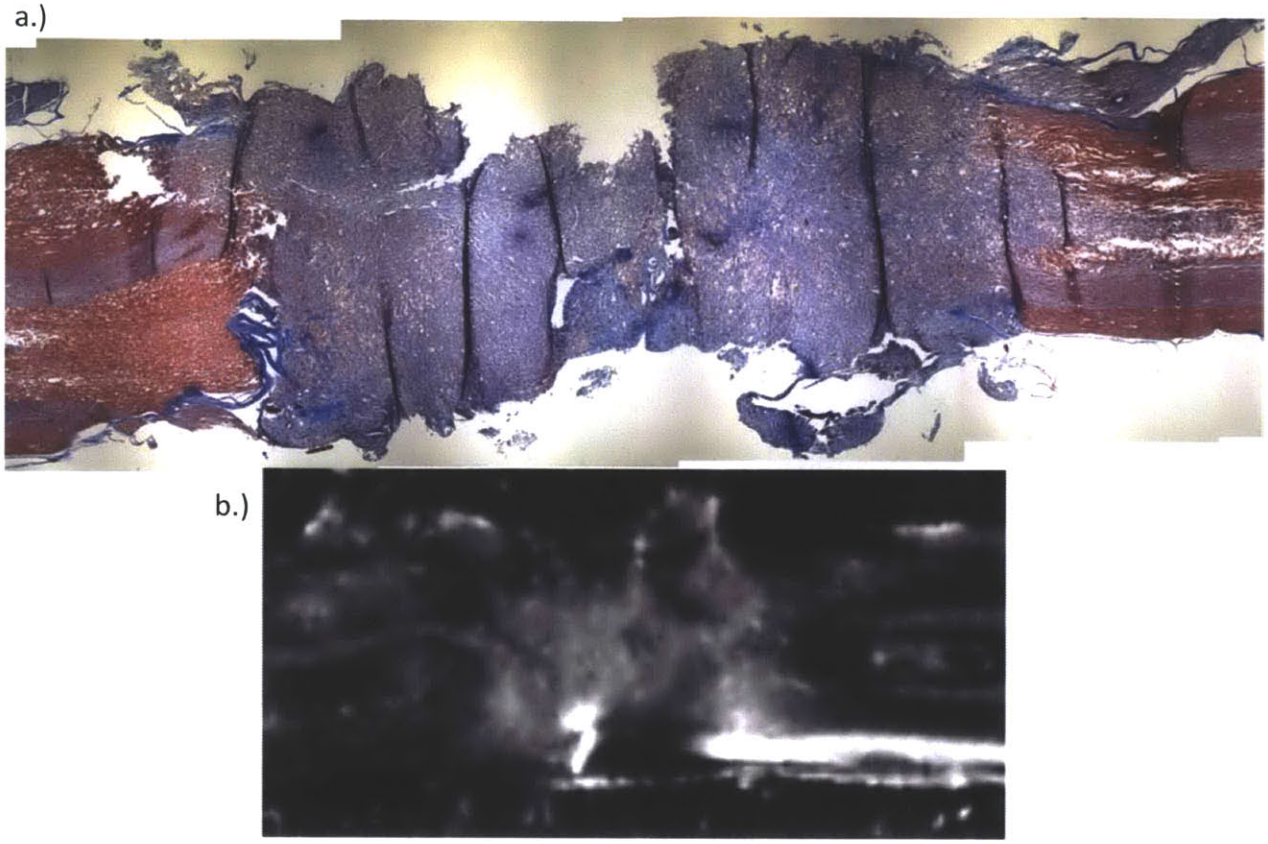

Figure 7-5: Dorsal aspect of the defect area at one week for the Col-Gen treated animal **a.)** Masson's trichrome stained section showing the extensive connective tissue infiltration of the entire width of the defect, destruction of the dorsal column white matter, and overlying muscle fascia within the defect. **b.)** MRI section corresponding to the image in a. regions of connective tissue infiltration and dorsal column destruction appear bright. Pockets of back within the defect correspond to blood. **c.)** Transverse section through the center of the defect showing the region of muscle fascia (bright spot on top right) which fell into the defect.

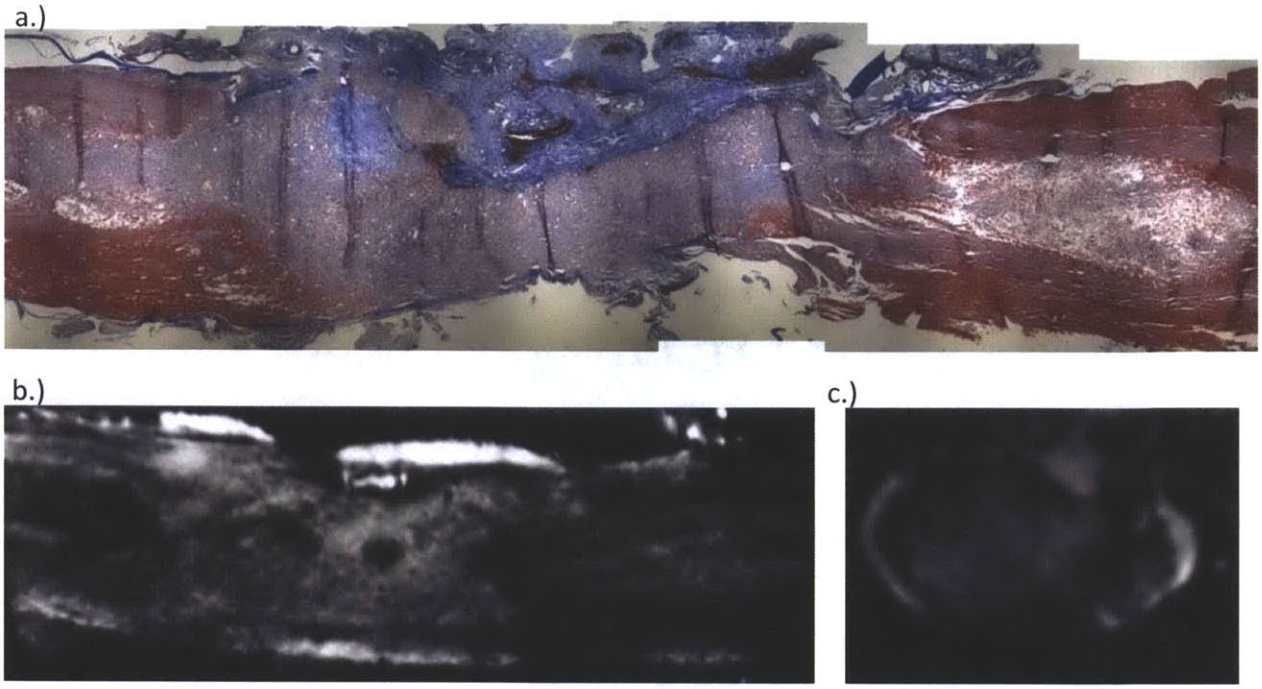

Figure 7-6: Dorsal aspect of the defect area at one week for the control animal **a.)** Masson's trichrome stained section showing the extensive connective tissue infiltration of the entire width of the defect and destruction of the dorsal column white matter,. **b.)** MRI section corresponding to the image in a. regions of connective tissue infiltration and dorsal column destruction appear bright. Pockets of back within the defect correspond to blood.

7.4.3 Four-weeks post injury: Control, Col-Gen, and Col-Gen LMT FGF-2 gel

By four-weeks post injury, MRI provides excellent contrast between the viable white and gray matter, areas of secondary damage, and fibrous connective tissue regions of the defect for control **Figure 7-7**, Col-Gen **Figure 7-8**, and Col-Gen LMT FGF-2 **Figure 7-9** animals. The three animals in this study are also illustrative of the three major responses to injury found at 4 weeks as described in chapter 6.

In general, dark regions within the defect correspond to denser connective tissue, medium contrast areas correspond to granular loose connective tissue, and bright areas correspond to areas of edema/increased macrophage infiltration. In all samples, there was a noticeable atrophy of the white matter close to the injury (mostly on the defect side) and a resulting curvature of the spinal cord towards the side of the defect (indicated by bright CSF area contralateral to the defect).

The Col-Gen LMT FGF-2 sample exhibited significant secondary damage after the original SCI **Figure 7-9**. A comparison of MRI and histological sections for this animal demonstrates the advantage of using *in situ* MRI for assessment of the defect and secondary damage as compared to histological sections,

which are prone to tearing in areas of very soft tissue such as macrophage filled cavities. Serial transverse sections through the defect **Figure 7-10** best illustrate the full extent of secondary damage in this animal.

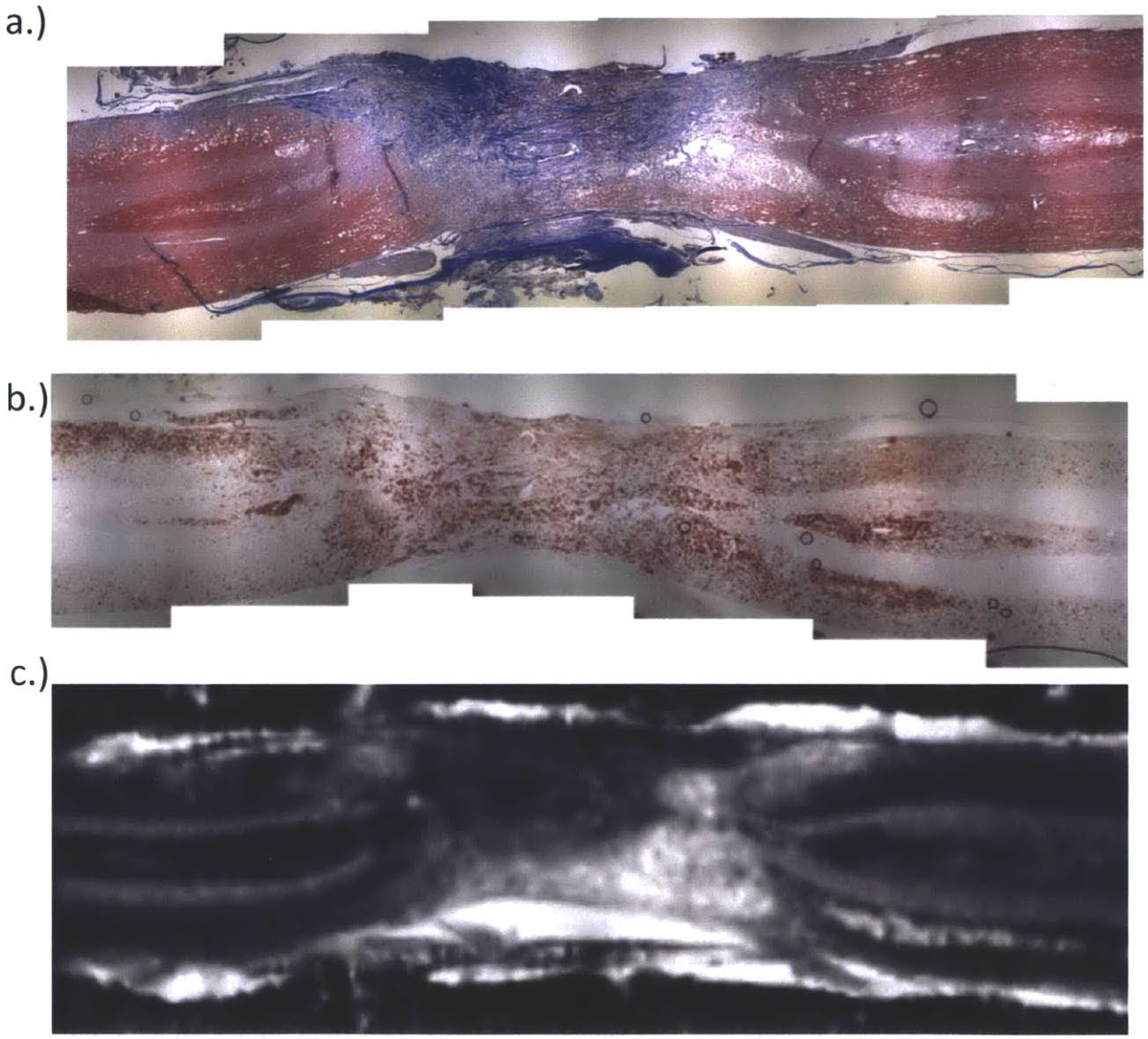

Figure 7-7: Upper-mid defect images of a control animal four-weeks post injury exhibiting a type C response to injury. **a.)** Masson's trichrome stained section **b.)** CD-68 IHC section **c.)** MRI section. Dense collagenous scar tissue appear black on MRI, regions of cellular infiltration with a less dense matrix appear gray, and edematous regions corresponding to the cavitary areas of dense macrophage infiltration which appear bright on MRI. Areas of secondary damage with dense macrophage staining can be seen spreading into the white matter.

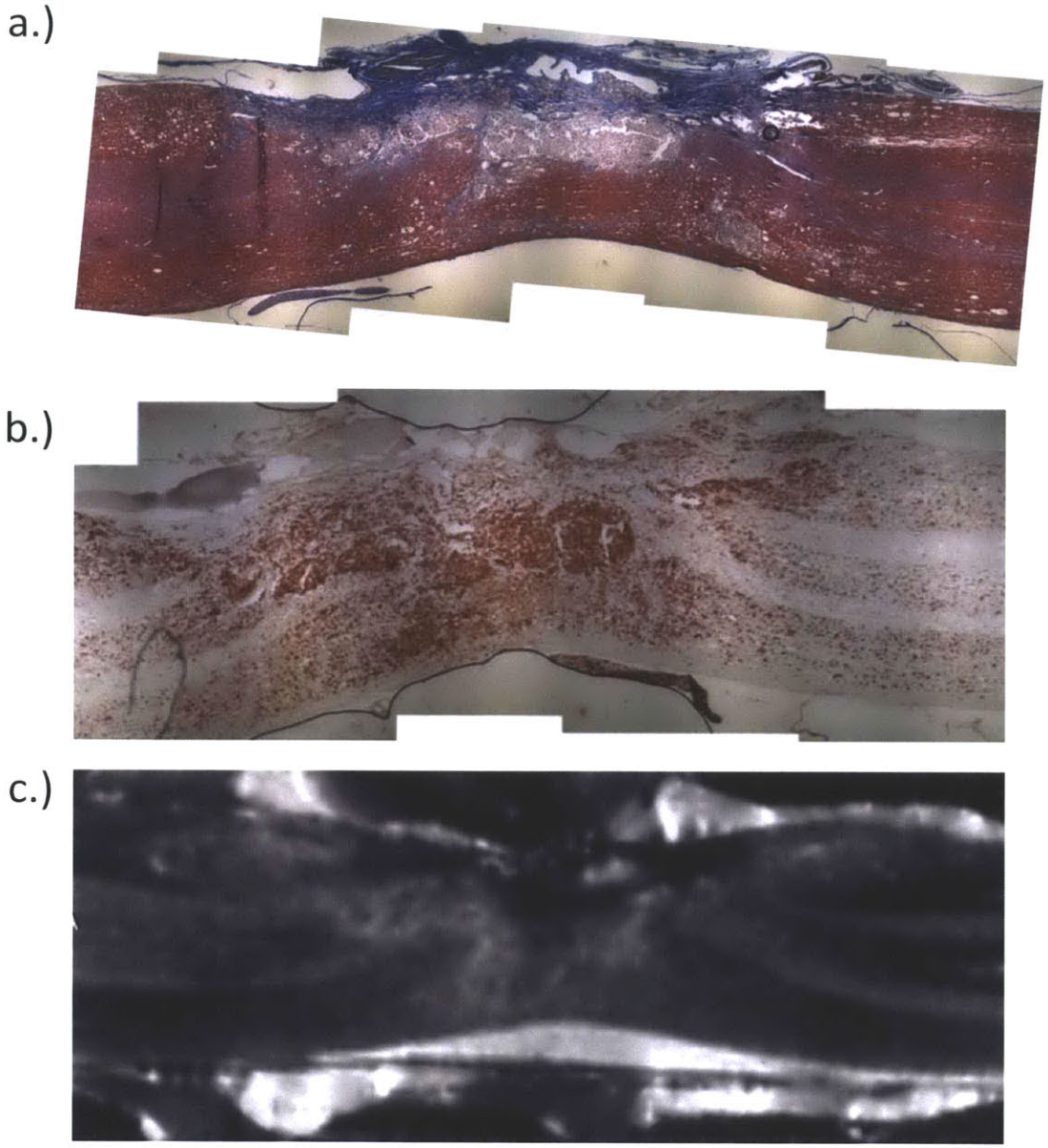

Figure 7-8: Mid defect images of a Col-Gen treated animal four-weeks post injury, exhibiting a type A response. **a.)** Masson's trichrome stained section **b.)** CD-68 IHC section **c.)** MRI section. Dense collagenous scar tissue (blue on trichrome) on the lateral border of the defect appears black on MRI, regions of cellular infiltration with a less dense matrix appear gray, and edematous regions corresponding to the cavitary areas of dense macrophage infiltration within the defect appear brighter than the gray matter on MRI.

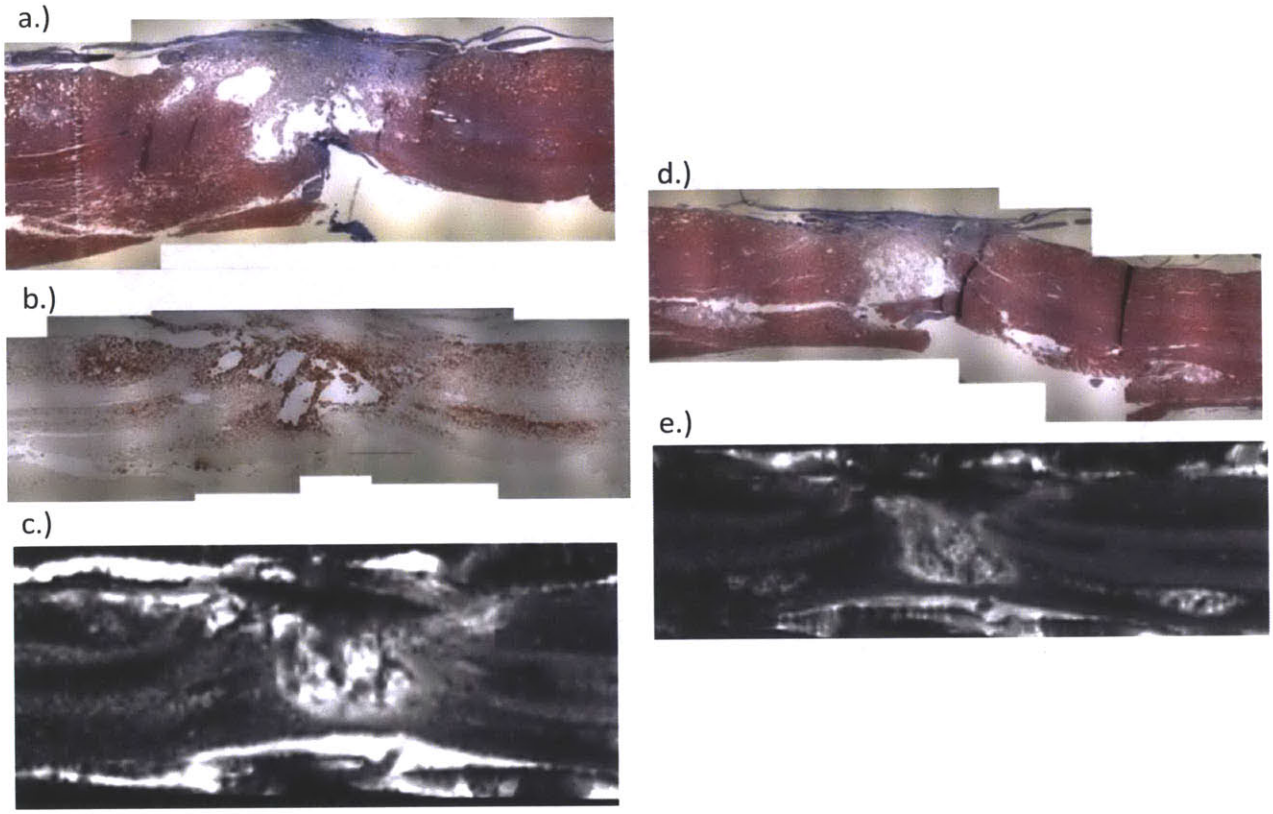

Figure 7-9: Mid defect images of a Col-Gen LMT FGF-2 treated animal four-weeks post injury, exhibiting a type B response. **a.)** Masson's trichrome stained section corresponding to the upper middle plane of the defect **b.)** CD68 stained section showing macrophage infiltration of the defect corresponding to the plane of section in a.) **c.)** MR image of the planes in b.) **d.)** Masson's trichrome stained section corresponding to the lower middle plane of the defect. **e.)** MR image of the planes in d.) A thin band of fibrous tissue is noted on the lateral border of the defect (blue a,d black c,e). Cavitary fluid filled regions are noted by the bright areas of MRI contrast.

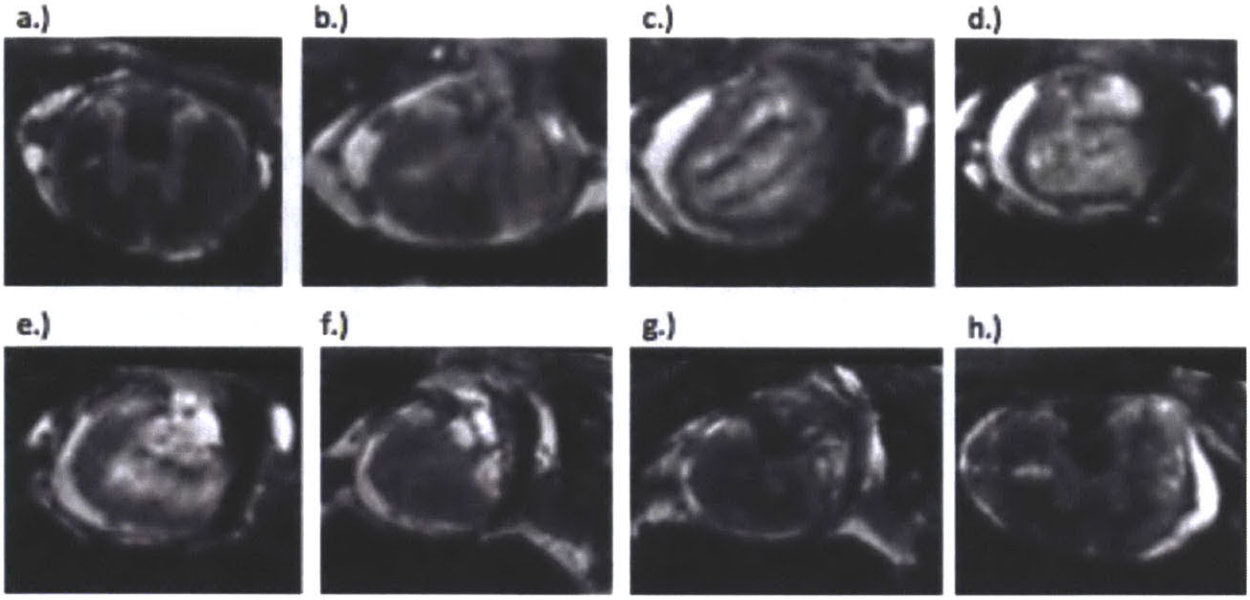

Figure 7-10: Serial transverse sections through the defect of Col-Gen LMT FGF-2 treated animal at 4 weeks going a.) caudal through h.) rostral to the defect. Extensive secondary damage can be seen in c-e. There is a band of fibrous tissue (dark) localized to the lateral border of the defect. Extra CSF on the left side of the image in c-e reflect the curvature of the spinal cord towards the defect side. Atrophy of the cord tissue on the caudal end of the lesion is noted by the extra CSF on the right (defect) side of the cord.

7.5 Discussion:

MRI of the hemi-resection SCI provided valuable insight into the progression of injury and remodeling of the tissue within the defect.

7.5.1 Early extent of initial injury and gel localization: The collagen-genipin gel is capable of conforming to and filling the defect area and is adhered directly to the spinal cord tissue **Figure 7-2**. The MR images were able to capture several features of the injury, which could then be related back to the histology including areas of edema (hyper-intense) and hemorrhage (very hypo-intense). The area of edematous abnormal cord tissue adjacent to the defect (most evident on the contralateral side) helps us to better understand the increased size of the lesion noted in 1 and 4 week samples caused by secondary damage. Disruption of the cord tissue as a result of mechanical trauma results in areas of ischemia, disruption of the blood spinal cord barrier, and infiltration of inflammatory cells.[10, 11] If these events are severe enough, they will result in necrosis of the involved tissue. Likewise, it is possible that the swelling noted in **Figure 7-2** is transient and would have resolved without further injury resulting in the half-width Type A responses seen at 4 weeks.

Although the gel was injected into a clean (non-hemorrhagic) defect, the gel was not devoid of cells at 1 day due to mixing with blood in the post surgical period. The appearance of the gel in MRI varied depending on the amount of mixing with blood. Since blood appears dark in T2 weighted images due to hemoglobin, gel that was mixed with blood appeared gray **Figure 7-1**. Un-mixed gel (bright) was localized more towards the lateral and dorsal side of the spinal cord. Collagen-genipin gels reach their gelation point (G'=G") after approximately one minute at 37°C, however the gel structure is still very weak until about 15 minutes.[12] It is possible that the overlying musculature or severed large anterior artery and dorsal veins in the midline of the spinal cord had residual bleeding after hemostasis was achieved during the surgical procedure. Blood from these sources would then be able to pool at the bottom of the defect thus causing the newly formed gel at the bottom to mix or be pushed upwards and away from the midline. Continued bleeding from the surrounding back musculature (a source of bleeding during the surgical procedure) into the defect is another potential source of blood.

The mixing of gel with blood is not necessarily an unwanted event. Blood can create more pores and imperfections in the gel, which can facilitate cellular migration into the scaffold. The formation of a fibrin clot in the areas of hemorrhage and blood-gel mixing serves as an additional cell permissive scaffold. Finally, nucleated blood cells (leukocytes) contained within the gel, have the capability to release pro-regenerative growth factors.[13]

The limitations of the histology at one day prevent us from preserving most of the loose tissue contained within the defect. Histological processing of samples at such an early time point presents many unique challenges. The process of detaching the overlying fascia and removing the spinal cord from the vertebra may result in a loss of some defect tissue, predominantly from the lateral border and dorsal aspect. This was mitigated as much as possible with substantial post fixation in 4% PFA and careful dissection technique. Paraffin processing of the tissue also results in shrinking of the spinal cord tissue and the collagen gel due to the dehydration steps and high temperatures. Finally, sectioning the tissue may result in rips and tears, which affects the very fragile clot/gel portions within the defect more than the spinal cord tissue. Despite all of these factors, it was still possible to obtain histological images for comparison with the MRI data. In histology, the gel had many appearances including a light blue amorphous area for unmixed gel which was fully preserved during processing, light blue fibrillar structures highly mixed with red blood cells for the gel-blood mix, and finally dense blue ribbon like structures which border empty areas for gel that severely shrunk during processing **Figures 7-1, 7-2, 7-3**.

7.5.2: Secondary damage and cellular infiltration at one week post injury

At one-week, MRI of the defect shows a hypo-intense center surrounded by areas of hyper-intensity, which spread into the surrounding spinal cord parenchyma **Figure 7-4b,f**. The areas of hyper-intensity can be attributed to edema from inflammatory events causing secondary damage to the spinal cord tissue adjacent to the defect. Within these regions, there is also substantial infiltration of elongated connective tissue cells, which are secreting a collagenous matrix. It is unclear if the hypo-intensity within the core of the defect is due to an increased density of tissue formation or the collection residual red blood cells. Interestingly, this area of the defect has a lower density of macrophage staining **Figure 7-4d** indicating something (either clot or fibrous tissue) is impeding their entry.

The control animal provided a good example of how the area of edema noted at one day in **Figure 7-2** can lead to an area of secondary damage **Figure 7-4e**. Unfortunately, in this sample there were unexplained areas of hypo-intensity on the MR images, such as the circular region at the bottom of **Figure 7-4f** where there is an abrupt cutoff in the CSF signal. One likely cause of this stems from the removal of the bone and some fascia close to the defect prior to imaging in this sample, which could have allowed fomblin oil to seep into the defect. Since the sample is immersed in fomblin oil prior to imaging in order to remove contrasting interference from air or water surrounding a sample, the presence of oil within the sample could have led to the observed results.

Towards the upper parts of the defect **Figures 7-5, 7-6**, it was also possible to distinguish the inflammatory/fibrotic infiltrate of the dorsal columns stemming from the hemorrhage noted earlier in the 1 day samples, as well as budging of the overlying fascia into the defect. The remarkable degree of elongated fibroblast-like cells and fibrous tissue formation across the entire top of the defect in both control and Col-Gen treated animals suggests these cells are entering the defect from the overlying connective tissue and back musculature and are not impeded in doing so by the autologous fascia draped over the defect after surgery. It is also possible that the sections are being taken through a portion of the fascia, which was pressed into the defect during paraffin processing. However, the appearance of a majority of the tissue is largely unorganized and unlike the architecture of the original fascia.

7.5.3: Remodeling of the defect by four weeks post injury

The animals examined at four-weeks post injury exhibited the three main responses to injury described in chapter 6, Type A: half width defect **Figure 7-8**, Type B: greater than half width defect **Figure 7-9**, Type C: full width defect **Figure 7-7**. The MRI modality used in this study was able to effectively discriminate between the types of tissue present in the defect at this time-point for each type of injury response. Unlike earlier time-points, there was very little or no blood remaining in the defect so the hypo-intense dark regions corresponded well to the presence of dense collagenous tissue. There was a

good correlation between the hyper-intense areas of the MR images and the cavitary macrophage filled areas within the defect as well as areas of secondary damage to the surrounding gray and white matter. The moderate intensity signal on MRI (gray) within the defect corresponded to cellular infiltration and loose matrix formation.

In all samples, there was a noticeable atrophy of the white matter close to the injury (mostly on the defect side) and a resulting curvature of the spinal cord towards the side of the defect (indicated by bright CSF area contralateral to the defect). It is possible that the scar tissue that forms towards the lateral border of the defect is pulling the cord towards the wall of the spinal canal.

One of the most compelling reasons to add *in situ* MR imaging for assessment of the defect and secondary damage after spinal cord injury is highlighted in **Figures 7-9,7-10**. A comparison of MRI and histological sections for this animal demonstrate the amount of information about the shape of the cavity and degree of tissue sparing, which was lost due to tearing and disruption of the section in areas of very soft tissue such as the macrophage filled cavities. Transverse sections through the defect **Figure 7-10** best illustrate the heterogeneous nature of the secondary damage in this animal.

Overall, the implications of the high correlation between histology-MRI mean that both degenerative and regenerative changes in the spinal cord parenchyma after injury can be determined *in situ* using MR imaging.

7.6 References:

[1] Lammertse D, Dungan D, Dreisbach J, Falci S, Flanders A, Marino R, et al. Neuroimaging in traumatic spinal cord injury: an evidence-based review for clinical practice and research. J Spinal Cord Med. 2007;30:205-14.
[2] Narayana PA, Grill RJ, Chacko T, Vang R. Endogenous recovery of injured spinal cord: longitudinal in vivo magnetic resonance imaging. J Neurosci Res. 2004;78:749-59.
[3] Schwartz ED, Hackney DB. Diffusion-weighted MRI and the evaluation of spinal cord axonal integrity following injury and treatment. Exp Neurol. 2003;184:570-89.
[4] Sundberg LM, Herrera JJ, Narayana PA. In vivo longitudinal MRI and behavioral studies in experimental spinal cord injury. J Neurotrauma. 2010;27:1753-67.
[5] Mihai G, Nout YS, Tovar CA, Miller BA, Schmalbrock P, Bresnahan JC, et al. Longitudinal comparison of two severities of unilateral cervical spinal cord injury using magnetic resonance imaging in rats. J Neurotrauma. 2008;25:1-18.
[6] Sandner B, Pillai DR, Heidemann RM, Schuierer G, Mueller MF, Bogdahn U, et al. In vivo high-resolution imaging of the injured rat spinal cord using a 3.0T clinical MR scanner. J Magn Reson Imaging. 2009;29:725-30.
[7] Weber T, Vroemen M, Behr V, Neuberger T, Jakob P, Haase A, et al. In vivo high-resolution MR imaging of neuropathologic changes in the injured rat spinal cord. AJNR Am J Neuroradiol. 2006;27:598-604.
[8] Iannotti C, Li H, Stemmler M, Perman WH, Xu XM. Identification of regenerative tissue cables using in vivo MRI after spinal cord hemisection and schwann cell bridging transplantation. J Neurotrauma. 2002;19:1543-54.
[9] Austin JW, Kang CE, Baumann MD, DiDiodato L, Satkunendrarajah K, Wilson JR, et al. The effects of intrathecal injection of a hyaluronan-based hydrogel on inflammation, scarring and neurobehavioural outcomes in a rat model of severe spinal cord injury associated with arachnoiditis. Biomaterials. 2012;33:4555-64.
[10] Hagg T, Oudega M. Degenerative and spontaneous regenerative processes after spinal cord injury. J Neurotrauma. 2006;23:264-80.
[11] Mautes AE, Weinzierl MR, Donovan F, Noble LJ. Vascular events after spinal cord injury: contribution to secondary pathogenesis. Physical therapy. 2000;80:673-87.
[12] Macaya D, Ng KK, Spector M. Injectable Collagen-Genipin Gel for the Treatment of Spinal Cord Injury: In Vitro Studies. Adv Funct Mater. 2011;21:4788-97.
[13] Trivedi A, Olivas AD, Noble-Haeusslein LJ. Inflammation and Spinal Cord Injury: Infiltrating Leukocytes as Determinants of Injury and Repair Processes. Clinical neuroscience research. 2006;6:283-92.

Chapter 8:
Conclusions

As a whole, this thesis follows the development of an injectable gel for the treatment of spinal cord injury from materials characterization, through *in vitro* assessment of cell-biomaterial interactions, and finally *in vivo* examination in a rodent hemi-resection model of SCI.

Materials characterization:

The reaction kinetics of collagen gels with the cross-linking plant-based extract genipin was characterized using absorbance and fluorescence measurements as well as rheological testing and degradation assays. Collagen cross-linked with genipin formed robust gels and were resistant to enzymatic degradation, and had tunable gelation and mechanical properties. The pH and ionic strength of the gel was also found to influence its shear modulus and gel time. The addition of LMTs (a secondary drug release vehicle) at 0.1 mg/ml did not impair the gelation properties or stiffness of the material.

Of importance is that *in vitro*, collagen solutions were capable of undergoing gelation and cross-linking when injected directly to a liquid medium. The same gels were also able of encapsulating cells for up to 10 days while maintaining cell viability. Genipin diffusion out of the gel into the medium was slow enough that a significant amount of genipin was retained to cross-link the gel, suggesting that when collagen-genipin gels are injected into tissue, enough genipin will remain within the gelling solution to provide substantial cross-linking *in vivo*. From the viability studies, there was a linear relationship between the effective concentration of genipin cells were exposed in the assay and their viability. These results suggest that 0.25-0.5 mM is an appropriate genipin concentration to use for a scaffold delivering cells cells while 1 mM can be an applicable concentration for a scaffold forming *in situ*, which is in contact with a relatively large volume of cells and tissue compared to the volume of the gel.

In vitro astrocyte infiltration studies:

Collagen gels alone and those covalently cross-linked with genipin, are permissive of astrocyte infiltration. FGF-2 incorporated directly into the gels, or released by LMTs added to the gels, enhances astrocyte infiltration into the gel and causes them move in a chain-like pattern. Cells can be found at distances up to 2mm into select gels after 10 days, which has relevance to the clinical application in which the gel is injected into astrocyte-surrounded defects up to 4mm in diameter. While exposure of astrocytes to genipin, at concentrations up to 0.5 mM does not affect cell viability, it does impair the ability of astrocytes to migrate. This genipin-induced impairment of astrocyte migration can, however, be offset by the incorporation of FGF-2 directly into the collagen-genipin gel or in LMT's incorporated into the gels. The results of this study paved the way for the *in vivo* evaluation of the effects of Col-Gen hydrogels incorporating FGF-2 on the astrocyte infiltration of the gel-filled SCI defect

In vivo rodent SCI:

The wound healing response to a hemi-resection SCI in rodents resulted in substantial early connective tissue and inflammatory cell infiltration into the defect which resolved into varying degrees of dense connective scar tissue, loose granular tissue, and cystic macrophage filled tissue. Interestingly, the actual surgery and amount of bleeding in the peri-operative period appeared to have substantial effects on the degree of tissue sparing and functional recovery of the animals regardless of the applied therapy.

The pilot animal studies using gels selected based on the *in vitro* astrocyte migration experiments demonstrated that implantation of the gel was well tolerated by the animals. However, the formulations of the gels were determined to be either too fragile or invoke too aggressive of a fibrotic tissue response (in the case of the first generation FGF-2 containing gels). Therefore, the second more complete animal study utilized a more robust collagen gel (50% more protein, 100% higher genipin concentration) with a 50 fold lower concentration of FGF-2.

The results of the second animal study suggested that regardless of treatment group (control injury, gel alone, or gel with FGF-2), regenerating axons could be found within the defect site on tissue bridges staining positive for laminin and consisted of astrocytes, blood vessels, and fibroblast-like cells. Importantly, the high concentration of genipin (1 mM) did not appear to elicit any adverse effects on the spinal cord tissue. Interestingly, there seemed to be a niche for astrocyte, axon, and endothelial cell ingrowth directly adjacent to the parallel oriented fibrous scar, which formed on the lateral border of the defect in some animals. The addition of LMTs loaded with FGF-2 increased the number of endothelial cells, astrocytes, and laminin, within the defect over control and Col-Gen treatment groups. The tissue formed within the defect therefore has a greater potential for future axonal regeneration. The FGF-2 containing group also increased contralateral tissue sparing with trends towards a lower defect size, a greater percentage of contralateral gray and white matter, more animals exhibiting a type A response to injury. There was also a trend towards increased functional recovery with these animals.

MRI is a suitable modality to non-destructively observe the features of the injury *in situ* at a reasonable resolution (68 μm) including defect volume, hemorrhage, edema, gel localization, and other morphologic parameters. MRI was able to successfully distinguish the different tissue components (*i e.* dense fibrous, granular, and cystic/edemedous/macrophage infiltrated tissue) within the defect and areas of secondary damage at a high correlation to histology. At one day post injury, pure Col-Gen gel could be distinguished from fluid/tissue within the defect, however mixing of the gel with blood altered its signal significantly, making it difficult to distinguish from other tissues within the defect seen at later time-

points. Additionally, MRI provided insight into the shape of the defect and spared tissue in cases were the histological processing disrupted or altered sections.

Chapter 9:
Limitations and Future Directions

I. Limitations:

The work presented in this thesis provides a comprehensive exploration of the materials characterization, *in vitro,* and *in vivo* development of an injectable gel for the treatment of spinal cord injury. Despite the extensiveness of the assays performed, there were several limitations to the studies conducted.

Materials characterization:

- Gels formed *in situ* on the rheometer could only be analyzed for a limited amount of time due to constraints on instrument availability. Therefore, *in situ* experiments were able to capture the initial period of gelation (<1 hr) but could not observe the saturation of genipin cross-linking, which occurs over days.
- For pre-formed gels tested on the rheometer, care was taken to best match the parameters of the machine (geometry height, shear speed, etc.) to yield consistent results with the data from the *in situ* tests, however variability in properties was introduced based on the degree of gel compression, contraction of the scaffolds due to cross-linking, degree of hydration, and potential slipping between the gel and machine geometry.
- Collagen-genipin gels were tested *in vitro* under ideal conditions (i.e. without the presence of blood and proteins), which would be found *in vivo*. The interaction of genipin with these amine rich components could affect the final properties of the gel.

***In vitro* cell assay:**

- Using the outgrowth assay, it was difficult to parse out the individual contributions of migration and proliferation to the observed response. It should be noted however that this limitation is less important in the context of this thesis since the overall goal was to increase the population of astrocytes within the graft.
- Outgrowth assay was an idealized version of growth into the injectable gel, which did not include other cell populations (i.e. leukocytes, endothelial cells, fibroblasts) that enter the defect site early on and may begin to remodel the gel and release a variety of growth factors/cytokines that could affect astrocyte behavior.
- The astrocyte study did not go into detail in determining why certain groups of cells exhibited a chain-like migration phenotype. The expression of cellular markers and release of growth factors was not fully explored since it is currently unclear which would be beneficial or detrimental to regeneration. Growth factor expression is also complicated by the relatively large mass of

astrocytes in the center of the assay, which may be producing different factors than the ones undergoing chain-migration.

- While FGF-2 exerts pro-migratory actions on astrocytes, its actions are more widespread and cause a variety of effects on many other cell types, which could be both pro- and anti-regenerative.

***In vivo* rodent experiments:**

- While the hemi-resection injury provides a clear standardized model for the growth of cells into the collagen-genipin gel contained within the defect, it is a large open injury, which exposes the cord to peripheral blood cells and is easily infiltrated by surrounding connective tissue resulting in scar formation. Therefore, a more ideal model for an injectable gel would be a closed defect (i.e. contusion model) contained within the dura. This type of model is also more clinically relevant to human spinal cord injury.
- The gel implantation procedure was not optimized with respect to injection time. The liquid gel was pipetted directly into the defect since the gel was filling a large volume and controlling the delivery time using an automatic syringe injector was cumbersome in surgery.
- Intraoperative and post operative bleeding into the defect from the surrounding muscle and bone caused variations in the secondary damage to the spinal cord and degree of fibrosis. If the blood continued to pool into the defect, it could impede the gelation of the collagen-genipin gel and also displace it laterally and dorsally.
- By 1 week post injury, the 2 mg/ml col + 0.5 mM gen gel as well as the more robust 3 mg/ml col + 1 mM gen gel were heavily infiltrated by cells and little original gel could be identified within the defect. This could have been due to an altered gelation effect (i.e. mixing with blood) leading to a weakened material, or the gels not being intrinsically strong enough to withstand the connective tissue infiltration induced by the present model. It would have been more ideal for the gels to persist for 2-3 weeks to prevent early filling of the defect site with fibroblasts and macrophages.
- Our analysis of the defect site was observed only up to 28 days post injury. While the defect is largely stable at this time, the tissue is still actively remodeling and the astrocyte-blood vessel network may continue to mature. Additionally, axon sprouting begins between 3 weeks and 3 months post injury so our data is only covering the beginning of this process.
- Histological processing of the tissue (in particular the gel and newly damaged tissue) was technically challenging, which sometimes led to an incomplete picture of the lesion or identification of the gel *in situ*.

- Quantification of the histological sections was performed on one section per stain per animal, in the middle of the defect. While this gives a good overall comparison between groups, a volumetric approach would be required for a more complete assessment of the cellular response to injury between groups.
- This study used an open field locomotor behavioral outcome metric to assess the functional recovery after injury. In general, these metrics are useful in grading recovery after injury but are limited in that they are non linear and do not take into account other important parameters of recovery such as sensation, pain, and bladder function.
- MRI of the spinal cords in this thesis were performed in an *ex vivo* fashion. In order to translate this work to live animals, techniques to account for artifacts due to respiration and blood flow will have to be used.

II. Future directions:

The work presented in this thesis lays the groundwork for further investigation of injectable gels for the treatment of spinal cord injury. The areas of future investigation flow from both the limitations and main findings of the current study:

Materials:

- Increase the gelation speed of collagen-genipin gels: lowering the ionic strength of the gel was touched upon in this thesis for this purpose, however there may be alternate ways. Follow up studies on the long-term mechanical properties and microstructure of low ionic strength gels should also be performed to ensure the properties are not significantly altered from prior gels.
- Alternate injectable hydrogel materials with tunable mechanical and gelation properties such as gelatin cross-linked with hydroxyphenylpropionic acid (HPA) can also be explored using the assays described in this thesis.

In vitro:

- The chain-like migration phenomena observed in astrocytes exposed to FGF-2 should be further investigated to determine how these cells are phenotypically different than the other astrocytes in the gel. This may include gene activation, protein synthesis, cell surface marker expression, ECM production, and growth factor secretion.
- Other stimulators of astrocyte outgrowth should be explored in the cell outgrowth assay described in this thesis. Examples include growth factors (HGF, TGF-a, EGF, TGF-b) or molecules (Ro3303544, a glycogen synthase kinase inhibitor), which show promise in their ability to promote astrocyte migration into the defect site. Such factors may encourage a targeted migratory effect on astrocytes, however caution should be taken since they may or may not have other widespread effects on inflammatory and connective tissue cells.
- Incorporating macrophages or fibroblasts into the encapsulating gel in the cellular outgrowth assay may be able to provide a better prediction of astrocyte growth into the gel *in vivo*.

In vivo:

- The experimental groups, which show promise at 28 days should be followed up at 2-3 months post injury to observe any maturation of the astrocyte-fibroblast-endothelial cell network and increased infiltration of the defect with axons.

- A more thoroughly investigate the fibroblast-like cells which seemed to promote axon regeneration within the defect should be conducted to determine what these cells are and why axons tended to grow along the tissue bridges formed by these cells.
- The collagen-genipin gels developed in this thesis should be tested in other models of SCI to determine their effectiveness in different contexts. For example, moving towards a contusion model would be more clinically relevant and more appropriate for an injectable therapy due to the closed contained nature of the injury. In this case, the injection procedure and gelation time must be optimized to reduce intraparenchymal pressure and ensure the gel remains in the defect. It is also plausible to utilize MRI to determine the area of cyst formation after SCI, aspirate out the contents of the cyst, and inject the gel to fill the defect.
- Since the optimum time for administering an injectable therapy for SCI may be slightly after the initial inflammatory response but before formation of the glial scar, future animal experiments may want to administer the gel in the subacute phase of SCI (7-14 days post injury)
- MR imaging can be used to follow individual animals, serially through the course of regeneration. The extent of the initial injury and zones of ischemia and hemorrhage can be identified and predictions can be made and tested about the evolution of the secondary injury. Understanding these factors will help us better comprehend and categorize the functional recovery of animals based on their individual injuries and help us best compare the regenerative response. It can also give us a sense of the neuroprotective effects of our therapies (limiting secondary damage).
- A more detailed histological-MR imaging comparison should be conducted to allow us to make an accurate prediction of the composition of the defect based on the imaging data. These experiments can include T2 mapping of the defect area, which would give us a signature relaxation time for different tissue and gel components and increase our certainty in identifying them. One can also incorporate information from other MR imaging modalities including T1 and diffusion tensor imaging (DTI) to discriminate between the tissue or gel within the defect.
- Finally, one may consider adding cells into the injectable scaffold for delivery into the defect site. The exact type of cell should be determined by the intended goal of the therapy (i.e. replacement of neurons, myelination, immunomodulation, secretion of trophic factors). Appropriate tests of the gel containing the specified cells should be conducted to ensure the gel still fits within the intended design parameters. Such tests include gelation time, gel mechanical properties, and cell viability/behavior within the gels.

Appendix:

Rheology procedure (gelation during testing):

For rat-tail collagen:

Instrument: TA instruments AR-G2 rheometer in a cone and plate geometry (40 mm 2 °) McKinley Lab 3-237 contact Sean Buhrmester for training [*fatsean@mit.edu*]

Parameters: Oscillation procedure, only check middle step

Experiment type: Time sweep for 60 min (really only use 1500 sec). Delay time 1 sec
Temperature: 37°C, don't click wait.
Mechanics: Controlled stress @ 0.1 Pa, 1 rad/s
Data collection: Sampling and conditioning time 10 sec each

Procedure:

*Sign up for time at calendar.yahoo.com (name: non_newtonian password: deborah)
*Remember to sign in and out of the book

1.) Calibrate instrument, follow instructions on the sheet on top of the computer. *Make sample during rotational mapping to save time. Use 1.5 ml centrifuge tubes and make 0.7 ml.
Keep collagen in refrigerator to keep it cold. There is no easy source of ice nearby.

2.) Change the bottom plate temperature to 8°C to prevent gelation

3.) Pipette 640 μl onto the center of the stage (marked as slightly in front of the circle on the lower platen). Make sure there are no bubbles (remove with pipette).

4.) Use the instrument control tab to lower the geometry to 500 μm, 100 μm, and finally 54 μm. Sample must be even around the entire geometry and must come right up to the edge without overflowing.

5.) Start the run and wait 150 sec before applying light mineral oil, dropwise around the edge of the geometry to prevent evaporation. The oil will spread so not much is needed.

6.) Data is automatically saved at every point to the file you specified. Data file automatically opens with the TA Analysis program. Right click on the file name on the left-hand panel and click export to text. The txt file will be in the same folder as the data file.
*To get the full data set you must close and reopen it at the end of the run!

7.) At the end of the run, press the stop button. Raise the geometry and clean it with a kipwipe. Wipe the stage clean with a kimwipe.

8.) Turn the temperature back to 8°C, recalibrate geometry inertia and rotational mapping before the next sample.

9.) Sample analysis: open txt file in excel.

Gelation time (G'=G" or delta =45). Plot delta vs time, zoom in on x-axis and make y-axis between 45-46. The gel point will now be the intersection of the line on the x-axis.

Modulus at a specific time: Read directly from text file. It is a little easier to put all data on the same sheet because all of the rows will be at essential the same time (+/- a few sec discrepancy per run).

For an unknown sample:

1.) Determine the linear viscoelastic regime (LVR) of the material.

Allow material to gel in the machine

Perform a stress sweep from 0.01-10 Pa 6 pts/decade @ 1 rad/s

Want a stress that is in the linear range of the modulus vs. stress plot

2.) Determine frequency dependence of modulus

Frequency sweep at a controlled stress determined in 1.)

1 rad/s – 100 rad/s

3.) Determine if stress affects the gel procedure (i.e. prevents gelation)

Within the LVR find the stress at which the gel point no longer changes

LMT Fabrication Procedure

Materials:

- 1,2-bis-(triscosa-10,12-diynoyl)-sn-glycero-3-phosphocholine ($DC_{8,9}PC$) AKA 23:2 Diyne PC: 1,2-di-(10Z,12Z-tricosadiynoyl)-*sn*-glycero-3-phosphocholine *Cat # 870016 Avanti Polar lipids*
- D^+/D^- Trehalose MW= 378.33 g/mol
- Ethanol
- DI H_2O
- 1x Phosphate Buffered Saline (PBS)
- Temperature controlled water bath (Cole-Palmer 6-liter Programmable Controller Heated Circulating Bath, 240VAC, CAT# EW-12116-35)

Fabrication Procedure:

1.) Preheat water bath to 55°C
2) In separate 15 ml conical tubes, warm 7 ml of 100% ethanol and 3 ml sterile water to 55°C
3) Dissolve 10 mg lipid in the 7 ml of warm ethanol
4) Slowly add the water to the lipid/ethanol solution and discard the empty water tube
5.) Use the following program to slowly cool the lipid solution at 1°C in the water bath (total running time of 51 hours)

Step	Ramp(°C)	Time (hr)
1	55-55	5
2	55-25	30
3	25-33	8
4	33-25	8

6) Incubate the lipid solution for two weeks at room temperature protected from light to allow the microtubules to completely form
7) Add 50mM trehalose (18.9mg/ml) to the lipid solution and mix gently. Since trehalose is poorly soluble in EtOH, dissolve the appropriate amount in 1 ml DiH_2O before adding. Incubate-overnight at room temperature
8) Centrifuge the lipid microtubules for 10 min at 1500*g*, remove the supernatant
9) Resuspend the microtubules in 0.5 ml sterile water, freeze and lyophilize the microtubules overnight
10) Load the microtubules by rehydrating the dried microtubules in the protein solution of interest (40µl per mg of lipid) and incubate overnight at 4°C. Be gentle with pipetting.
11) Add 2 ml 1x PBS per mg microtubule, centrifuge for 10 min at 1500*g* and remove the supernatant
12) Repeat the rinse (step 11) and dilute to the desired concentration in 1x PBS

Astrocyte Migration Assay Procedure:

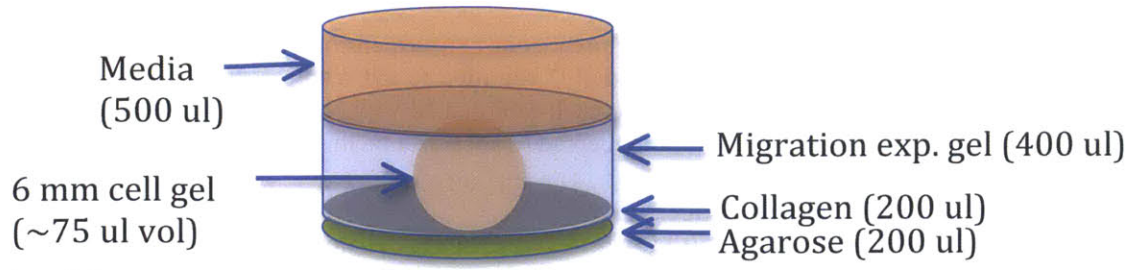

Materials:

Collagen gel: Always keep components on ice

- Type I rat tail collagen (BD Biosciences) 3.6-3.9 mg/ml
- 5x Phosphate buffered saline (PBS)
- 1N NaOH
- 1x PBS or cell culture media
- 3 mg/ml genipin in 5x PBS*: make sure it solubilizes, then filter*
- Lipid microtubules (LMTs): See LMT procedure document
- Growth factor of choice (ie. FGF-2)

Migration assay

- 12 well plate – for initial astrocyte seeding
- 24 well plate- for migration assay
- 6 mm biopsy punch
- forceps
- 2% sterile agarose solution
- Trypan blue & hemocytometer

Cell Culture:

- Media: DMEM high glucose + pyruvate + glutamate
- Media additives: 10% FBS, 1% Penn/Strep antibotics
- Accutase- for harvesting

Procedure:

Day 1:

- Obtain astrocytes from Charlestown. Use Styrofoam box with heating pack inside
- Harvest cells:
  - Remove media & rinse with PBS
  - Add warmed Accutase solution (3 ml for T25, 5 ml for T50) incubate 5-10 min. Tap bottom of flask with palm of hand.
    - By microscope: most cells should be seen floating
  - Add equal parts media & transfer to centrifuge tube
    - 300x g, 5 min
  - Remove supernatant and re-suspend gently in 1 ml media
    - Count on hemocytomter, 1:9 dilution w/ trypan blue

        - #cells= Avg 4 squares * dilution * vol media * 10^4
- Seed at $1x10^6$ cells/ml in 2 mg/ml collagen gel
    - Use Col, 5x, NaOH, cell culture media, cell suspension
    - **Want volume of # gels needed /7 rounded to nxt whole #**
    - Add 1 ml gel-cell solution to each well of a 12 well plate
    - Allow to gel for 15-30 min then add 1 ml warm media
- Load LMTs with growth factor or PBS
    - 40 µl/mg LMTs, keep in refrigerator
        - Previously 1 mg/ml, 0.11 mg/ml FGF-2 in 5% trehalose
- Coat bottom of 24 well migration plates with agarose
    - **Only have 2-3 groups/plate- temp control when plating & imaging**
    - Heat agarose solution to 60°C
    - Pipette **200 µl** on the bottom of each plate,
    - Keep in hood overnight

Day 2:

- Coat 24 well plates with type I collagen solution
    - 200 µL, let gel in incubator for 30-60 min
- Rinse LMTs
    - Transfer to 15 ml tube and re-suspend in 2 ml 1x PBS
    - Centrifuge 1500 x g, 10 min
    - Remove supernatant and re-suspend at 1 mg/ml
- Make 2 mg/ml collagen gel solutions
    - Use spreadsheet to calculate volumes of all components
        - **Want final volume of 0.4 ml x (# samples +1)**
    - Make 3 mg/ml genipin soln in 5x PBS
        - Mix thoroughly using vortex until solubilized, then filter (0.22 µm)
    - Genipin groups were done at 0.25 mM
    - For LMT groups load at 0.1 mg/ml
    - **Hold everything on ice till ready to plate**
- Setup migration assay
    - Biopsy punch 6 mm gels (7 per 12 well plate)
    - Carefully remove with forceps and place in the center of the 24 well plate
    - Immediately coat with **0.4 ml** Col migration gel
    - Incubate for 30 min before adding **0.5 ml** media

Day 3-9:

- Replace media on all samples at 24 hours
- Replace every 48 hours thereafter
- Imaging can be done on the light microscope (usually Day 4,6)

Day 10:

- Imaging:
    - Remove media from wells & replace with 0.5-1 ml staining solution
        - 1-2 µl Calcein AM (1mg/ml aliquots) per 1 ml PBS
        - Incubate for 30-60 min
    - Remove from well, place on microscope slide and blot dry along edges
    - Image at 4x in fluorescent microscope 5-6 FOV along edge per gel

        - Be sure to capture both interface and furthest cells even if it takes multiple FOV
    - Also take an image at the center of the gel
- Fixation:
    - Place gel into new well with 1 ml 4% PFA, leave at RT for 1 hr
    - Rinse with 1x PBS
    - Add 1 ml 0.5% triton-x 100, leave for 30 min-1 hr
    - Rinse with 1x PBS
    - Add DAPI (5 mg/ml stock) 1 ml (1-2 µl/10 ml PBS) leave overnight
- Imaging again for DAPI staining

Analysis: Using Image J

For each image:

- Measure the interface length between the cell seeded and migration gel
- Manually count the number of migrated cells using the cell counter function
    - Careful to make sure you are catching each cell in Calcein AM images
- Measure the distance from the interface to the longest cell
    - Measure using a line perpendicular to the interface

For the image with the longest migration (using DAPI images)

- Create a histogram of all the cells
    - Using the cell counter function, place a marker at the interface of the gel
        - If the surface is highly curved, you may have to place several markers after rotating the image
    - Mark the positions of each cell that has migrated
    - Subtract the XY coordinates from nucleus of the cell from the XY coordinate of the gel interface to determine the migration distance
        - Images were scaled to 62 pixels= 100 microns
- Graphs
    - # cells/mm interface
    - Avg migration distance of longest cell
        - Averaged over all images of all gels per group
    - Histogram of distance cells migrated
        - 100 µm intervals

Image Analysis:

1.) Select your image for analysis in Photoshop CS5

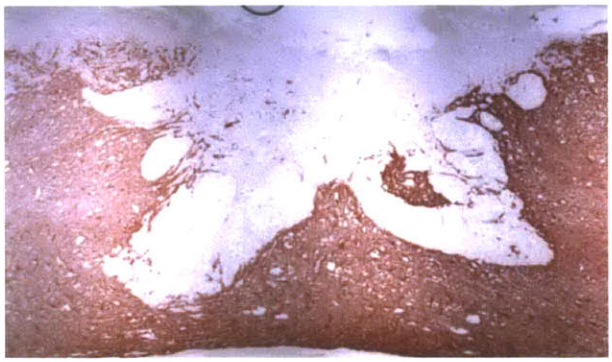

2.) Draw a border around the defect or region of interest using the brush tool

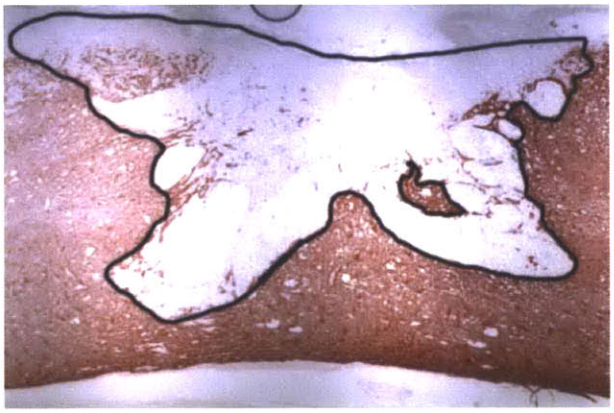

3.) Select the region of interest using the quick selection tool

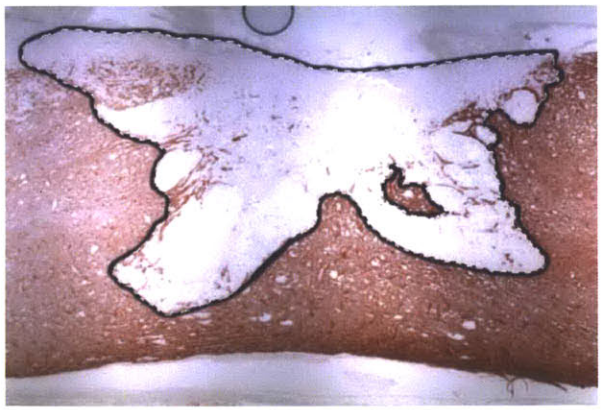

4.) If recording an absolute area measurement:

Analysis- set measurement

4x histology= (542 pixels/1000μm)

If recording a percent area, leave in default scale (easier to switch between Photoshop and image J

Analysis- Record measurement (gives area of the selection)

5.) *Image- calculations*- Green channel subtract red channel.

This creates a new grayscale channel based only on the red staining in the image

Image-mode-grayscale (deletes all other channels

6.) *Select-inverse*

Press delete and fill with black

Images with high background staining can be thresholded to include only the appropriate staining by

Image-adjustments-threshold

7.) Save as JPEG image

8.) Open in Image J 1.45S

Process-Binary- Make binary

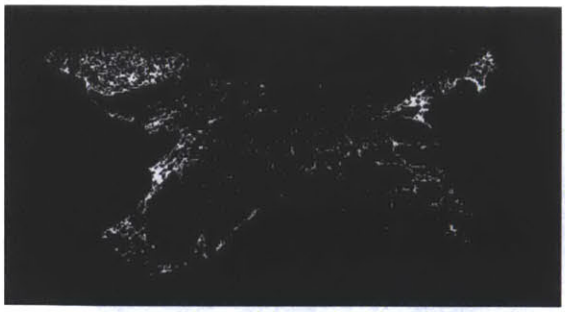

Analyze-analyze particles- size 0-infinity, circularity 0-1

Use the "total area" for analysis (area of white in the image)

9.) For percent area analysis:

% area= $A_{\text{binary from image J}}/A_{\text{selct from photoshop}}$

Validation: Correlation of cell number and area

1.) Primary cortical astrocytes seeded in a collagen gel. Gels were embedded in paraffin, sectioned at 6 μm and stained with Masson's Trichrome. Image taken at 4x objective

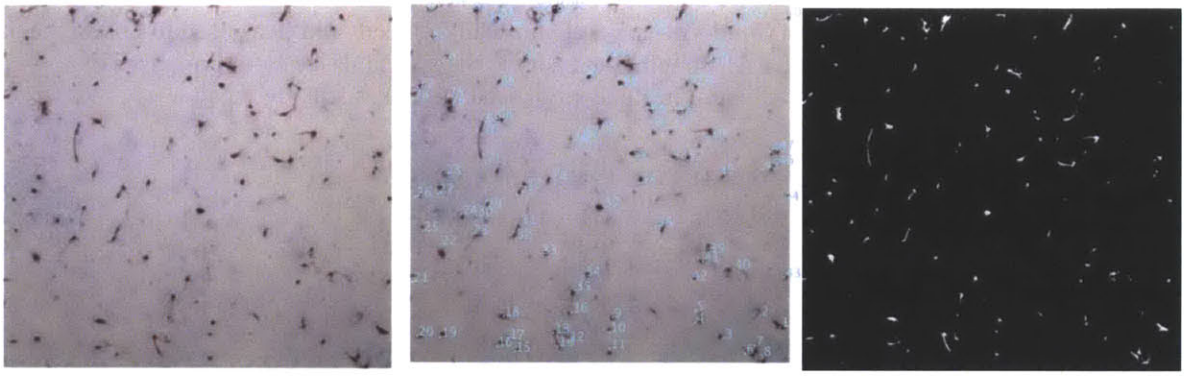

Original Image Counting Post processing as above

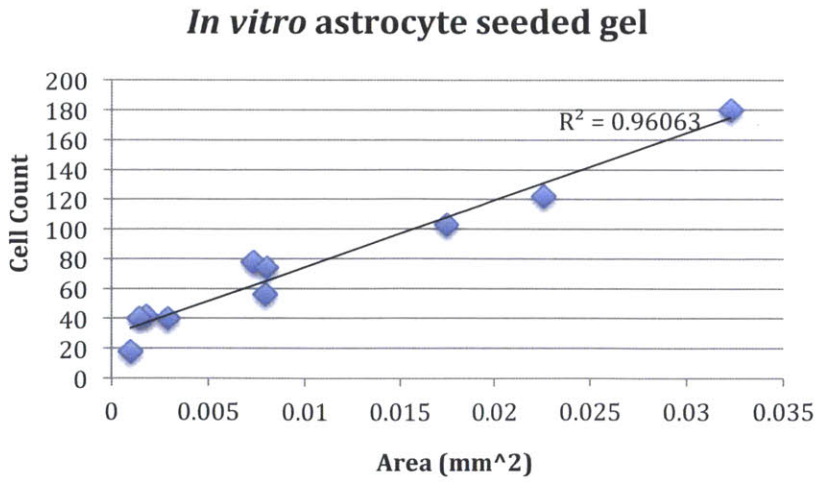

Images of the spared white/gray matter of GFAP IHC stained slides were used to validate the method of separating areas IHC staining and correlating area to number of cell bodies present. A number of astrocytes in the images below are also hypertrophic.

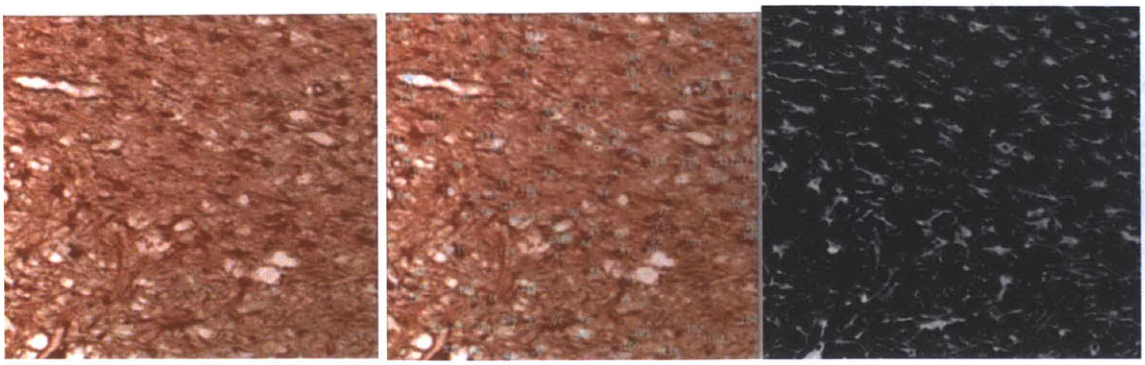

Original Image Counting Post processing*

*A slightly different image calculation (blue- inverse green instead of green –red) was used to obtain the post-processed image due to the high GFAP staining intensity in the spared tissue from processes of astrocytes whose bodies are not in the image. The concept of separation was still identical.